

Copyright

by

Larry Seth Memberg

2002

**Bridges with Premature Concrete Deterioration: Damage Indices,
Strand-Pullout Tests, and Field Observations**

by

Larry Seth Memberg, B.S.C.E.

Thesis

Presented to the Faculty of the Graduate School of

The University of Texas at Austin

in Partial Fulfillment

of the Requirements

for the Degree of

Master of Science in Engineering

The University of Texas at Austin

August 2002

**Bridges with Premature Concrete Deterioration: Damage Indices,
Strand-Pullout Tests, and Field Observations**

**Approved by
Supervising Committee:**

Richard E. Klingner

Michael E. Kreger

Dedication

For my parents, Donald and Francine Memberg,
my grandmothers, Belle Memberg and Anne M. Zwirn,
and for my grandfather, Irving Memberg.

Acknowledgements

I first want to thank the Structural Engineering faculty and staff of The University of Texas at Austin for creating an environment that is world-class, relaxed, helpful, encouraging, and collaborative. Thank you for providing all of the support and resources that students need.

This research and my master's education were funded by the Texas Department of Transportation under Study 1857. Brian Merrill, our TxDOT Project Director, deserves to be recognized for his assistance and cooperation. He took an active interest in our work, and whenever I asked him for anything, he responded almost immediately. Also, Darren Crenwelge and Bobby Chenault of the Junction Area Office were more than willing to help me track down a lot of old information from the Lake Ivie bridge.

Thank you to my research advisor, Dr. Richard E. Klingner, for his guidance and direction throughout the laboratory testing, classes, and writing of this thesis. Thank you, also, to my second reader, Dr. Michael E. Kreger, and Dr. Timothy J. Fowler for their support and assistance.

Thanks and appreciation are due to the members of my research team, Piya Chotickai, Amy Eskridge, Yong-Mook Kim, and Joe Roche, for their help. I am grateful to Anna Boenig, whose research I followed, for staying in touch and answering my questions even though she had already graduated.

Thank you to the technical FSEL staff, Mike Bell, Dennis Phillip, Ray Madonna, and Blake Stasney, for always having good, practical ideas.

I appreciate the helpfulness and friendliness of the FSEL staff: Regina Forward, Ruth Goodson, Wanda Kitts, Barbara Lafferty, Hortensia Peoples, Dijaira Smith, and Lindsay Rogers. José Acosta was also part of the team.

Thank you to all of the professors who spent time helping me, even though they weren't involved with my project, especially Dr. Oguzhan Bayrak, Dr. John E. Breen, and Dr. Michael D. Engelhardt. Thank you to the students who spent time helping me test, figure out difficult concepts, and choose the right wordings for my thesis, even though they had many other things to do, especially Gabriela Arce, Nat Ativitavas, Baris Binici, Alfredo Castro, Greg Cohen, Michael Hagenberger, Matthew Memberg, Taichiro Okazaki, Marcel Poser, Onur Sonuvar, Jenny Tanner, Fernando Ulloa, and Jorge Varela. The support and camaraderie of my fellow students made the experience at UT what it was.

Thank you especially to all of the Latinos. They know what it means to be true friends.

I am honored to have been a part of the FSEL research machine.

August 2002

Abstract

Bridges with Premature Concrete Deterioration: Damage Indices, Strand-Pullout Tests, and Field Observations

Larry Seth Memberg, MSE

The University of Texas at Austin, 2002

Supervisor: Richard E. Klingner

This thesis describes part of the work associated with TxDOT Study 1857 (“Structural Assessment of In-Service Bridges With Premature Concrete Deterioration”). The primary objective of this thesis is to determine the effects of premature concrete deterioration on the bond between prestressing strands and concrete, using damage indices and strand-pullout tests. Sixty-four strand-pullout tests were performed on sixty strands from four laboratory specimens taken from full-size precast concrete box girders. The field observation program, begun earlier in this study, of five large TxDOT structures in different parts of Texas was continued for two additional years. Recommendations are made for addressing deterioration in the FM 1929 structure over the Lake Ivie Reservoir in Concho, Texas. Results from the laboratory tests and the field observation

program are used to relate external damage to reductions in structural capacity of in-service structures with premature concrete deterioration.

Table of Contents

List of Tables.....	xvi
List of Figures	xvii
Chapter 1 Introduction	1
1.1 Information on TxDOT Study 1857.....	1
1.2 Scope and Objectives of Study 1857.....	2
1.3 Scope of This Thesis	3
1.4 Objectives of This Thesis	3
1.5 Complementary Work.....	4
Chapter 2 Literature Review	6
2.1 Previous Studies of Prestressing Bond.....	6
2.1.1 Bond Between Prestressing Strand and Concrete	6
2.1.2 Bond-Stress Distribution in Pullout Tests.....	7
2.2 Previous Techniques For Conducting Pullout Tests of Bars and Strands.....	8
2.2.1 Stocker and Sozen (1970)	8
2.2.2 Salmons and McCrate (1977).....	9
2.2.3 Abrishami and Mitchell (1993).....	9

2.2.4	Rose and Russell (1997).....	10
2.3	Gaps in Knowledge Regarding Pullout of Strands.....	11
Chapter 3	Development of Test Program.....	13
3.1	Objectives and Plan.....	13
3.2	Test Specimens.....	13
3.2.1	Box Girders	13
3.2.2	Cutting of Slice Specimens	15
3.2.3	Slice and Strand Nomenclature	18
3.2.4	Location of Slices in Girders.....	19
3.2.5	Pre-existing Condition of Slices.....	21
3.2.6	Rationale for Slice Preparation	30
3.2.7	Slice Preparation Procedure	31
3.3	Test Setup and Procedure	35
3.3.1	Test Setup.....	36
3.3.2	Instrumentation and Data Acquisition	40
3.4	Strand-Pullout Test Procedure	43
3.5	Correlation With Visual Damage	44
Chapter 4	Test Results.....	47

4.1	Presentation of Data	47
4.2	Results From Strand-Pullout Tests.....	51
4.2.1	No Significant Change in P with Increasing N	52
4.2.2	Decrease in P with Increase in N	59
4.2.3	Increase in P with Increase in N	62
4.3	Measured Damage Indices of Specimens.....	70
4.3.1	Slice BG1S	70
4.3.2	Slice BG2N	71
4.3.3	Slice BG4S1	71
4.3.4	Slice BG4S2	72
Chapter 5	Significance of Test Results	73
5.1	Mechanisms Governing the Load-Displacement Response of Strands in Concrete	73
5.2	Bond Mechanism.....	74
5.3	Friction Mechanism.....	78
5.4	Twist Mechanism	79
5.5	Combination of Resistance Mechanisms	82
5.6	Significance of Damage Indices of Specimens	85

Chapter 6 Continuation of Field Observation Program	89
6.1 Objectives and Plan.....	89
6.2 Structures Observed	89
6.2.1 I-10 Over AT & SF RR.....	89
6.2.2 US-90 Over the San Jacinto River	91
6.2.3 Robinson Road Over I-45	92
6.2.4 Beltway 8 Over State Highway 3.....	93
6.2.5 FM 1929 Over Lake Ivie.....	95
6.3 Inspection Procedure	95
6.4 Brief Summary of Field Visits	100
Chapter 7 Results from Field Observations	103
7.1 Nomenclature	103
7.2 Observations From Structures Studied.....	104
7.2.1 I-10 over AT & SF RR.....	104
7.2.2 US-90 over the San Jacinto River	110
7.2.3 Robinson Road over I-45	116
7.2.4 Beltway 8 over State Highway 3.....	123
7.2.5 FM 1929 over Lake Ivie.....	131

7.3 Results From Crack-Width Measurements	145
7.3.1 I-10 over AT & SF RR.....	145
7.3.2 US-90 over the San Jacinto River	146
7.3.3 Robinson Road over I-45	147
7.3.4 Beltway 8 over State Highway 3.....	148
7.3.5 FM 1929 over Lake Ivie.....	149
Chapter 8 Significance of Field Results	154
Chapter 9 Recommendations for Addressing Deterioration in Lake Ivie	
Structure	165
9.1 Introduction	165
9.2 General Discussion of Replacement or Repair	165
9.2.1 Steel Jackets	166
9.2.2 Concrete Shells.....	166
9.2.3 Column Splints.....	167
9.2.4 Sister Columns	168
9.3 General Discussion of Mitigation	169
9.3.1 Flexible Wrap around Bent Columns.....	170
9.3.2 Cofferdams around Bent Columns.....	170

9.3.3 Seal Cracks and Coat Affected Elements.....	171
9.3.4 TxDOT Mitigation Technique	172
9.4 Probable Useful Life of the Lake Ivie Structure Without Mitigation.....	172
9.4.1 Probable Reduced Strengths	173
9.4.2 Probable Reduced Strengths of Girders	176
9.4.3 Probable Reduced Strength of Columns	177
9.5 Options for Addressing Deterioration at Lake Ivie.....	184
9.5.1 Repair or Replace Affected Elements.....	184
9.5.2 Mitigate Deterioration.....	184
9.5.3 Monitor Deterioration	184
9.6 Recommendations for Addressing Deterioration at Lake Ivie.....	185
Chapter 10 Summary, Conclusions, and Recommendations	186
10.1 Summary	186
10.2 Conclusions	187
10.2.1 Effects of Premature Concrete Deterioration on the Pullout Response of Strands.....	187
10.2.2 Conclusions with Respect to the FM 1929 Structure over Lake Ivie.....	188

10.3 Recommendations	189
10.3.1 Recommendations Regarding the Effects of Premature Concrete Deterioration on the Pullout Response of Strands	189
10.3.2 Recommendations with Respect to the FM 1929 Structure over Lake Ivie.....	189
Appendix A Fabrication Details of Box Girders.....	191
Appendix B Fabrication Drawing for Box Girders with Non-Standard Spans	195
Appendix C Data from Strand-Pullout Tests	197
References	254
Vita	256

List of Tables

Table 4.1:	Summary of Test Results for Strand BG2N_8L	55
Table 4.2:	Summary of Test Results for Strand BG4S1_17R.....	57
Table 4.3:	Summary of Test Results for Strand BG4S2_1L.....	58
Table 4.4:	Summary of Test Results for Strand BG4S1_15L.....	60
Table 4.5:	Summary of Test Results for Strand BG4S1_4R.....	62
Table 4.6:	Summary of Test Results for Strand BG2N_9R	64
Table 4.7:	Summary of Test Results for Strand BG1S_13R.....	66
Table 4.8:	Summary of Test Results for Strand BG1S_2R.....	67
Table 4.9:	Summary of Test Results for Strand BG4S2_5R.....	69
Table 4.10:	Damage Indices for Slice BG1S	71
Table 4.11:	Damage Indices for Slice BG2N.....	71
Table 4.12:	Damage Indices for Slice BG4S1	72
Table 4.13:	Damage Indices for Slice BG4S2	72
Table 5.1:	Derivation of load-displacement relationship for twist mechanism.....	81
Table 5.2:	Average bond strengths for selected strands in Slice BG4S2	87
Table 7.1:	Field damage indices for bent cap, Bent 5, Lake Ivie	152
Table 7.2:	Field damage indices for bent cap, Bent 9, Lake Ivie	152

List of Figures

Figure 3.1	Side view of box girders	14
Figure 3.2:	Cross-section of box girders used for strand-pullout tests	14
Figure 3.3:	Cross-section of typical slice taken from box girder	16
Figure 3.4:	Side view of typical slice taken from box girder	16
Figure 3.5:	Front view of slice cut from Girder BG2N	17
Figure 3.6:	Back view of slice cut from Girder BG2N.....	17
Figure 3.7:	Strand numbering system.....	19
Figure 3.8:	Location of slice from Girder BG1S	20
Figure 3.9:	Location of slice from Girder BG2N	20
Figure 3.10:	Location of slices from Girder BG4S	21
Figure 3.11:	Crack through Strand 9L in back face of Slice BG1S	22
Figure 3.12:	Cracking on left face of Slice BG1S	23
Figure 3.13:	Cracks at left inner corner of Slice BG1S.....	23
Figure 3.14:	Cracking on right face of Slice BG2N	24
Figure 3.15:	Large cracks in back face of Slice BG2N	25
Figure 3.16:	Cracking on middle of bottom face of Slice BG2N.....	25

Figure 3.17: Cracking on Bottom Face of Slice BG4S1	26
Figure 3.18: Cracking on left face of Slice BG4S1	27
Figure 3.19: Damage to cross-section of Slice BG4S1 (back face)	28
Figure 3.20: Cracking in back face of Slice BG4S2.....	29
Figure 3.21: Cracking on bottom face of Slice BG4S2	29
Figure 3.22: Front view of right inside corner of Slice BG4S2.....	30
Figure 3.23: Test setup to mimic service conditions in a solid end block.....	31
Figure 3.24: Cardboard formwork used for front face	33
Figure 3.25: Formwork for web sections.....	34
Figure 3.26: Cardboard formwork for top of web	34
Figure 3.27 Level Hydrostone bearing surface on top of web section	35
Figure 3.28: Schematic drawing of test setup.....	36
Figure 3.29: Slice specimen in loading machine for strand-pullout tests.....	37
Figure 3.30: Testing positions for specimens	38
Figure 3.31: Steel plate between loading head and slice specimen	39
Figure 3.32: Steel spacer and plate used for middle strands.....	39
Figure 3.33: Linear potentiometers at loaded end	40
Figure 3.34: Linear potentiometer attached to back of strand	42

Figure 3.35: Linear potentiometers recording relative movement of strand at free end.....	43
Figure 3.36: Representative areas for bottom face damage indices	45
Figure 3.37: Representative square for left side damage index.....	45
Figure 3.38: Representative square for right side damage index.....	46
Figure 4.1: Loading history for strand-pullout tests	48
Figure 4.2: Typical load-displacement response from strand-pullout tests	49
Figure 4.3: Identifying first slip without reliable free-end data.....	50
Figure 4.4: Identifying resumption of slip without reliable free-end data.....	51
Figure 4.5: Back view of Strand BG2N_8L (right) and Strand BG2N_9L (left).....	53
Figure 4.6: Load-displacement Relationship for Strand BG2N_8L.....	54
Figure 4.7: Crack in back of Slice BG4S1 at Strand 17R (Center)	55
Figure 4.8: Load-displacement Relationship for Strand BG4S1_17R	56
Figure 4.9: Load-displacement Relationship for Strand BG4S2_1L.....	58
Figure 4.10: Load-displacement Relationship for Strand BG4S1_15L.....	59
Figure 4.11: Back view of Strand BG4S1_4R (right) and Strand BG4S1_5R (left).....	61
Figure 4.12: Load-displacement Relationship for Strand BG4S1_4R	62

Figure 4.13: Load-displacement Relationship for Strand BG2N_9R.....	63
Figure 4.14: Load-displacement Relationship for Strand BG1S_13R	65
Figure 4.15: Load-displacement Relationship for Strand BG2N_2R.....	67
Figure 4.16: Back View of Strand BG4S2_5R (Top Row, Second From Left)	68
Figure 4.17: Load-displacement Relationship for Strand BG4S2_5R.....	69
Figure 5.1: Free-body diagram of a length dx of a smooth bar in concrete.....	74
Figure 5.2: Free-body diagram of a smooth bar in concrete.....	76
Figure 5.3: Experimental setup used to determine u_{avg}	76
Figure 5.4: Load-displacement relationship assuming uniform bond stress	77
Figure 5.5: Approximate load-displacement relationship for bond mechanism.....	78
Figure 5.6: Load-displacement relationship for friction mechanism.....	79
Figure 5.7: Twist of a cylindrical bar	80
Figure 5.8: Load-displacement relationship for twist mechanism.....	82
Figure 5.9: Superposition of the three independent mechanisms	82
Figure 5.10: Load-displacement Relationship for Strand BG4S2_17R	83
Figure 5.11: Average bond strength vs. damage index for strand-pullout tests.....	85

Figure 5.12: Cracking in back face of Slice BG4S2.....	86
Figure 6.1: I-10 over AT & SF RR in Beaumont, Texas (facing east).....	90
Figure 6.2: Overview of West Abutment of I-10 structure in Beaumont, Texas.....	90
Figure 6.3: US-90 over the San Jacinto River near Houston, Texas	91
Figure 6.4: West Abutment of US-90W bridge over the San Jacinto River.....	92
Figure 6.5: Robinson Road over I-45 in The Woodlands, Texas	93
Figure 6.6: Underside of Robinson Road over I-45 (facing east).....	93
Figure 6.7: Beltway 8 over State Highway 3, Houston, Texas (facing north) ...	94
Figure 6.8: Beltway 8 over State Highway 3, Houston, Texas (facing west).....	94
Figure 6.9: FM 1929 over the Lake Ivie Reservoir in Concho, Texas (facing west).....	95
Figure 6.10: Crack comparator card	97
Figure 6.11: Measuring crack widths with optical scope	97
Figure 6.12: Taking readings with Demec gauge.....	98
Figure 6.13: One set of Demec discs for monitoring crack width.....	99
Figure 6.14: Holding set of Demec discs in place with reference bar	99
Figure 6.15: Representative areas used for crack ratios, I-10 structure.....	100
Figure 7.1: Nomenclature used to identify faces of girders.....	103

Figure 7.2: Schematic of crack-measurement locations on I-10 structure (plan view)	104
Figure 7.3: New diagonal cracks on I-10 SW Girder 4, Face 5 (10/7/00).....	105
Figure 7.4: Representative areas on I-10 SW Girder 2, south face (10/7/00).....	106
Figure 7.5: Cracks at first bent east of west abutment, I-10 (10/7/00)	107
Figure 7.6: Location of new cracks on I-10 structure (plan view) (12/10/01).....	108
Figure 7.7: New cracks on south face of SW Girder 3 at west abutment, I-10 (12/10/01)	109
Figure 7.8: Cracks at first bent east of west abutment, I-10 (12/10/01)	110
Figure 7.9: Schematic of crack-measurement locations on US-90 structure (plan view)	111
Figure 7.10: Typical crack under drain at US-90 structure (10/6/00)	112
Figure 7.11: Extension of existing cracking on north surface (Face 5) of NW Girder 2, US-90 (6/22/01)	113
Figure 7.12: Cracks at end of NW Girder 1, US-90 (6/22/01)	114
Figure 7.13: Close-up view of Point 10 (bottom, left pair of Demec discs) and Point 8 (top), US-90 (12/11/01)	115
Figure 7.14: Apparent cracking through sealant, US-90 (12/11/01)	116

Figure 7.15: Schematic of crack-measurement locations on Robinson Road structure (plan view)	117
Figure 7.16: Extension of new cracking on south face of NW Girder 3, Robinson Road (10/7/00)	118
Figure 7.17: Extension of cracking on NW Girder 2, Robinson Road (6/21/01)	119
Figure 7.18: Extension of cracking on underside of NW Girder 2, Robinson Road (6/21/01)	120
Figure 7.19: Extension of cracking on north surface of NW Girder 2, Robinson Road, at west abutment (12/10/01)	121
Figure 7.20: Extension of cracking past sealant on south surface of NW Girder 2, Robinson Road, at west abutment (12/10/01)	121
Figure 7.21: Location of new cracks on Robinson Road structure (plan view) (12/10/01)	122
Figure 7.22: New cracks on north surface of NW Girder 3, Robinson Road, at west abutment (12/10/01)	123
Figure 7.23: Overview of Beltway 8 over State Highway 3 (facing north)	124
Figure 7.24: Schematic of crack-measurement locations on Beltway 8 structure (plan view)	125
Figure 7.25: Overall view of Points 3-5, Beltway 8 (facing south) (6/22/01)	126

Figure 7.26: Overall view of Point 1, Beltway 8 structure (facing north) (6/22/01).....	127
Figure 7.27: Close-up view of Point 1, Beltway 8 structure (6/22/01).....	128
Figure 7.28: Close-up view of Point 6, Beltway 8 structure (6/22/01).....	128
Figure 7.29: Overall view of Point 7, Beltway 8 structure (facing north) (6/22/01).....	129
Figure 7.30: Cracking near Point 6, Beltway 8 structure (12/11/01).....	130
Figure 7.31: Sealed cracks along girder flange near Point 6, Beltway 8 structure (12/11/01).....	131
Figure 7.32: North profile of Lake Ivie structure	131
Figure 7.33: Plan view of Lake Ivie structure	132
Figure 7.34: Schematic drawing of typical bent for Lake Ivie structure	132
Figure 7.35: Schematic drawing of crack-measurement locations on Bent 5	133
Figure 7.36: Overall view of Bent 5 (facing north)	133
Figure 7.37: Schematic drawing of crack-measurement locations on Bent 9	134
Figure 7.38: Overall view of Bent 9 (facing west)	135
Figure 7.39: Schematic drawing of crack-measurement location on Bent 11	135
Figure 7.40: Map cracking on tie beam, Bent 5 (12/18/00).....	136
Figure 7.41: Cracking on bent cap, Bent 9 (12/18/00)	137

Figure 7.42: 12 in. (0.31 m) square on south end of bent cap, Bent 5 (12/19/00).....	138
Figure 7.43: 12 in. (0.31 m) square on south end of bent cap, Bent 9 (4/24/01).....	139
Figure 7.44: Example of column cracking near waterline of Bent 5 (4/24/01).....	140
Figure 7.45: Example of column cracking near waterline of Bent 11 (Point 10) (4/24/01).....	140
Figure 7.46: New cracks on 12 in.. (0.31 m) square on south end of bent cap, Bent 5 (10/15/01).....	141
Figure 7.47: New cracks on exterior faces of south girders at Bent 9 (10/15/01).....	142
Figure 7.48: Close-up of new cracks on south girder at Bent 9 (10/15/01).....	142
Figure 7.49: Column cracking at Point 10 near waterline, Bent 11 (10/15/01).....	143
Figure 7.50: Close-up of vertical cracking at Point 10 near waterline, Bent 11 (10/15/01)	144
Figure 7.51: Close-up of horizontal crack at Point 10 near waterline, Bent 11 (10/15/01)	144
Figure 7.52: Crack width over time for I-10 structure.....	145
Figure 7.53: Crack width over time for US-90 structure.....	146

Figure 7.54: Crack width over time for Robinson Road structure.....	148
Figure 7.55: Crack width over time for Beltway 8 structure	149
Figure 7.56: Crack width over time for FM 1929 at Lake Ivie	150
Figure 7.57: Crack comparator readings over time for FM 1929 at Lake Ivie.....	151
Figure 7.58: Damage Index over time for FM 1929 at Lake Ivie.....	153
Figure 8.1: Crack width versus age of girder for the I-10 structure	155
Figure 8.2: Change in crack width versus age of girder for the I-10 structure.....	156
Figure 8.3: Crack width versus age of girder for the US-90 structure	157
Figure 8.4: Change in crack width versus age of girder for the US-90 structure.....	158
Figure 8.5: Crack width versus age of girder for the Robinson Road structure.....	159
Figure 8.6: Change in crack width versus age of girder for the Robinson Road structure	160
Figure 8.7: Incremental change of crack width versus age of girder for the I-10 structure	162
Figure 8.8: Incremental change in crack width versus age of girder for the US-90 structure	163

Figure 8.9: Incremental change in crack width versus age of girder for the Robinson Road structure	164
Figure 9.1: Steel jacket around bent columns.....	166
Figure 9.2: Concrete shells poured around bent columns.....	167
Figure 9.3: Splints installed on bent columns.....	168
Figure 9.4: Sister columns installed at bent.....	169
Figure 9.5: Flexible wrap around bent columns	170
Figure 9.6: Cofferdams constructed around bent columns	171
Figure 9.7: Concrete compressive strength of cores from box girders versus damage index (Boenig 2000)	173
Figure 9.8: Ratio of tested to specified concrete compressive strength versus damage index for pretensioned, precast concrete	174
Figure 9.9: Probable ratio of actual to specified concrete compressive strength versus damage index for cast-in-place elements with Class C concrete.....	176
Figure 9.10: Cross-section of lower column in Bent 5, Lake Ivie structure.....	178
Figure 9.11: Typical vertical cracking on south lower column of Bent 5	179
Figure 9.12: Ratio of design axial capacity to design axial load versus damage index, south column, Bent 5, Lake Ivie	181

Figure 9.13: Predicted Damage Index versus time for south column, Bent 5,
Lake Ivie..... 182

Figure 9.14: Predicted ratio of axial capacity to design axial load versus time,
south column, Bent 5, Lake Ivie 183

CHAPTER 1

Introduction

1.1 INFORMATION ON TxDOT STUDY 1857

In late 1995, the Texas Department of Transportation (TxDOT) became aware of premature concrete deterioration in several in-service structures throughout Texas. Most of the affected structural elements are prestressed girders, though substructures, including abutments, columns, and bents, are also damaged at some bridge sites. Typical damage to prestressed girders is described as horizontal cracking in the bottom flanges, longitudinal cracks in the underside of the bottom flange, and distributed “map cracking,” concentrated at but not limited to the end regions.

Also in late 1995, TxDOT became aware of premature concrete deterioration in 56 prestressed concrete box girders fabricated and in storage in San Marcos, Texas (Klingner and Fowler 1998). These affected box beams were never incorporated in their intended structure(s) due to the deterioration that occurred while the box beams were still in storage¹.

This premature concrete deterioration has been attributed to two expansive distress mechanisms: Alkali-Silica Reaction (ASR) and Delayed Ettringite Formation (DEF). TxDOT is currently deciding what actions to take with respect to this damage. In past instances, structures have been removed from service or repaired after only several years of service. As statewide inspection of in-service concrete structures progresses, more structures with this problem are being

¹ Personal communication, Lee Lawrence (TxDOT), January 1998.

identified. The cost for replacing and repairing these structures is already significant, and will continue to increase (TxDOT 1998).

This situation was the motivation for TxDOT Study 1857 (“Structural Assessment of In-Service Bridges With Premature Concrete Deterioration”). In this thesis, specific portions of Study 1857 are reviewed and reported. Section 1.1 is taken almost verbatim from a previous thesis (Boenig 2000).

1.2 SCOPE AND OBJECTIVES OF STUDY 1857

TxDOT Study 1857, “Structural Assessment of In-Service Bridges With Premature Concrete Deterioration,” focuses on seven specific tasks that were outlined in the project proposal (Klingner and Fowler 1998):

1. Conduct field investigations to confirm and monitor existing premature concrete deterioration, the rate of increase of such deterioration, and the effect of different remedial measures on that rate of increase.
2. Conduct laboratory investigations of local effects of premature concrete deterioration.
3. Develop nondestructive evaluation (NDE) techniques for determining degree and type of concrete deterioration.
4. Develop petrographic techniques for assessing severity of deterioration from samples taken from field investigations.
5. Develop engineering models for evaluating the global reduction in capacity of a structural element due to local premature concrete deterioration.
6. Develop an overall methodology for predicting the probable loss in capacity over time of a deteriorated structural element, based on external evidence, NDE, and engineering models.

7. Develop recommended actions by TxDOT for handling any given case of premature concrete deterioration. The recommendations will include specific guidelines for assessing the probable capacity of the structure as a function of time, and specific techniques for extending the useful life and maintaining the capacity of the structure for as long as possible.

1.3 SCOPE OF THIS THESIS

The parts of Study 1857 reported here concern Tasks (1) and (2). The field observation program developed by Boenig (2000) was continued for this thesis, as part of Task 1. Crack patterns, crack widths, and the progression of damage were documented for five in-service TxDOT bridge structures for an additional two years.

The laboratory testing program for this part of the study was designed to investigate the effect of premature concrete deterioration on the bond between prestressing strands and concrete (Task 2). Strand-pullout tests were performed on slice specimens removed from full-scale box girder specimens. Changes in the pullout response of strands were correlated with different indices of external damage to the concrete.

In addition, recommendations are given for addressing deterioration of the FM 1929 structure over the Lake Ivie Reservoir in Concho, Texas. The probable capacity of bent columns over time is projected, and options for addressing premature concrete deterioration in those columns are discussed. While the recommendations made for the Lake Ivie structure are intended specifically for that structure, the methodology pertains to Tasks (6) and (7) and can be applied to other cases of premature concrete deterioration.

1.4 OBJECTIVES OF THIS THESIS

The primary objective of this thesis is to determine the effect of premature concrete deterioration on the bond between prestressing strands and concrete. External visible damage in laboratory specimens is correlated with reductions in bond strength as part of the structural assessment of bridges with premature concrete deterioration. The effect of transverse clamping loads on the load-displacement response of a prestressing strand in concrete is explored.

Another key objective of this thesis is to predict the remaining useful life of the FM 1929 structure over Lake Ivie in Concho, Texas. Previous work (Boenig 2000) is used to estimate the reduced structural capacity of the bent columns, and options are discussed for addressing the premature concrete deterioration of that structure.

1.5 COMPLEMENTARY WORK

As part of Study 1857, several other students have conducted research on laboratory specimens and field structures under the direction of Dr. Richard E. Klingner, Dr. Michael E. Kreger, and Dr. Timothy J. Fowler. Luz Marina Fúnez presented the background and field work in a report in December 1999 that included monitoring crack patterns and crack widths for prestressed I-beams in four TxDOT bridge structures, and for prestressed concrete box girders in the laboratory (Task 1) (Fúnez 1999). Anna Boenig conducted laboratory tests and developed a field observation program for five TxDOT bridge structures, including the four observed by Fúnez (Task 1). Boenig performed full-scale static flexural tests and static shear tests on prestressed concrete box girders and also compressive strength tests and modulus of elasticity tests on cores taken from those girders (Task 2). Using test results, Boenig correlated the damage in prestressed girders with their structural capacities (Boenig 2000). Joe Roche

conducted full-scale fatigue tests on prestressed concrete box girders to determine the effects of premature concrete deterioration on shear-fatigue strength of pre-cracked prestressed concrete girders (Task 2) (Roche 2001). Yong-Mook Kim conducted laboratory tests similar to those performed by Boenig on prestressed concrete I-beams (Type C girders). He also conducted strand-pullout tests on slice specimens removed from those girders. Kim is developing strut-and-tie models to predict structural capacities of similar I-beams, given a level of deterioration (Task 5)².

Brian Tinkey investigated the use of nondestructive test methods (Task 3), including acoustic emission, impact echo, and short pulse radar, to assess the degree of distributed damage in laboratory specimens tested by Boenig and Kim (Tinkey 2000). Piya Chotickai developed nondestructive testing procedures for use in the field (Task 3) and used acoustic emission to monitor damage in the shear-dominated fatigue specimens tested by Roche and in the strand-pullout test specimens discussed in this thesis (Chotickai 2001).

Amy Eskridge conducted research as part of the related TxDOT Study 4069 (“Mitigation Techniques for In-Service Structures with Premature Concrete Deterioration”). She investigated several different types of concrete coatings and their effectiveness in mitigating damage due to ASR or DEF (Eskridge 2002).

² Kim, Y.M., “Structural Evaluation of Pretensioned Concrete Bridge Girders Damaged by Premature Concrete Deterioration.” Ph. D. dissertation (in progress) prepared for The Graduate School of The University of Texas at Austin, August 2002.

CHAPTER 2

Literature Review

This chapter presents a literature review of previous studies of bond between prestressing strand and concrete, focusing on pullout tests. The goal of this literature review was to identify previous experimental methods for determining the pullout behavior of prestressing strand in concrete. Gaps in knowledge of premature concrete deterioration and its effect on bond strength are explored and addressed by TxDOT Study 1857.

2.1 PREVIOUS STUDIES OF PRESTRESSING BOND

Extensive research has been conducted on bond between concrete and reinforcing steel. Several articles and textbooks discuss bond characteristics of smooth and deformed steel reinforcement. Particularly relevant research is discussed in this thesis.

2.1.1 Bond Between Prestressing Strand and Concrete

Three factors contribute to bond between prestressing strand and concrete:

1. adhesion between the concrete and strand;
2. friction between the concrete and steel; and
3. mechanical resistance provided by the twisting of the outer wires of the strand (Janney 1954).

In this thesis, slip is defined as rigid-body motion of the strand with respect to the surrounding concrete. After slip occurs, adhesion is lost and can no longer contribute to bond (Janney 1954). During subsequent slip, friction acts between the steel wires and concrete as the outer wires twist through the helical grooves in the concrete.

2.1.2 Bond-Stress Distribution in Pullout Tests

Pullout tests have been performed to study bond characteristics and stress-slip relationships. Early research (Mylrea 1948) showed that bond stress is not uniform along the length of a smooth or deformed bar in a pullout test. Based on Mylrea, the variation of bond stress, $u(x)$, with distance from the loaded end, x , is shown schematically in Figure 2.1. The bond stress is equal to zero at the loaded end, and also at the free end inside the concrete. The bond stress reaches its peak close to the loaded end, and then drops off to zero.

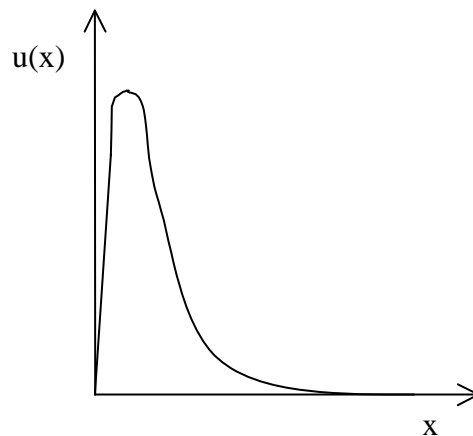


Figure 2.1: *Bond stress versus distance from loaded end*

Researchers have attempted to measure the actual distribution of bond and bar stresses along the length of the embedded bar. A common method of doing this is to place strain gauges on the bar prior to pouring concrete, and to use the variation of measured strains along the bar to calculate the corresponding variation of bond stress. However, these strain gauges can disturb the bond between the steel and concrete at these points, causing inaccurate results.

Some researchers (Mains 1951) have tried to circumvent this problem by saw-cutting deformed steel bars in half along the longitudinal axis and installing strain gauges in the center of the cross-section. This technique allows the

measurement of strains in deformed reinforcement without disturbing bond on the outside surface of the bar. It is not practical to install strain gauges in the interior of seven-wire prestressing strands, however.

The bond characteristics of prestressing strand are usually given in terms of an average bond strength over a known length. Limited work has been reported on the actual distribution of bond stress along the length of a strand.

2.2 PREVIOUS TECHNIQUES FOR CONDUCTING PULLOUT TESTS OF BARS AND STRANDS

Techniques used by researchers to conduct pullout tests of bars and strands are reviewed, and relevant examples are discussed in this section.

2.2.1 Stocker and Sozen (1970)

Stocker and Sozen conducted a very comprehensive testing program to develop a fundamental understanding of bond between prestressing strand and concrete, and to establish the effects of various parameters on the anchorage length for strand. The parameters investigated were strand diameter, concrete strength, shrinkage, settlement of concrete, confining pressure, and time.

While most strand-pullout tests were performed on specimens with a bonded length of 1 in. (25.4 mm), bonded lengths for some specimens ranged up to 20 in. (0.51 m). Relationships between bond force and slip were found that were nearly independent of the bonded length of strand. The writers discussed the mechanisms of bond between strand and concrete and reported that maximum bond strength was linearly proportional to externally applied lateral pressure.

The investigation of the effect of confining pressure was particularly relevant to this thesis (Section 1.4). The test setup for this thesis (Section 3.3) was intended to subject the test specimens to conditions similar to those present in service in a solid end block of a precast, prestressed concrete box girder.

2.2.2 Salmons and McCrate (1977)

Salmons and McCrate tested untensioned, bonded prestressing strand in concrete. All strands were composed of twisted wires. Some strands were bent to form hooks, while others were straight. Straight strands were tested in rectangular specimens that were supported in the test frame against translating or rotating in any direction. Results were reported in terms of steel stress at the loaded end, versus displacement of the strands at the loaded end.

Those writers noted that the strands tended to unscrew as they were pulled out of the concrete. In contrast to the pullout behavior of deformed reinforcement, no mechanical resistance was present. As the strand continued to elongate, however, the pitch of the strand changed as the end rotated within the helical grooves in the concrete. As explained by the writers: “This effect causes increased normal and frictional forces which more than compensates (sic) for the effect of radian (sic) contraction associated with the strand at elongation.” Those writers concluded, in essence, that axial elastic elongation of the strand is not as important as the pitch of the seven-wire strand to the post-slip load-displacement response.

The testing program developed for this thesis (Chapter 3) involves strand-pullout tests of bonded prestressing strand in concrete. The behavior observed in those tests is compared with the observations made by Salmons and McCrate (Section 5.4).

2.2.3 Abrishami and Mitchell (1993)

Abrishami and Mitchell introduced a method to determine the relationship between bond stress and slip of prestressing strand along the transfer length and flexural bond length, using tensioned pullout tests instead of beam tests. A length of strand was pretensioned, and concrete was cast in a cylindrical shape around

the tensioned strand. After curing, the concrete was held in a test frame, and bond stress was created along the strand by reducing the strand tension at one end. At each load increment, the relative displacement between the strand and the concrete was recorded at each end of the specimen.

Abrishami and Mitchell studied bond characteristics over the transfer and flexural bond lengths of strands in prestressed beams. The testing program for this thesis (Chapter 3) does not classify the specimen length over which strands are tested as transfer or flexural bond length; the procedures used by Abrishami and Mitchell to measure and compute bond strength, however, are useful because they are similar to the procedures used in this thesis (Section 5.2). Load-displacement relationships reported by those writers are compared to experimental data obtained in this study (Section 4.1).

2.2.4 Rose and Russell (1997)

Rose and Russell investigated three different types of tests of bond between prestressing strand and concrete: simple pullout tests, in which the strand is only embedded in the concrete specimen (no prestress), and is subsequently pulled out; tensioned pullout tests, in which the strand is tensioned prior to pouring concrete, and is subsequently pulled out; and “measured end slips,” in which displacement of strands is measured at the ends of prestressed beam specimens, after release of the strands. The tensioned pullout tests were patterned after those performed by Abrishami and Mitchell (1993). The purpose of Rose and Russell’s tests was to evaluate each test method and to recommend a reliable and repeatable standardized method for studying bond characteristics of prestressing strands. The results of each test method were compared to the measured transfer lengths of companion specimens to determine which of the

three correlated most strongly with bond between prestressing strand and concrete.

When the ends of pretensioned strands in concrete are released, strand diameter increases due to Poisson's effect. The resulting wedging action, known as "Hoyer's effect," increases the bond between those strands and the surrounding concrete. Tensioned pullout tests involve Hoyer's effect, while simple pullout tests do not.

Based on a comparison of results from each type of test, the writers concluded that simple pullout tests are not completely adequate for evaluating bond between concrete and prestressing strand. The complexity of tensioned pullout tests, however, makes them problematic. The writers recommended measured end slips as a more reliable method than the other two options for assessing the bond behavior of strands in concrete.

The writers' discussion of their simple pullout tests was particularly useful in the development of the strand-pullout test setup (Section 3.3). Load-displacement relationships reported by Rose and Russell are compared to experimental data obtained in this thesis (Section 4.1). Because test specimens for this study were taken from full-size members and not constructed in the laboratory, the writers' recommendation of measuring strand end-displacements in beams was not particularly relevant to this study.

2.3 GAPS IN KNOWLEDGE REGARDING PULLOUT OF STRANDS

The studies discussed above of bond between prestressing strand and concrete and the load-displacement response of strands in pullout tests have focused on specimens with undamaged concrete and with no applied normal pressure. Some of the Stocker and Sozen pullout tests were tested with a confining lateral pressure. The strand-pullout specimens in Study 1857 were

taken from prestressed box girders experiencing premature concrete deterioration. It is known that cracking and expansion of cracks occurs inside the concrete, and it is logical to predict that premature concrete deterioration may separate bonded prestressing strands from the surrounding concrete.

As part of the overall structural assessment of bridges displaying premature concrete deterioration, three gaps in knowledge remain:

1. How does premature concrete deterioration affect bond between prestressing strands and concrete?
2. Can external visible damage to the affected element be correlated with a reduction in bond strength?
3. What effect does a transverse clamping load have on the load-displacement response of a prestressing strand in concrete with premature concrete deterioration?

Tests performed as part of TxDOT Study 1857 are used to fill those gaps. Results and observations from the testing program will be used to evaluate the overall structural integrity of full-scale specimens. These evaluations may be applied to existing in-service structures displaying similar damage patterns.

Future researchers may be able to apply conclusions about the load-displacement response of strands in deteriorated concrete to strands embedded in undamaged concrete. Correlations between the degree of external damage and the changes in pullout response can be used by engineers to estimate the decrease in structural capacity of prestressed concrete girders with premature concrete deterioration.

CHAPTER 3

Development of Test Program

3.1 OBJECTIVES AND PLAN

The testing program was designed to investigate the effect of premature concrete deterioration on the bond between prestressing strands and concrete. Strand-pullout tests were performed to determine the average bond strength and to examine the load-displacement behavior of strands as they are pulled out of concrete. Changes in this pullout response of strands were correlated with different indices of external damage to the concrete.

3.2 TEST SPECIMENS

Specimens for the strand pullout tests were taken from full-size members and prepared for laboratory tests. The pre-existing conditions for each specimen were detailed and documented. This section describes the procedure for preparation and testing of the specimens.

3.2.1 Box Girders

Pullout tests were performed on slice specimens cut from the prestressed box girders investigated earlier in this study by Boenig (2000) and Roche (2001). In summary, four prestressed concrete box girders, fabricated at Heldenfels Brothers, Inc. in San Marcos, Texas between June and September 1991, were brought to Ferguson Structural Engineering Laboratory (FSEL) at The University of Texas at Austin (UT Austin) for examination and assessment. The strand pullout tests were performed on specimens cut from three of those girders.

The girders were reinforced with six 3/4-inch (19.1 mm) ASTM A615 Grade 60 (420 MPa) bars and 30 1/2-inch (12.7 mm) diameter, 270 ksi (1,862 MPa) strands. The specified design compressive strength of the concrete was 6,000 psi (41 MPa).

Figure 3.1 shows the side view and size of those girders, and Figure 3.2 shows their cross-sectional dimensions.

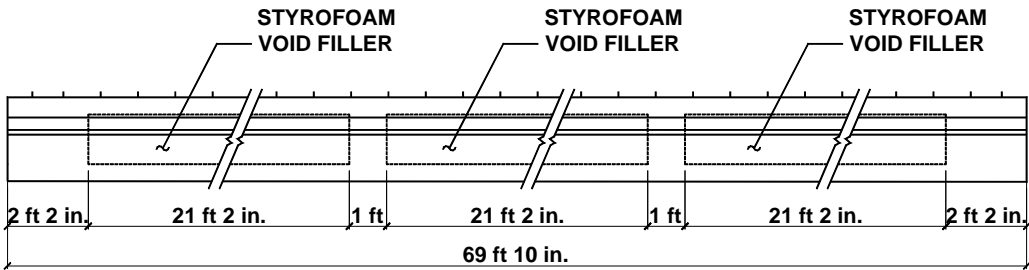
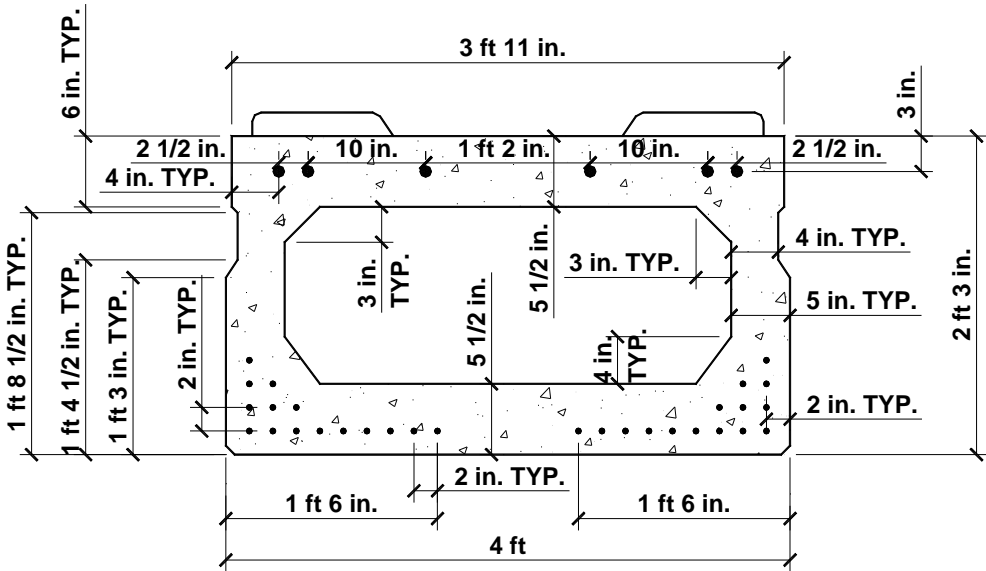


Figure 3.1: Side view of box girders



NOTE: MANY DIMENSIONS ARE APPROXIMATE

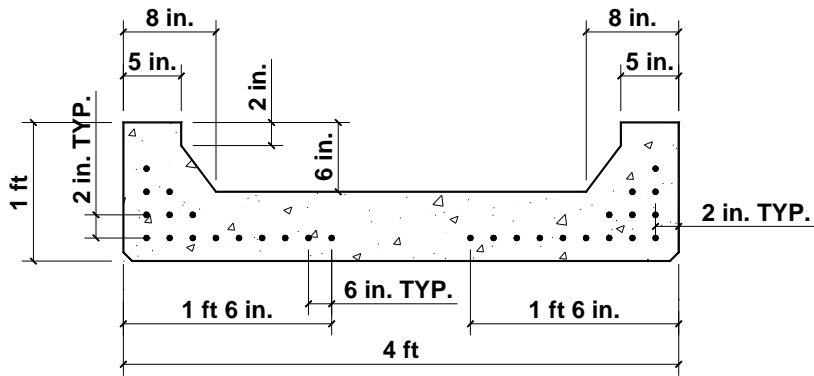
Figure 3.2: Cross-section of box girders used for strand-pullout tests

The box girders were identified as BG1, BG2, BG3, and BG4. Additionally, the suffix “N” or “S” indicated the girder’s north half or south half. Generally, BG2 and BG3 were more damaged than BG1, and BG4 featured the most extensive damage and was in worse condition than the other three box girders. The condition of the box girders at the time of arrival at FSEL is given in Boenig (2000). This thesis specifically describes the damage found in the individual specimens taken from the girders.

3.2.2 Cutting of Slice Specimens

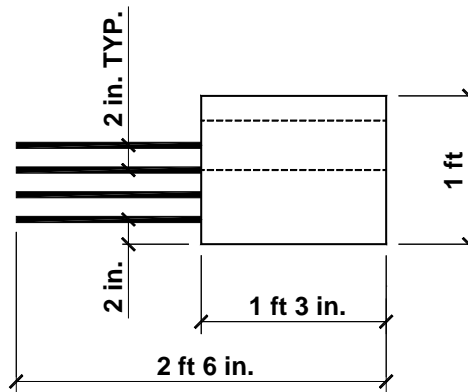
A total of four slices were cut from Girders BG1S, BG2N, and BG4S for use as specimens for strand pullout tests. One slice each was cut from Girder BG1S and Girder BG2N, and two slices were cut from Girder BG4S. The slices were cut using specialized water-cutting equipment using high-pressure cutting jets and water containing garnet abrasive powder.

The approximate cross-sectional dimensions of a slice are shown in Figure 3.3. The slices were cut with approximately a 30 in. (0.76 m) length to provide a sufficient length of strand in concrete (approximately 12 in. (0.305 m) to 15 in. (0.381 m)) to develop bond stress for testing. Figure 3.4 shows the side view of a typical slice taken from a box girder.



NOTE: MANY DIMENSIONS ARE APPROXIMATE

Figure 3.3: Cross-section of typical slice taken from box girder



NOTE: MANY DIMENSIONS ARE APPROXIMATE

Figure 3.4: Side view of typical slice taken from box girder

Some exposed length of strand was needed to pull the strands and mount measurement devices. Roughly half of the concrete was blasted off with water so that 12 in. (0.31 m) to 15 in. (0.38 m) of prestressing strand remained bonded to concrete, leaving the rest exposed. The excess concrete was removed with high-pressure water instead of a jackhammer because the vibrations from a jackhammer could have introduced local cracking in the concrete surrounding the

strands. Additionally, it would have been difficult to distinguish between pre-existing damage and jackhammer-induced damage.

Figure 3.5 and Figure 3.6 show an example of a slice cut from the girders.



Figure 3.5: *Front view of slice cut from Girder BG2N*



Figure 3.6: *Back view of slice cut from Girder BG2N*

It is likely that the strands in the slice specimens retained some of the prestress that was present in the box girders. For this reason, strand-pullout tests performed in this study are not simple pullout tests, as described by Rose and Russell (1997). The tests described in this thesis are more similar to the tensioned

tests described by those writers; pullout behavior is likely influenced somewhat by Hoyer's effect (Section 2.2.4).

3.2.3 Slice and Strand Nomenclature

The slices were given the same name as the girder from which they were cut. Since two slices were cut from Girder BG4S, however, those two specimens gained an arbitrarily assigned suffix of "1" or "2" in order to distinguish between them.

The face of the slice containing the exposed strands is termed as the front face or the front of the slice. The opposite side, characterized by a relatively smooth and flat surface, is termed as the back face. The front of the slice is associated with the loaded end of the strand during strand tests, and the back face is associated with the free end.

The strands were numbered based on the nomenclature specified on a TxDOT fabrication drawing for prestressed concrete box beams with non-standard spans (Appendix B). Each strand was labeled by its position in the cross section of the girder; an "L" or "R" was added to the number to indicate whether the strand was in the left strand group or the right strand group. Left and right were defined with respect to the front face of the slice (Figure 3.7).

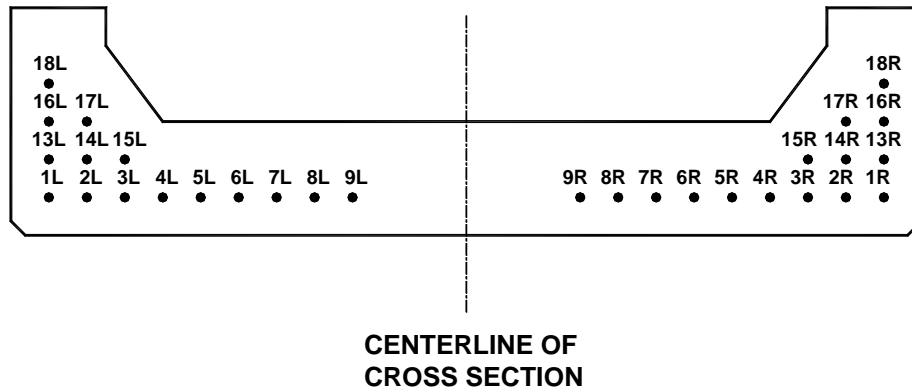


Figure 3.7: Strand numbering system

The strand numbering skips from 9 to 13 because Spaces 10, 11, and 12 are available for strands but are unfilled.

The strands were divided into four principal groups: left cluster strands (1L-3L, 13L-15L, 16L-17L, 18L); left middle strands (4L-9L); right middle strands (4R-9R); and right cluster strands (1R-3R, 13R-15R, 15R-17R, 18R).

3.2.4 Location of Slices in Girders

The most heavily damaged regions for each of the box girders were the solid end blocks. This is partly due to the large amount of heat produced in these regions during hydration. Field observations have shown that the ends of girders are most likely to be exposed to water (for example, at expansion joints or abutments). Water is known to exacerbate premature concrete deterioration in bridge girders (Boenig 2000). Because the ends of the girders contained the most damage and are most susceptible to further damage in the field, they are the critical sections for bond failure of prestressing strands. Ideally, slices for the strand-pullout tests would have been cut from the solid end blocks; the concrete there was in such poor condition, however, that cutting was not practical in these regions.

Alternatively, locations in the girders were chosen that would provide a representative sample of the premature degradation. Slices were cut in the middle of the girders at locations displaying typical damage, and the slices were later prepared to facilitate pullout tests intended to replicate service conditions in a solid end block (Section 3.2.6). Figures 3.8 through 3.10 indicate the location of each slice in its respective girder.

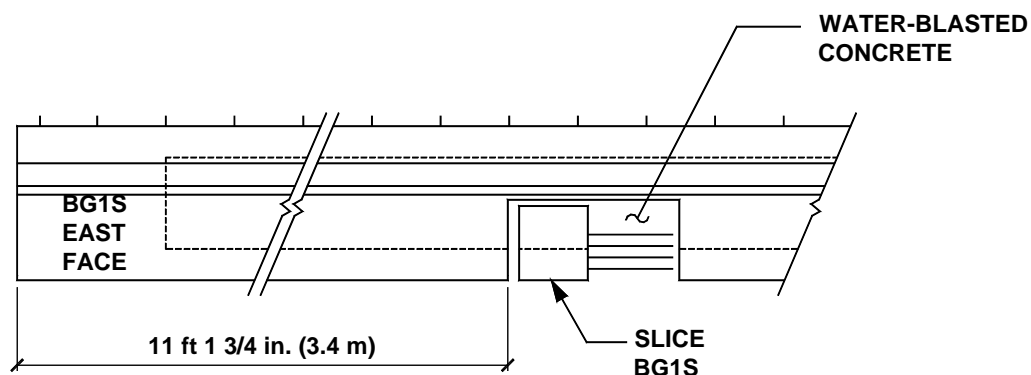


Figure 3.8: Location of slice from Girder BG1S

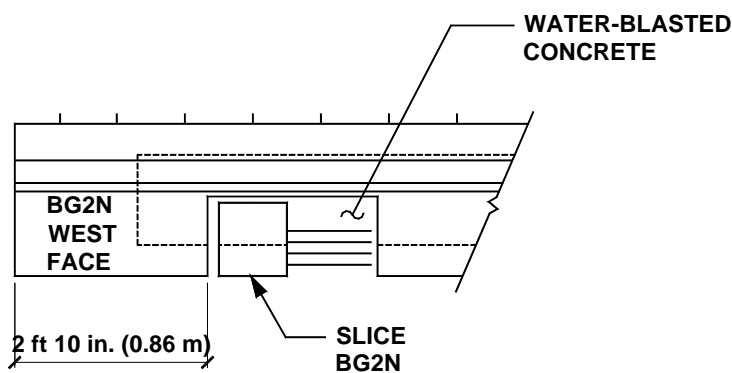


Figure 3.9: Location of slice from Girder BG2N

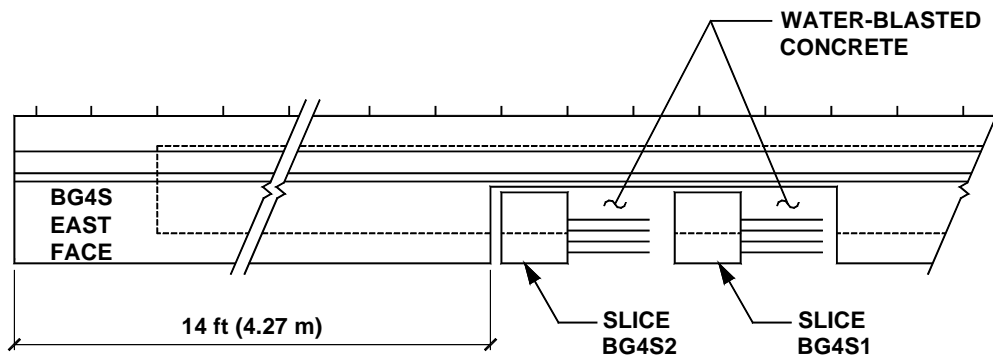


Figure 3.10: Location of slices from Girder BG4S

3.2.5 Pre-existing Condition of Slices

Each of the specimens displayed varying degrees of damage. The pre-existing condition was important in correlating visible damage due to premature concrete deterioration and the pullout response of the strands.

Slice BG1S

The overall condition of Slice BG1S was good. The concrete had some minor cracks on all surfaces, but in general, damage was less than the other three specimens. Several cracks existed on the front face, but these were difficult to measure because the concrete surface was roughened due to water blasting.

The most significant crack on Slice BG1S was a medium-wide crack (about 0.5 mm) on the bottom face corresponding with the longitudinal direction of the box girders. That crack extended into the cross-section to the void and propagated through Strand 9L in the back face (Figure 3.11).



Figure 3.11: Crack through Strand 9L in back face of Slice BG1S

The left side of Slice BG1S was the most damaged surface of the specimen. Several cracks extended throughout the entire length of the slice parallel to the longitudinal axis of the girder. Figure 3.12 shows the left face of Slice BG1S, which also displayed some spalling from the water-blasting process.

Figure 3.13 shows a close-up of typical damage to the concrete in the left inside corner. Cracking through the aggregate was typical of the damage observed in the specimens.



Figure 3.12: Cracking on left face of Slice BG1S



Figure 3.13: Cracks at left inner corner of Slice BG1S

Slice BG2N

Slice BG2N contained many cracks on each of its side faces and some longitudinal cracks on the right half of its bottom face. Very few cracks were evident on the left half of the bottom face.

Wide cracks (0.64 mm and wider) existed on the left and right side faces. Figure 3.14 shows the right web of Slice BG2N in which a wide crack is present. Also, longitudinal cracks aligned with the bottom of the void can be seen (Boenig 2000).



Figure 3.14: Cracking on right face of Slice BG2N

Large cracks were apparent in the back face of the slice, as shown in Figure 3.15. Very wide cracks propagated from the inner corners of the void to the corner strands (Strand 15L and Strand 15R). These cracks continued in the plane of the cross section to the adjacent strands. As shown in Figure 3.15, concrete was no longer in contact with a portion of Strand 15R. The photo also shows that the crack extended through the remaining Styrofoam void filler.

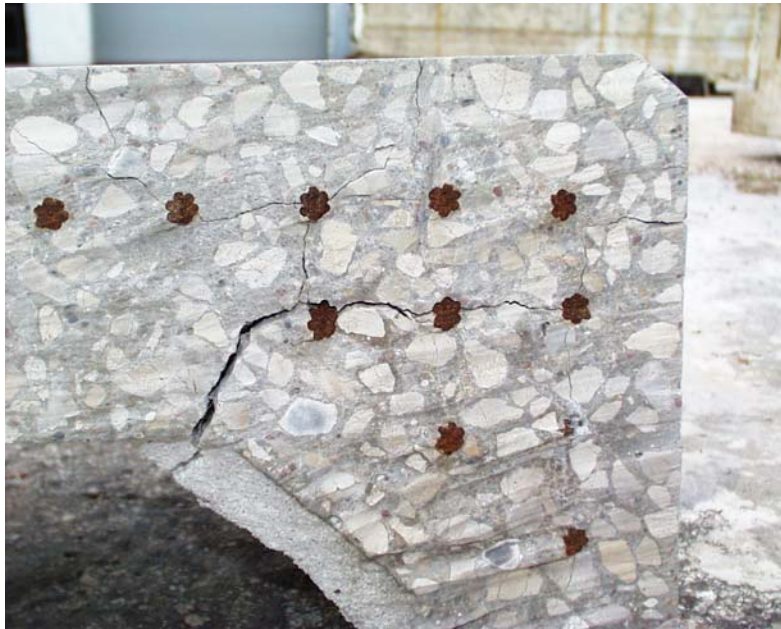


Figure 3.15: Large cracks in back face of Slice BG2N

Narrow longitudinal cracks were present on the bottom face (Figure 3.16).

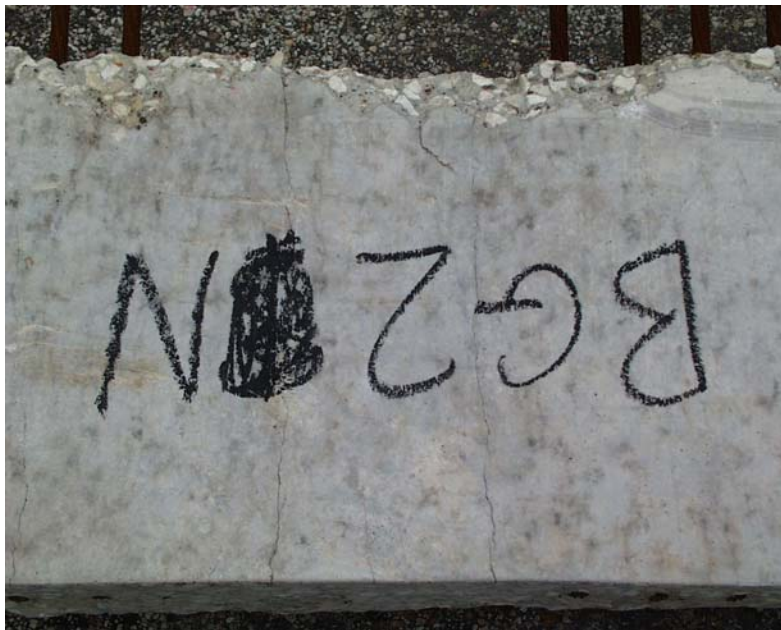


Figure 3.16: Cracking on middle of bottom face of Slice BG2N

Slice BG4S1

The bottom face of Slice BG4S1 had extensive longitudinal cracking. Most of the cracks were narrow (0.05 mm - 0.13 mm), but some were wider. Figure 3.17 shows the left side of the bottom surface of Slice BG4S1.



Figure 3.17: Cracking on bottom face of Slice BG4S1

The right web surface was lightly damaged compared to the bottom face. On the other hand, the left face contained several cracks, some of them of medium width (0.18 mm – 0.51 mm). Figure 3.18 shows the visible damage on the left web face.



Figure 3.18: Cracking on left face of Slice BG4S1

Cracking in the cross-section, while not nearly as bad as for Slice BG2N, was still present. Figure 3.19 shows a typical example of damage in the concrete in the back face of Slice BG4S1. Separation is seen between the strands and the surrounding concrete.



Figure 3.19: Damage to cross-section of Slice BG4S1 (back face)

Slice BG4S2

Damage in Slice BG4S2 was similar to the damage present in Slice BG4S1 since both slices were cut at the same location in Girder BG4S. Crack patterns were similar, but the degree of damage was slightly less in Slice BG4S2. Figure 3.20 shows significant cracking between prestressing strands in the left side of the back face, and Figure 3.21 shows more typical longitudinal cracks on the bottom face.



Figure 3.20: Cracking in back face of Slice BG4S2



Figure 3.21: Cracking on bottom face of Slice BG4S2

Figure 3.22 shows a good example of cracking in the cross section that can be seen from the front face. Both the left and right inside corners of the void had cracks extending along the entire width of the specimen. Figure 3.22 shows the front view of the right corner. This is the same crack shown in Figure 3.20.



Figure 3.22: Front view of right inside corner of Slice BG4S2

3.2.6 Rationale for Slice Preparation

To perform pullout tests on the prestressing strands, the concrete box girder slices were prepared. Because a hydraulic ram was used to pull the strands, a flat bearing surface was needed on the face of the slice with the prestressing strands exposed. The concrete at this location had been blasted away with a high-pressure water jet, leaving the surface rough (Figure 3.5). This rough surface was smoothed by a layer of high-strength non-shrink grout.

The pullout tests were intended to mimic service conditions in the solid end blocks of the box girders. This was accomplished by applying a transverse

clamping load to the specimen while strands were pulled and tested. A flat, level bearing surface was needed on the webs of the girder slice. The surfaces were smoothed with a layer of gypsum plaster (Hydrostone) (Figure 3.23).

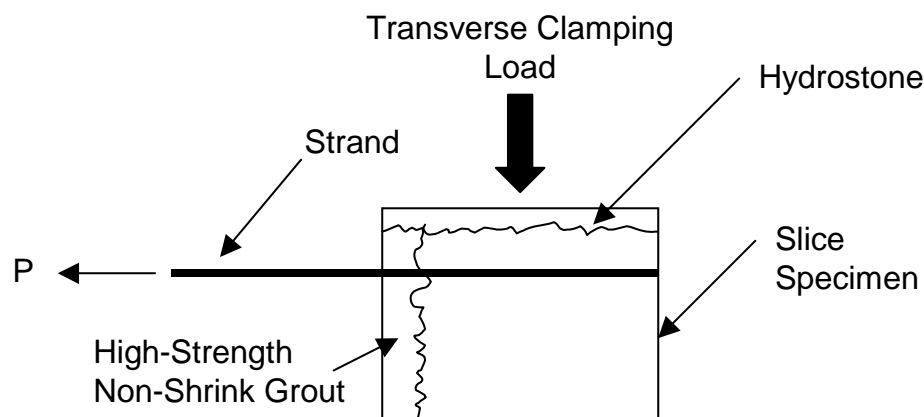


Figure 3.23: Test setup to mimic service conditions in a solid end block

The concrete in these girder slices was prematurely deteriorated due to Alkali-Silica Reaction (ASR) and Delayed Ettringite Formation (DEF). Many cracks existed in the slices, both close to and far away from the strands. Pouring grout or Hydrostone directly onto the cracked surfaces could have influenced the test results, as the capping materials would probably have seeped into the cracks. This problem was averted by coating the surfaces of the slices with clear silicone sealant before pouring any grout or Hydrostone.

3.2.7 Slice Preparation Procedure

Slices were prepared as follows:

1. Cut selected strands with plasma torch. The strands to be tested had to be identified before pouring any grout onto the slices. Those strands immediately adjacent to the strands earmarked for testing were cut to make room for the testing equipment. Fifteen out of thirty strands could

be tested in each slice. A plasma torch was used because it can quickly cut high-strength prestressing strand without heating it significantly.

When preparing the first specimen for testing (Slice BG2N), excess strands were not cut before pouring the topping material. Instead, strands were cut as needed with a plasma torch while the specimen was set in the test machine. The typical pullout behavior of the strands was not known in the early stages of the test program, so a cautious approach was followed. After several tests had been completed, it was determined that pulling of prestressed strands did not damage surrounding concrete. To speed up the slice preparation and strand testing, excess strands were then cut prior to sealing the slices and pouring capping material.

2. Wrap remaining strands. The strands that were not cut were wrapped with clear plastic wrap near the slice surface to prevent bonding between the capping material and strands. Bond between the capping material and strands could have influenced the pullout test results.
3. Seal strand face of slice. The slice surfaces containing the exposed strands were sealed with clear silicone to prevent any grout or Hydrostone from seeping into the cracks and possibly bonding with the prestressing strands. The silicone was applied to the entire surface and was allowed to dry for 24 hours before casting the grout or Hydrostone.
4. Construct cardboard form around slice perimeter. Cardboard was a simple and effective material for formwork. The form was bound tightly around the specimen with steel bands. The edges of the form were sealed with clear silicone to prevent leaks when pouring the capping material. Figure 3.24 shows an example of the cardboard formwork used for the strand faces.



Figure 3.24: Cardboard formwork used for front face

5. Pour capping material onto face containing exposed strands. High-strength non-shrink grout was used as the capping material on the strand face. Hydrostone was used on the first specimen, but it proved to be susceptible to cracking and spalling on the edges. It also deformed under the bearing pressure of the ram as the strands were pulled. The grout provided a much more rigid bearing surface.
6. Seal slice web sections and construct formwork for top bearing surfaces. Figure 3.25 and Figure 3.26 show examples of the formwork for the web sections.



Figure 3.25: Formwork for web sections



Figure 3.26: Cardboard formwork for top of web

7. Pour capping material onto web sections. Hydrostone was used as the capping material on the web sections for Slices BG1S, BG2N, and BG4S2, and grout was used for Slice BG4S1. Figure 3.27 shows the level bearing surface on top of a slice web section.



Figure 3.27 Level Hydrostone bearing surface on top of web section

3.3 TEST SETUP AND PROCEDURE

The test setup was designed to subject the slice specimen to conditions similar to those found in a solid end block. The procedure developed to test the pullout response of the strands is detailed in this section. While the strand-pullout tests are more similar to tensioned pullout tests (Section 3.2.2), the test setup is more similar to the simple pullout tests performed by Rose and Russell (1997). Those writers constructed their pullout test specimens in the laboratory; that was not possible in the testing program described in this thesis.

3.3.1 Test Setup

The slice specimens were tested at FSEL in a screw-type universal testing machine with a 600,000 lb (2,700 kN) capacity and thick steel bed. A transverse clamping load was applied to the slice specimen with the machine while strands were pulled out with a hydraulic ram and hand pump. Figure 3.28 shows a schematic drawing of the test setup, and Figure 3.29 shows a slice specimen in the loading machine.

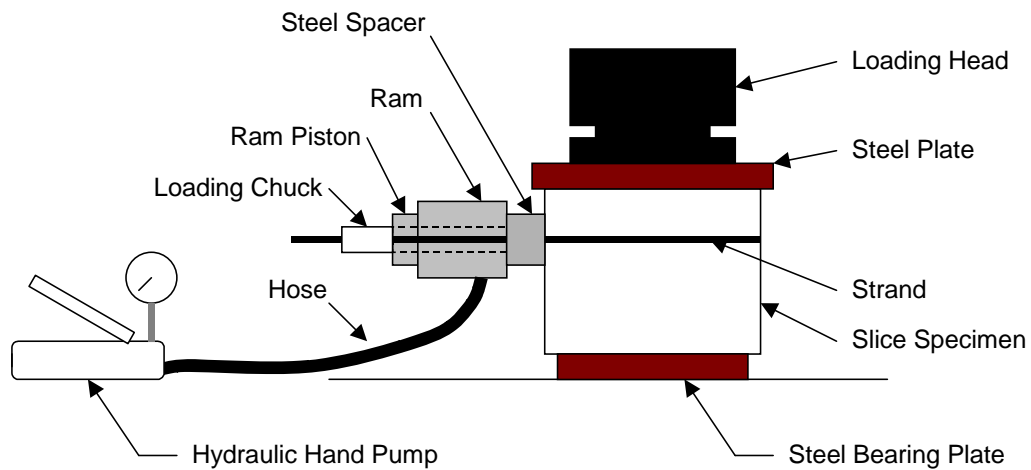


Figure 3.28: Schematic drawing of test setup



Figure 3.29: Slice specimen in loading machine for strand-pullout tests

Slice specimens were set in place so that a clamping load would be applied to the group of strands being tested. A hemispherical loading head was used to apply the clamping load. There were four different positions in the testing machine for each slice specimen so that the loading head would compress the proper area: center of the left web to test the left cluster strands; above the left middle strands; above the right middle strands; and center of the right web to test the right cluster strands. Figure 3.30 shows a schematic diagram of the four testing positions for each specimen.

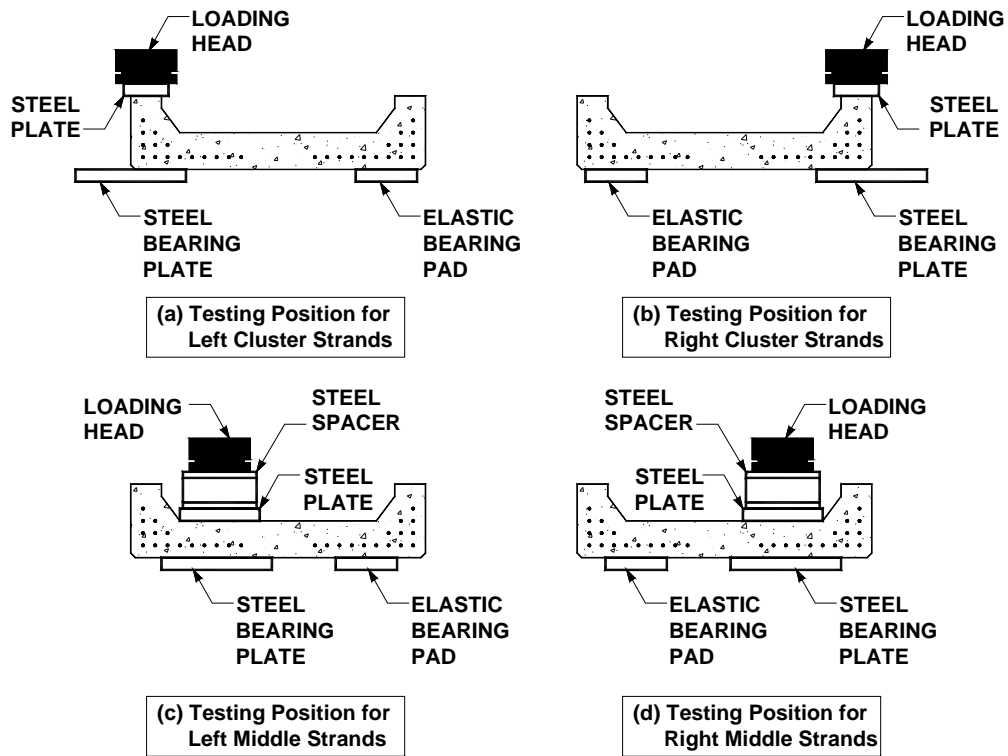


Figure 3.30: Testing positions for specimens

The specimens were simply supported by a steel bearing plate and an elastic bearing pad. The steel bearing plate was placed under the loaded portion under the test machine loading head (Figure 3.31). Hydrostone was poured between the steel plate and the specimen to ensure a solid connection with no voids. The other end of the specimen was not grouted to the elastic bearing pad so that vertical motion was not restrained. This was done to avoid cracking of the specimen under load.

A 2 in. (51 mm) thick steel bearing plate was placed between the loading head and the specimen in order to ensure uniform bearing stress (Figure 3.31). For the middle strands, a stiff steel spacer was used (Figure 3.32). Otherwise, the machine crosshead would have crushed the specimen.



Figure 3.31: Steel plate between loading head and slice specimen



Figure 3.32: Steel spacer and plate used for middle strands

The strands were pulled with a 30 kip (133 kN) center-hole hydraulic ram and a reusable, three-piece 0.5 in. (12.7 mm) diameter loading chuck. The chuck jaws were greased with release compound prior to each test. A 2 in. (51 mm) thick steel spacer was placed between the ram body and the face of the specimen to ensure uniform compressive stress on the specimen. An elastic pad was used between the steel spacer and the face of the specimen. A small steel washer was used between the ram piston and loading chuck to make sure that the piston pushed on the chuck barrel, because the diameter of the barrel was close to the diameter of the center hole of the ram.

3.3.2 Instrumentation and Data Acquisition

Displacement of the loaded end of the strand was measured with two 6 in. (0.15 m), 10 volt linear potentiometers. A custom-made aluminum clamp connected the potentiometers to the strand being pulled, and the spring-loaded shafts of the potentiometers were extended against the ram body (Figure 3.33).



Figure 3.33: Linear potentiometers at loaded end

The average of the readings from the two potentiometers was taken to be the displacement at the loaded end.

In early tests, 2 in. (51 mm) potentiometers were used at the loaded end, but they were replaced to allow for more displacement. Also, a longer loading chuck barrel was used which required longer potentiometer shafts to record displacement data. The pressure in the ram was recorded with a pressure transducer, and was also monitored using a dial gauge (Figure 3.29). Rigid-body motion (slip) of the strand was measured at the free end with a 6 in. (0.15 m) linear potentiometer affixed to the back of the strand with epoxy (Figure 3.34). An extender rod was used to make it easier for the potentiometer shaft to follow the strand through the specimen, and to allow for a greater range of measurement. In the first few tests, a 2 in. (51 mm) potentiometer was used to measure slip at the free end before switching to a 6 in. (0.15 m) potentiometer. Various methods of attaching the potentiometer shafts to the back of the strand were attempted before deciding on 5-minute epoxy with threaded spacers.



Figure 3.34: Linear potentiometer attached to back of strand

A 2 in. (51 mm) linear potentiometer was placed on the back of the specimen to measure movement of the specimen during testing. The difference between the readings of the two potentiometers on the back of the specimen was the relative slip of the strand. Figure 3.35 shows the instrumentation setup on the back of a specimen during testing.



Figure 3.35: Linear potentiometers recording relative movement of strand at free end

3.4 STRAND-PULLOUT TEST PROCEDURE

The procedure for setting up and running a strand-pullout test was:

1. Increase pressure in ram a small amount (approximately 50-100 psi (345-689 kPa)) to stabilize it for setup.
2. Glue potentiometer shaft to free end of strand. Remove excess epoxy after it hardens to prevent the shaft from sticking to the specimen and not traveling with the strand.
3. Clamp potentiometers to loaded end of strand. Zero all channels with the data acquisition system.
4. Apply a 25 kip (111 kN) transverse clamping load on the specimen with the testing machine.

5. Increase pressure in ram to pull strand. Pull strand until it slips at a constant load or until the pullout force is decreasing as Δ increases.
6. Decrease pressure in ram until it is very close to the small amount of pressure utilized in Step 1. Since the data acquisition channel was zeroed in Step 3, the measured pressure in the ram will essentially be zero.
7. Increase clamping load by 25 kips (111 kN).
8. Repeat Steps 5-7. The highest clamping load used for the tests is 125 kips (556 kN). Exceeding this clamping load risks cracking the specimen.
9. Terminate the strand pullout test when the ram piston has extended its full stroke or when the potentiometers at the loaded end have extended fully and are no longer in contact with the ram body.

3.5 CORRELATION WITH VISUAL DAMAGE

Part of the test program included quantifying visible damage on the specimens and correlating degree of damage with the effect on bond between the prestressing strands and concrete using the method introduced by Boenig (2000) earlier in this study. Damage indices were computed for representative squares drawn on the exterior surfaces of each specimen.

The damage index (DI) was calculated as follows:

$$DI = \sum w^2 l \quad (3-1)$$

where w is the crack width in thousandths of an inch, and l is the crack length in inches (Boenig 2000).

This damage index is based on cracks measured in a 12 in. (0.31 m) by 12 in. (0.31 m) square. Squares were drawn on the exterior faces of each specimen

as shown in Figure 3.36 through Figure 3.39. Where possible, 12 in. (0.31 m) by 12 in. (0.31 m) squares were drawn, but in several cases, there was not sufficient surface area on the face of the slice to draw a large enough square for crack measurement. To correct for this, the computed damage index was multiplied by the appropriate scale factor required to match 144 in.² (0.093 m²) of area. For example, the damage index for a 10 in. (0.25 m) by 10 in. (0.25 m) square was multiplied by 1.44. In some cases, rectangles with an equivalent area of 144 in.² (0.093 m²) were drawn (Figure 3.36).



Figure 3.36: *Representative areas for bottom face damage indices*



Figure 3.37: Representative square for left side damage index



Figure 3.38: Representative square for right side damage index

Five different damage indices for each specimen were computed and tabulated for correlation with test results.

CHAPTER 4

Test Results

Sixty-four strand-pullout tests, described in Chapter 3, were performed on sixty strands from the slice specimens. The results and observations made during the tests are presented in this chapter, along with damage indices for the slice specimens.

4.1 PRESENTATION OF DATA

Strand-pullout tests were conducted with an initial transverse clamping load of 25 kips (111 kN), which was increased in 25-kip (111 kN) increments to a maximum value of 125 kips (556 kN). Each value of clamping load was associated with a separate test segment, or stage. The clamping load history for the strand-pullout tests is shown schematically in Figure 4.1. In that figure, the stage when the transverse clamping load was 75 kips (334 kN) is labeled and marked by an arrow.

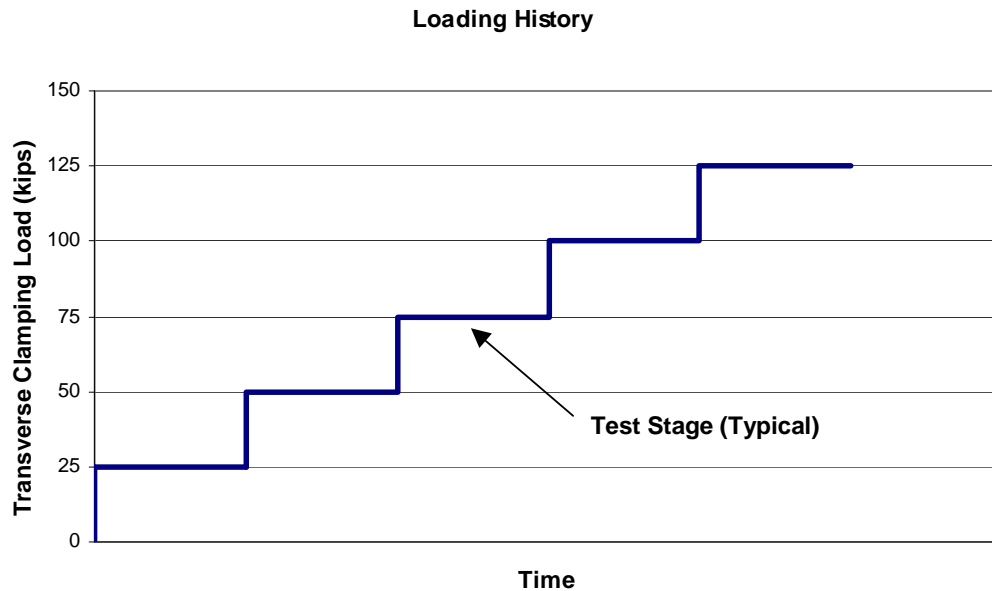


Figure 4.1: Loading history for strand-pullout tests

In each stage, the pressure in the ram was increased so that axial tension was applied on the strand. In this thesis, slip is defined as rigid-body motion of the strand with respect to the surrounding concrete. The start of slip was denoted by the first observed displacement at the free end of the loaded strand.

During the first stage (the lowest level of clamping force) of the test, when the transverse clamping load N was 25 kips (111 kN), some bond was present between the strands and concrete. Therefore, identifying the load associated with the start of slip (first slip) in that first stage was key to determining the average bond strength of the strand. First slip corresponded to the loss of bond along the entire embedded length of the strand.

It was also important to identify the resumption of slip of the strand in later stages of the test. Since first slip of the strand had already occurred, it was assumed that no bond remained between the strand and concrete.

Figure 4.2 shows a typical load-displacement curve recorded during a strand-pullout test. Key points are identified, and the presentation of test results is explained.

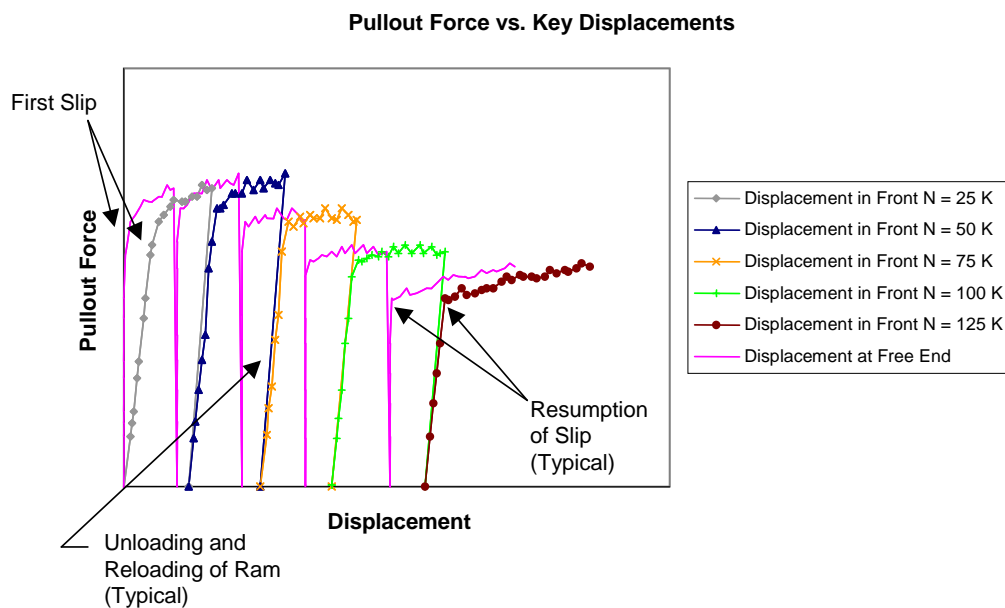


Figure 4.2: *Typical load-displacement response from strand-pullout tests*

Pullout force was determined by multiplying the recorded pressure in the ram by the cross-sectional area of the ram. The linear potentiometers described in Section 3.3.2 were used to measure displacement of the strand at the loaded end and at the free end. A range of 0.005 in. (0.13 mm) to 0.01 in. (0.25 mm) was determined to be the sensitivity of the instruments. Readings lower than this were not considered significant.

Different line types for the “Displacement in Front” curves indicate different test stages. The curve “Displacement at Free End” is used to identify the start or resumption of slip in all stages. The ram was unloaded between stages (Section 3.4), and the linear portions of each “Displacement in Front” curve show those unloading and reloading cycles.

Before first slip, there is no recorded displacement at the free end of the loaded strand. After first slip, the displacement curves at the loaded end and free end have the same values for Pullout Force and are separated by a constant difference, except for the unloading and reloading cycles (Figure 4.2). This observed behavior illustrates that the loaded strand is slipping with respect to the surrounding concrete. Abrishami and Mitchell (1993) and Rose and Russell (1997) reported similar load-displacement curves, which apparently verify the experimental plots presented in this thesis.

In several tests, the connection between the potentiometer shaft and the free end of the strand was not secure; in these cases the shaft did not move with the strand, and no displacement of the free end was recorded. In these cases, first slip was estimated as the point at which the load-displacement relationship for the loaded end first became nonlinear (Figure 4.3). This method of identifying first slip was verified using tests for which reliable displacement measurements had been obtained at the free end of the loaded strand, as shown above in Figure 4.2.

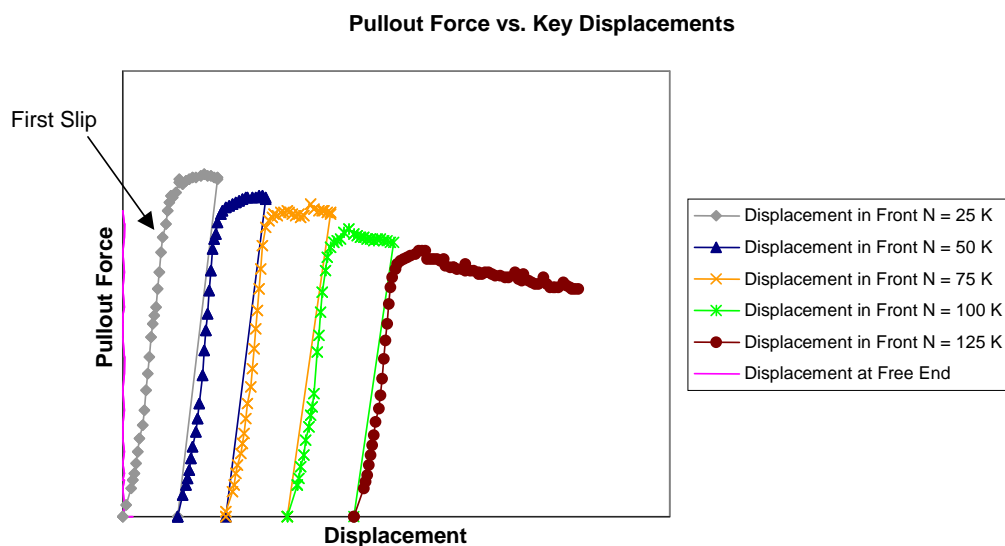


Figure 4.3: *Identifying first slip without reliable free-end data*

In other tests, the potentiometer shaft was initially connected to the free end of the strand, but became disconnected after first slip had been observed. Since bond between the strand and concrete was assumed to have been broken at first slip, for subsequent stages, the resumption of slip was taken as the point at which the load-displacement relationship for the loaded end first became nonlinear. This point usually coincided with the instant that displacement at the loaded end first exceeded the maximum loaded-end displacement recorded in the previous stage. It was simple to identify this point graphically (Figure 4.4).

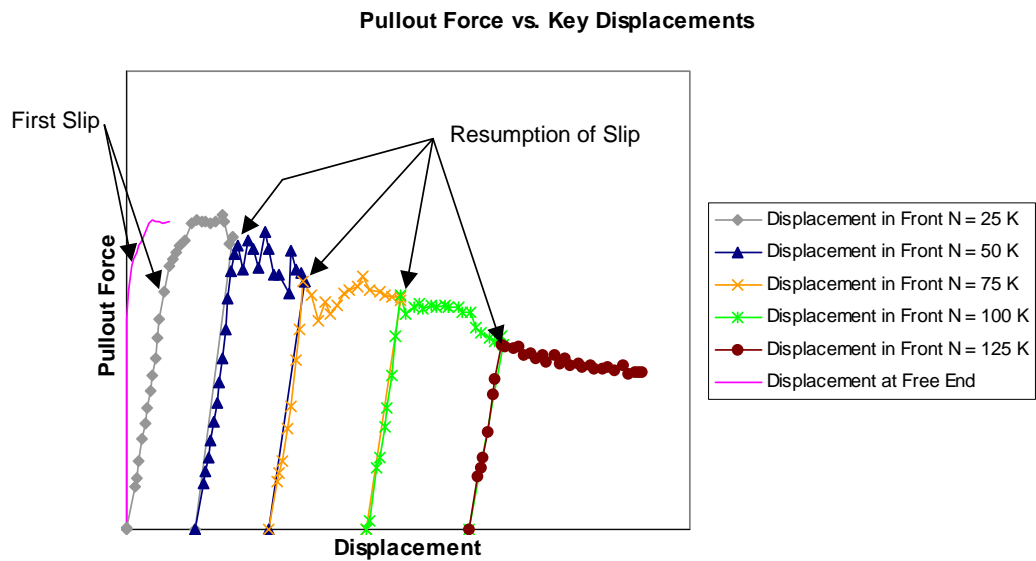


Figure 4.4: *Identifying resumption of slip without reliable free-end data*

4.2 RESULTS FROM STRAND-PULLOUT TESTS

Typical test results are presented in this section. Strand-pullout test names identify both the strand that was pulled and the slice specimen containing the strand. For example, the test name “Strand BG2N_17R” refers to Strand 17R in Slice BG2N, which was taken from Girder BG2N. Slice specimens and

individual strands were labeled according to the nomenclature described in Section 3.2.3.

The load-displacement relationship was recorded during the test and was used to compute the average bond strength for the strand. The different line types in each load-displacement plot indicate the load and displacement at the loaded end of the strand for the different levels of transverse clamping load.

Results are organized into three main groups:

1. Pullout force P did not significantly increase or decrease with increasing transverse clamping force N . Approximately 30 percent of the test results fall into this category.
2. P decreased somewhat with increasing N . Approximately 55 percent of the test results fall into this category.
3. P increased somewhat with increasing N . Approximately 15 percent of the test results fall into this category.

The data collected in 8 of the 64 strand pullout tests were not reported because of errors in the test setup mistakes or errors in data collection. In some of those tests, the capping material broke under the pressure exerted by the hydraulic ram. Load-displacement relationships recorded in the other 56 strand tests are provided in Appendix C.

Typical examples of the three different types of results are shown in this section.

4.2.1 No Significant Change in P with Increasing N

In these cases, the general behavior showed that the load required to cause slip of the strand did not significantly increase or decrease as the transverse clamping load was increased. In the later stages of the tests, the curve appeared to reach a maximum pullout load that was independent of the clamping load.

These results are in contrast to those reported by Stocker and Sozen (1970). In those tests, lateral pressure on the test specimens was applied from all sides with a hydraulic pressure chamber. In the testing program developed for this thesis, lateral pressure was applied in the form of a transverse clamping load with the testing machine (Section 3.3). One possible explanation for the apparent discrepancy in test results is the difference in test setup.

Strand BG2N_8L

Strand BG2N_8L was tested on October 25, 2001. The concrete was cracked around the strand in the back face. Cracks propagated from the strand to adjacent strands and through the surrounding aggregates (Figure 4.5). The length of BG1S_13R embedded in concrete in the specimen prior to testing was measured to be approximately 13 in. (0.33 m).



Figure 4.5: Back view of Strand BG2N_8L (right) and Strand BG2N_9L (left)

Figure 4.6 shows the load-displacement relationship recorded during the test. The pullout force in the strand is plotted on the vertical axis and is simply taken as the pressure in the ram multiplied by the area of the ram. Displacement is plotted along the horizontal axis.

First slip occurred during the first stage of the test, when N was 25 kips (111 kN). The load required to cause first slip was 1.98 kips (8.81 kN). Average bond strength was computed to be 97 psi (670 kPa).

BG2N_8L: Pullout Force vs. Key Displacements

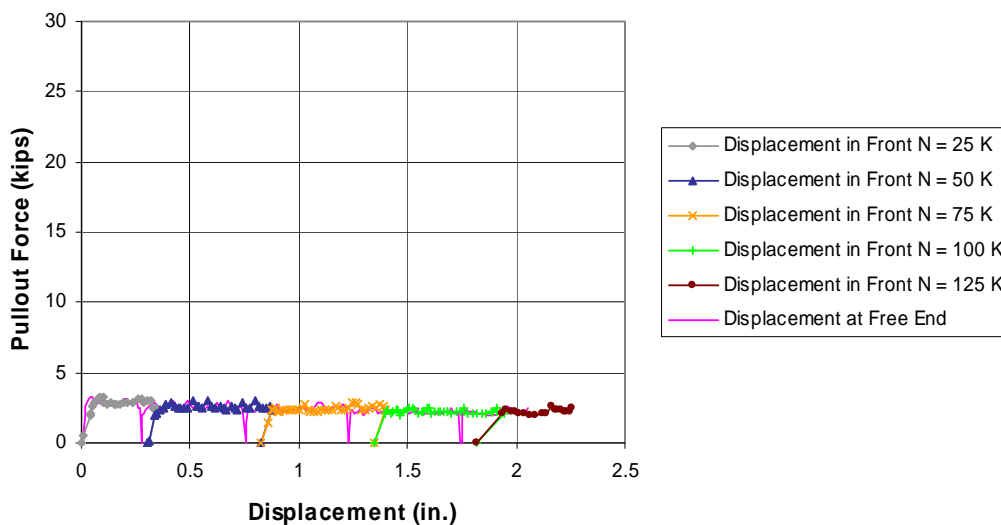


Figure 4.6: Load-displacement Relationship for Strand BG2N_8L

Table 4.1 summarizes the values of pullout force required to cause slip for varying transverse clamping forces for Strand BG2N_8L.

Table 4.1: Summary of Test Results for Strand BG2N_8L

Clamping Load N	Slip Occurred or Resumed At
25 kips (111 kN)	1.98 kips (8.81 kN)
50 kips (222 kN)	2.15 kips (9.56 kN)
75 kips (334 kN)	2.32 kips (10.3 kN)
100 kips (445 kN)	2.35 kips (10.4 kN)
125 kips (556 kN)	2.37 kips (10.5 kN)

Strand BG4S1_17R

Strand BG4S1_17R, tested on February 19, 2002, had a significant initial crack at the back of the strand. The crack extended from the edge of the inner void of the girder cross section, around Strand BG4S1_17R, and towards Strand BG4S1_14R (Figure 4.7).



Figure 4.7: Crack in back of Slice BG4S1 at Strand 17R (Center)

The length of Strand BG4S1_17R embedded in concrete prior to testing was measured to be approximately 15 in. (0.38 m). First slip occurred at 3.72 kips (16.6 kN), at an average bond strength of 158 psi (1,090 kPa).

Figure 4.8 shows the load-displacement relationship recorded during the test. During the last stage, when the transverse clamping load was 125 kips (556 kN), the pullout force increased slightly as displacement increased.

BG4S1_17R: Pullout Force vs. Key Displacements

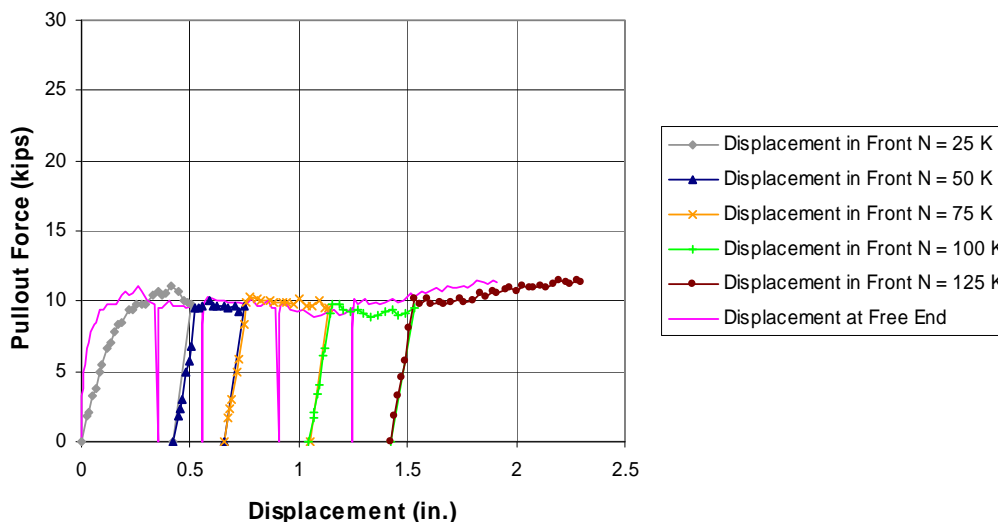


Figure 4.8: Load-displacement Relationship for Strand BG4S1_17R

Table 4.2 summarizes the values of pullout force required to cause slip for varying transverse clamping forces for Strand BG4S1_17R.

Table 4.2: Summary of Test Results for Strand BG4S1_17R

Clamping Load N	Slip Occurred or Resumed At
25 kips (111 kN)	3.72 kips (16.6 kN)
50 kips (222 kN)	9.56 kips (42.5 kN)
75 kips (334 kN)	10.32 kips (45.9 kN)
100 kips (445 kN)	9.76 kips (43.4 kN)
125 kips (556 kN)	10.24 kips (45.6 kN)

Strand BG4S2_1L

Strand BG4S2_1L was tested on January 13, 2002. The concrete surrounding the back of the strand seemed to be in good condition; there was a crack near the strand in the back face, however. The length of Strand BG4S2_1L embedded in concrete prior to testing was measured to be approximately 13.2 in. (0.34 m).

Figure 4.9 shows the load-displacement relationship recorded during the test. The load required to cause first slip at the free end of the strand was 5.81 kips (25.8 kN). Average bond strength was computed to be 280 psi (1,930 kPa).

BG4S2_1L: Pullout Force vs. Key Displacements

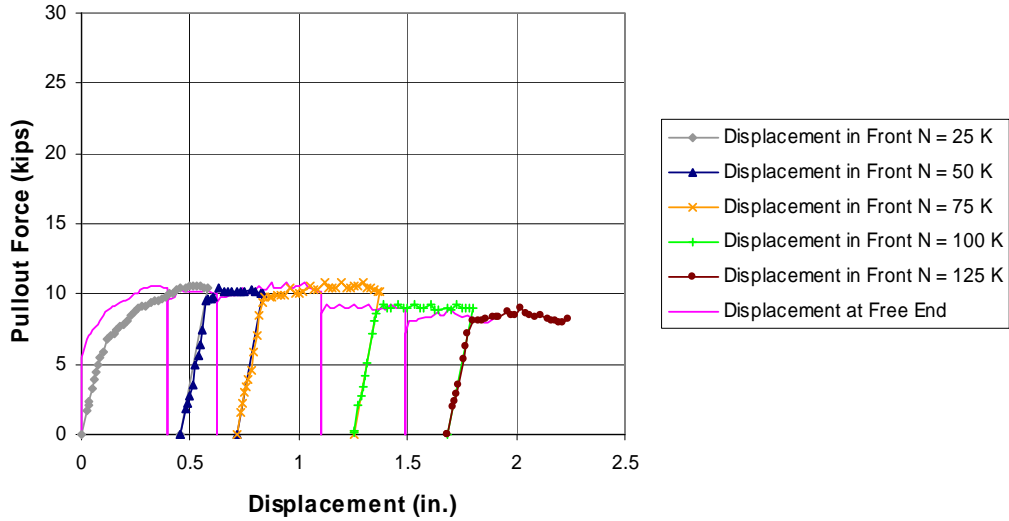


Figure 4.9: Load-displacement Relationship for Strand BG4S2_1L

Table 4.3 summarizes the values of pullout force required to cause slip for varying transverse clamping forces for Strand BG4S2_1L.

Table 4.3: Summary of Test Results for Strand BG4S2_1L

Clamping Load N	Slip Occurred or Resumed At
25 kips (111 kN)	5.81 kips (25.8 kN)
50 kips (222 kN)	9.61 kips (42.8 kN)
75 kips (334 kN)	9.72 kips (43.2 kN)
100 kips (445 kN)	8.63 kips (38.4 kN)
125 kips (556 kN)	8.1 kips (36.0 kN)

4.2.2 Decrease in P with Increase in N

As discussed similarly in the preceding section, these results are in contrast to those reported by Stocker and Sozen (1970).

Strand BG4S1_15L

Strand BG4S1_15L was tested on February 8, 2002. No cracks were apparent in the back face around the free end of the strand. The length of strand BG4S1_15L embedded in concrete prior to testing was measured to be approximately 14 in. (0.36 m).

Figure 4.10 shows the load-displacement relationship recorded during the test. The load required to cause first slip at the free end of the strand was 14.77 kips (65.7 kN). Average bond strength was computed to be 672 psi (4,630 kPa).

BG4S1_15L: Pullout Force vs. Key Displacements

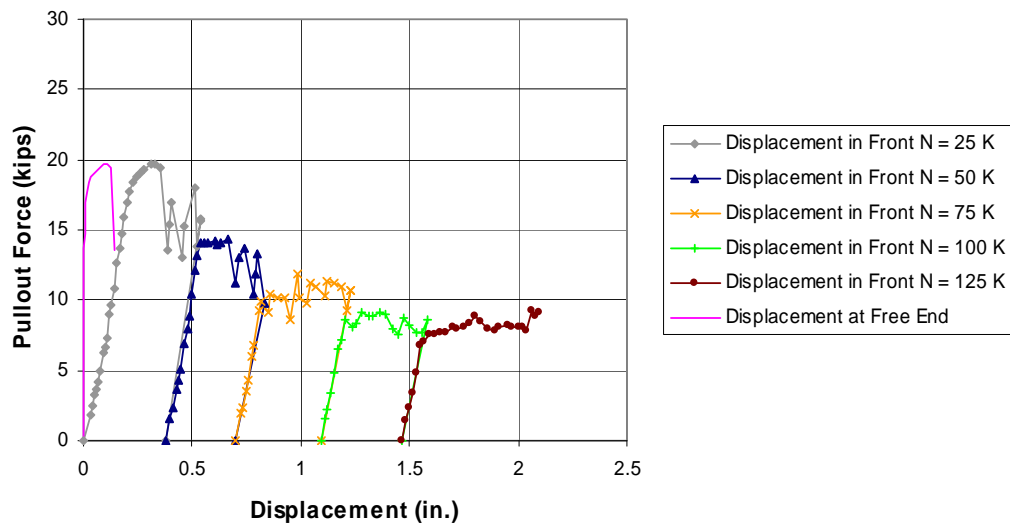


Figure 4.10: Load-displacement Relationship for Strand BG4S1_15L

The linear potentiometer attached to the back of the strand became disconnected at approximately 0.3 in. (7 mm) of displacement at the front end.

During the test, the strand surged forward and apparently pulled the strand off of the potentiometer shaft. This explains why the curve “Displacement at Free End” does not continue throughout the remainder of the test.

Table 4.4 summarizes the values of pullout force required to cause slip for varying clamping forces for Strand BG4S1_15L.

Table 4.4: Summary of Test Results for Strand BG4S1_15L

Clamping Load N	Slip Occurred or Resumed At
25 kips (111 kN)	14.77 kips (65.7 kN)
50 kips (222 kN)	14.02 kips (62.4 kN)
75 kips (334 kN)	9.97 kips (44.4 kN)
100 kips (445 kN)	8.63 kips (38.4 kN)
125 kips (556 kN)	7.06 kips (31.4 kN)

Strand BG4S1_4R

Strand BG4S1_4R was tested on February 15, 2002. The concrete around the strand in the back face had some cracking through the concrete paste and aggregates (Figure 4.11). The length of Strand BG4S1_4R embedded in concrete prior to testing was measured to be approximately 13.8 in. (0.35 m).



Figure 4.11: Back view of Strand BG4S1_4R (right) and Strand BG4S1_5R (left)

Figure 4.12 shows the load-displacement relationship recorded during the test. The load required to cause first slip at the free end of the strand was 8.3 kips (36.9 kN). Average bond strength was computed to be 384 psi (2,650 kPa).

BG4S1_4R: Pullout Force vs. Key Displacements

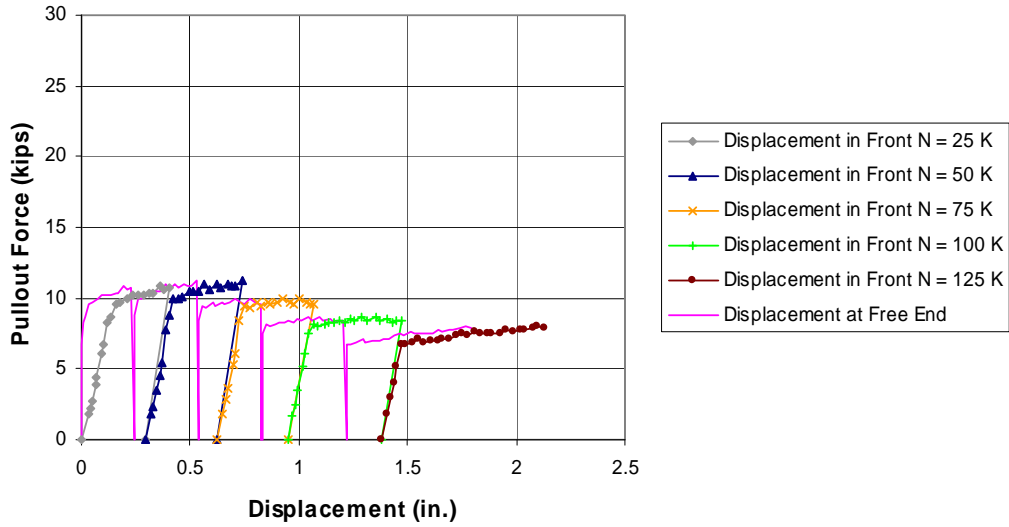


Figure 4.12: Load-displacement Relationship for Strand BG4S1_4R

Table 4.5 summarizes the values of pullout force required to cause slip for varying clamping forces for Strand BG4S1_4R.

Table 4.5: Summary of Test Results for Strand BG4S1_4R

Clamping Load N	Slip Occurred or Resumed At
25 kips (111 kN)	8.3 kips (36.9 kN)
50 kips (222 kN)	9.99 kips (44.4 kN)
75 kips (334 kN)	9.49 kips (42.2 kN)
100 kips (445 kN)	8.12 kips (36.1 kN)
125 kips (556 kN)	6.75 kips (30.0 kN)

Strand BG2N_9R

Strand BG2N_9R was tested on November 5, 2001. The concrete around the strand was in good condition; no cracks were apparent at the back of the strand. The length of Strand BG2N_9R embedded in concrete prior to testing was measured to be approximately 14.3 in. (0.36 m).

Figure 4.13 shows the load-displacement relationship recorded during the test. The load required to cause first slip was 18.84 kips (83.8 kN). Average bond strength was computed to be 842 psi (5,800 kPa).

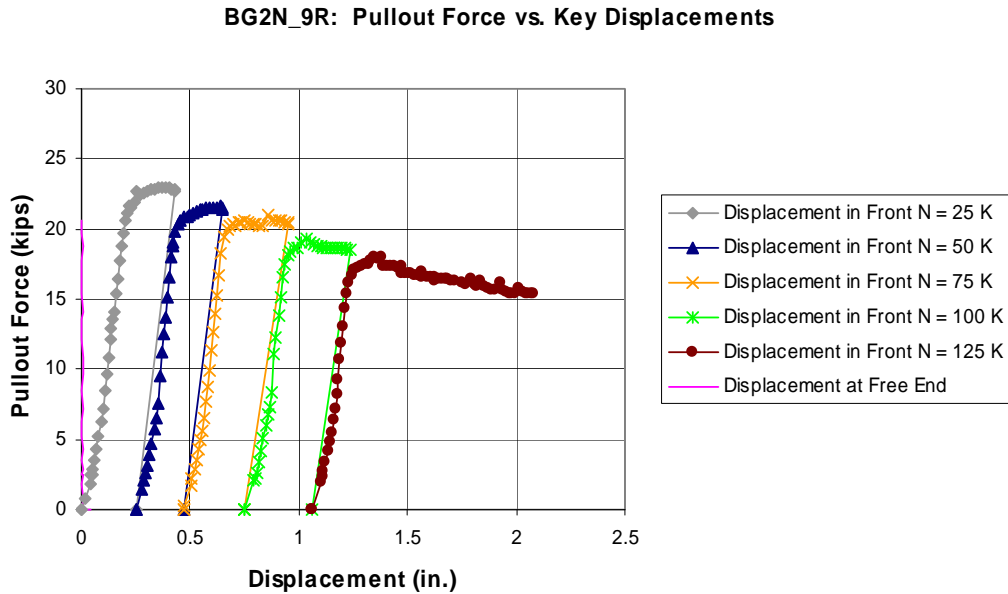


Figure 4.13: Load-displacement Relationship for Strand BG2N_9R

The linear potentiometer attached to the back of the strand was inadvertently glued to the back of the specimen, and did not move with the free end of the strand. This explains why the curve “Displacement at Free End” does not show any displacement of the free end during the test.

Table 4.6 summarizes the values of pullout force required to cause slip for varying clamping forces for Strand BG2N_9R.

Table 4.6: Summary of Test Results for Strand BG2N_9R

Clamping Load N	Slip Occurred or Resumed At
25 kips (111 kN)	18.84 kips (83.8 kN)
50 kips (222 kN)	19.82 kips (88.2 kN)
75 kips (334 kN)	19.46 kips (86.6 kN)
100 kips (445 kN)	17.51 kips (77.9 kN)
125 kips (556 kN)	16.17 kips (71.9 kN)

4.2.3 Increase in P with Increase in N

Strand BG1S_13R

Strand BG1S_13R was tested on August 9, 2001. Concrete around the strand was fairly sound and did not have many cracks. The length of Strand BG1S_13R embedded in concrete prior to testing was measured to be approximately 12.6 in. (0.32 m).

Figure 4.14 shows the load-displacement relationship recorded during the test. The load required to cause first slip was 16.97 kips (75.5 kN). Average bond strength was computed to be 856 psi (5,900 kPa).

BG1S_13R: Pullout Force vs. Key Displacements

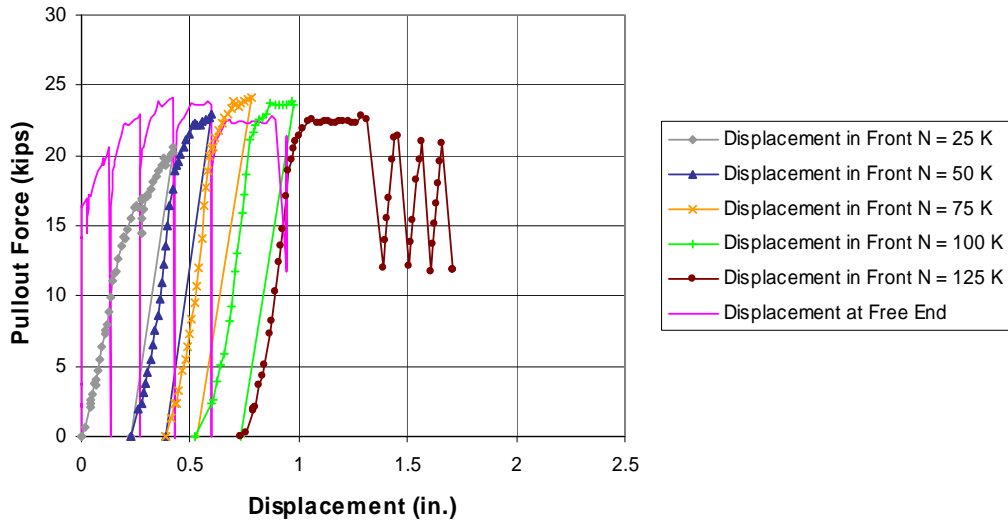


Figure 4.14: Load-displacement Relationship for Strand BG1S_13R

The large decreases in pressure and increases in displacement during the stage when the clamping load was 125 kips (556 kN) indicate moments when the strand jumped and surged forward during the test. These jumps were accompanied by a loud popping noise. The linear potentiometer shaft at the free end was pulled from the strand by the first surge, so subsequent potentiometer data were disregarded.

Table 4.7 summarizes the values of pullout force required to cause slip for Strand BG1S_13R.

Table 4.7: Summary of Test Results for Strand BG1S_13R

Clamping Load N	Slip Occurred or Resumed At
25 kips (111 kN)	16.97 kips (75.5 kN)
50 kips (222 kN)	18.94 kips (84.3 kN)
75 kips (334 kN)	19.96 kips (88.8 kN)
100 kips (445 kN)	21.16 kips (94.1 kN)
125 kips (556 kN)	20.46 kips (91.0 kN)

Strand BG2N_2R

Strand BG2N_2R was tested on November 9, 2001. The concrete around the strand was not nearly as damaged as the concrete surrounding the adjacent strands. Figure 3.14 shows the pre-test condition for the back face of the right cluster strands of Slice BG2N. The length of Strand BG2N_2R embedded in concrete prior to testing was measured to be approximately 14 in. (0.36 m).

Figure 4.15 shows the load-displacement relationship recorded during the test. The load required to cause first slip was 4.81 kips (21.4 kN). Average bond strength was computed to be 219 psi (1,510 kPa).

During the stage when N was 100 kips (445 kN), the pullout force increased as displacement increased. This test did not show a stepped increase of P with increasing N ; it was one of the few tests that showed an increase in resistance, however. Because the pressure in the ram continued to increase, the test was continued until the ram extended fully; this occurred before a transverse clamping load of 125 kips (556 kN) could be reached.

BG2N_2R: Pullout Force vs. Key Displacements

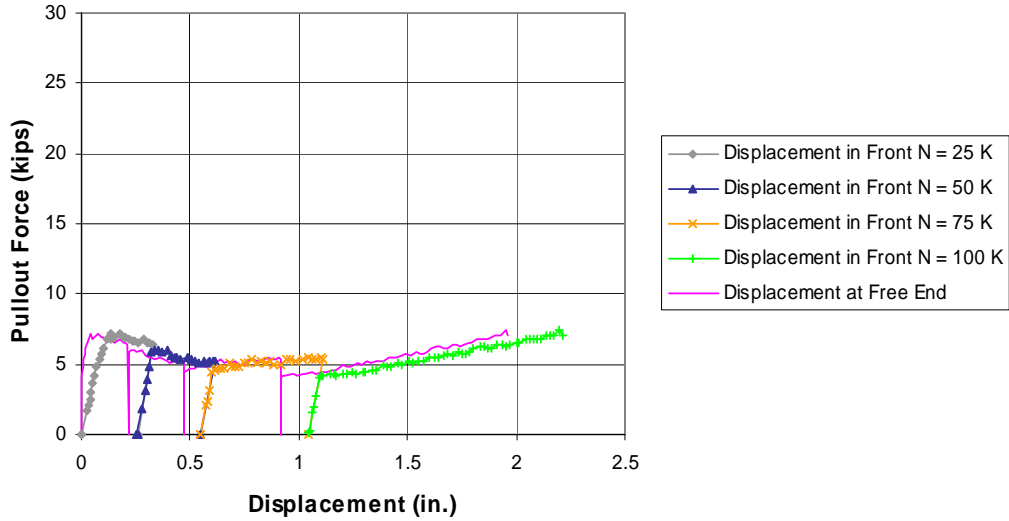


Figure 4.15: Load-displacement Relationship for Strand BG2N_2R

Table 4.8 summarizes the values of pullout force required to cause slip for Strand BG2N_2R.

Table 4.8: Summary of Test Results for Strand BG1S_2R

Clamping Load N	Slip Occurred or Resumed At
25 kips (111 kN)	4.81 kips (21.4 kN)
50 kips (222 kN)	6.06 kips (27.0 kN)
75 kips (334 kN)	4.61 kips (20.5 kN)
100 kips (445 kN)	4.2 kips (18.7 kN)

Strand BG4S2_5R

Strand BG4S2_5R was tested on January 18, 2002. Cracking was significant around the back of the strand and the adjacent strands (Figure 4.16).

The length of Strand BG4S2_5R embedded in concrete prior to testing was measured to be approximately 12.4 in. (0.31 m).



Figure 4.16: Back View of Strand BG4S2_5R (Top Row, Second From Left)

Figure 4.17 shows the load-displacement relationship recorded during the test. The load required to cause first slip at the free end of the strand was 5.28 kips (23.5 kN). Average bond strength was computed to be 272 psi (1,870 kPa).

The resistance increased significantly as displacement increased during the stage when N was 75 kips (334 kN), and it also increased slightly during the last two stages of the test. Even though the pullout force increased during the stages, the load required to cause slip stayed about the same.

BG4S2_5R: Pullout Force vs. Key Displacements

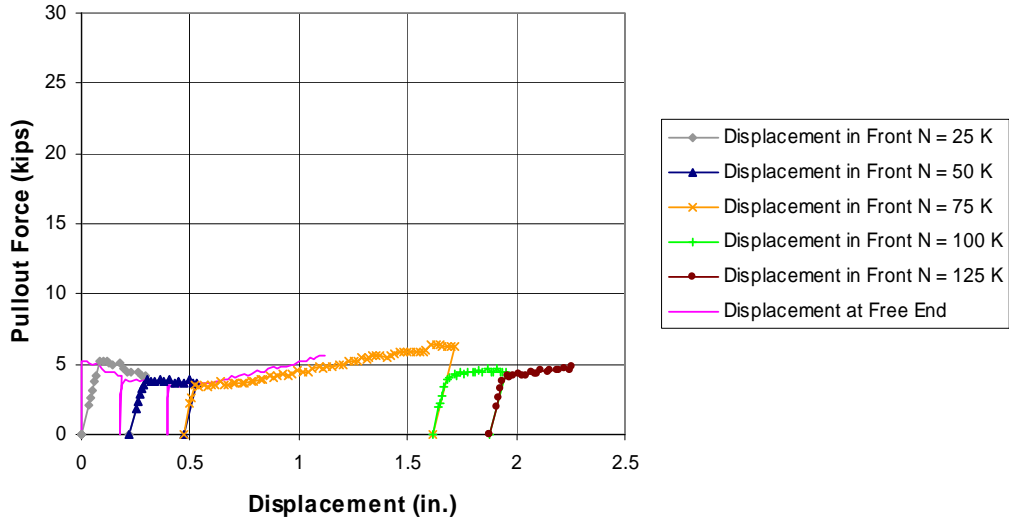


Figure 4.17: Load-displacement Relationship for Strand BG4S2_5R

The potentiometer shaft attached to the free end of the strand became disconnected during the stage when N was 75 kips (334 kN). Data collected by that potentiometer past this point were disregarded.

Table 4.9 summarizes the values of pullout force required to cause slip for Strand BG4S2_5R.

Table 4.9: Summary of Test Results for Strand BG4S2_5R

Clamping Load N	Slip Occurred or Resumed At
25 kips (111 kN)	5.28 kips (23.5 kN)
50 kips (222 kN)	3.56 kips (15.8 kN)
75 kips (334 kN)	3.49 kips (15.5 kN)
100 kips (445 kN)	4.01 kips (17.8 kN)
125 kips (556 kN)	4.14 kips (18.4 kN)

4.3 MEASURED DAMAGE INDICES OF SPECIMENS

Five damage indices for each slice specimen were computed as described in Section 3.5. Cracks were measured with a crack comparator card and classified by width. To compensate for some of the subjectivity of using a crack comparator and to make crack measurement easier, five ranges of crack widths were established:

1. Hairline: < 0.002 in. (0.05 mm)
2. Narrow: 0.002 in. (0.05 mm) – 0.005 in. (0.13 mm)
3. Medium: 0.007 in. (0.18 mm) – 0.020 in. (0.51 mm)
4. Wide: 0.025 in. (0.64 mm) – 0.06 in. (1.52 mm)
5. Extra Wide: > 0.06 in. (1.52 mm)

To compute the damage index, the width and length of all cracks in the representative square were measured. Each crack was classified in one of the five ranges. To further simplify the required calculations, a single average crack width was used for each crack range in Equation 3-1:

1. Hairline: 0.001 in. (0.03 mm)
2. Narrow: 0.0035 in. (0.09 mm)
3. Medium: 0.013 in. (0.33 mm)
4. Wide: 0.04 in. (1.02 mm)
5. Extra Wide: exact width

4.3.1 Slice BG1S

Table 4.10 lists the five damage indices computed for Slice BG1S.

Table 4.10: Damage Indices for Slice BG1S

Location on Slice	Damage Index ($\Sigma w^2 l$)
Left Side	1,700
Bottom Left	15
Bottom Middle	1,600
Bottom Right	24
Right Side	240

The representative squares on the side of the left web and the middle of the bottom face have the most cracking on this specimen.

4.3.2 Slice BG2N

Table 4.11 lists the five damage indices computed for Slice BG2N.

Table 4.11: Damage Indices for Slice BG2N

Location on Slice	Damage Index ($\Sigma w^2 l$)
Left Side	16,900
Bottom Left	1,000
Bottom Middle	840
Bottom Right	1,100
Right Side	18,300

The external faces of the webs are heavily damaged on this specimen, and are much more deteriorated than the bottom face.

4.3.3 Slice BG4S1

Table 4.12 lists the five damage indices computed for Slice BG4S1.

Table 4.12: Damage Indices for Slice BG4S1

Location on Slice	Damage Index ($\Sigma w^2 l$)
Left Side	3,700
Bottom Left	4,600
Bottom Middle	3,100
Bottom Right	330
Right Side	650

More intense damage is concentrated towards the left half of this specimen. The damage indices on the left web and the left and middle portions of the bottom face are significantly higher than the other two indices.

4.3.4 Slice BG4S2

Table 4.13 lists the five damage indices computed for Slice BG4S2.

Table 4.13: Damage Indices for Slice BG4S2

Location on Slice	Damage Index ($\Sigma w^2 l$)
Left Side	2,500
Bottom Left	2,700
Bottom Middle	1,400
Bottom Right	640
Right Side	780

The damage indices follow the same pattern as Slice BG4S1, the specimen taken from the same area of Girder BG4S. Higher degrees of damage are found on the left and middle portions of the specimen when compared to the right half.

CHAPTER 5

Significance of Test Results

In this chapter, the three resistance mechanisms influencing the load-deformation response of the strand pullout tests are discussed, and conclusions are drawn regarding the relative significance of each mechanism based on the experimental data. Conclusions are also drawn regarding the correlation between damage indices for the specimens and changes in the pullout response of strands embedded in those specimens.

5.1 MECHANISMS GOVERNING THE LOAD-DISPLACEMENT RESPONSE OF STRANDS IN CONCRETE

Based on the literature survey of Chapter 2, three mechanisms govern the load-displacement response of strands embedded in concrete: bond between the strands and the concrete; friction between the strands and concrete; and twisting of the strand as it is pulled out of the concrete.

When a strand is loaded, all three mechanisms act simultaneously. How much each mechanism contributes to the overall pullout behavior is generally not known. Typical results of strand-pullout tests, however, show that one or two of the mechanisms dominates different stages of the load-displacement response of prestressing strands in concrete.

To determine the dominant mechanism(s), plots of experimental data (Appendix C) were compared with the fundamental load-displacement relationships for each mechanism.

5.2 BOND MECHANISM

When a strand embedded in concrete is loaded in tension, displacement of the strand is resisted partly by bond between the strand and the concrete. Bond between a smooth bar and the surrounding concrete is due primarily to adhesion between the concrete and the bar. Bond between deformed reinforcement and concrete is due primarily to mechanical anchorage between the bar deformations and the concrete. Bond failure of a deformed bar usually occurs by shearing of the concrete on a cylindrical failure surface roughly coincident with the outside of the deformations. A prestressing strand does not have such deformations, and its bond characteristics are similar to those of a smooth bar.

The governing differential equation for bond is developed using a free-body diagram of a bar in concrete subjected to tensile force (Figure 5.1).

Figure 5.1 shows a length dx of a smooth bar in concrete:

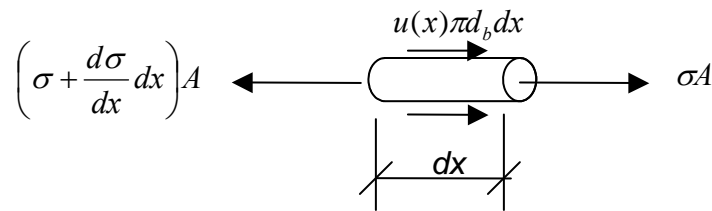


Figure 5.1: *Free-body diagram of a length dx of a smooth bar in concrete*

In Figure 5.1,

d_b = bar diameter

A = cross-sectional area of bar = $\frac{\pi d_b^2}{4}$

σ = stress in the bar

Imposing axial equilibrium, the bond stress at any point along the bar, $u(x)$, is:

$$u(x) = \frac{\left(\frac{d\sigma}{dx}\right)A}{\pi d_b} \quad (5-1)$$

Equation 5-1 can be simplified to Equation 5-2.

$$u(x) = \frac{\left(\frac{d\sigma}{dx}\right)d_b}{4} \quad (5-2)$$

The variation of differential stress in the bar, $d\sigma$, must be determined experimentally or analytically. Because the specimens used for the strand-pullout tests were cut from prefabricated bridge girders, it was not possible to install strain gauges inside the specimens along the strands, and also impossible to know the actual distribution of bar stress, and the corresponding distribution of bond stress, for each pullout test. Experimental methods to measure $d\sigma$ were therefore unavailable for the pullout tests of this thesis.

Direct evaluation of the variation of bond stress along the length of the bar, $u(x)$ (Equation 5-2) is generally not possible. The actual distribution of bond stress is complex, and can be affected by cracking in the concrete and slip between the bar and concrete. Analytical solutions obtained with the finite element method are not useful because bond is lost after the bar slips.

An approximate bond stress can be measured by assuming that bond stress is uniform along the length of the strand in concrete. The derivation of the uniform average bond stress, u_{avg} , is similar to the procedure shown above for a length dx of a smooth bar in concrete. Figure 5.2 shows a free-body diagram of a smooth bar in concrete with length dl and known bar stresses at each end of the bar.

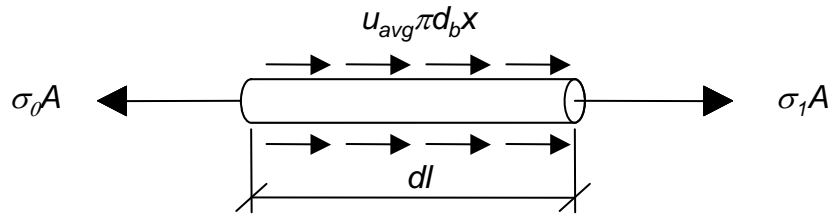


Figure 5.2: Free-body diagram of a smooth bar in concrete

$$u_{avg} = \frac{(\sigma_0 - \sigma_1)(A)}{\pi d_b dl} \quad (5-3)$$

Equation 5-3 can be simplified to Equation 5-4.

$$u_{avg} = \frac{(\sigma_0 - \sigma_1)(d_b)}{4dl} \quad (5-4)$$

The average bond strength for each strand was computed as the force required to cause first slip of the strand at the free end divided by the circumference of the strand multiplied by the length of strand embedded in concrete. Figure 5.3 illustrates the experimental setup used to determine u_{avg} for each strand (Section 3.3).

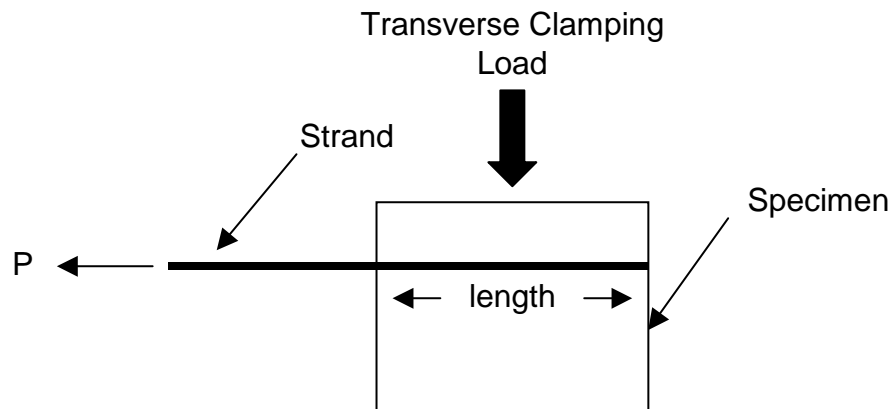


Figure 5.3: Experimental setup used to determine u_{avg}

Equation 5-5 shows Equation 5-3 updated for values obtained with strand tests.

$$u_{avg} = \frac{P}{\pi d_b * length} \quad (5-5)$$

In Equation 5-5, P is the force required to cause first slip of the strand, and $length$ is the embedded length of strand in concrete in the slice specimen prior to testing, as shown in Figure 5.3. A similar procedure to determine bond stress over a known length was used by Abrishami and Mitchell (1993).

Equation 5-5 can be arranged to express P in terms of u_{avg} .

$$P = u_{avg} \pi d_b * length \quad (5-6)$$

The corresponding load-displacement relationship for the bond mechanism, assuming uniform bond stress, is shown in Figure 5.4.

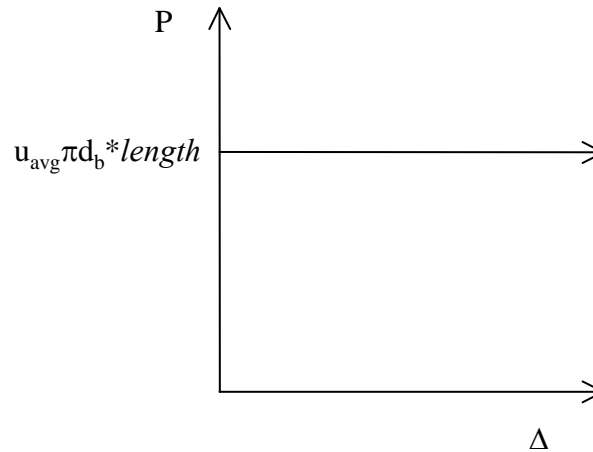


Figure 5.4: *Load-displacement relationship assuming uniform bond stress*

In actuality, the variation of bond stress is not uniform along the length of a strand in concrete subject to tensile force. Because the variation of bond stress is not uniform, displacement at the loaded end is greater than zero as P is increased from 0 to its maximum value (Equation 5-6). Previous research on the pullout behavior of smooth bars in concrete (Mylrea 1948) corroborates this and provides an approximate load-displacement relationship for the bond mechanism (Figure 5.5).

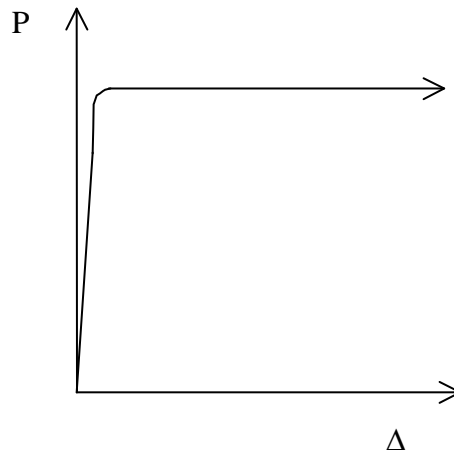


Figure 5.5: *Approximate load-displacement relationship for bond mechanism*

5.3 FRICTION MECHANISM

Strand pullout is also resisted by friction between the prestressing strand and the concrete. The available friction capacity is the product of the coefficient of friction between the strand and concrete, μ , and the normal force acting perpendicular to the surface of the strand, N . As the pullout force is increased in the strand, the strand begins to slip when the available friction capacity is exceeded (that is, $P > \mu N$). The corresponding load-displacement relationship is shown in Figure 5.6.

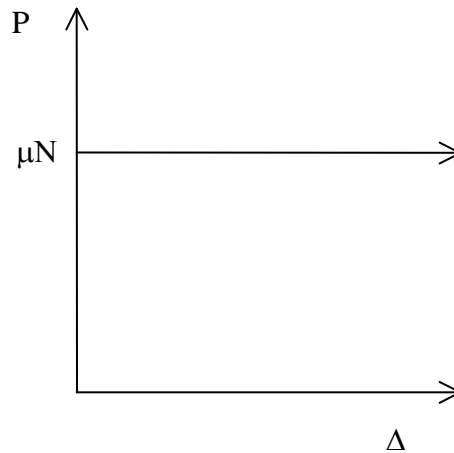


Figure 5.6: *Load-displacement relationship for friction mechanism*

In evaluating the strand pullout tests at The University of Texas at Austin, the value of N was taken as the transverse clamping load shown in Figure 5.3.

5.4 TWIST MECHANISM

The third mechanism resisting pullout is twisting of the strands. As a strand is pulled out, the strand essentially unscrews out of the concrete, leaving the spiral grooves in the concrete intact. This observed behavior matches that observed in tests conducted by Salmons and McCrate (1977). Friction between the loading chuck and washer prevents the loaded end of the strand from twisting. Because the loaded end is not permitted to rotate freely, a torque is applied to the strand.

To understand this mechanism, the strand can be compared to a threaded screw embedded in a frictionless material of infinite strength. If the screw is pulled out of the material without restraining its rotation at the loaded end, the required axial force is zero. The screw will simply rotate out of the threaded hole. The angle through which the screw rotates, θ , depends on the pitch of the screw, or rate of rotation. This rate is defined as the change in angle per unit length.

$$rate = \frac{d\theta}{dx} \quad (5-7)$$

If rotation at the free end is restrained, then the screw cannot rotate freely. Pulling the screw out of the material produces a torque in the free length of the screw, L_0 (Figure 5.7).

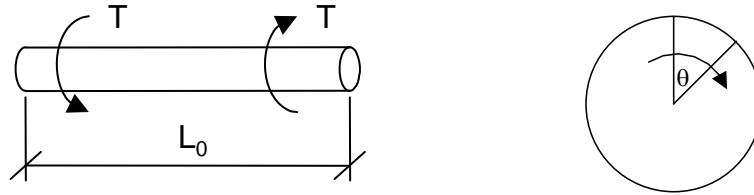


Figure 5.7: Twist of a cylindrical bar

The general equation for torque, T , is given in Equation 5-8, where G is the shearing modulus of the material, J is the torsional constant for the cross-section, and L is the length over which the torsional deformation occurs.

$$T = \frac{GJ}{L}\theta \quad (5-8)$$

For the strand-pullout tests, L_0 is the length of strand between the strand chuck and the face of the specimen. This is the initial length of strand undergoing twist. G , J , and $\frac{d\theta}{dx}$ are assumed constant over the entire length of the strand.

For the example of the screw, the torsional deformation depends upon the rate of rotation and the distance the bar is pulled out, Δ .

$$\theta = \frac{d\theta}{dx}\Delta \quad (5-9)$$

As the screw is pulled out of the material, the elastic strain energy associated with this torsional deformation is equal to the work required to pull the bar out the corresponding distance.

The relationship between the pullout force P and the displacement of the bar can be derived as shown in the series of equations in Table 5.1.

Table 5.1: Derivation of load-displacement relationship for twist mechanism

External Work	Internal Strain Energy
$P = K\Delta$ (5-10a)	$T = \left(\frac{GJ}{L}\right)\left(\frac{d\theta}{dx}\right)\Delta$ (5-10b)
$Energy = \frac{1}{2}P\Delta$ (5-11a)	$Energy = \frac{1}{2}T\theta$ (5-11b)
$Energy = \frac{1}{2}K\Delta^2$ (5-12a)	$Energy = \frac{1}{2}\left(\frac{GJ}{L}\right)\left(\frac{d\theta}{dx}\right)^2 \Delta^2$ (5-12b)

$$\frac{1}{2}K\Delta^2 = \frac{1}{2}\left(\frac{GJ}{L}\right)\left(\frac{d\theta}{dx}\right)^2 \Delta^2 \quad (5-13)$$

$$K = \frac{GJ}{L}\left(\frac{d\theta}{dx}\right)^2 \quad (5-14)$$

$$P = \left(\frac{GJ}{L}\right)\left(\frac{d\theta}{dx}\right)^2 \Delta \quad (5-15)$$

If the length of strand subjected to torsional deformation, denoted by L in Equation 5-15, remained constant throughout the test, P would have a linear relationship to Δ . As the strand is pulled out of the concrete, however, the affected length of strand increases from its initial value of L_0 to a final value of $(L_0 + \Delta)$. As Δ increases, so does L ; therefore, the slope of the load-displacement curve decreases. The relationship between P and Δ for the twist mechanism is shown schematically in Figure 5.8.

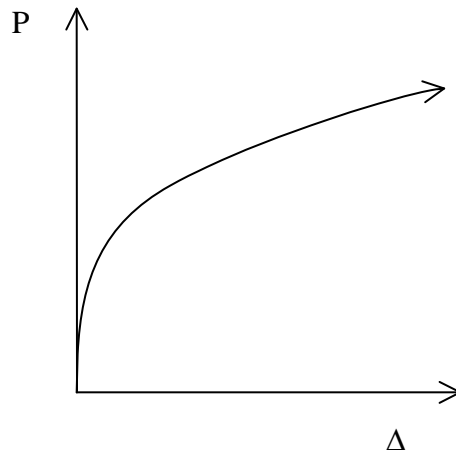


Figure 5.8: *Load-displacement relationship for twist mechanism*

5.5 COMBINATION OF RESISTANCE MECHANISMS

As the strand is pulled out of the concrete, all three mechanisms act simultaneously. Figure 5.9 shows the schematic superposition of the fundamental load-displacement relationships for all three mechanisms. Because the actual relative contribution of each mechanism to pullout behavior is generally not known, the vertical scale for the combined plot is arbitrary.

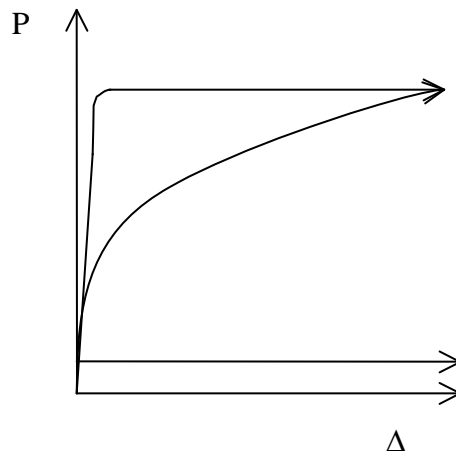


Figure 5.9: *Superposition of the three independent mechanisms*

As shown in Chapter 4, the experimental load-displacement relationships observed in this study were characterized by a sharp increase (similar to the bond mechanism), and a gradually increasing curve (similar to the twist mechanism). Figure 5.10 shows the load-displacement relationship recorded for Strand BG4S2_17R. The plot is used to illustrate the typical shape of the experimental load-displacement curves and is compared with the fundamental load-displacement relationships for the three mechanisms.

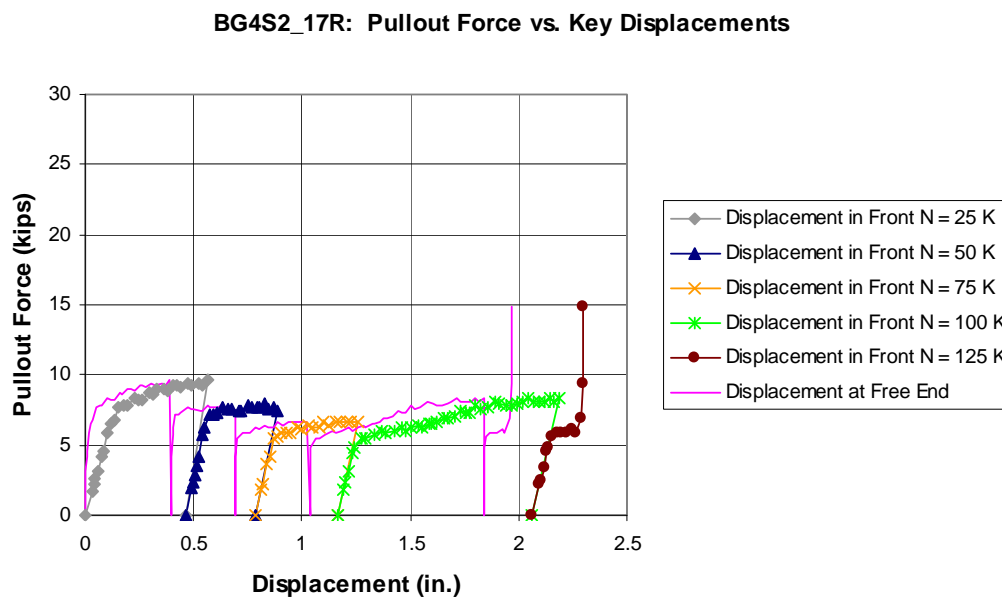


Figure 5.10: Load-displacement Relationship for Strand BG4S2_17R

Because the strand-pullout tests are more similar to tensioned pullout tests, Hoyer’s effect may have influenced the bond between the strands and concrete in the slice specimens (Rose and Russell 1997). Because the test setup in this thesis is more similar to that of the simple pullout tests performed by Rose and Russell, the results presented in Chapter 4 and discussed here are probably conservative.

The following conclusions were drawn from the test results:

1. Because the experimental data curve is characterized before first slip has occurred by a sharp increase similar to the bond mechanism, the bond mechanism dominates before first slip.
2. Because pullout force P does not increase significantly with transverse clamping force N , the friction mechanism is not very important.
3. Because the load-displacement curves for the loaded end of the strands show elastic unloading and reloading behavior after first slip of the strands, and because the load-displacement curves for the loaded end of the strands increase gradually in a manner similar to the twist mechanism after first slip of the strand, the twist mechanism dominates after first slip.
4. Because premature concrete deterioration leads to material failure of the concrete, a lower pullout force P is required to produce a displacement Δ in concrete with premature concrete deterioration, than in normal concrete.
5. Because there is less concrete in contact with the prestressing strand, premature concrete deterioration lowers the average bond strength and therefore lowers the pullout force P required to cause first slip of the strand.
6. The unloading and reloading cycle of the strands is not likely to decrease the coefficient of friction μ between the prestressing strand and the concrete. Because the test results show no significant increase in P even though N increases, it is concluded that μ is small and therefore, the friction mechanism is much less important than the adhesion and twist mechanisms in the pullout resistance of strands in concrete.

5.6 SIGNIFICANCE OF DAMAGE INDICES OF SPECIMENS

Figure 5.11 shows the average bond strengths of 54 tested strands, determined using Equation 5-8, versus the damage index nearest to the strand, computed as described in Section 3.5. For a particular specimen, the Left Side damage index was considered nearest to Strands 1L and 13L-18L, Bottom Left damage index for Strands 2L-7L, Bottom Middle damage index for Strands 8L, 9L, 8R, and 9R, Bottom Right damage index for Strands 2R-8R, and Right Side damage index for Strands 1R and 13R-18R. For example, the average bond strength for Strand BG2N_8L, 97 psi, was plotted against the Bottom Middle damage index for Slice BG2N, 844.

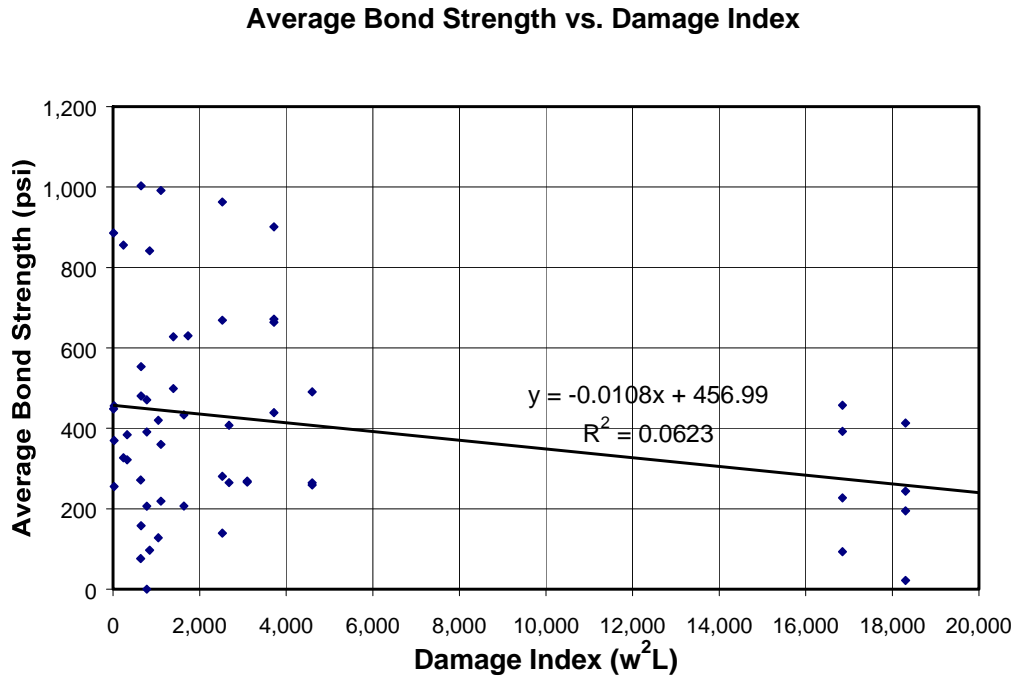


Figure 5.11: Average bond strength vs. damage index for strand-pullout tests

The measured damage indices from the four slice specimens fall into two groups: less than 5,000 and greater than 16,000. For a damage index less than

5,000, the mean average bond strength, \bar{u}_{avg} , is 442 psi (3,040 kPa), with a coefficient of variation of 0.58. For a damage index greater than 16,000, \bar{u}_{avg} is 255 psi (1,760 kPa), with a coefficient of variation of 0.66.

Increases in damage index are associated with decreases in average bond strength. It is not possible to determine with external damage indices whether internal cracks involve individual strands in the cross-section, however. For example, Figure 5.12 shows the left-hand strands of Slice BG4S2, as visible from the back face. The crack propagating from the left corner of the interior void in Slice BG4S2 affects Strand BG4S2_15L but not other nearby strands.

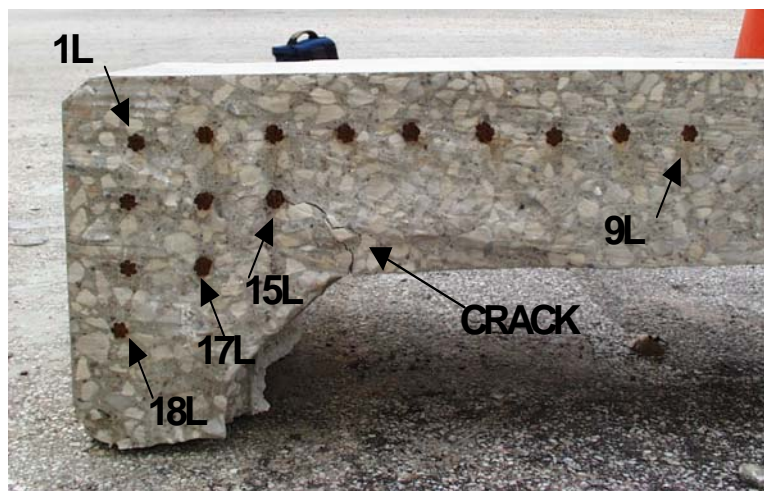


Figure 5.12: Cracking in back face of Slice BG4S2

The left side damage index for Slice BG4S2 was computed to be 2,525 (Table 4.13). As discussed above, this damage index was considered nearest to Strands 1L, 15L, 17L, and 18L. Table 5.2 lists the average bond strengths estimated from pullout tests for those strands.

Table 5.2: Average bond strengths for selected strands in Slice BG4S2

Strand Tested	Average Bond Strength, u_{avg}
BG4S2_1L	280 psi (1,930 kPa)
BG4S2_15L	139 psi (960 kPa)
BG4S2_17L	963 psi (6,640 kPa)
BG4S2_18L	667 psi (4,610 kPa)

The following conclusions were drawn from the experimental data:

1. Because a large range of average bond strengths was found for each external damage index, Figure 5.11 suggests that the pullout response of strands is highly dependent on the local conditions of concrete surrounding each individual strand.
2. Statistically, external damage to the specimens did not correlate very well with changes in the pullout response of the strands. Figure 5.11 suggests, however, that \bar{u}_{avg} decreases with increasing damage index, as shown with a trendline based on least-squares fit.

Because \bar{u}_{avg} decreases as damage index increases, it follows that structural capacity of prestressed girders, as governed by bond strength of strands, decreases as damage index increases. Bond strength may not be critical, however, for the capacity of a girder with premature concrete deterioration. For bond failure of a strand to occur, bond stress between a portion of that strand and the surrounding concrete must exceed the bond strength. High bond stresses (that is, stresses that could approach or exceed the bond strength of strands) are caused by high internal shear forces, which usually exist at girder ends. The ends were the most heavily damaged regions for the box girders in this study. Additionally,

field observations have shown that the ends of girders are most likely to be exposed to water and therefore contain the most damage (Boenig 2000). Because the ends of girders are the most likely to have reduced strand-pullout strengths, and because the critical sections for shear are close to the ends of girders, premature concrete deterioration could eventually lead to bond failure of strands in the ends of those girders.

Previous work by Boenig (2000) and Roche (2001), however, suggests that capacity of girders with premature concrete deterioration concentrated in the ends was limited by flexural or shear capacity, rather than by bond failure of prestressing strands. In laboratory tests, bond stress evidently did not exceed the reduced bond strength before failure of the girder specimens occurred by other mechanisms, such as crushing of the webs. Bond failure of strands did not govern the response of girders in static flexure and shear tests (Boenig 2000), nor in fatigue shear tests (Roche 2001), even in specimens with severe deterioration at the ends. This leads to the conclusion that even with a high damage index and corresponding reduced bond strength, bond failure is probably not critical for the capacity of girders with premature concrete deterioration.

CHAPTER 6

Continuation of Field Observation Program

6.1 OBJECTIVES AND PLAN

The field observation program developed by Boenig (2000) was continued for this thesis. The structures observed as part of this study were monitored further, and the progression of damage was documented over an additional two-year period. While no new bridges were added to the study, crack-measurement points were identified on one of the structures as one of the specific tasks for Study 1857.

6.2 STRUCTURES OBSERVED

The five structures observed for Study 1857 were:

1. Interstate Highway 10 (I-10) over the Atchison Topeka & Santa Fe Railroad (AT & SF RR) in Beaumont, Texas
2. US Highway 90 (US-90) over the San Jacinto River near Houston, Texas
3. Robinson Road over Interstate Highway 45 (I-45) in The Woodlands, Texas
4. Beltway 8 (BW8) over State Highway 3 in Houston, Texas
5. FM 1929 over the Lake Ivie Reservoir in Concho, Texas

6.2.1 I-10 Over AT & SF RR

The bridge structure for I-10 over the Atchison Topeka and Santa Fe railway lines in Beaumont, Texas (Figure 6.1), was monitored throughout the duration of this study. This structure was first inspected by researchers from The

University of Texas at Austin on November 28, 1998. Figure 6.2 shows an overview of the portion of the west abutment where cracks were measured and recorded. The ends of the girders at the abutment were among the affected elements at the structure.



Figure 6.1: I-10 over AT & SF RR in Beaumont, Texas (facing east)



Figure 6.2: Overview of West Abutment of I-10 structure in Beaumont, Texas

The bridge girders shown in Figure 6.2 are standard AASHTO Type C prestressed girders and were fabricated in 1987. Premature deterioration existed in the ends of these girders. Other examples of damage were evident but were not reachable without lifting equipment.

6.2.2 US-90 over the San Jacinto River

The US-90 bridge over the San Jacinto River, northeast of Houston, Texas, (Figure 6.3) was first monitored on February 6, 1999. Figure 6.4 shows the west abutment for the westbound lanes. All readings and measurements were taken in this part of the structure.



Figure 6.3: US-90 over the San Jacinto River near Houston, Texas



Figure 6.4: *West Abutment of US-90W bridge over the San Jacinto River*

Members affected at this site were Type 54 prestressed girders, cast in 1986 (Figure 6.4).

6.2.3 Robinson Road over I-45

The Robinson Road bridge crosses over I-45 in The Woodlands, Texas (Figure 6.5). It was first monitored as part of this study on February 6, 1999. Figure 6.6 shows a view of the underside of the bridge facing east. The west abutment of this structure was observed and inspected by researchers. Cracking was apparent in the Type IV prestressed girders, fabricated in 1987.



Figure 6.5: Robinson Road over I-45 in The Woodlands, Texas



Figure 6.6: Underside of Robinson Road over I-45 (facing east)

6.2.4 Beltway 8 over State Highway 3

The Beltway 8 structure over State Highway 3 was added to the study on the April 9, 1999 field visit. The affected elements are Type IV prestressed girders, fabricated in 1987. Figure 6.7 and Figure 6.8 show an overall view of locations where specific cracks were measured and documented.



Figure 6.7: Beltway 8 over State Highway 3, Houston, Texas (facing north)



Figure 6.8: Beltway 8 over State Highway 3, Houston, Texas (facing west)

6.2.5 FM 1929 over Lake Ivie

FM 1929 crosses the Lake Ivie Reservoir near Concho, Texas (Figure 6.9), approximately 45 miles (72.4 km) east of San Angelo.



Figure 6.9: FM 1929 over the Lake Ivie Reservoir in Concho, Texas (facing west)

This first visit to this structure was a visual inspection conducted on September 29, 1999. Over the course of this thesis, cracking in the columns, bent caps, tie beams, and prestressed girders was measured and documented. The girders are Type C prestressed girders, cast in 1989.

6.3 INSPECTION PROCEDURE

The following procedure was developed for inspecting in-service bridge structures with premature concrete deterioration:

1. Identify high-risk areas for damage due to premature concrete deterioration. Cracking due to ASR or DEF, while relatively insignificant, worsens with exposure to water (Boenig 2000). Consequently, high-risk areas on a structure include exposed columns

or bent caps; girder ends under expansion joints; near drains and drain scuppers; and near the waterline of submerged columns.

2. Locate typical damage. Map cracking and discoloration of the concrete are good indicators of premature concrete deterioration due to ASR and DEF (Boenig 2000).
3. Draw 12 in. (0.31 m) x 12 in. (0.31 m) representative areas on affected elements. Select locations on the structure (i.e. girders, bent caps, etc.) that provide a representative sample of the overall damage in the indicated elements. Measure crack widths and lengths to be used to compute the damage index for each element as described in Section 3.5.
4. Select representative cracks to monitor. Crack widths and lengths should be monitored over time to determine the rate of deterioration for the structure and elements.
5. Measure crack widths. Take crack width readings with a crack comparator card (Figure 6.10), optical scope (Figure 6.11), and Demountable Mechanical (Demec) Strain Gauge (Figure 6.12).



Figure 6.10: Crack comparator card



Figure 6.11: Measuring crack widths with optical scope



Figure 6.12: Taking readings with Demec gauge

The Demec gauge (“DEmountable MEChanical gauge”) is a mechanical dial gauge used to measure the distance between two steel reference discs attached to a surface. For measuring changes in crack width over time, two discs (one set of discs) are affixed to a structure with epoxy so that one disc is on each side of the crack, as shown in Figure 6.13. While the epoxy is setting, the discs are maintained at an initial gauge length of 1.97 in. (50 mm) with a reference bar, as shown in Figure 6.14. In this thesis, a “Demec point” refers to a location along a crack on a structure where one set of Demec discs has been installed.



Figure 6.13: *One set of Demec discs for monitoring crack width*



Figure 6.14: *Holding set of Demec discs in place with reference bar*

Crack ratios were also used to quantify damage on the monitored structures. The crack ratio for a specified representative area was defined as the

ratio of the total area of cracks in the representative area to the gross representative area. Figure 6.15 shows two such representative areas drawn on the I-10 structure for crack ratio measurements: one on the sloped face of the girder bottom flange and one on the vertical face. The area of one crack was estimated by multiplying its approximate length by its width as determined from crack comparator measurements.



Figure 6.15: Representative areas used for crack ratios, I-10 structure

Crack ratios for representative areas on the I-10 structure, the US-90 structure, and the Beltway 8 structure were calculated and discussed by Kim (2002); they are not discussed further in this thesis.

6.4 BRIEF SUMMARY OF FIELD VISITS

The five structures in Texas were monitored on ten additional trips after Boenig's thesis. Brief summaries of the research trips are listed below.

Trip on May 19, 2000

On May 19, 2000, the four structures in southeast Texas (I-10 in Beaumont, US-90 over the San Jacinto River, Robinson Road over I-45, and

Beltway 8 over State Highway 3) were monitored again. Crack widths were measured with a crack comparator, optical scope, and Demec gauge.

Trip on October 6, 2000

On October 6, 2000, I-10 in Beaumont, US-90, and Robinson Road were monitored again. Crack comparator, optical scope, and Demec readings were taken.

Trip on October 12, 2000

On October 12, 2000, Beltway 8 was monitored again. Crack widths were measured with a crack comparator and optical scope; however, all of the Demec discs were no longer present on the bridge. No Demec readings could be taken. Some acoustic emission (AE) data were collected by Chotickai (2001) as part of the collateral research for Study 1857.

Trip on December 18, 2000

On December 18, 2000, Demec points were installed on the FM 1929 structure over Lake Ivie. Initial readings and measurements were taken with the crack comparator, optical scope, and Demec gauge.

Trip on January 24, 2001

On January 24, 2001, the I-10 structure in Beaumont was monitored again.

Trip on February 19, 2001

On February 19, 2001, the US-90, Robinson Road, and Beltway 8 structures were monitored again. No Demec points were available for readings at Beltway 8.

Trip on April 23, 2001

On April 23, 2001, the Lake Ivie structure was monitored again. The Demec discs, set on December 18, 2000, with 5-minute epoxy, were replaced with new discs set with 30-minute epoxy.

Trip on June 21, 2001

On June 21, 2001, the four structures in southeast Texas were monitored again. Some Demec points were replaced at US-90, and seven new Demec points were installed at Beltway 8.

Trip on October 15, 2001

On October 15, 2001, the Lake Ivie structure was monitored again. Two new locations were identified for crack width monitoring but no new Demec points were added to the structure.

Trip on December 10, 2001

On December 10, 2001, the four structures in southeast Texas were monitored again. The girders at US-90 and Beltway 8 had been sealed and painted by TxDOT prior to the trip, so it was not possible to continue measuring crack widths with a crack comparator or optical scope. Most Demec points were still usable.

CHAPTER 7

Results from Field Observations

This chapter presents the results from the continued field observation as described in Chapter 6.

7.1 NOMENCLATURE

Girders in the monitored structures were designated according to their position in the structure. At each structure, adjacent girders were monitored near one abutment as shown in the figures in this chapter. The label “1” was assigned to the exterior girder. For example, “SW Girder 1” refers to Southwest Girder 1, is the exterior girder on the south side of the structure at the west abutment. Figure 7.1 shows the nomenclature used to identify faces of the girders (Boenig 2000).

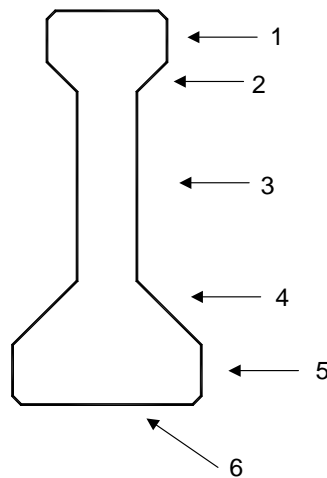


Figure 7.1: Nomenclature used to identify faces of girders

7.2 OBSERVATIONS FROM STRUCTURES STUDIED

7.2.1 I-10 over AT & SF RR

Figure 7.2 is a schematic drawing of crack-measurement locations on the I-10 structure. In the figure, numbers indicate relative locations of points along the girders.

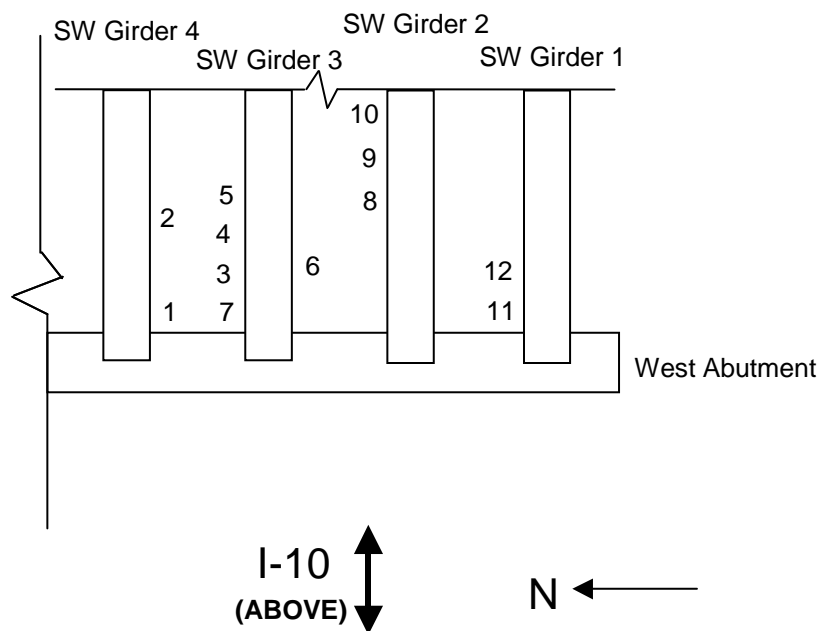


Figure 7.2: *Schematic of crack-measurement locations on I-10 structure (plan view)*

On May 19, 2000, it was noted that the crack width at Point 7 had steadily increased over the previous year while no other cracks showed significant changes in width. SW Girder 1 and the girder east of SW Girder 1 were observed to have severe deterioration at the first bent east of the west abutment.

Four representative areas were defined on the structure to monitor crack ratios over time. Two of these areas were drawn on the north surface of SW

Girder 1 and two more on the south surface of SW Girder 2. On each girder, the first area was drawn on Face 4, and the second area was drawn on Face 5 so that representative areas shared one edge.

On October 7, 2000, diagonal cracks had become visible on the side faces of the bottom flanges (Face 5) on several girders near the west abutment. Figure 7.3 shows an example of this cracking (below Point 1 on SW Girder 4).



Figure 7.3: *New diagonal cracks on I-10 SW Girder 4, Face 5 (10/7/00)*

On October 7, 2000, cracks in the representative areas were observed to be significantly wider than the previous visit. Figure 7.4 shows the representative areas defined on SW Girder 2 near the west abutment.



Figure 7.4: Representative areas on I-10 SW Girder 2, south face (10/7/00)

At the first bent east of the west abutment, cracks in Face 5 at the ends of the two south exterior girders were noticeably wider (Figure 7.5). An expansion joint is present at this bent. Staining on the bent cap indicates that the joint seal had not protected the girders or bent cap from exposure to rainwater. Cracks were not monitored closely at this location because lifting equipment would have been required.



Figure 7.5: Cracks at first bent east of west abutment, I-10 (10/7/00)

On January 24, 2001, Demec readings indicated that the cracks had widened at all points except at Point 7, where they had narrowed slightly. High-resolution digital photos were taken of the representative areas on the structure for use in computing crack ratios using digital photo-processing software.

On June 21, 2001, the west abutment was very wet and dirty following rain showers. Cracks were observed to be wider at all points. Demec readings had increased significantly from the previous visit, with the largest increase at Point 7.

On December 10, 2001, cracking in the structure was overall worse than the previous visit. Cracks were not plotted over the representative areas defined previously on May 19, 2000; cracks in the square on Face 4 of SW Girder 2 were measured to be wider than 1/8 in. (3.2 mm), however.

New cracks had become apparent on SW Girders 2 and 3. Vertical cracks had formed in the web (Face 3) close to the end of the girders; and horizontal cracks had formed at the intersection of the web and top flange (intersection of Face 3 and Face 2), and had extended towards the middle of the span. A schematic diagram of the location of these new cracks is shown in Figure 7.6. Figure 7.7 shows an example of the newly visible cracking on the south face of SW Girder 3. New, small cracks were also noted on the underside (Face 6) of SW Girder 2.

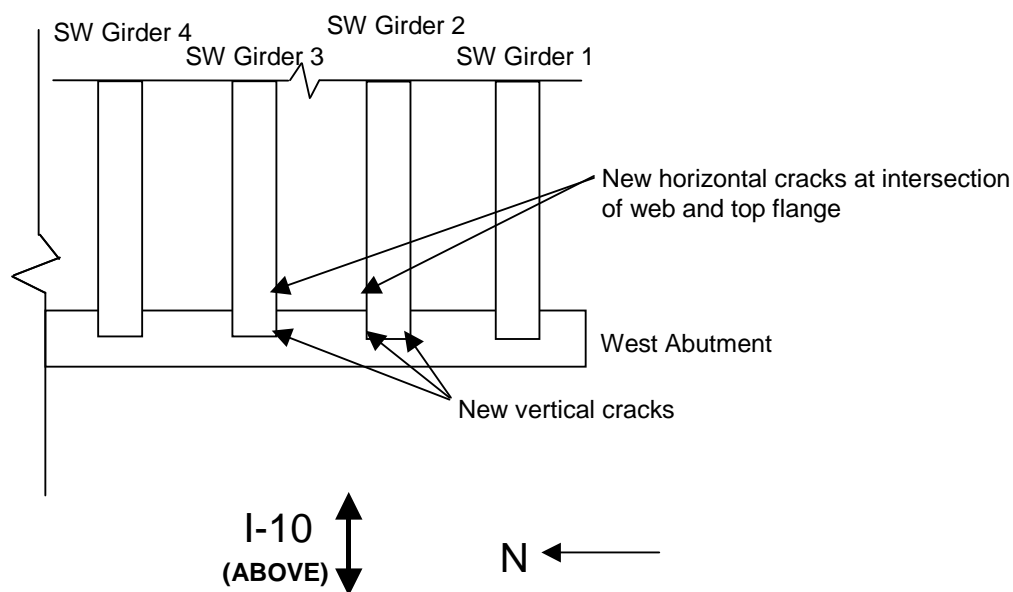


Figure 7.6: Location of new cracks on I-10 structure (plan view) (12/10/01)



***Figure 7.7: New cracks on south face of SW Girder 3 at west abutment, I-10
(12/10/01)***

Figure 7.8 shows more staining on the bent cap, indicating extensive exposure to rainwater since October 7, 2000 (Figure 7.5).



Figure 7.8: Cracks at first bent east of west abutment, I-10 (12/10/01)

7.2.2 US-90 over the San Jacinto River

Figure 7.9 shows a schematic drawing of crack-measurement locations on the US-90 structure. In that figure, numbers and letters indicate relative locations of points along the girders.

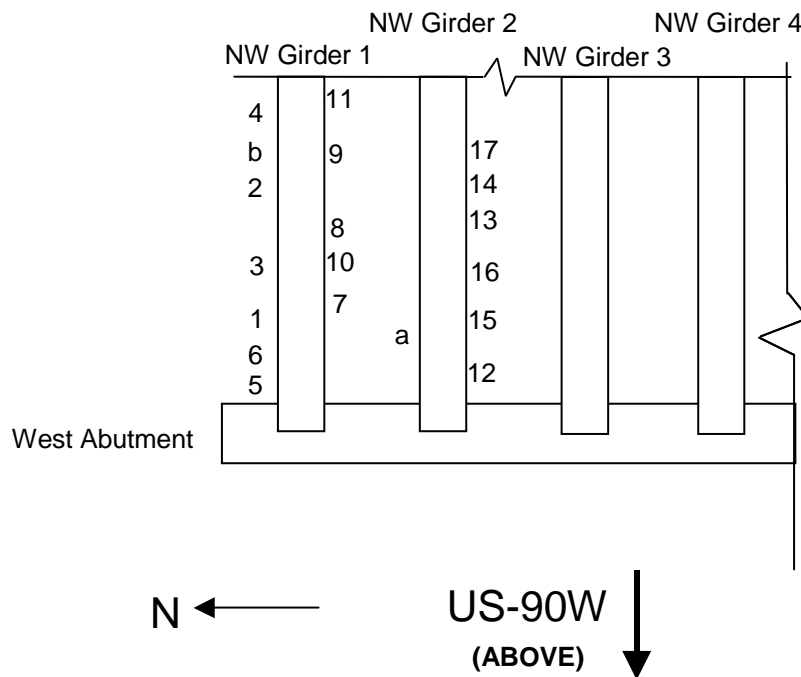


Figure 7.9: Schematic of crack-measurement locations on US-90 structure (plan view)

On May 19, 2000, crack widths at Points 2, 3, and 7 were observed to have changed substantially from the previous visit to the structure. Two new sets of Demec discs were added at newly observed cracks parallel to existing cracks, because it was suspected that the newly observed cracks were affecting the widths of the nearby existing cracks. Four representative areas for crack-ratio measurements were defined as for the I-10 structure. Two areas were drawn on the south surface of NW Girder 1, and two on the north surface of NW Girder 2.

On October 6, 2000, no significant new cracks were noted; existing cracks had widened, however. Two cracks near Point 11 on the south surface of NW Girder 1 were measured to be approximately 0.2 in. (5.1 mm) wide. Cracks were plotted over the representative areas identified on May 19, 2000. Cracks under the drains on the exterior girders had continued to widen. Figure 7.10 shows an

example of significant cracking underneath a drain on Face 5 of the north surface of NW Girder 1.



Figure 7.10: Typical crack under drain at US-90 structure (10/6/00)

On February 19, 2001, most of the monitored cracks showed relatively large increases in width since October 6, 2000. Points 1, 3, 7, and 12, which were located at some of the widest cracks, had continued to widen. High-resolution digital photos were taken of the representative areas on the structure for use in computing crack ratios using digital photo-processing software.

Demec discs were removed from the structure. They had originally been set with 5-minute epoxy on February 6, 1999; at three points, the epoxy had weakened over two years, causing movement of the Demec discs and inconsistent readings.

On June 22, 2001, cracking generally seemed worse than before. Previously noted cracks had extended towards midspan along Face 5 on the

interior girders (Figure 7.11). In addition, many new hairline cracks were noted on the bottom flanges of most girders. Cracks over the representative areas had not changed significantly, however.



Figure 7.11: Extension of existing cracking on north surface (Face 5) of NW Girder 2, US-90 (6/22/01)

Figure 7.12 shows the status of Points 1, 3, 5, and 6 and cracking at the end of NW Girder 1 at the west abutment. Several cracks were visible in the bottom flange on Face 4 and Face 5, and paint was peeling in the deteriorated regions.



Figure 7.12: Cracks at end of NW Girder 1, US-90 (6/22/01)

New Demec discs were mounted at Points 5, 10, 13, 15, and 17 with 30-minute epoxy. Initial measurements were not taken, because the initial separation of the discs was imposed by the setting apparatus.

On December 11, 2001, the girders were discovered to have been sealed and painted. Surface treatment had been applied to the girders. Some cracks were sealed with flexible caulk while others were primed with surface sealant. While all cracks appeared to have been sealed, several sealed cracks had reopened.

Most Demec discs were still attached to the girders. The grease pencil markings and labeling of crack measurement points had been painted over, however. Sixteen of the 19 Demec points were found, and it was possible to take Demec readings at 15 of these points. The specific point numbers and locations were deduced later from previous photos and records. Figure 7.13 shows Point 10 and Point 8, located on the south surface of NW Girder 1.



Figure 7.13: Close-up view of Point 10 (bottom, left pair of Demec discs) and Point 8 (top), US-90 (12/11/01)

Figure 7.14 shows an example of cracks that have apparently occurred in the sealant on Face 4 of the north surface of NW Girder 1. These cracks were located approximately 3 ft (0.91 m) from the end of the girder, and ranged from 0.002 in. (0.05 mm) to 0.02 in. (0.51 mm) wide.

Evidence of cracking in the sealant indicated that the girders at the US-90 structure are continuing to deteriorate. If the girders had not been primed and sealed, the cracks may have looked worse.



Figure 7.14: Apparent cracking through sealant, US-90 (12/11/01)

7.2.3 Robinson Road over I-45

Figure 7.15 shows a schematic drawing of crack-measurement locations on the Robinson Road structure. In the figure, numbers and letters indicate relative locations of points along the girders.

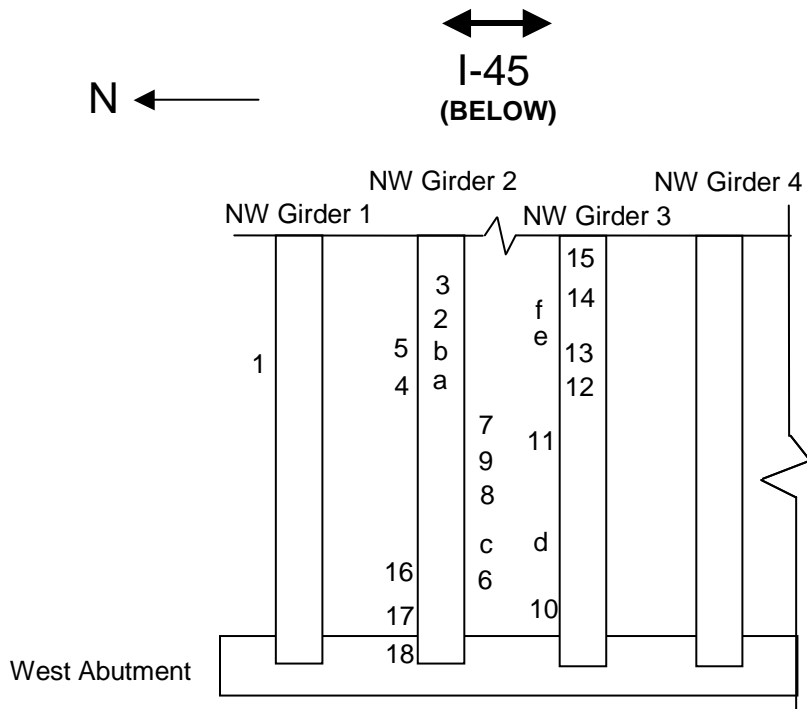


Figure 7.15: Schematic of crack-measurement locations on Robinson Road structure (plan view)

On May 19, 2000, the Robinson Road structure was again monitored, and no substantial changes were noted at any of the cracks. The crack width at Point 9 had decreased slightly. Paint covered the entire bottom flange (Faces 4, 5, and 6) of each girder, and no visible cracks were present on the girder webs (Face 3) at the structure.

On October 7, 2000, narrow cracks had propagated on the girders along the intersection between the top flange and web (intersection between Face 2 and Face 3). This type of cracking was typical of NW Girder 1, NW Girder 2, and NW Girder 3. Figure 7.16 shows an example of this cracking on NW Girder 3, and also illustrates the armor joint seal specific to the Robinson Road structure.



Figure 7.16: Extension of new cracking on south face of NW Girder 3, Robinson Road (10/7/00)

On February 19, 2001, damage on the girders was again observed to be relatively minor compared to the other monitored structures in this study. Most cracks increased slightly in width since the previous visit. One of the Demec discs at Point 17 was no longer present on NW Girder 2, rendering that point unusable.

On June 21, 2001, it was observed that narrow cracks had continued to propagate. Figure 7.17 shows an extension of cracking near the end of NW Girder 2 at the west abutment. The status and locations of Points 16, 17, and 18 are also shown.



Figure 7.17: Extension of cracking on NW Girder 2, Robinson Road (6/21/01)

Longitudinal cracking was also apparent on the underside (Face 6) of NW Girder 2. Cracks extended from the west abutment to the middle of the span, as shown in Figure 7.18. Points 4, 5, and b were originally placed at this location to monitor the widths of the longitudinal cracks.



Figure 7.18: Extension of cracking on underside of NW Girder 2, Robinson Road (6/21/01)

On December 10, 2001, Demec readings were lower than those taken on June 21, 2001 at all points; it was noted, however, that narrow cracks had continued to propagate. Figure 7.19 provides an example of the extension of cracking on NW Girder 2 throughout the course of the field study. Figure 7.20 shows a crack propagating past the point where it had been previously sealed.

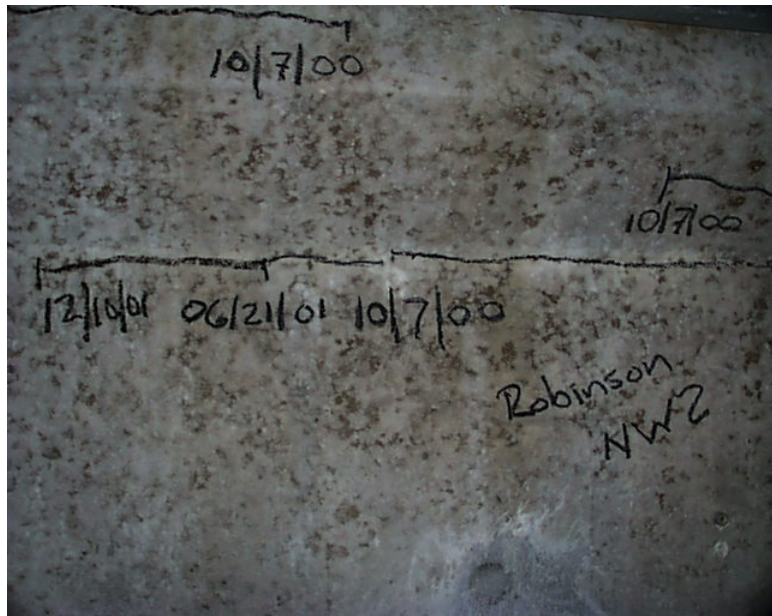


Figure 7.19: Extension of cracking on north surface of NW Girder 2, Robinson Road, at west abutment (12/10/01)

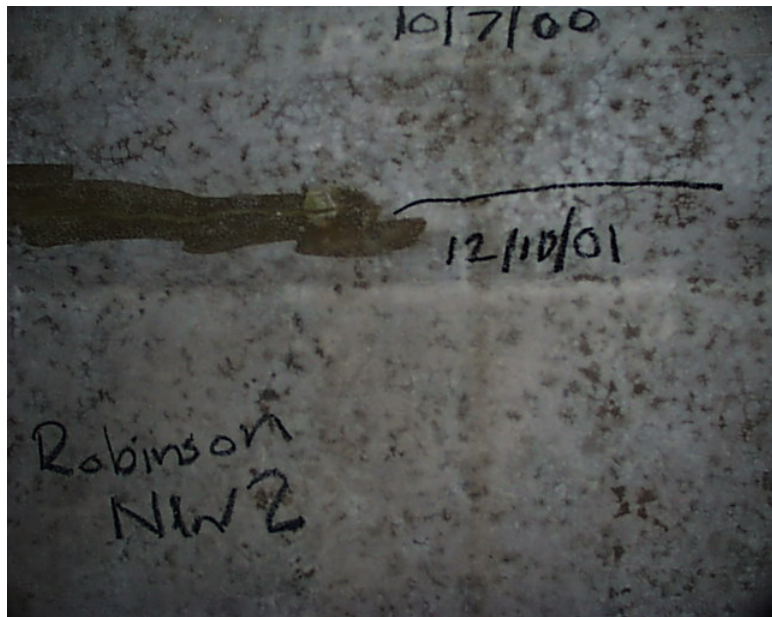
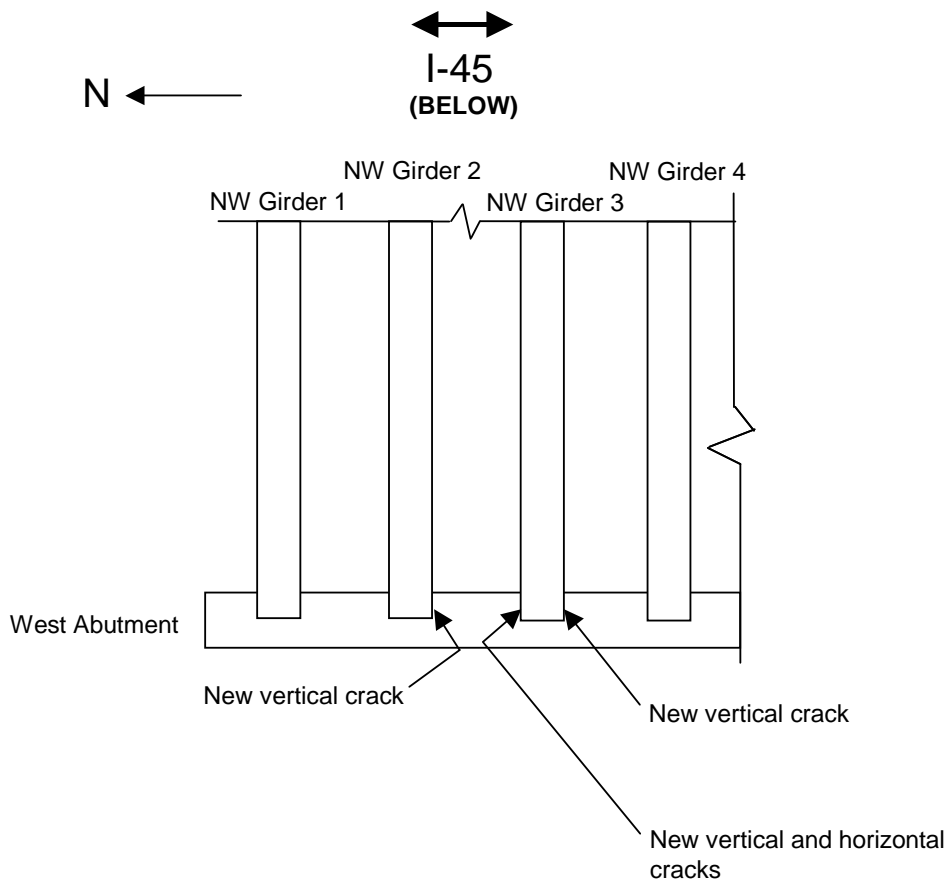


Figure 7.20: Extension of cracking past sealant on south surface of NW Girder 2, Robinson Road, at west abutment (12/10/01)

New cracks had become apparent on NW Girder 2 and NW Girder 3 at the site. A schematic diagram of the location of new cracks is shown in Figure 7.21. Figure 7.22 shows an example of new cracks on NW Girder 3.



**Figure 7.21: Location of new cracks on Robinson Road structure (plan view)
(12/10/01)**

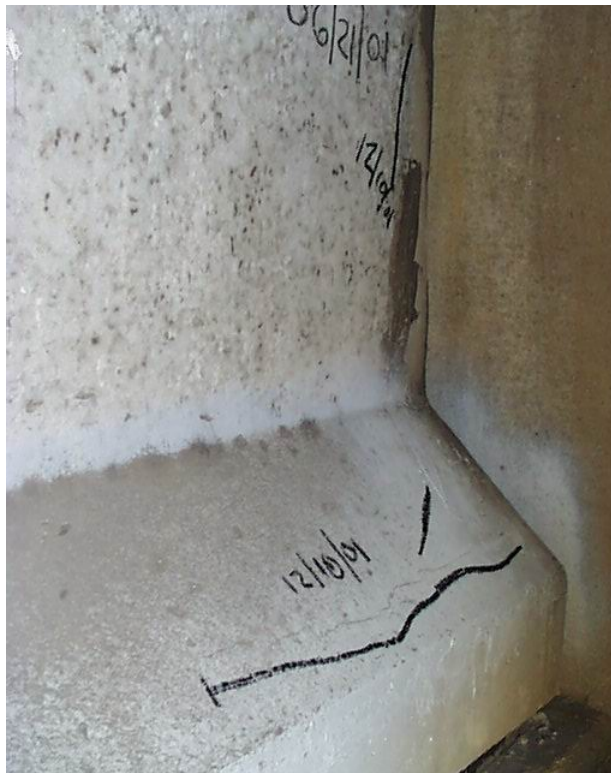


Figure 7.22: New cracks on north surface of NW Girder 3, Robinson Road, at west abutment (12/10/01)

7.2.4 Beltway 8 over State Highway 3

An overview of the bridge site is shown in Figure 7.23.



Figure 7.23: Overview of Beltway 8 over State Highway 3 (facing north)

Figure 7.24 shows a schematic drawing of crack-measurement locations on the Beltway 8 structure. The structure consists of four independent bridges spanning State Highway 3 in the east-west direction: eastbound frontage road; eastbound Beltway 8 main lanes; westbound Beltway 8 main lanes; and westbound frontage road. Each bridge contained eight Type-IV prestressed girders, as shown in Figure 7.25. Because of the limited maneuverability of the lifting equipment provided by TxDOT, cracks were monitored only on exterior faces of exterior girders.

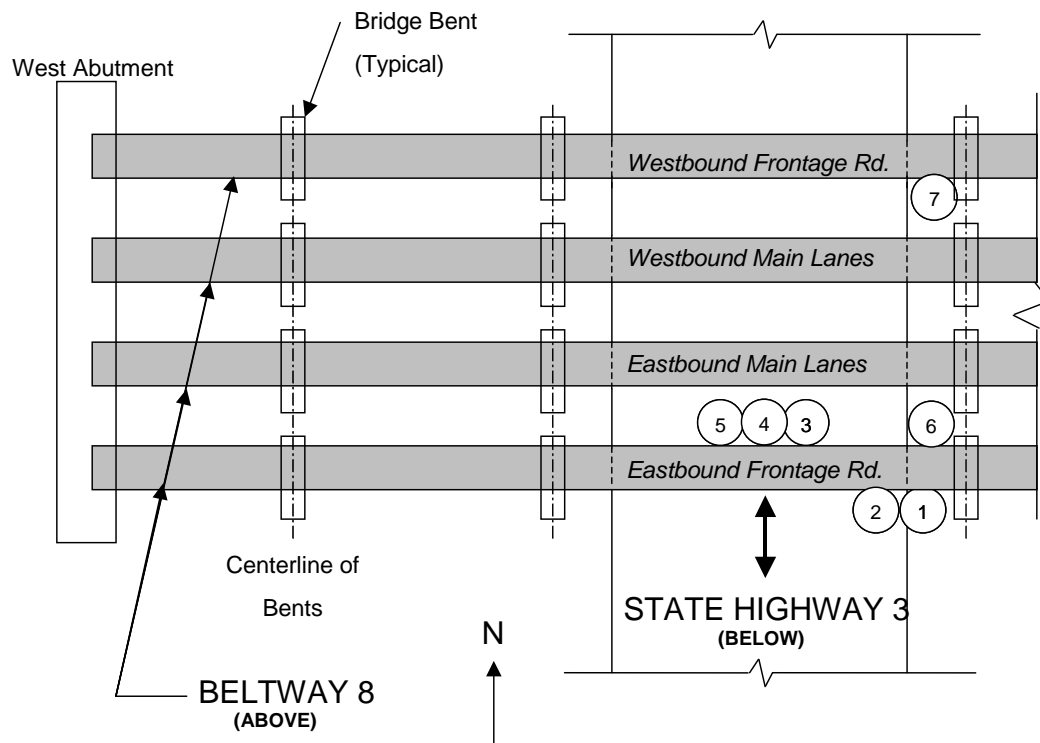


Figure 7.24: Schematic of crack-measurement locations on Beltway 8 structure (plan view)



Figure 7.25: Overall view of Points 3-5, Beltway 8 (facing south) (6/22/01)

On May 19, 2000, the only remaining set of Demec discs on the Beltway 8 structure was at Point 3. Crack widths were measured with a crack comparator card and optical scope, and none of the cracks was observed to have changed substantially from the previous visit on February 11, 2000. Two representative areas were defined to monitor crack ratios on the exterior girder of the south structure, similarly to the other structures in the study. The monitored areas were located on Face 4 and Face 5 of the exterior surface, approximately 2 ft. (0.61 m) from the end of the girder (near Point 1).

On October 12, 2000, none of the Demec discs placed on June 5, 1999 remained on the structure. Crack widths were measured with a crack comparator card and optical scope. An increase in crack width was noted in the representative area on Face 5 of the exterior girder in the south structure. A considerable change in crack width was observed on Face 5 of the north girder in the south structure, at the support. Acoustic emission (AE) data were collected by Chotickai (2001) at the site as part of the collateral work for this study.

On February 20, 2001, crack monitoring was again performed. None of the cracks had changed substantially from the previous observations on October 12, 2000. High-resolution digital photos were taken of the representative areas on the exterior girder for crack-ratio calculations.

On June 22, 2001, the previously marked crack-measurement points were located. Demec discs were reinstalled at Points 1-5 with 30-minute epoxy (Figure 7.23). An overall view of Point 1 is shown in Figure 7.26. The contrast between damaged and undamaged girders is visible in the figure.



***Figure 7.26: Overall view of Point 1, Beltway 8 structure (facing north)
(6/22/01)***

Figure 7.27 shows a close-up view of Point 1 and the representative areas previously defined on Face 4 and Face 5 for crack-ratio calculations.



Figure 7.27: Close-up view of Point 1, Beltway 8 structure (6/22/01)

Two new sets of Demec discs were added to the structure at Point 6 and Point 7 (Figure 7.24). A wide crack existed at Point 6 on Face 5 of the girder, as shown in Figure 7.28.



Figure 7.28: Close-up view of Point 6, Beltway 8 structure (6/22/01)

Similar cracking was observed at Point 7 on Face 5 of the south girder of the westbound frontage road bridge. Figure 7.29 shows an overall view of Point 7.



**Figure 7.29: Overall view of Point 7, Beltway 8 structure (facing north)
(6/22/01)**

On December 11, 2001, it was discovered that the girders had been recently painted. In some cases, cracks on the girders had been sealed with flexible caulk and primed. All Demec discs set on the previous visit were still present, except for one missing Demec disc at Point 2. The new discs at Point 1 were too far apart to take a reading; and at Point 7, the discs were too close. The most likely reason for the out-of-range state of discs at Points 1 and 7 is that the

30-minute epoxy did not cure quickly enough when the points were set on June 22, 2001.

Paint was removed from the discs, and readings were taken with the Demec gauge at Points 3-6. Because of the paint, it was not possible to measure crack widths with the crack comparator card or optical scope. Some remaining exposed cracks to the left of Point 6 (Figure 7.30) were measured to be 0.03 in. (0.76 mm) to 0.05 in. (1.27 mm) wide, however. It was not clear whether these cracks had not been filled and sealed completely, or whether continued expansion of the concrete had reopened them.



Figure 7.30: Cracking near Point 6, Beltway 8 structure (12/11/01)

Figure 7.31 shows a typical example of sealed cracks along the bottom flanges (Face 4 and Face 5) of several girders.



Figure 7.31: Sealed cracks along girder flange near Point 6, Beltway 8 structure (12/11/01)

Because of the cold, wet conditions on December 11, 2001, no Demec discs were replaced at any of the missing or unusable Demec point locations because the epoxy would not have set in those conditions.

7.2.5 FM 1929 over Lake Ivie

The east profile of the Lake Ivie bridge structure is shown in Figure 7.32, and a plan map is shown in Figure 7.33. Figure 7.34 shows a schematic of a typical bent.

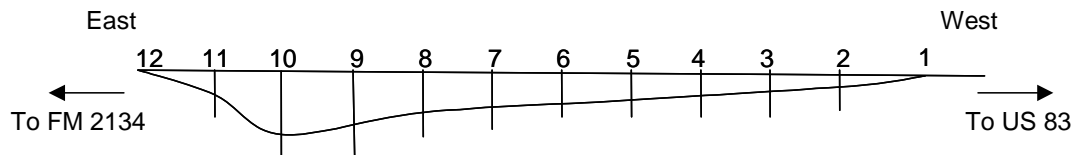


Figure 7.32: North profile of Lake Ivie structure

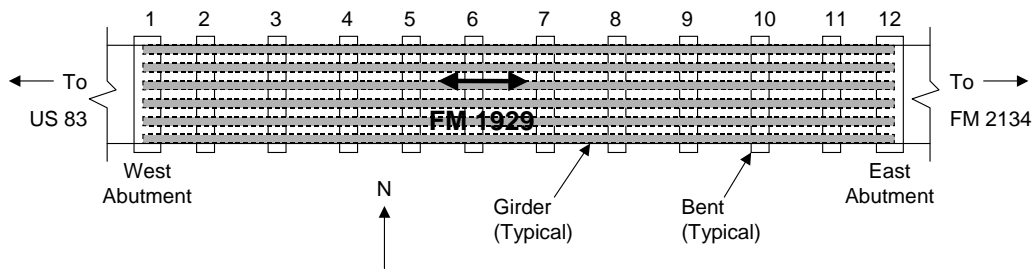


Figure 7.33: Plan view of Lake Ivie structure

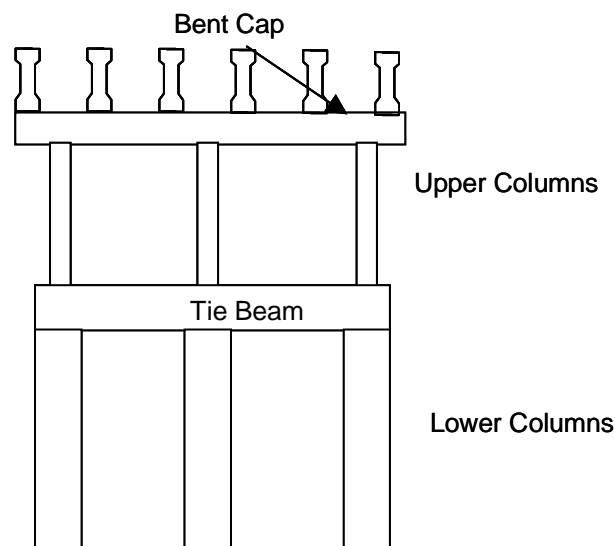


Figure 7.34: Schematic drawing of typical bent for Lake Ivie structure

The lower columns in Bents 2-4 have a diameter of 36 in. (0.91 m), and the lower columns in Bents 5-11 have a diameter of 48 in. (1.22 m). Each lower column is supported by a drilled shaft of the same diameter, at least 33 ft. (10 m) deep¹.

Cracks were marked and Demec discs installed at seven points on Bent 5, as shown in Figure 7.35: Points 1 and 2 on the interior face of the south girder; Point 3 in the top of the bent cap, between the first and second girders; Point 4 on the west side of the bent cap, between the first and second girders; Points 5 and 6

¹ Personal communication, Brian Merrill (TxDOT), April 2002.

on the top of the tie beam; and Point 7 on the west side of the south column. An overall view of Bent 5 is shown in Figure 7.36.

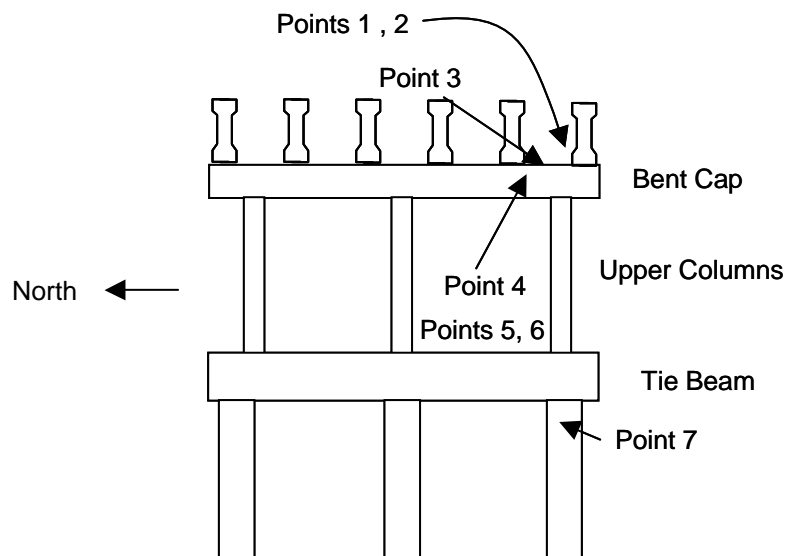


Figure 7.35: Schematic drawing of crack-measurement locations on Bent 5



Figure 7.36: Overall view of Bent 5 (facing north)

In a similar fashion, cracks were marked and Demec discs installed at three points on Bent 9, as shown in Figure 7.37: Point 8 on the top of the bent cap, between the first and second girders; Point 9 on the west side of the bent cap, between the first and second girders; and Point 11 on the exterior face of the south girder. An overall view of Bent 9 is shown in Figure 7.38.

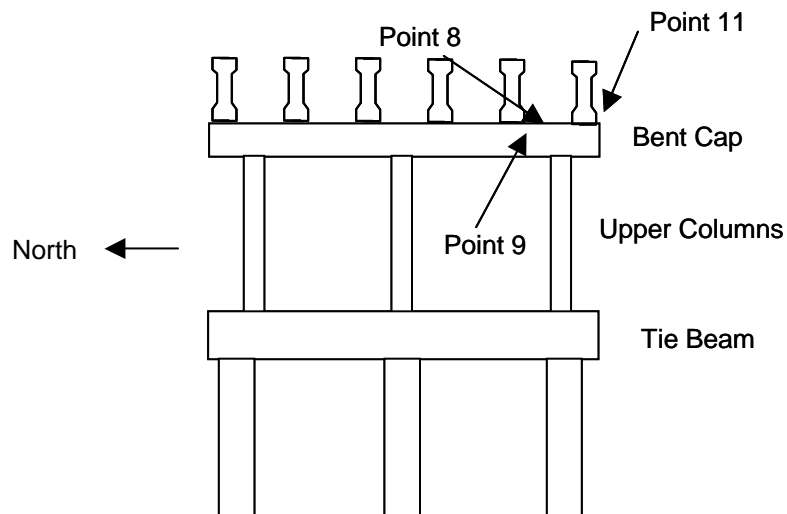


Figure 7.37: Schematic drawing of crack-measurement locations on Bent 9



Figure 7.38: Overall view of Bent 9 (facing west)

Point 10 was located near the waterline on the north column of Bent 11 (Figure 7.39). No Demec discs were affixed to the structure at this point; crack-width measurements were made with a crack comparator card.

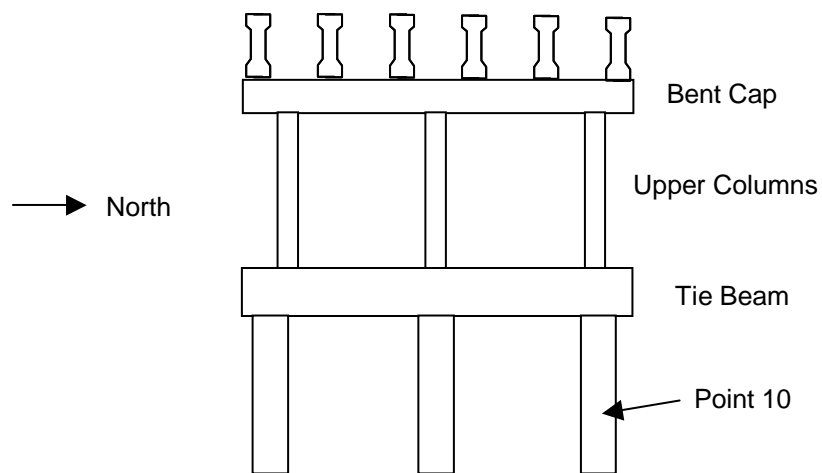


Figure 7.39: Schematic drawing of crack-measurement location on Bent 11

On December 18, 2000, the degree of deterioration of the Lake Ivie structure was observed to be approximately the same as that observed during the first visit on September 29, 1999.

Nine crack locations were marked, and Demec points were set on the structure for crack width monitoring. Bents 5 and 9 were chosen for closer inspection due to the concentration of damage at these bents. Expansion joints were located at these bents, and Bent 5 and Bent 9 therefore had greater exposure to rainwater than the other bents. Greater exposure to rain leads to higher premature concrete deterioration (Boenig 2000).

Cracking was apparent at Bent 5 in the bent caps, tie beams, and columns, and also at the ends of the girders. Figure 7.40 shows the condition of the tie beam at Bent 5 during the inspection on December 18, 2000.



Figure 7.40: Map cracking on tie beam, Bent 5 (12/18/00)

Bent 9 also displayed cracking in the bent caps, tie beams, columns, and ends of the girders (Figure 7.41). Damage was similar to Bent 5 but generally less severe.



Figure 7.41: Cracking on bent cap, Bent 9 (12/18/00)

Representative squares were drawn on the south end of the bent cap at Bent 5 (Figure 7.42) and Bent 9. Cracks were plotted in the 12 in. (0.31 m) squares throughout the field study.



*Figure 7.42: 12 in. (0.31 m) square on south end of bent cap, Bent 5
(12/19/00)*

On April 24, 2001, damage to the structure was overall slightly worse than the previous visit. Cracks were wider on the south ends of the bent caps at Bent 5 and Bent 9, but the increase in width was minimal. New cracks had formed in these locations as well. Figure 7.43 shows cracking in the 12 in. (0.31 m) square on the south face of the bent cap at Bent 9.

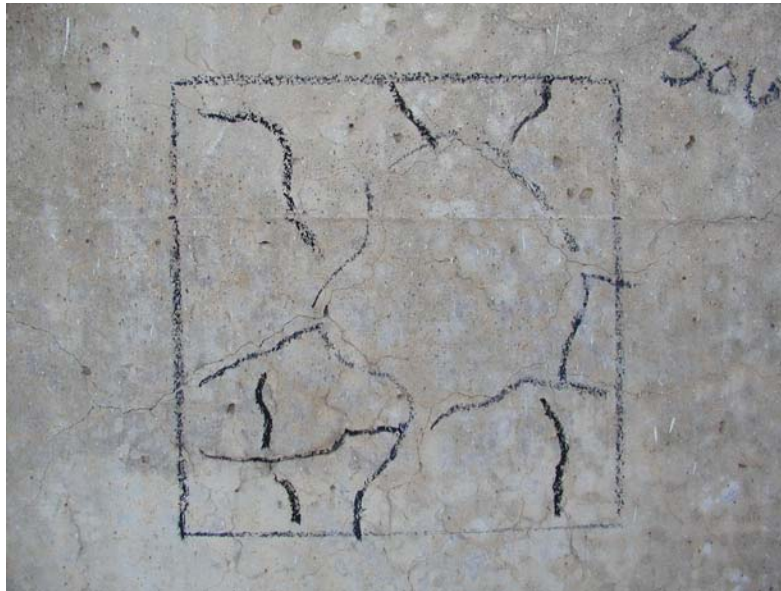


Figure 7.43: 12 in. (0.31 m) square on south end of bent cap, Bent 9 (4/24/01)

Cracking in the columns near the waterline had become more pronounced in several bents. Figure 7.44 shows vertical cracking in Bent 5. Point 10 was marked on the north column of Bent 11 (Figure 7.45). A new horizontal crack, 0.002 in. (0.05 mm) wide, was apparent at Point 10.



Figure 7.44: Example of column cracking near waterline of Bent 5 (4/24/01)



*Figure 7.45: Example of column cracking near waterline of Bent 11 (Point 10)
(4/24/01)*

On October 15, 2001, deterioration was slightly worse than the previous visit; in some areas, cracks were not noticeably different, however. Some new

cracks had formed on the south ends of the bent caps at Bent 5 and Bent 9. Figure 7.46 shows map cracking on the south end of the bent cap at Bent 5. New cracks are labeled with the date 10/15/01.

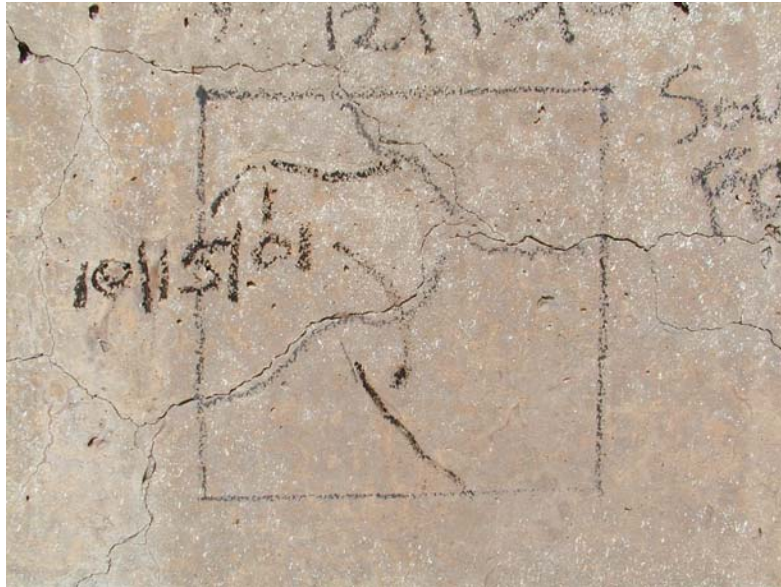


Figure 7.46: New cracks on 12 in. (0.31 mm) square on south end of bent cap, Bent 5 (10/15/01)

Point 11 was placed on October 15, 2001, on the exterior face of one of the south girders at Bent 9. New cracks had formed at that location since the previous visit to the bridge on April 24, 2001 (Figure 7.47 and Figure 7.48). Similar cracks became apparent on the exterior faces of the south girders at Bent 5.



*Figure 7.47: New cracks on exterior faces of south girders at Bent 9
(10/15/01)*



Figure 7.48: Close-up of new cracks on south girder at Bent 9 (10/15/01)

Vertical cracks at Point 10 on Bent 11 had widened to 1/8 in. (3.2 mm). These long, wide cracks extended upwards to the bottom of the tie beam. Figure

7.49 and Figure 7.50 show the status of cracks near the waterline on Bent 11 on October 15, 2001. The horizontal crack visible at Point 10 had widened to approximately 0.013 in. (0.25 mm) (Figure 7.51).



Figure 7.49: Column cracking at Point 10 near waterline, Bent 11 (10/15/01)



Figure 7.50: Close-up of vertical cracking at Point 10 near waterline, Bent 11
(10/15/01)



Figure 7.51: Close-up of horizontal crack at Point 10 near waterline, Bent 11
(10/15/01)

7.3 RESULTS FROM CRACK-WIDTH MEASUREMENTS

7.3.1 I-10 over AT & SF RR

Figure 7.52 shows crack widths over time at each point for the I-10 structure as determined from Demec measurements. With the exception of Point 7, all Demec discs were installed on November 28, 1998. Demec discs were added to the structure at Point 7 on February 6, 1999. Readings were first taken at Point 4 on October 22, 1999. All Demec discs were set with 30-minute epoxy, and remained on the structure throughout the field study.

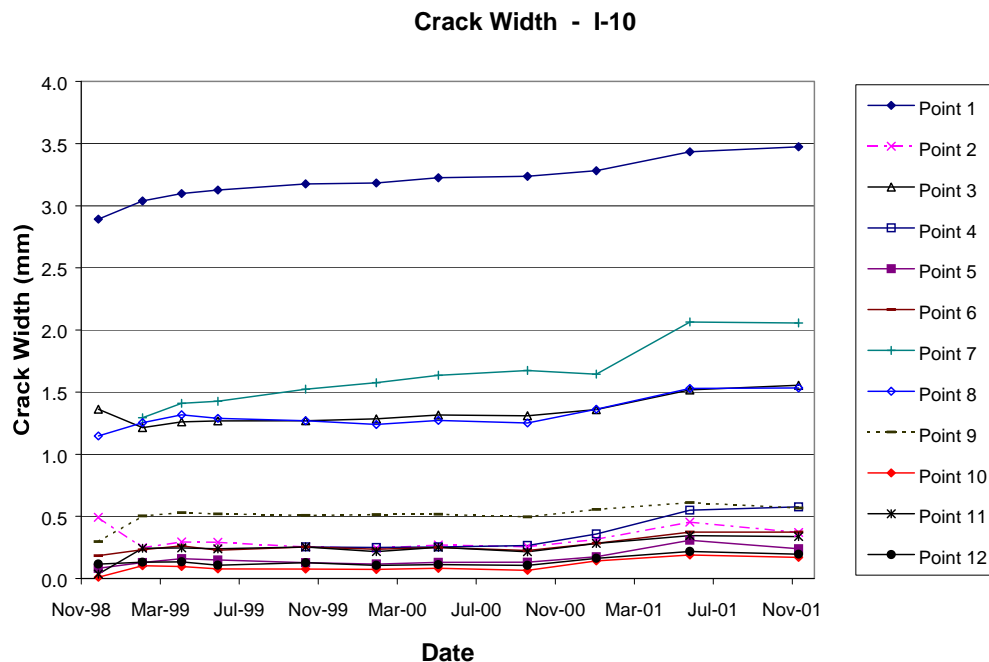


Figure 7.52: Crack width over time for I-10 structure

Cracks gradually widened over the course of the field study; they widened more rapidly between October 7, 2000 and June 21, 2001.

7.3.2 US-90 over the San Jacinto River

Figure 7.53 shows crack widths over time at each point for the US-90 structure as determined from Demec measurements. Demec discs were installed and initial measurements were taken on February 6, 1999.

On June 21, 2001, Demec discs were replaced and set with 30-minute epoxy at Points 5, 10, 13, 15, and 17. Initial readings were taken for these new discs on December 11, 2001. A second set of Demec readings at the new points is needed in order to show the crack width at these points over a greater time range. Unfortunately, those data are not available at this time.

Data for Point 10 were unavailable until December 11, 2001, and are not presented here. Demec discs were missing from the structure on December 11, 2001 at Points 2, 4, 6, and b.

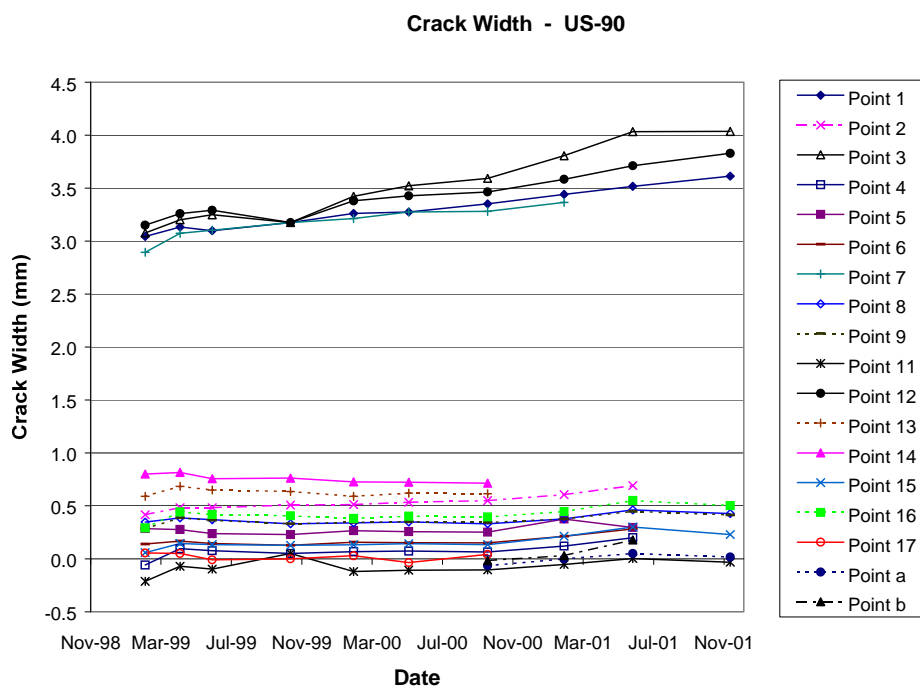


Figure 7.53: Crack width over time for US-90 structure

Cracks at Points 1, 3, 7, and 12 were significantly wider than at all other monitored points, and experienced dramatic increases in width compared to the majority of measurement points on the US-90 structure. Crack widths at other points remained below 1 mm and displayed gradual increases and decreases.

7.3.3 Robinson Road over I-45

Figure 7.54 shows the crack width over time at each point for the Robinson Road structure as determined from Demec measurements. Demec discs were installed at Points 1-15 on February 6, 1999, and at Points 16-18 on April 9, 1999.

On June 21, 2001, Demec discs were replaced and set with 30-minute epoxy at Points 2, 3, 8, 10, and 17. Initial readings were taken for these new discs on December 11, 2001. A second set of Demec readings at the new points is needed in order to show the crack width at these points over a greater time range. Unfortunately, data are not available at this time.

Data for Points 2, 3, and 10 are unavailable between February 6, 1999 and December 10, 2001, and are not presented here.

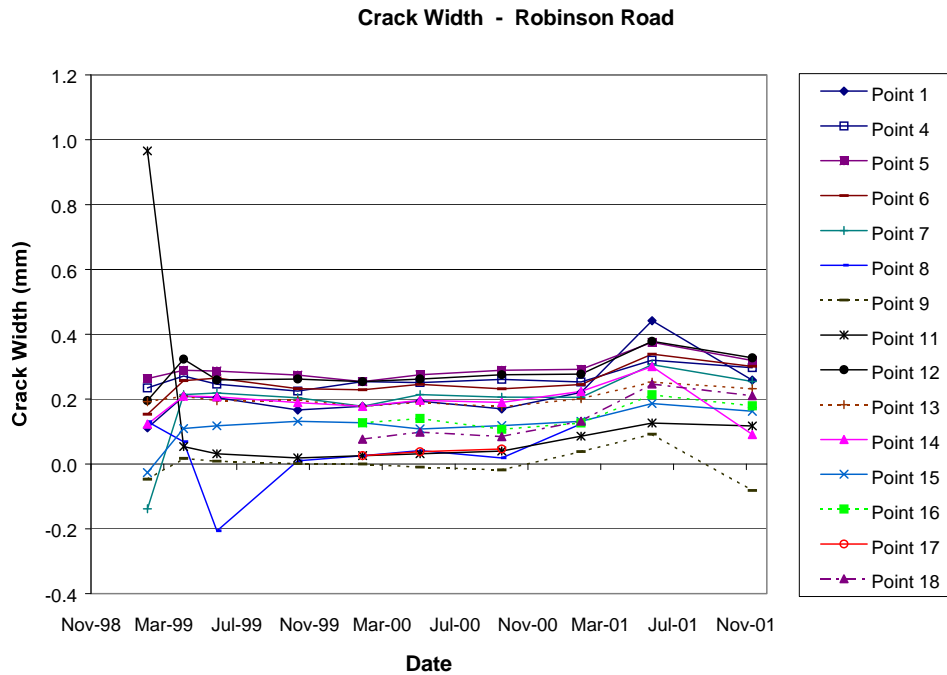


Figure 7.54: Crack width over time for Robinson Road structure

Cracks at the Robinson Road structure behaved like those of the other bridges monitored in this study. Most crack widths were about 0.3 mm throughout the field-observation program. Between February 19, 2001 and June 21, 2001, cracks generally widened at all points; between June 21, 2001 and December 10, 2001, they generally narrowed.

7.3.4 Beltway 8 over State Highway 3

Figure 7.55 shows crack widths over time at each point for the Beltway 8 structure as determined from crack comparator card measurements. All Demec discs which had originally been set on June 5, 1999 with 5-minute epoxy were missing from the structure on October 12, 2000. The discs were replaced on June 22, 2001 and set with 30-minute epoxy at Points 3-6. Initial readings were taken for these new discs on December 11, 2001. A second set of Demec readings at

the new points is needed in order to show the change in crack width at these points over time. Unfortunately, those data are not available at this time. Because insufficient Demec data are not available for crack width calculations, crack comparator measurements are presented for the Beltway 8 structure.

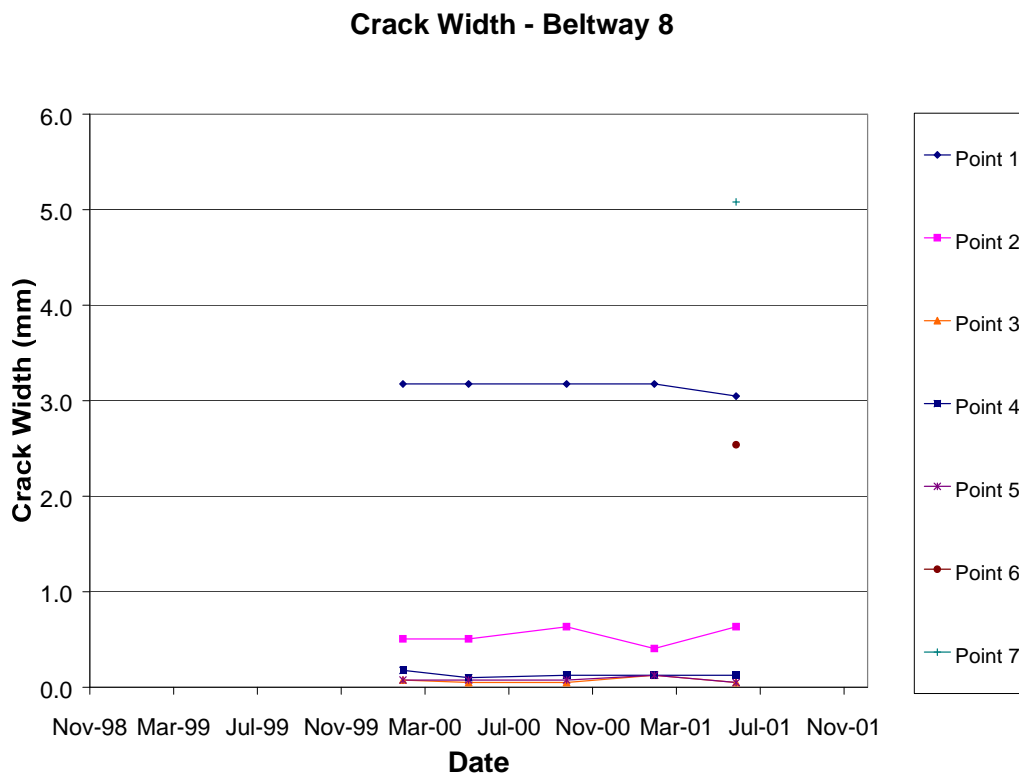


Figure 7.55: Crack width over time for Beltway 8 structure

Cracks did not generally widen or narrow significantly; Demec readings, however, may have shown greater changes between visits to the structure. It is very difficult to evaluate gradual changes with a crack comparator card.

7.3.5 FM 1929 over Lake Ivie

Figure 7.56 shows crack widths over time at each point for the Lake Ivie structure as determined from Demec measurements.

On April 24, 2001, all Demec discs, which had been affixed to the structure with 5-minute epoxy on December 18, 2000, were replaced with new discs set with 30-minute epoxy. Initial readings were taken with the new discs at Points 1, 3-6, 8, and 9 on October 15, 2001. The discs set on December 18, 2000, continued to be used for Point 2 and Point 7. A second set of Demec readings at the new points is needed in order to show crack widths over a greater time range. Unfortunately, those data are not available at this time.

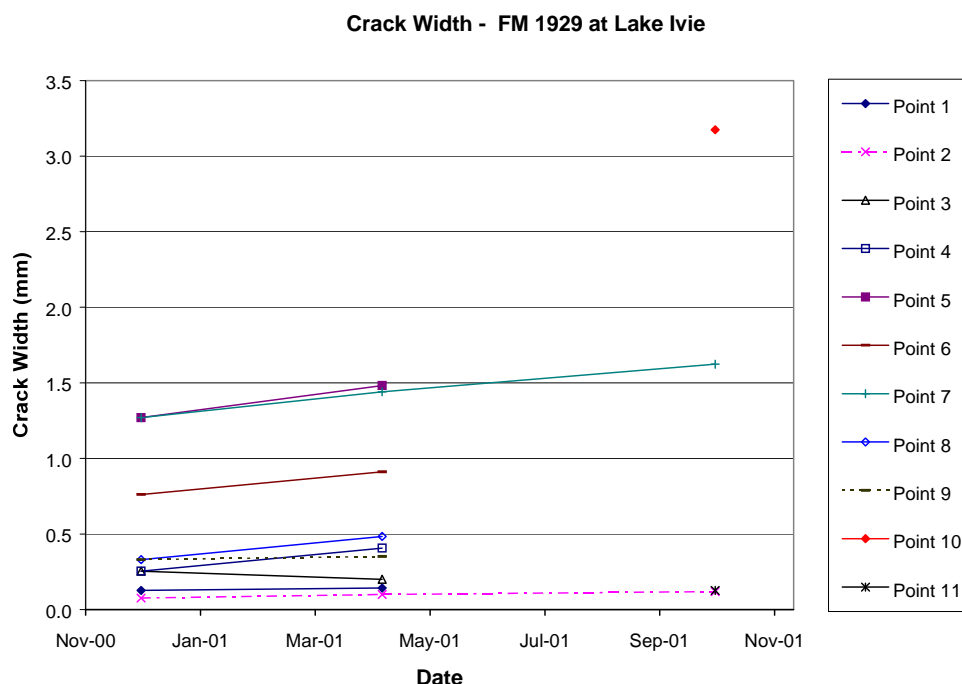


Figure 7.56: Crack width over time for FM 1929 at Lake Ivie

Figure 7.57 shows crack comparator card measurements over time for the Lake Ivie structure. As discussed previously by Boenig (2000), this method of crack measurement is subjective. It is often difficult to measure the crack accurately with the crack comparator card. Using the Demec gauge to measure change in crack width is considered to be the most accurate. Although a crack

comparator is not as accurate, the data show some consistency, at least for the period between December 18, 2000, and April 24, 2001.

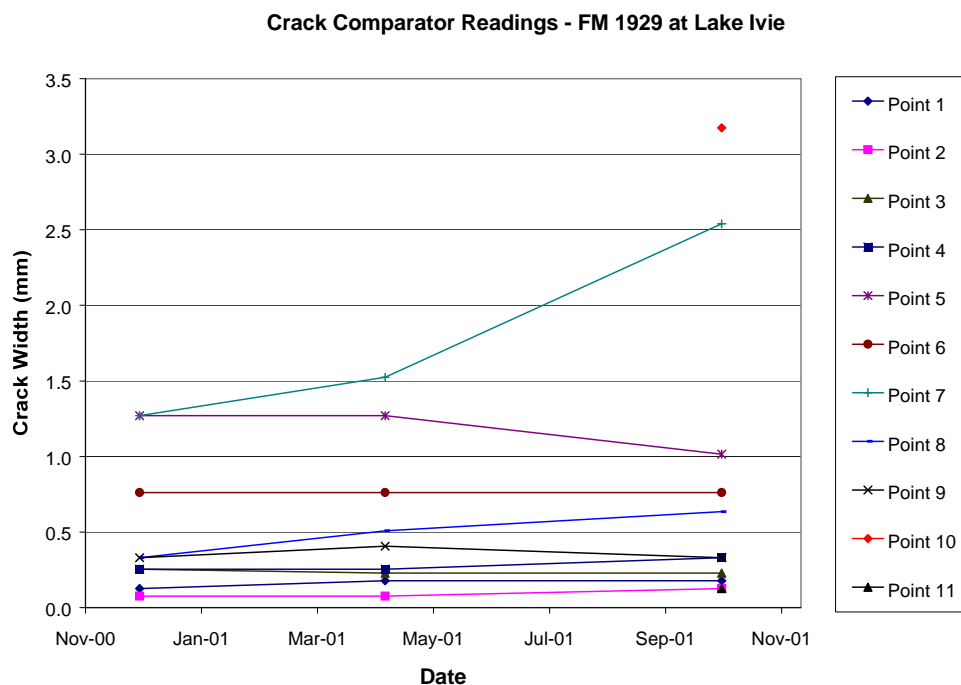


Figure 7.57: Crack comparator readings over time for FM 1929 at Lake Ivie

Cracks on the Lake Ivie structure are gradually widening or unchanging. Crack comparator measurements at Point 5 and Point 9 on October 15, 2001, however, indicate that these cracks narrowed following the April 24, 2001 visit.

Damage indices were computed using Equation 3-1 for the two representative areas on the south ends of the bent caps at Bent 5 and Bent 9. Table 7.1 and Table 7.2 list field damage indices recorded at Lake Ivie during the field study. Figure 7.58 shows damage indices over time on the bent caps.

Table 7.1: *Field damage indices for bent cap, Bent 5, Lake Ivie*

Date	Damage Index
December 19, 2000	49,000
April 24, 2001	50,000
October 15, 2001	50,420

Table 7.2: *Field damage indices for bent cap, Bent 9, Lake Ivie*

Date	Damage Index
December 19, 2000	2,260
April 24, 2001	2,308
October 15, 2001	2,308

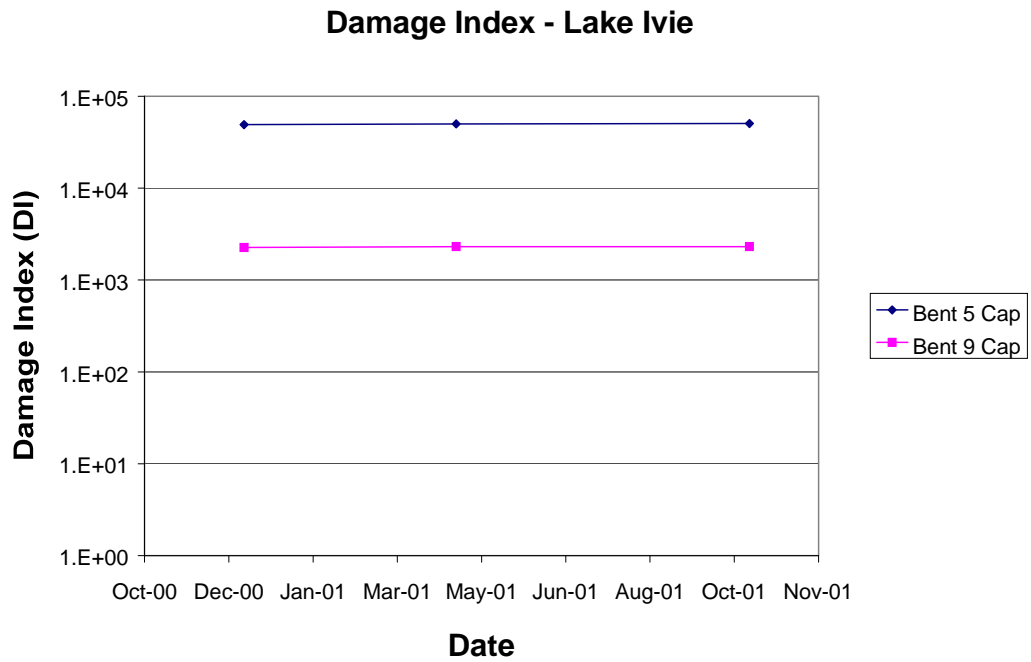


Figure 7.58: Damage Index over time for FM 1929 at Lake Ivie

The damage index for representative area on the south end of the Bent 5 cap is increasing at an average rate of 1729 units/year (3.5% per year), and the damage index for the representative area on the south end of the Bent 9 cap is increasing at an average rate of 59 units/year (2.5% per year).

CHAPTER 8

Significance of Field Results

This chapter discusses the significance of the results presented in Chapter 7 from the field observation program.

The damage trends and patterns observed by Boenig (2000) continued. Cracks continued to grow at approximately the same rate. New cracks formed on similar regions of the girders at the five different structures throughout the study. In general, observations made between May 2000 and December 2001 were similar to those made between November 1998 and February 2000, except that the degree of damage was slightly worse in the latter half of the field study.

The results from the field observation of five structures in different parts of Texas have shown that damage is concentrated in elements with a severe exposure to wetting. In all structures monitored, the most intense cracking has been observed close to the ends of girders, directly below expansion joints. Other elements displaying accelerated deterioration have included girder flanges underneath drain spouts, and columns at Lake Ivie.

Severity of exposure to water continued to affect the rate of deterioration of the structures. For example, cracks grew significantly in the I-10 structure, US-90 structure, and Beltway 8 structure. These three structures were considered to have severe exposure because they were located in areas of high rainfall and had poorly sealed expansion joints (Boenig 2000).

Except for the vertical cracks in the columns, crack widths at Lake Ivie tended to be narrower than those at the I-10, US-90, and Beltway 8 structures. The Lake Ivie structure had moderate exposure because Concho, Texas receives approximately half the amount of annual rainfall as southeast Texas (National

Climatic Data Center 2002). The degree of exposure for the Robinson Road structure was defined as mild because The Woodlands receives slightly less rainfall, and the structure's expansion joints were well sealed (Boenig 2000). No significant crack growth was observed on the Robinson Road structure.

Results from the field observation program illustrate the effect of exposure on visible damage. Figures 8.1 through 8.6 show crack widths and changes in crack widths, determined from Demec readings, versus the age of the girders monitored in the I-10, US-90, and Robinson Road structures. Information was not available regarding the exact casting dates for the Beltway 8 structure; therefore, relationships between crack width and age for that structure are not presented here. The casting dates for the Lake Ivie girders and bents are known; not enough data are available, however, to show crack widths versus age over a significant time range for that structure.

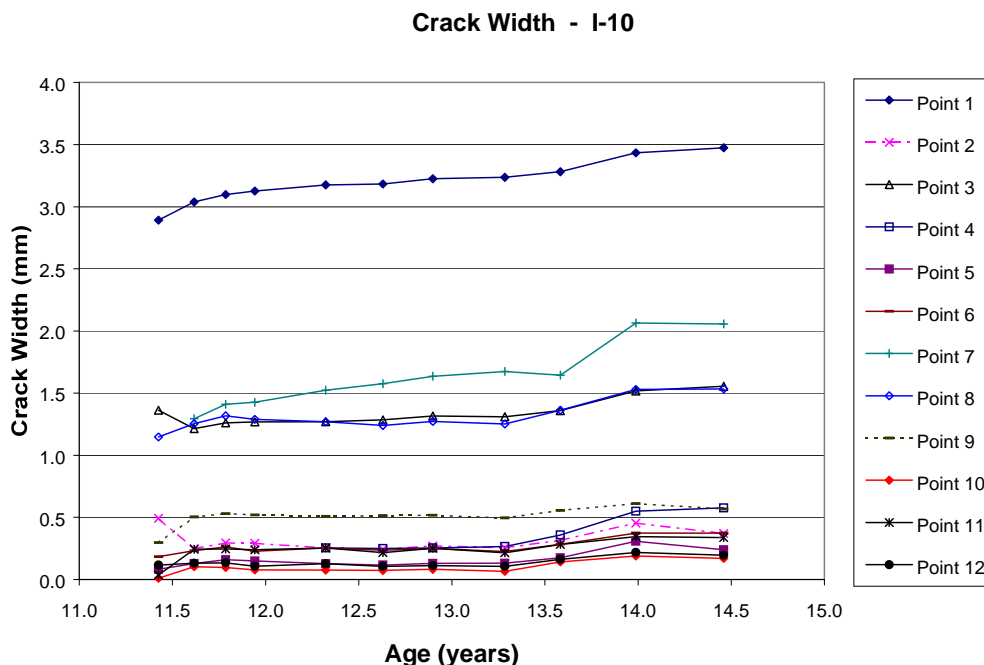


Figure 8.1: Crack width versus age of girder for the I-10 structure

Change in Crack Width - I-10 Beaumont

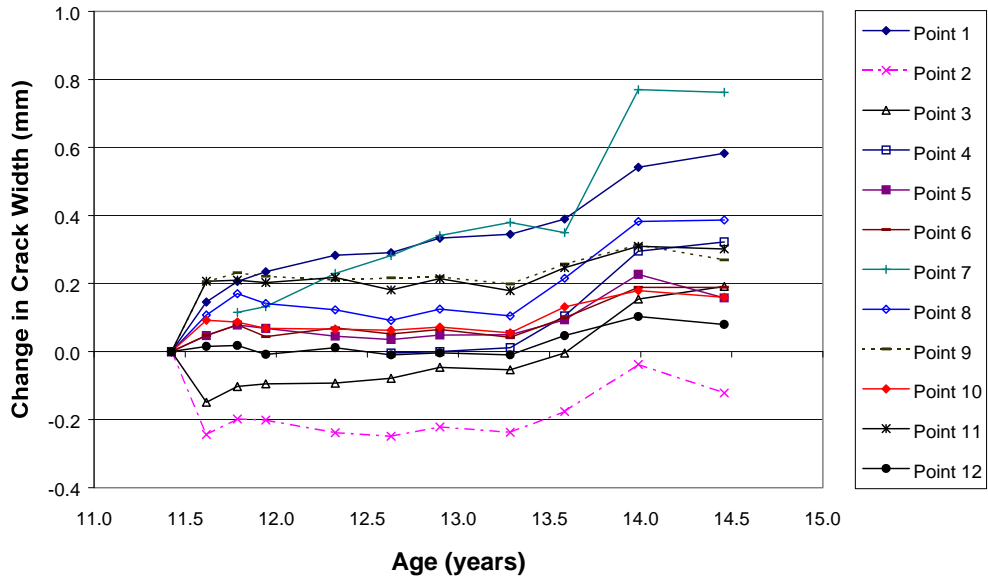


Figure 8.2: *Change in crack width versus age of girder for the I-10 structure*

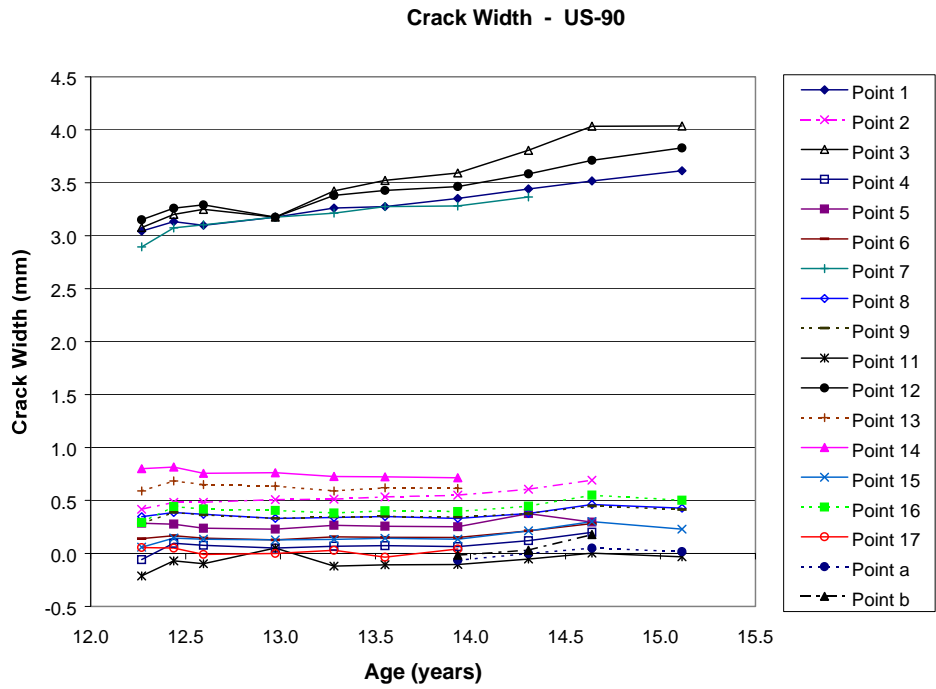


Figure 8.3: Crack width versus age of girder for the US-90 structure

Change in Crack Width - US-90

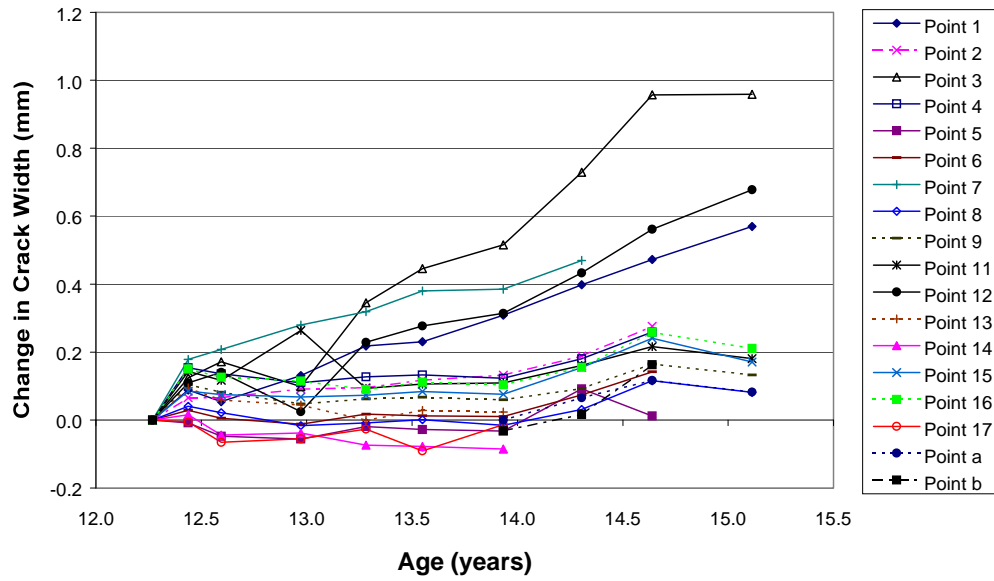


Figure 8.4: Change in crack width versus age of girder for the US-90 structure

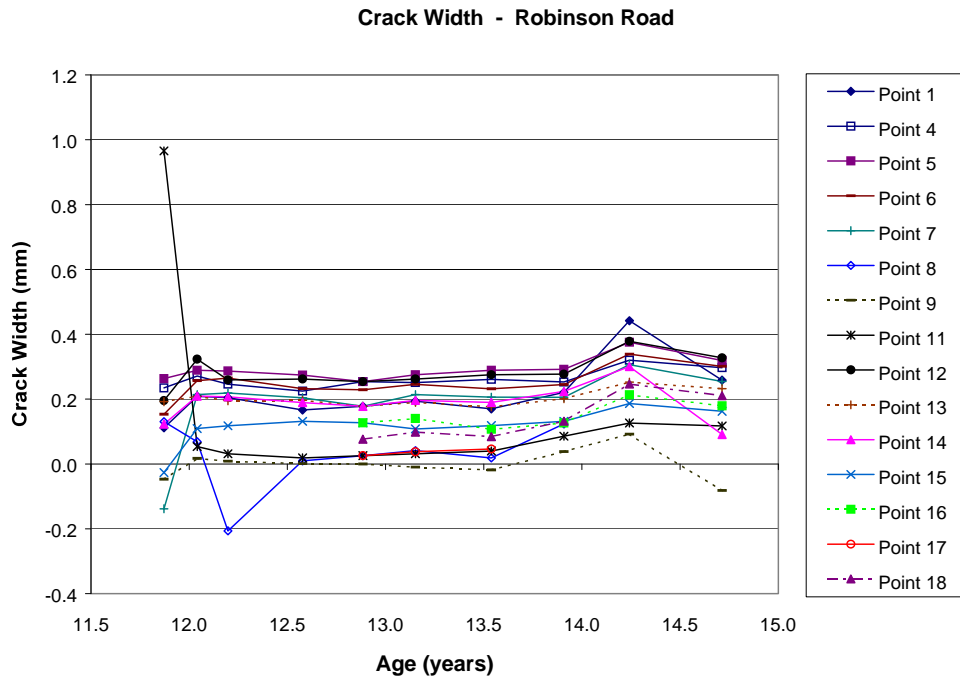


Figure 8.5: Crack width versus age of girder for the Robinson Road structure

Change in Crack Width - Robinson Road

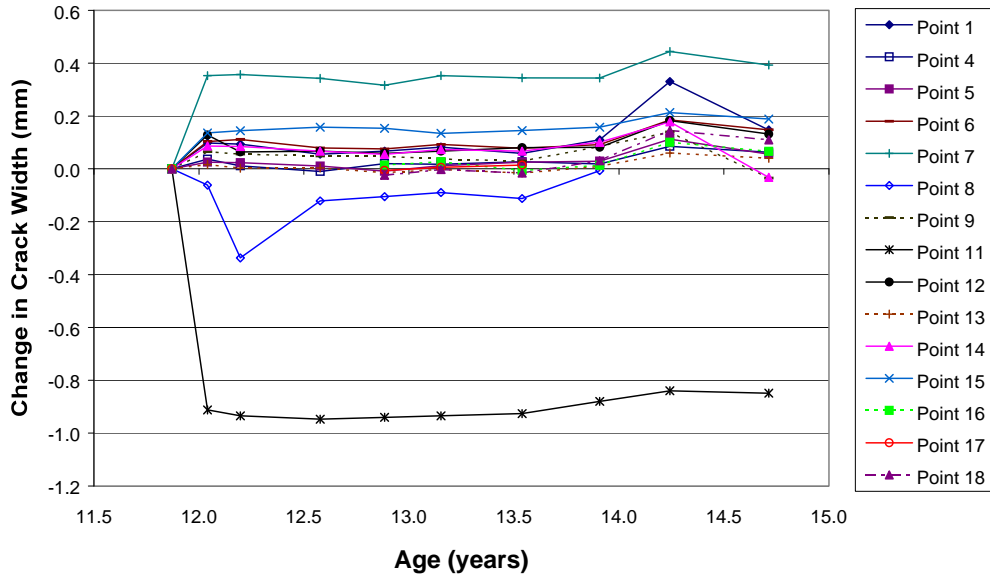


Figure 8.6: Change in crack width versus age of girder for the Robinson Road structure

The widest and fastest-growing cracks in the I-10 and US-90 structures were located in the bottom flanges, close to the ends of the girders. At the I-10 structure, cracks at Points 1, 3, 7, 8 were significantly wider than cracks at other measurement points. Those cracks grew at a slightly faster rate than the other monitored cracks; all cracks in the I-10 structure continued to increase in width, however. Points 1, 3, 7, 8 were either on Face 4 or Face 5, and were all within 65 in. (1.65 m) of the ends of their respective girders at the west abutment.

At the US-90 structure, cracks at Points 1, 3, 7, and 12 were significantly wider than at other measurement points. Those four cracks were the only ones to widen substantially; other cracks experienced only slight widening. Points 1, 3, 7,

and 12 were on Face 4 or Face 5 and were all within 53 in. (1.35 m) of the ends of their respective girders at the west abutment.

The behavior of cracks at those eight points on the I-10 and US-90 structures shows that severe exposure to water can be directly linked to accelerated crack growth. These observations match those of Boenig (2000) in earlier stages of the field observation program.

Of the five structures studied, the Robinson Road structure had the narrowest cracks and the slowest rate of deterioration. Much of this can be attributed to the armor joint seal that kept rainwater from flowing onto the abutment and girder ends (Figure 7.16). That evidence supports the hypothesis that keeping rainwater out of existing cracks on a structure greatly reduces the rate of deterioration and is a very effective strategy for damage mitigation.

All monitored cracks in a particular structure tended to widen or narrow about the same as other cracks in the same structure between research visits. This indicates that the rate of deterioration is roughly the same for cracks throughout the structure; cracks do not act independently. Boenig (2000) showed that overall damage progressed similarly in the monitored in-service structures and the box girders tested at FSEL, and that in some cases, focusing on the behavior of single cracks could lead to incorrect conclusions regarding the deterioration of an element.

Figures 8.7 through 8.9 show the incremental change in crack widths measured throughout the study for the I-10 structure, US-90 structure, and Robinson Road structure. The incremental change for the US-90 structure shows more variation among the crack measurement points than the other two structures.

Incremental Change in Crack Width - I-10 Beaumont

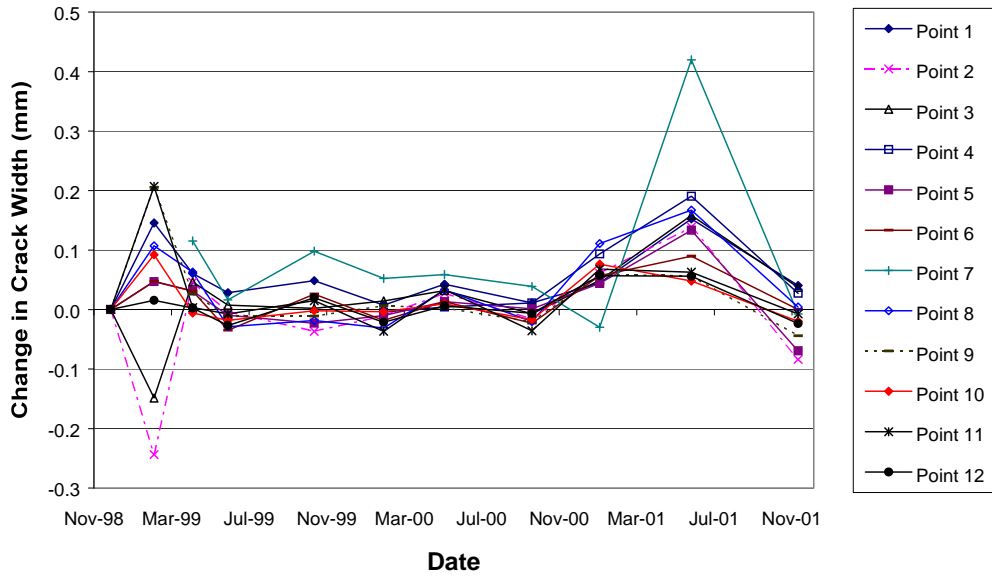


Figure 8.7: Incremental change of crack width versus age of girder for the I-10 structure

Incremental Change in Crack Width - US-90

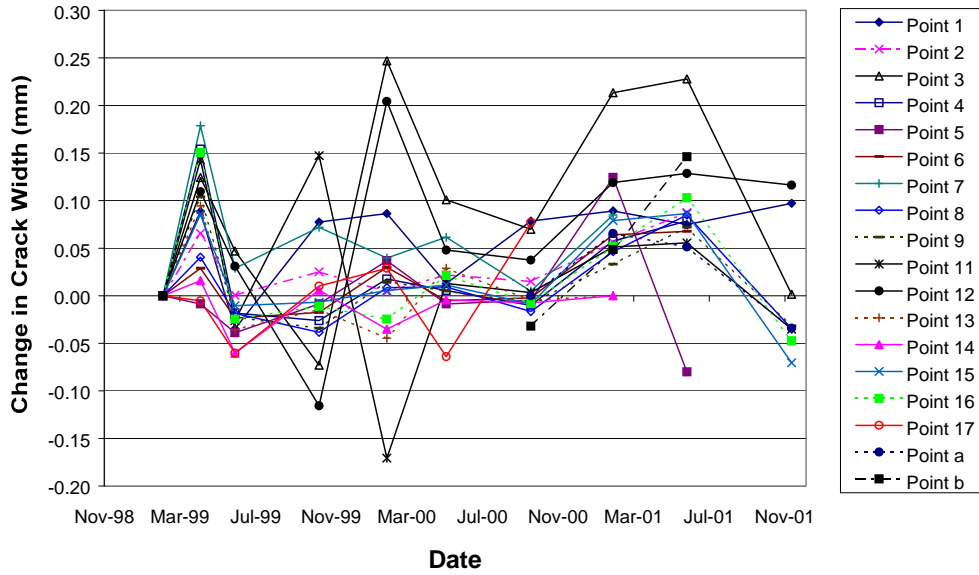


Figure 8.8: Incremental change in crack width versus age of girder for the US-90 structure

Incremental Change in Crack Width - Robinson Road

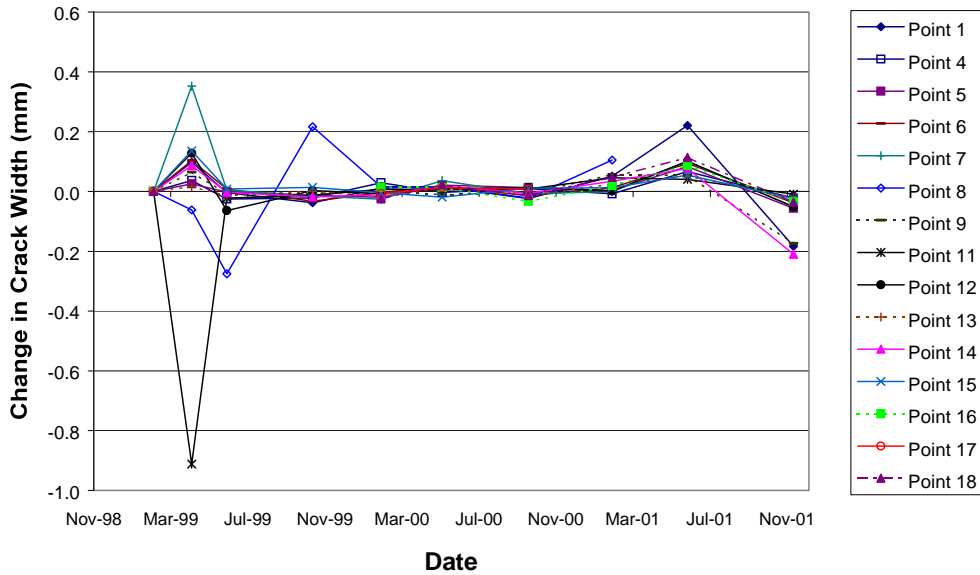


Figure 8.9: Incremental change in crack width versus age of girder for the Robinson Road structure

Field observations also showed that crack sealants were unable to stop cracks from propagating further (Figure 7.14 and Figure 7.20). Cracks were sealed at the four structures in southeast Texas: selected cracks were treated at the I-10 and Robinson Road structures; and all surfaces were primed and painted at the US-90 and Beltway 8 structures. Surface sealants and sealants injected into cracks did not stop deterioration; protecting the damaged concrete from further exposure to water appeared to hinder crack growth, however. It is unknown how effective the sealants were because rates of deterioration for cracks before and after treatment were not available.

CHAPTER 9

Recommendations for Addressing Deterioration in Lake Ivie Structure

9.1 INTRODUCTION

The Lake Ivie structure shows signs of premature concrete deterioration in girders, bent caps, and tie beams; the most significant deterioration is in the bent columns. Options for addressing this deterioration fall into the following general categories:

1. replace or repair the affected elements;
2. take practical mitigation measures to decrease the rate of deterioration;
or
3. continue to monitor the deterioration without repairing or replacing affected elements.

In this chapter, each option is discussed in more detail; criteria are presented for selecting the best option; and a specific option (continuing monitoring) is recommended.

9.2 GENERAL DISCUSSION OF REPLACEMENT OR REPAIR

The affected elements of the Lake Ivie structure are girders, bent caps, tie beams, and bent columns. Deterioration is concentrated at Bent 5 and Bent 9 (Section 7.2.5). Replacing those elements would involve a full or partial closure of FM 1929, removal of portions of the structure, and underwater construction and installation of bent columns. Repair would be less extensive. In this section, possible specific repair techniques are discussed.

9.2.1 Steel Jackets

Encase the bent columns with steel jackets, as shown in Figure 9.1.

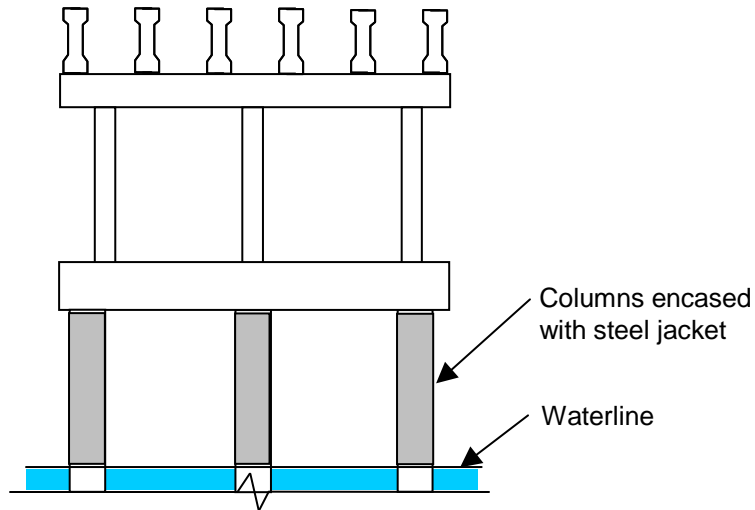


Figure 9.1: *Steel jacket around bent columns*

The steel may add some confinement to the damaged columns; its effectiveness is unknown, however, because the confinement for the column cores is already provided by spiral reinforcement.

The benefits of wrapping a steel jacket around damaged columns include easy technology and ease of installation. Steel is impermeable, however, and it can trap water in columns, which only perpetuates the deterioration-causing reactions. Damage would be hidden by the steel jacket; therefore, it would no longer be possible to continue crack monitoring. Additionally, the steel would rust and likely result in an unattractive and ineffective solution.

9.2.2 Concrete Shells

Pour concrete shell around bent columns, as shown in Figure 9.2.

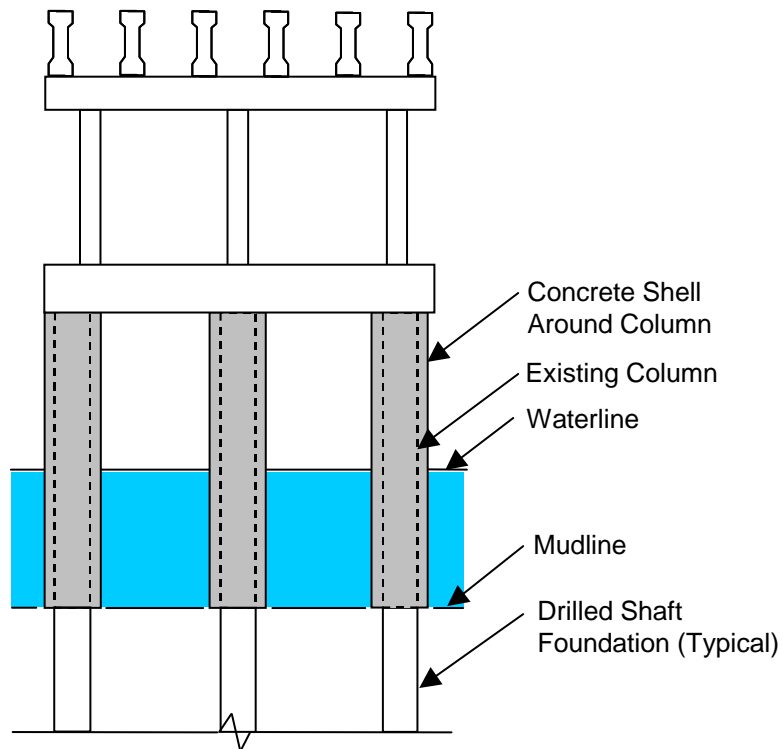


Figure 9.2: *Concrete shells poured around bent columns*

Pouring concrete shells around the bent columns would strengthen the damaged columns somewhat by increasing their diameter. Underwater construction would be difficult, however, and crack monitoring would no longer be possible.

9.2.3 Column Splints

Install “splints” on the bent columns, as shown in Figure 9.3.

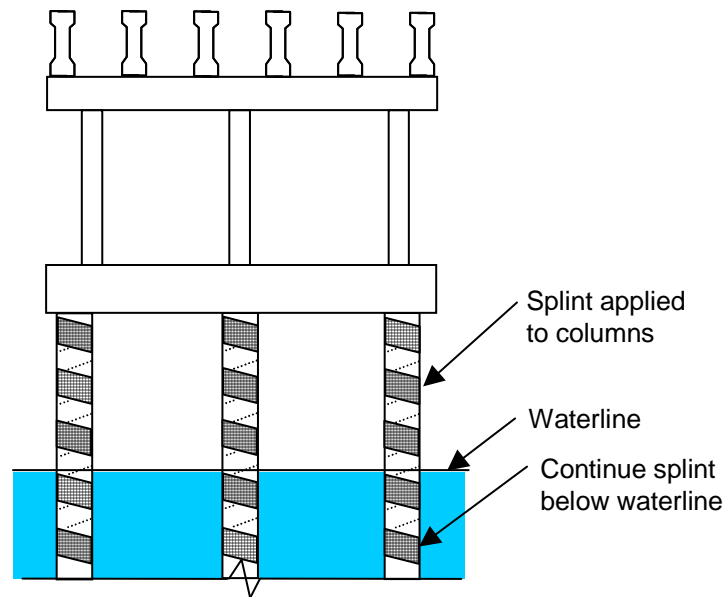


Figure 9.3: *Splints installed on bent columns*

A splint is a partial wrap for strength. It would be designed to strengthen the column by adding confinement. The core is already confined, however, by spiral reinforcement. Existing cracks would still be visible; inspectors could continue to monitor the progression of deterioration. Splints could be installed as an intermediate step; additional strengthening techniques could be applied at a later time if needed.

9.2.4 Sister Columns

Install sister columns, as shown in Figure 9.4.

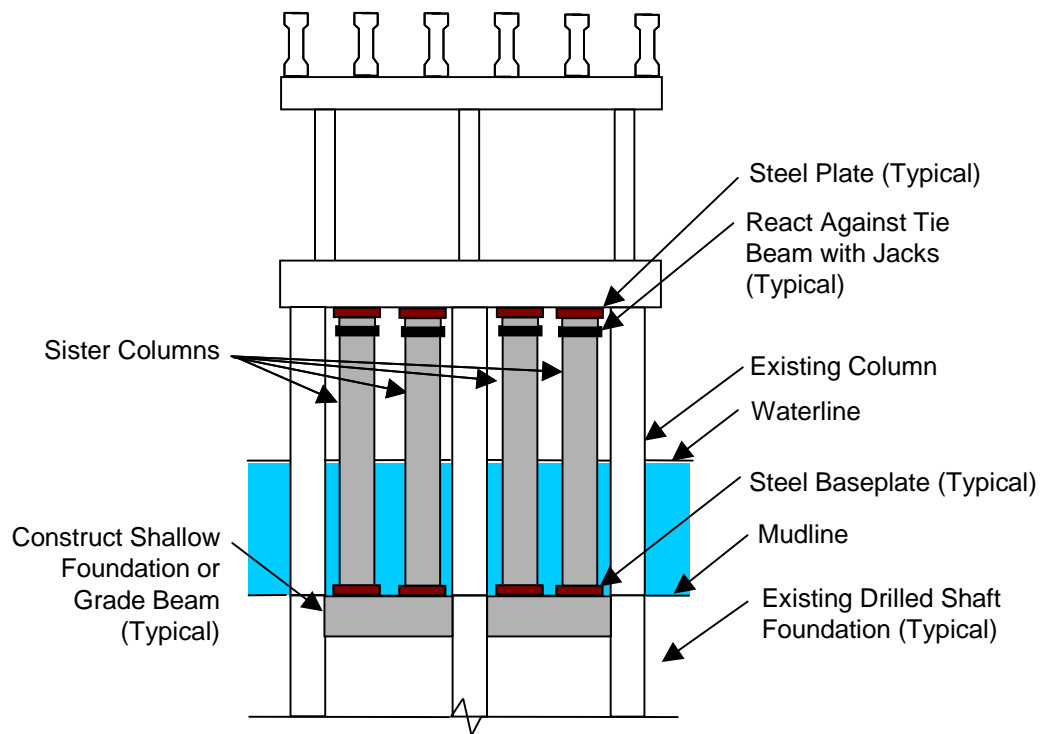


Figure 9.4: Sister columns installed at bent

Sister columns would strengthen the bents by taking some of the loads intended to be carried by the existing lower columns. Because each column is supported by a drilled shaft of the same diameter, shallow foundations or grade beams would have to be constructed to provide bearing surfaces for the sister columns. Because the existing columns are rigidly connected to the tie beam, the sister columns would have to react against the tie beam to transfer the load path away from the existing damaged columns.

9.3 GENERAL DISCUSSION OF MITIGATION

Premature concrete deterioration is the result of internal expansion in the concrete. It can be caused by Alkali-Silica Reaction (ASR) or Delayed Ettringite Formation (DEF). In both cases, deterioration is accelerated by water (Boenig 2000). For this reason, mitigation efforts should focus on keeping water out.

This is obviously problematic for columns submerged in water. In this section, possible mitigation approaches are reviewed.

9.3.1 Flexible Wrap around Bent Columns

Wrap bent columns with flexible, partially permeable material, as shown in Figure 9.5.

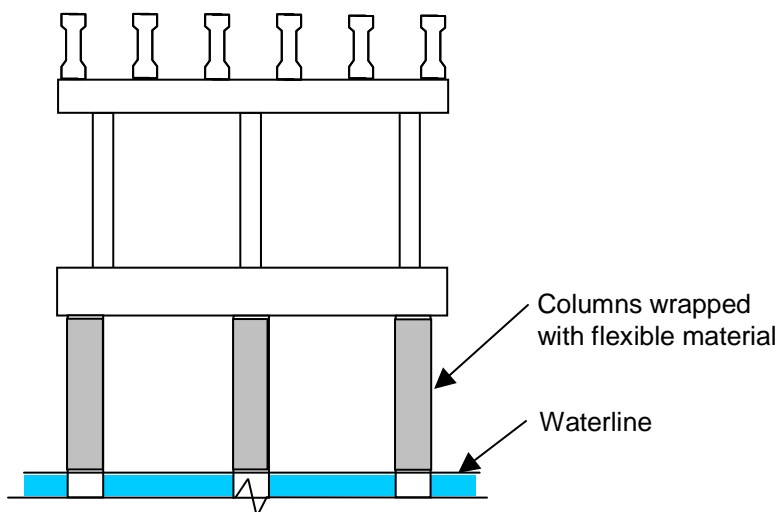


Figure 9.5: Flexible wrap around bent columns

A partially permeable wrap would keep water out of cracks above the waterline. It should be breathable for vapor to allow moisture inside the concrete to escape, but impermeable for liquid so that further exposure to rainwater is eliminated. This option will prevent large amounts of water from entering the cracks; however, it will prevent inspectors from determining the status of deterioration above the waterline. Because the lower columns are under water, it is not possible to eliminate exposure to water completely.

9.3.2 Cofferdams around Bent Columns

Construct cofferdams around the bent columns, as shown in Figure 9.6.

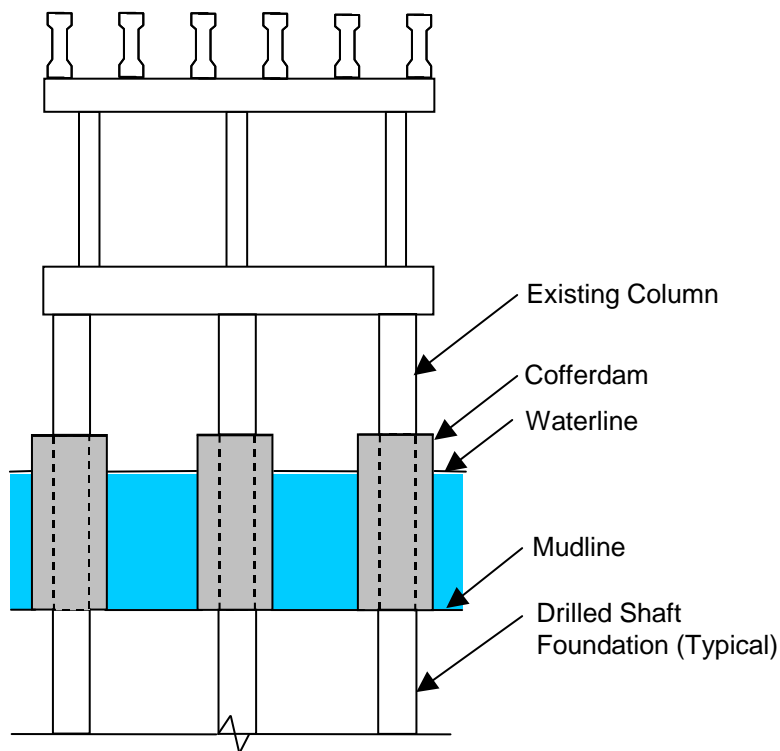


Figure 9.6: *Cofferdams constructed around bent columns*

The purpose of cofferdams would be to keep the columns dry below the waterline. This method is problematic, however, because of the expense and difficulty of construction and installation.

9.3.3 Seal Cracks and Coat Affected Elements

Seal cracks and coat affected elements using current TxDOT techniques. Mitigation efforts similar to those carried out at the US-90 and Beltway 8 structures could be applied in an effort to keep water out of the cracks above the waterline. In those structures, cracks in girders were sealed with surface sealant and primed, and girders were coated with some type of paint. Some cracks in the I-10 structure have also received treatment. An elastomeric sealant was injected into some wide cracks near the west abutment (Boenig 2000). In all treated

structures, however, it was observed that sealed cracks continue to widen and propagate, albeit at a slower rate than unsealed cracks.

Eskridge (2002) investigated several different types of coatings as part of TxDOT Study 4096. Her work should be taken into consideration when evaluating sealants and coatings.

9.3.4 TxDOT Mitigation Technique

The TxDOT treatment procedure for mitigating premature concrete deterioration in concrete bridge members involves the following steps:¹

1. Clean exposed surfaces by abrasive blasting or other approved method.
2. Apply silane-based penetrating surface treatment.
3. Seal cracks with 100% silicone sealant (either siloxane- or silane-based).
4. Paint, if required.

Examples of the existing TxDOT treatment procedure were observed on December 11, 2001 at the US-90 structure (Section 7.2.2) and the Beltway 8 structure (Section 7.2.4). Surface treatment and flexible crack sealant did not stop deterioration in those structures: cracks were apparent through sealant at US-90 (Figure 7.14).

9.4 PROBABLE USEFUL LIFE OF THE LAKE IVIE STRUCTURE WITHOUT MITIGATION

In the preceding sections, options were reviewed for addressing the premature concrete deterioration in the Lake Ivie structure. To select the best option, it is necessary to estimate the probable useful life of the Lake Ivie structure, assuming monitoring only (no replacement or mitigation). That is the

¹ Personal communication, Brian Merrill (TxDOT), July 2002.

objective of this section. Based on field observations, the probable decrease in concrete compressive strength can be estimated, and is used to estimate the decreasing ratio, over time, of design capacity to factored design load for the Lake Ivie columns. The useful life of the Lake Ivie structure is taken as the time required for that ratio to decrease from its present value to a value of unity.

9.4.1 Probable Reduced Strengths

The remaining strength of a pretensioned, precast element with premature concrete deterioration is estimated using the procedure developed by Boenig (2000). Figure 9.7, taken from that reference, shows the relationship between core compressive strength and damage index, determined experimentally on the prestressed box girders tested as part of Study 1857.

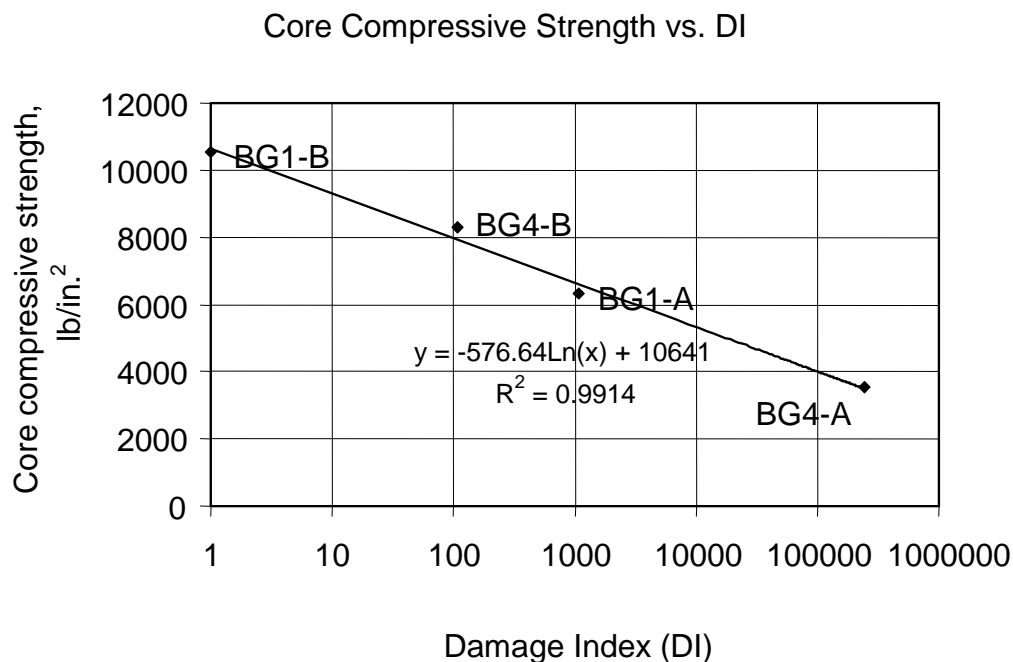


Figure 9.7: Concrete compressive strength of cores from box girders versus damage index (Boenig 2000)

The specified compressive strength of those girders was 6,000 psi (41.4 MPa) (Boenig 2000). Dividing the ordinates of Figure 9.7 by that value, it is possible to plot the ratio of actual compressive strength, f_c , to specified compressive strength, f_c' , for pretensioned, precast concrete (Figure 9.8).

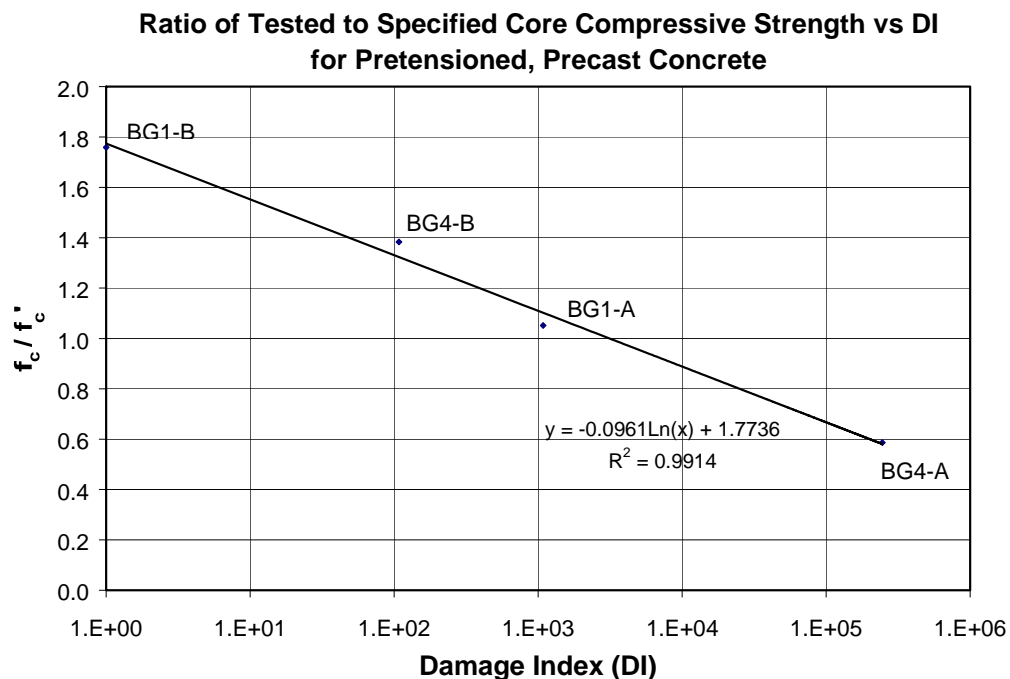


Figure 9.8: *Ratio of tested to specified concrete compressive strength versus damage index for pretensioned, precast concrete*

The relationship shown in Figure 9.8 cannot be directly applied to cast-in-place concrete however. Pretensioned, precast concrete requires high early strengths at release of the strands. Designers typically design concrete mixes for compressive strengths significantly higher than f_c' . It is not necessarily correct to assume that the ratio of actual to specified compressive strength for undamaged, cast-in-place concrete has the same value of 1.76.

TxDOT Class C structural concrete, with a specified 7-day modulus of rupture of 510 psi (3.5 MPa) and a specified 28-day compressive strength of 3,600 psi (24.8 MPa), was used for the bent columns in the Lake Ivie structure². In a previous TxDOT study, Fang et al. (1990) performed flexural and compressive strength tests on the same class of concrete, with the same specified tensile and compressive strengths. Their concrete was produced at roughly the same time as that used in the Lake Ivie structure, and their results can be expected to be similar to those of the Lake Ivie structure. Based on cylinder tests, Fang et al. found a 180-day compressive strength of 5,160 psi, or $1.43f_c'$. For the columns of the Lake Ivie structure, it is therefore reasonable to assume that same ratio. For cast-in-place concrete, the ratio of actual to specified compressive strengths is therefore estimated as the graph of Figure 9.8, multiplied by the ratio (1.43/1.76) or 0.81. That second graph is Figure 9.9.

² Personal communication, Brian Merrill (TxDOT), April 2002.

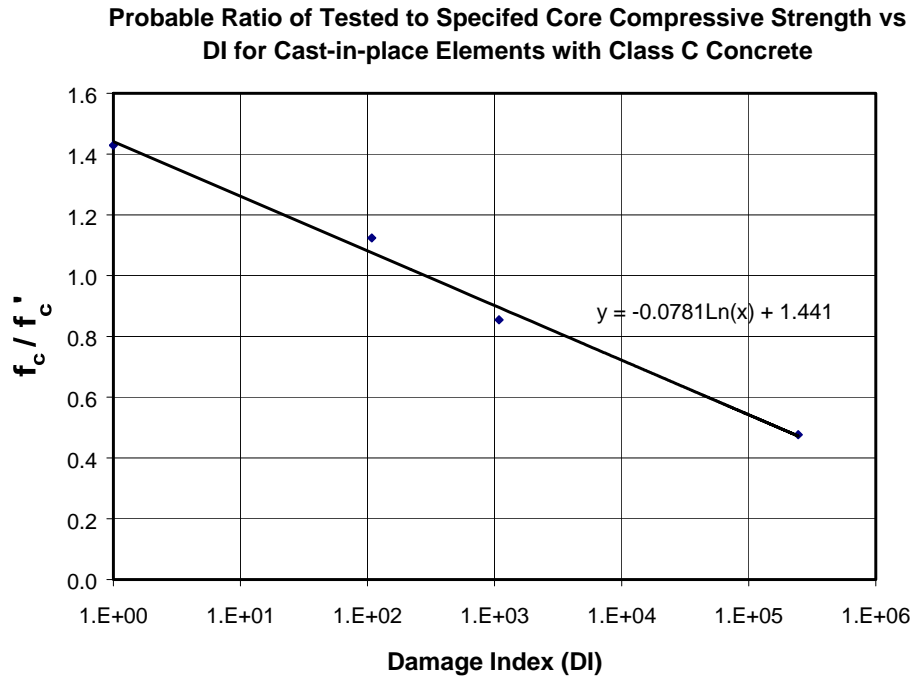


Figure 9.9: *Probable ratio of actual to specified concrete compressive strength versus damage index for cast-in-place elements with Class C concrete*

A damage index of an in-service element, determined as described in Section 3.5, is used with the appropriate relationship to estimate the compressive strength of the deteriorated concrete. Figure 9.8 is used for pretensioned, precast elements, and Figure 9.9 is used for cast-in-place elements. That reduced compressive strength can then be used to estimate a corresponding reduced structural capacity.

9.4.2 Probable Reduced Strengths of Girders

In general, for the structures examined in Study 1857, and in particular for the Lake Ivie structure, damage from premature concrete deterioration is concentrated at the girder ends rather than the middle. This is important, because flexural capacity of simply supported girders is not significantly reduced in

prestressed girders with premature concrete damage concentrated in the ends (Boenig 2000). In addition, Roche (2001) showed that in-service shear fatigue failure is not likely in prestressed girders with premature concrete damage concentrated in the ends, provided that the stress range in the shear reinforcement of the girders remains below the endurance limit of the steel. Therefore, limited premature concrete damage observed at the ends of some girders of the Lake Ivie structure, is not expected to reduce their strength significantly, and is not considered further in estimating that structure's useful life.

9.4.3 Probable Reduced Strength of Columns

Columns in several bents in the Lake Ivie structure have significant vertical cracking in their lower portions, extending from below the waterline to the bottom of the tie beams (Section 7.2.5). On October 15, 2001, typical column cracks were measured to be up to 1/8 in. (3.2 mm) wide. The effect of premature concrete deterioration on the axial capacity of those columns can be estimated using a modified version of Boenig's procedure.

Figure 9.10 shows the cross-sectional dimensions of the south lower column of Bent 5 for the Lake Ivie structure³. The circular column is 48 in. (1.22 m) in diameter. It is reinforced in the longitudinal direction with 18-#9 bars, which have a nominal diameter of 1.128 in. (28.7 mm), a nominal cross-sectional area of 1 in.² (645 mm²), and a specified yield strength, f_y , of 40,000 psi (276 MPa). The provided f_y of most of the longitudinal reinforcement is 60,000 psi (414 MPa), however⁴. TxDOT Class C structural concrete, with a specified compressive strength of 3,600 psi (24.8 MPa), was used for the column.

³ Personal communication, Brian Merrill (TxDOT), April 2002.

⁴ Personal communication, Brian Merrill (TxDOT), April 2002.

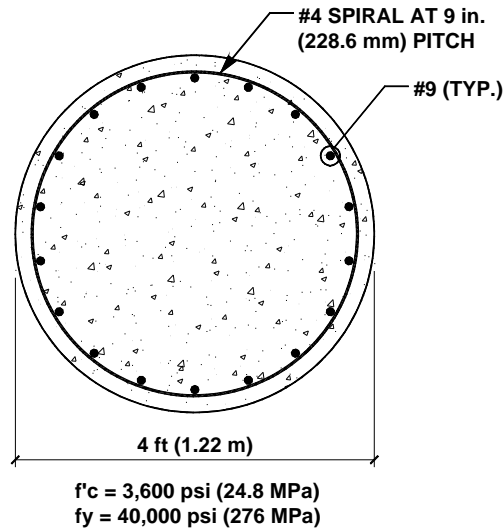


Figure 9.10: Cross-section of lower column in Bent 5, Lake Ivie structure

In this chapter, the probable capacities of the columns in the Lake Ivie structure are estimated. Because it is the latest reference, and will almost certainly be referenced by or repeated directly in AASHTO provisions, the design equations of ACI318-02 are used.

The nominal axial capacity, P_0 , of the column is given by Equation 9-1.

$$P_0 = 0.85 f'_c (A_g - A_{st}) + f_y A_{st} \quad (9-1)$$

In this equation, A_g is the gross cross-sectional area of the column, and A_{st} is the total cross-sectional area of the longitudinal reinforcement. Equation 9-1 assumes that the column is under concentric compression, and cannot buckle.

Realistically, some bending moments are applied on the column due to the 3% grade of the Lake Ivie bridge deck. These bending moments reduce the axial capacities of the columns somewhat. Equation 10-1 of ACI318-02 limits the design axial load for a spirally reinforced column to 0.85 times the factored nominal axial capacity, ϕP_0 . ACI318-02 Section 9.3.3.2 states that the resistance factor, ϕ , for spirally reinforced columns is 0.7. Because the bending moments in

the columns of the Lake Ivie structure do not reduce the axial capacity significantly, the value given by ACI318-02 Equation 10-1 is considered to be a good estimate for the design axial capacity of the Lake Ivie columns.

$$\phi P_{n,max} = 0.85\phi[0.85f'_c(A_g - A_{st}) + f_y A_{st}] \quad (9-2) \quad (\text{ACI 318-02 Equation 10-1})$$

Based on this equation, the design axial capacity of the south lower column of Bent 5, is computed by Equation 9-3.

$$\begin{aligned} \phi P_{n,max} &= (0.85)(0.7)[(0.85)(3,600 \text{ psi})(1809.6 \text{ in.}^2 - 18 \text{ in.}^2) \\ &+ (40,000 \text{ psi})(18 \text{ in.}^2)] = 3,690,366 \text{ lb} \sim 3690 \text{ kips} \end{aligned} \quad (9-3)$$



**Figure 9.11: Typical vertical cracking on south lower column of Bent 5
(10/15/01)**

Figure 9.11 shows typical damage (observed on October 15, 2001) near Point 7 on the south lower column of Bent 5. Based on these field observations, a damage index can be estimated for this column. On October 15, 2001, the vertical crack at Point 7 (Figure 9.9) was 0.064 in. (1.63 mm) wide, as determined from Demec measurements. If a representative 12 in. (0.31 m) square is drawn on the column, at most two or three vertical cracks can be expected to extend through

that square. Using Equation 3-1 and assuming three vertical cracks of the same width in the representative square, the damage index for the column as of October 15, 2001 can be estimated:

$$DI = \sum w^2l \quad (3-1), \text{ repeated}$$

In Equation 3-1, w is the crack width in thousandths of an inch, and l is the crack length in inches.

$$DI = 3[(64)^2(12 \text{ in.})] = 147,456 \sim 147,000 \quad (9-4)$$

From Figure 9.9, a damage index of 147,000 corresponds to a f_c / f_c' ratio of 0.51, and to almost the same ratio of probable to specified compressive capacity.

$$y = -0.0781 \ln(x) + 1.441 \quad (9-5) \quad (\text{from Figure 9.9})$$

$$\frac{f_c}{f_c'} = -0.0781 \ln(147,000) + 1.441 = 0.51 \quad (9-6)$$

$$f_c = 0.51(3,600 \text{ psi}) = 1,836 \text{ psi} \quad (9-7)$$

Using this reduced compressive strength in Equation 10-1 of ACI318-02, a probable design axial capacity is computed:

$$\begin{aligned} \phi P_{n,max} &= (0.85)(0.7)[(0.85)(1,836 \text{ psi})(1809.6 \text{ in.}^2 - 18 \text{ in.}^2) \\ &+ (40,000 \text{ psi})(18 \text{ in.}^2)] = 2,092,002.7 \text{ lb} \sim 2,092 \text{ kips} \end{aligned} \quad (9-8)$$

According to TxDOT, the unfactored axial design load of the drilled shaft foundation underneath the column at Bent 5 is 408 kips (1815 kN)⁵. An approximate load factor of 1.4 gives a factored design axial load of 572 kips (2545 kN) for the column. The initial design axial capacity of the column (Equation 9-3) exceeds this value by a factor of 6.45, and the reduced design axial capacity computed for October 15, 2001 (Equation 9-8) exceeds the factored design axial load by a factor of 3.66.

⁵ Personal communication, Brian Merrill (TxDOT), April 2002.

Because column design axial capacity varies linearly with concrete strength, the damage-related ratio f_c / f_c' (Figure 9.9) can also be expressed as a damage-related ratio of $\phi P_n / P_{design}$ for the columns in Bent 5 of the Lake Ivie structure (Figure 9.12). In the latter figure, the initial compressive strength, $f_c^{(0)}$, is taken as 1.43 times the specified value (Fang et al. 1984). Because the damage index is plotted on a logarithmic scale, its lower limit is taken as 1.0 on the horizontal axis.

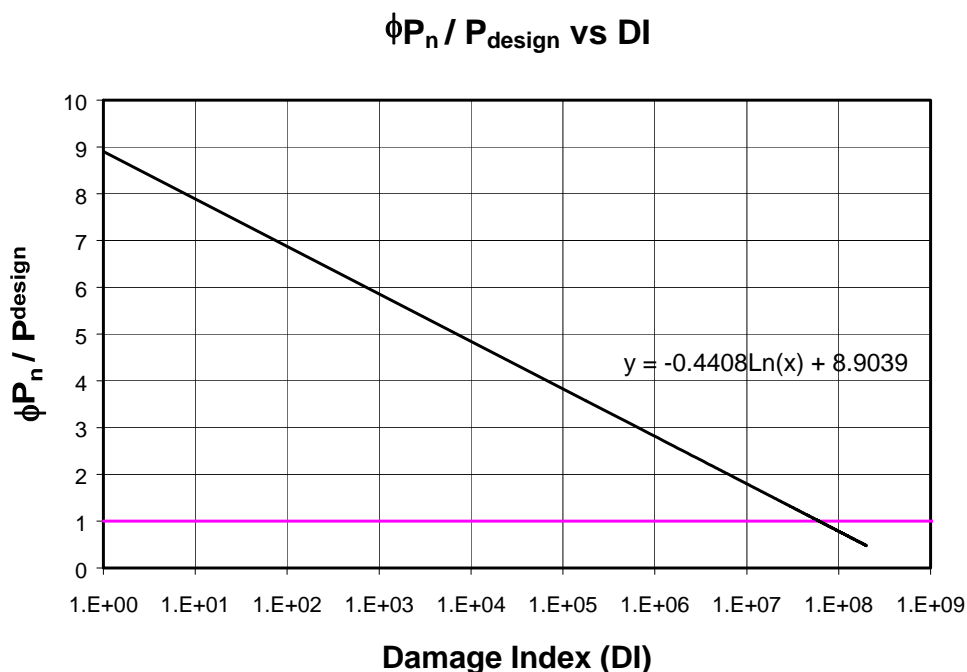


Figure 9.12: Ratio of design axial capacity to design axial load versus damage index, south column, Bent 5, Lake Ivie

According to Figure 9.12, the ratio of probable design axial capacity to factored load decreases to 1.0 when the damage index reaches 6.13×10^7 . The probable time required for the damage index to reach that value can also be estimated. The crack at Point 7 has widened at an average rate of 0.43 mm/year

(Figure 7.56). This observed rate is among the fastest observed rates in the field, and can be taken as a conservative estimate of the probable rate of widening. By comparison, Point 7 on the I-10 structure has widened at an average rate of 0.27 mm/year (Figure 7.52); Point 3 on the US-90 structure has widened at an average rate of 0.41 mm/year (Figure 7.53); and Point 1 on the Robinson Road structure has widened at an average rate of 0.14 mm/year (Figure 7.54). Starting from an assumed damage index of 1.0 at the casting date of August 11, 1989, assuming that the observed cracks in the south column of Bent 5 continue to widen linearly with time at the same rate, and that no new cracks form in the representative square, Figure 9.13 shows the corresponding increase in damage index with time for that column.

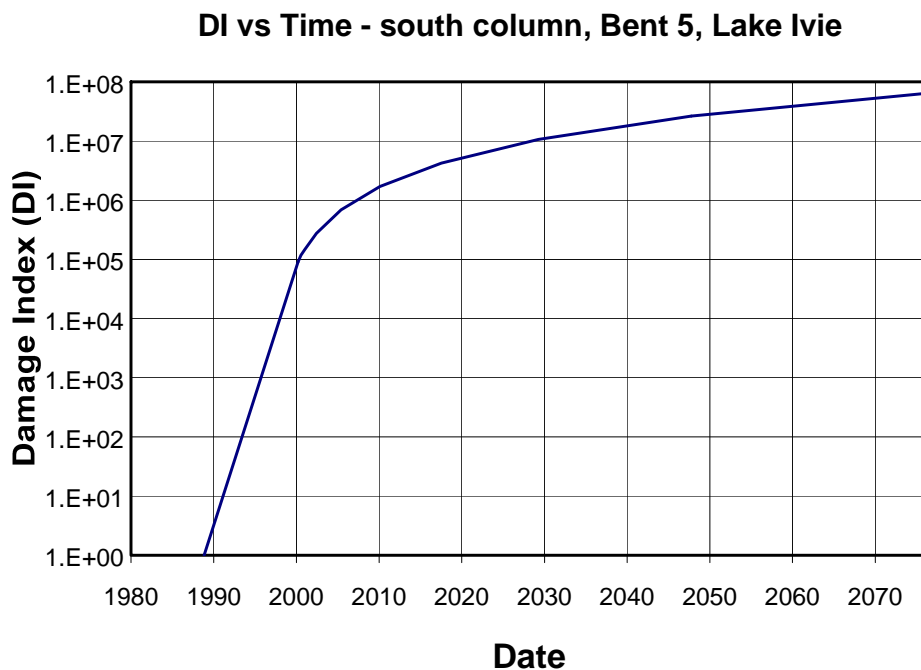


Figure 9.13: Predicted Damage Index versus time for south column, Bent 5, Lake Ivie

Finally, Figure 9.12 and Figure 9.13 can be combined to produce a graph predicting reduced ratio of axial capacity to design capacity over time (Figure 9.14).

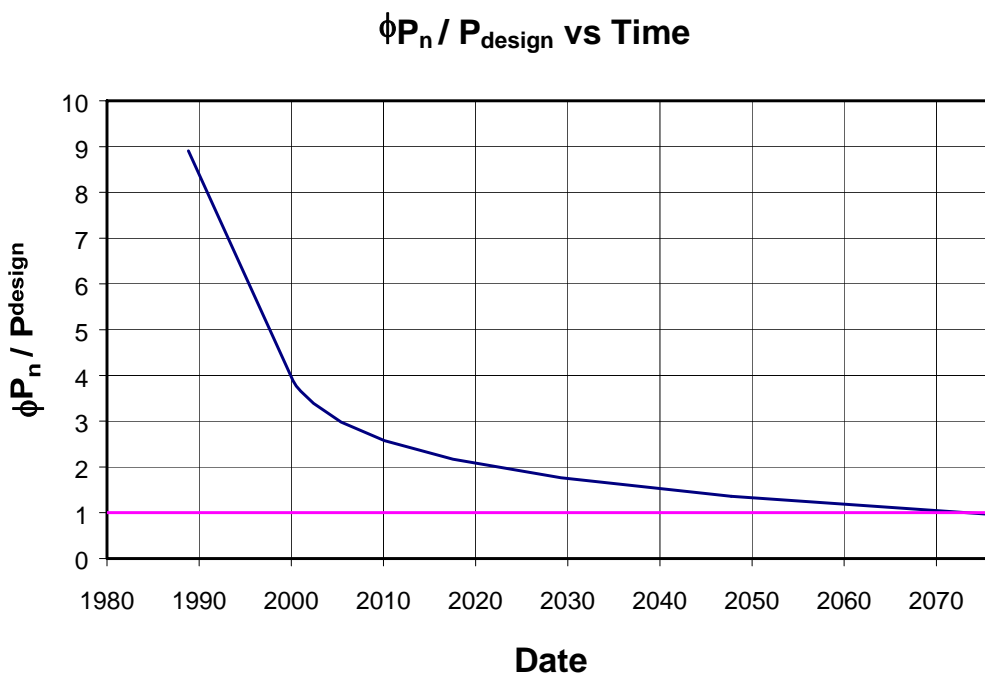


Figure 9.14: Predicted ratio of axial capacity to design axial load versus time, south column, Bent 5, Lake Ivie

When $\phi P_n / P_{design}$ is less than 1.0, the column no longer satisfies ACI318-02 requirements. Based on the model presented in this section, the axial capacity ratio is predicted to remain above 1.0 until at least 2070. This is well beyond the expected design life of that structure.

9.5 OPTIONS FOR ADDRESSING DETERIORATION AT LAKE IVIE

9.5.1 Replace or Repair Affected Elements

Because the useful life of the Lake Ivie structure will extend past the year 2070, it is unnecessary and impractical to replace the affected girders and bents now. Repair is always an option if the premature concrete deterioration (or subsequent corrosion) increases unexpectedly.

9.5.2 Mitigate Deterioration

Because girders, bent caps, and tie beams in the Lake Ivie structure have adequate strength and a slow rate of deterioration (Section 7.3.5), mitigation efforts do not need to be focused on those elements at this time. Simple mitigation techniques (Section 9.3.4), including surface sealants and sealants injected into girder cracks, have been attempted at the I-10, US-90, Robinson Road, and Beltway 8 structures by TxDOT personnel; these simple techniques do not stop the growth of existing cracks or the formation of new ones, however.

Sealing cracks and coating the affected girders, bent caps, and tie beams would cover the visible damage; crack growth is expected to continue, however, similar to the observed behavior of sealed cracks at the US-90 and Beltway 8 structures. If such simple mitigation techniques were used, their primary justification would be cosmetic improvements in the appearance of the Lake Ivie structure.

9.5.3 Monitor Deterioration

This course of action involves the least effort. Because the useful life of the Lake Ivie structure is estimated to extend past the year 2070, TxDOT can continue to monitor conditions of the Lake Ivie structure, and also continue to

postpone any corrective actions as long as monitoring shows that damage is increasing as predicted here.

9.6 RECOMMENDATIONS FOR ADDRESSING DETERIORATION AT LAKE IVIE

To provide continued information about the progression of damage and reductions of axial capacities, it is recommended that the Lake Ivie structure be inspected once or twice per year. Damage indices should be computed as described in Section 3.5 and used to update the estimates of the reduced strength of the Lake Ivie bent columns as described in Section 9.4. If damage increases more rapidly than estimated here, TxDOT should consider repair.

CHAPTER 10

Summary, Conclusions, and Recommendations

10.1 SUMMARY

This thesis describes work done as part of TxDOT Study 1857: “Structural Assessment of In-Service Bridges With Premature Concrete Deterioration.” That study focuses on seven specific tasks:

1. Conduct field investigations to confirm and monitor existing premature concrete deterioration, the rate of increase of such deterioration, and the effect of different remedial measures on that rate of increase.
2. Conduct laboratory investigations of local effects of premature concrete deterioration.
3. Develop nondestructive evaluation (NDE) techniques for determining degree and type of concrete deterioration.
4. Develop petrographic techniques for assessing severity of deterioration from samples taken from field investigations.
5. Develop engineering models for evaluating the global reduction in capacity of a structural element due to local premature concrete deterioration.
6. Develop an overall methodology for predicting the probable loss in capacity over time of a deteriorated structural element, based on external evidence, NDE, and engineering models.
7. Develop recommended actions by TxDOT for handling any given case of premature concrete deterioration. The recommendations will include specific guidelines for assessing the probable capacity of the

structure as a function of time, and specific techniques for extending the useful life and maintaining the capacity of the structure for as long as possible.

The parts of Study 1857 reported here concern Tasks (1) and (2). The field observation program developed by Boenig (2000) was continued for this thesis, as part of Task 1. Crack patterns, crack widths, and the progression of damage were documented in five in-service TxDOT bridge structures for an additional two years.

The laboratory testing program for this part of the study was designed to investigate the effect of premature concrete deterioration on the bond between prestressing strands and concrete (Task 2). Strand-pullout tests were performed on slice specimens removed from the full-scale box girder specimens. Changes in the pullout response of strands were correlated with different indices of external damage to the concrete.

In addition, recommendations are given for addressing deterioration to the FM 1929 structure over the Lake Ivie Reservoir in Concho, Texas. The probable capacity of bent columns over time is projected, and options for addressing premature concrete deterioration in those columns are discussed. While the recommendations made for the Lake Ivie structure are intended specifically for that structure, the methodology pertains to Tasks (6) and (7) and can be applied to other cases of premature concrete deterioration.

10.2 CONCLUSIONS

10.2.1 Effects of Premature Concrete Deterioration on the Pullout Response of Strands

1. Premature concrete deterioration causes a reduction in bond strength between prestressing strands and concrete. In slice specimens taken

from prestressed box girders, mean average bond strength was reduced to about 60% of the value for undamaged concrete (Figure 5.11).

2. Capacity of prestressed girders with premature concrete deterioration is limited by other mechanisms than bond failure of prestressing strands. No bond failure of strands was observed in tests of full-size girders by Boenig (2000) or Roche (2001).
3. Three mechanisms govern the load-displacement response of prestressing strands embedded in concrete: bond between the strands and concrete; friction between the strands and concrete; and twisting of the strand as it is pulled out of the concrete.
 - a. Before first slip of the strands has occurred, the bond mechanism is dominant.
 - b. After first slip of the strands has occurred, the twist mechanism is dominant.
4. Because it is not possible with external damage indices to determine whether internal cracks involve individual strands in the cross-section, damage on outside faces was not found to be a good indicator of interior damage.

10.2.2 Conclusions with Respect to the FM 1929 Structure over Lake Ivie

1. While the Lake Ivie structure is experiencing premature concrete deterioration, the rate of deterioration is consistent with a useful life until at least 2070.
2. The bent columns should continue to be monitored at yearly or 6-month intervals, and repair should be considered if damage increases more rapidly than expected.

10.3 RECOMMENDATIONS

10.3.1 Recommendations Regarding the Effects of Premature Concrete Deterioration on the Pullout Response of Strands

1. To evaluate the reduced pullout capacity of prestressing strands in girders with premature concrete deterioration, the following approach is recommended:
 - a. Compute damage indices on the bottom face of the girder and on the side faces (if possible) by measuring crack widths and lengths in representative squares (Section 3.5).
 - b. Use the damage indices with Figure 5.11 to estimate the corresponding reduced bond strength and corresponding reduced pullout capacity.
 - c. While the work of this study indicates that reduced pullout capacity is not a concern for typical TxDOT girders, its probable consequences can be evaluated further if desired.
2. Nondestructive evaluation (NDE) techniques should be developed to determine whether internal cracks involve individual strands.

10.3.2 Recommendations with Respect to the FM 1929 Structure over Lake Ivie

1. The Lake Ivie structure should continue to be monitored to assess the progression of damage. As in Chapter 9, damage indices should be computed and used to estimate the reduced strength of the Lake Ivie bent columns.
2. To evaluate the probable axial capacity of cast-in-place columns with premature concrete deterioration, the following approach is recommended:

- a. Compute damage indices by measuring crack widths and lengths in representative squares (Section 3.5).
- b. Use the damage index with Figure 9.9 to estimate the corresponding ratio of actual to specified concrete compressive strength.
- c. Compute the probable design axial capacity using the governing ACI equation, and compare the probable axial capacity to the factored design axial load.

Appendix A: Fabrication Details of Box Girders

Appendix B: Fabrication Drawing for Box Girders with Non-Standard Spans

Appendix C: Data from Strand-pullout Tests

SLICE BG1S

BG1S_4L: Pullout Force vs. Key Displacements

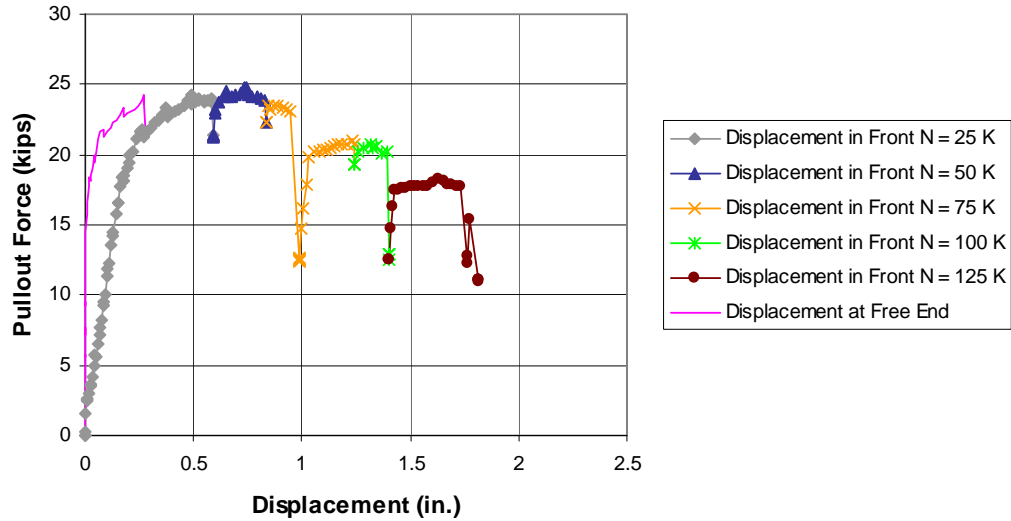


Figure C.1: Load-displacement Relationship for Strand BG1S_4L

Date Tested: July 13, 2001

Length embedded in concrete prior to test: 11.9 in. (0.30 m)

Average bond strength: 886 psi (6,110 kPa)

Table C.1: Summary of Test Results for Strand BG1S_4L

Clamping Load N	Slip Occurred or Resumed At
25 kips (111 kN)	16.52 kips (73.5 kN)
50 kips (222 kN)	Unknown
75 kips (334 kN)	Unknown
100 kips (445 kN)	Unknown
125 kips (556 kN)	Unknown

BG1S_7L: Pullout Force vs. Key Displacements

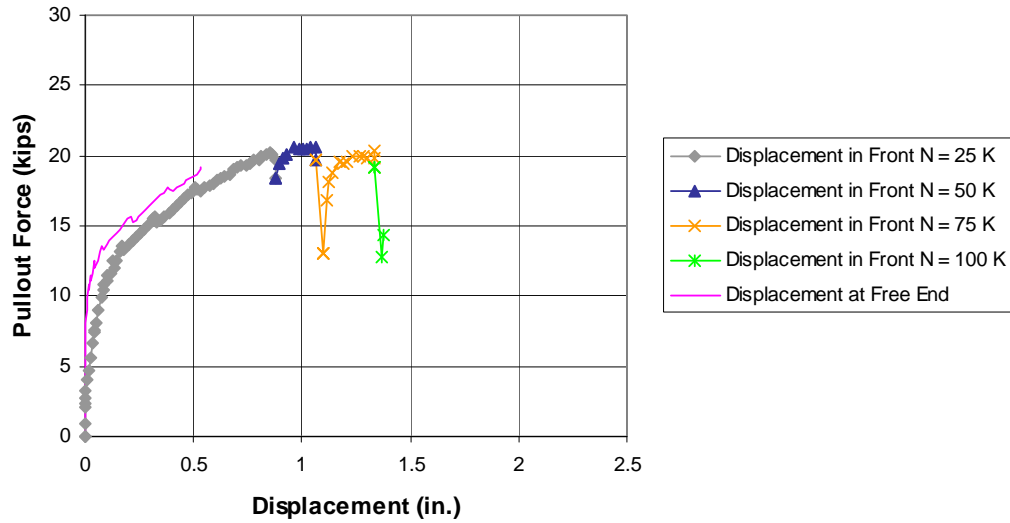


Figure C.2: Load-displacement Relationship for Strand BG1S_7L

Date Tested: July 13, 2001

Length embedded in concrete prior to test: 12.8 in. (0.33 m)

Average bond strength: 448 psi (3,090 kPa)

Table C.2: Summary of Test Results for Strand BG1S_7L

Clamping Load N	Slip Occurred or Resumed At
25 kips (111 kN)	9.01 kips (40.1 kN)
50 kips (222 kN)	Unknown
75 kips (334 kN)	Unknown
100 kips (445 kN)	Unknown

BG1S 9L: Pullout Force vs. Key Displacements

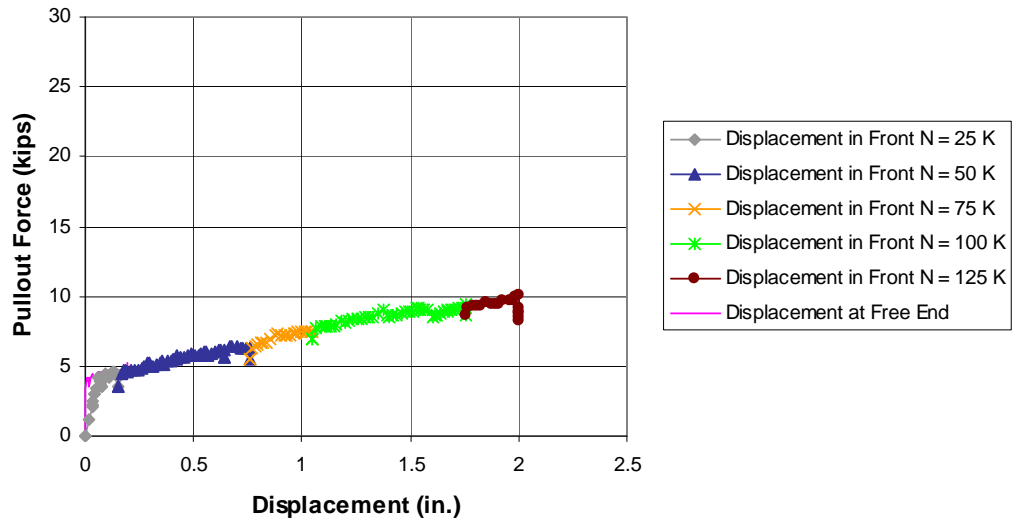


Figure C.3: Load-displacement Relationship for Strand BG1S_9L

Date Tested: July 12, 2001

Length embedded in concrete prior to test: 12.8 in. (0.32 m)

Average bond strength: 207 psi (1,430 kPa)

Table C.3: Summary of Test Results for Strand BG1S_9L

Clamping Load N	Slip Occurred or Resumed At
25 kips (111 kN)	4.14 kips (18.4 kN)
50 kips (222 kN)	Unknown
75 kips (334 kN)	Unknown
100 kips (445 kN)	Unknown
125 kips (556 kN)	Unknown

BG1S_13L_retest: Pullout Force vs. Key Displacements

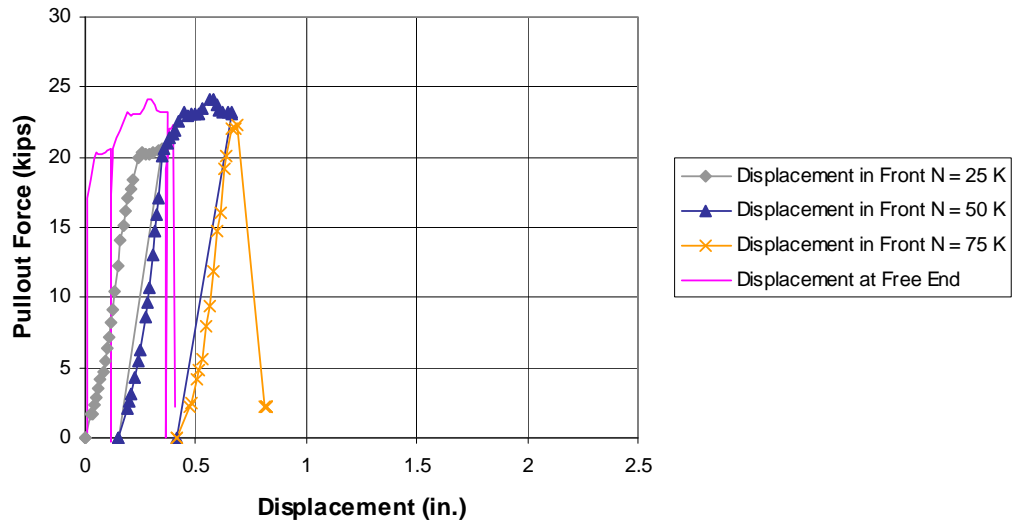


Figure C.4: Load-displacement Relationship for Strand BG1S_13L_retest

Date Tested: August 17, 2001

Length embedded in concrete prior to test: 12 in. (0.31 m)

Average bond strength: 907 psi (6,250 kPa)

Table C.4: Summary of Test Results for Strand BG1S_13L_retest

Clamping Load N	Slip Occurred or Resumed At
25 kips (111 kN)	17.09 kips (76.0 kN)
50 kips (222 kN)	20.63 kips (91.8 kN)
75 kips (334 kN)	22.07 kips (98.2 kN)

BG1S 15L: Pullout Force vs. Key Displacements

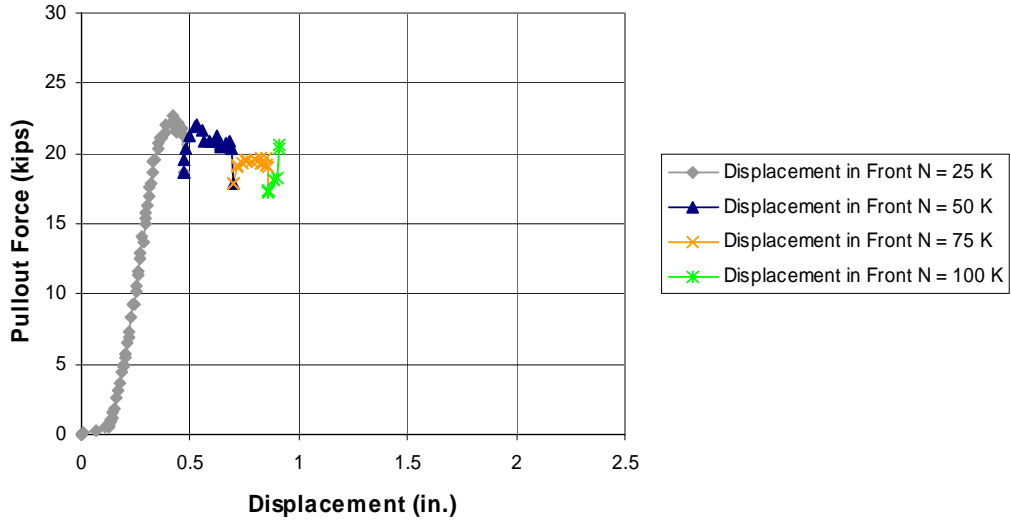


Figure C.5: Load-displacement Relationship for Strand BG1S_15L

Date Tested: April 4, 2001

Length embedded in concrete prior to test: 13 in. (0.33 m)

Average bond strength: 630 psi (4,350 kPa)

Table C.5: Summary of Test Results for Strand BG1S_9L

Clamping Load N	Slip Occurred or Resumed At
25 kips (111 kN)	12.87 kips (57.3 kN)
50 kips (222 kN)	Unknown
75 kips (334 kN)	Unknown
100 kips (445 kN)	Unknown

BG1S_2R: Pullout Force vs. Key Displacements

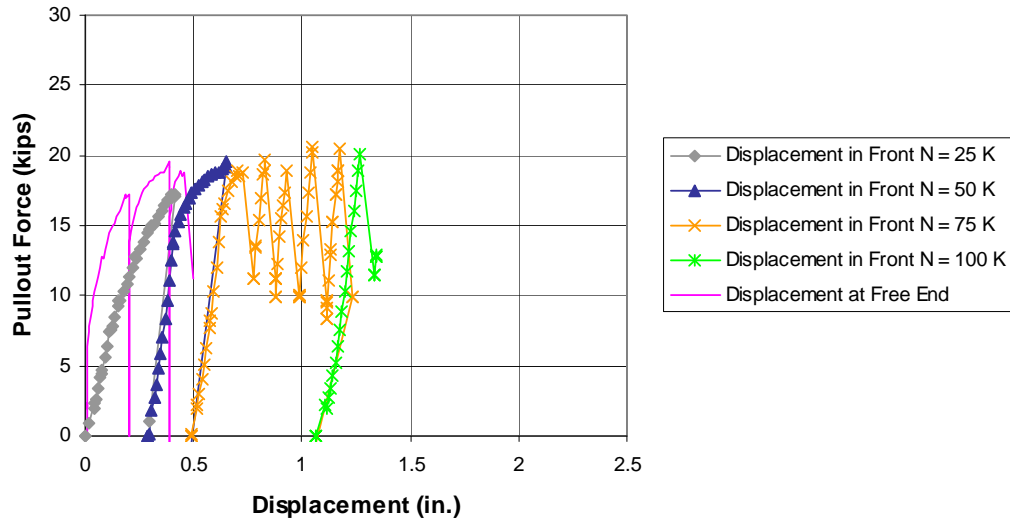


Figure C.6: Load-displacement Relationship for Strand BG1S_2R

Date Tested: August 1, 2001

Length embedded in concrete prior to test: 13 in. (0.33 m)

Average bond strength: 630 psi (4,350 kPa)

Table C.6: Summary of Test Results for Strand BG1S_2R

Clamping Load N	Slip Occurred or Resumed At
25 kips (111 kN)	7.55 kips (33.6 kN)
50 kips (222 kN)	14.64 kips (65.1 kN)
75 kips (334 kN)	16.54 kips (73.6 kN)
100 kips (445 kN)	20.14 kips (89.6 kN)

BG1S 5R: Pullout Force vs. Key Displacements

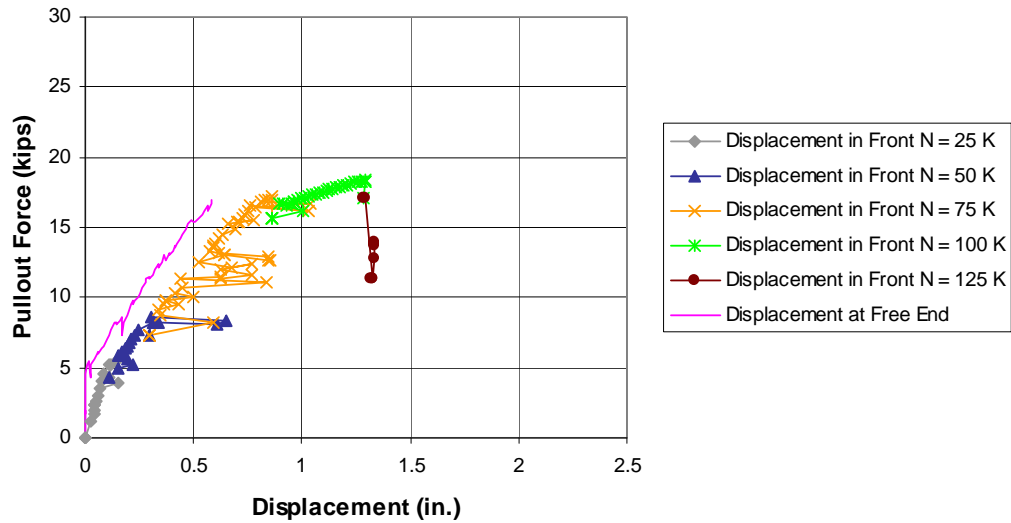


Figure C.7: Load-displacement Relationship for Strand BG1S_5R

Date Tested: July 6, 2001

Length embedded in concrete prior to test: 12.9 in. (0.33 m)

Average bond strength: 255 psi (1,760 kPa)

Table C.7: Summary of Test Results for Strand BG1S_5R

Clamping Load N	Slip Occurred or Resumed At
25 kips (111 kN)	5.17 kips (23.0 kN)
50 kips (222 kN)	Unknown
75 kips (334 kN)	Unknown
100 kips (445 kN)	Unknown
125 kips (556 kN)	Unknown

BG1S 7R: Pullout Force vs. Key Displacements

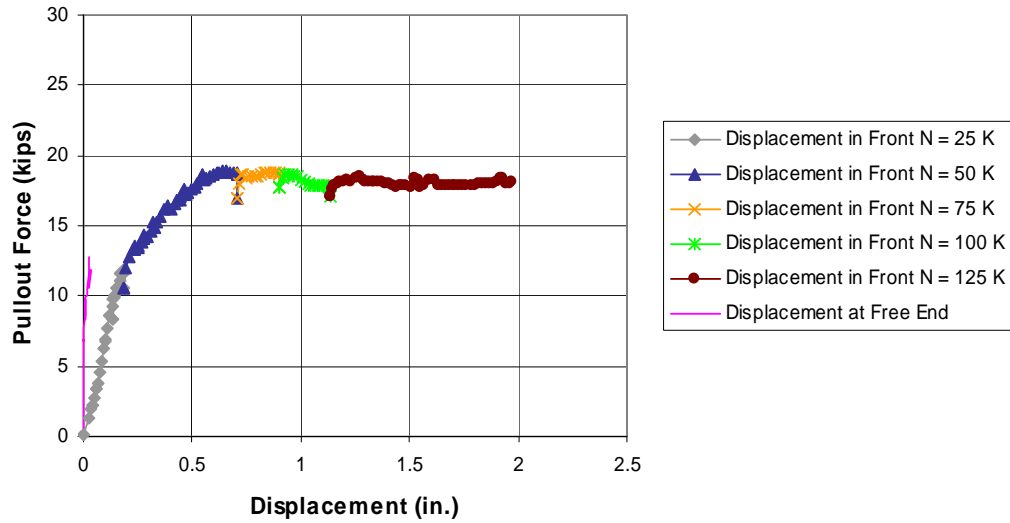


Figure C.8: Load-displacement Relationship for Strand BG1S_7R

Date Tested: July 6, 2001

Length embedded in concrete prior to test: 13.7 in. (0.35 m)

Average bond strength: 456 psi (3,140 kPa)

Table C.8: Summary of Test Results for Strand BG1S_7R

Clamping Load N	Slip Occurred or Resumed At
25 kips (111 kN)	9.81 kips (43.6 kN)
50 kips (222 kN)	Unknown
75 kips (334 kN)	Unknown
100 kips (445 kN)	Unknown
125 kips (556 kN)	Unknown

BG1S_9R: Pullout Force vs. Key Displacements

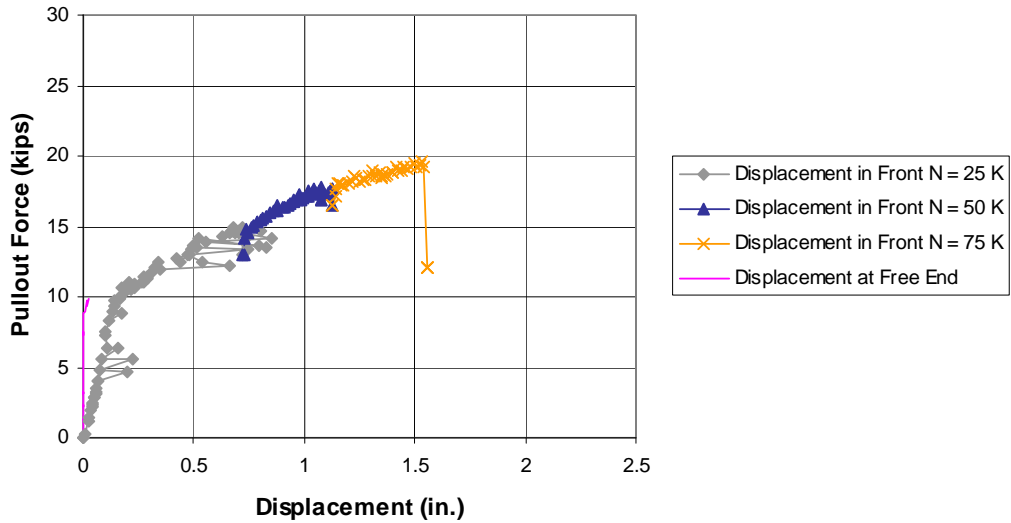


Figure C.9: Load-displacement Relationship for Strand BG1S_9R

Date Tested: July 5, 2001

Length embedded in concrete prior to test: 13.1 in. (0.33 m)

Average bond strength: 434 psi (2,990 kPa)

Table C.9: Summary of Test Results for Strand BG1S_9R

Clamping Load N	Slip Occurred or Resumed At
25 kips (111 kN)	8.94 kips (39.8 kN)
50 kips (222 kN)	Unknown
75 kips (334 kN)	Unknown

BG1S_13R: Pullout Force vs. Key Displacements

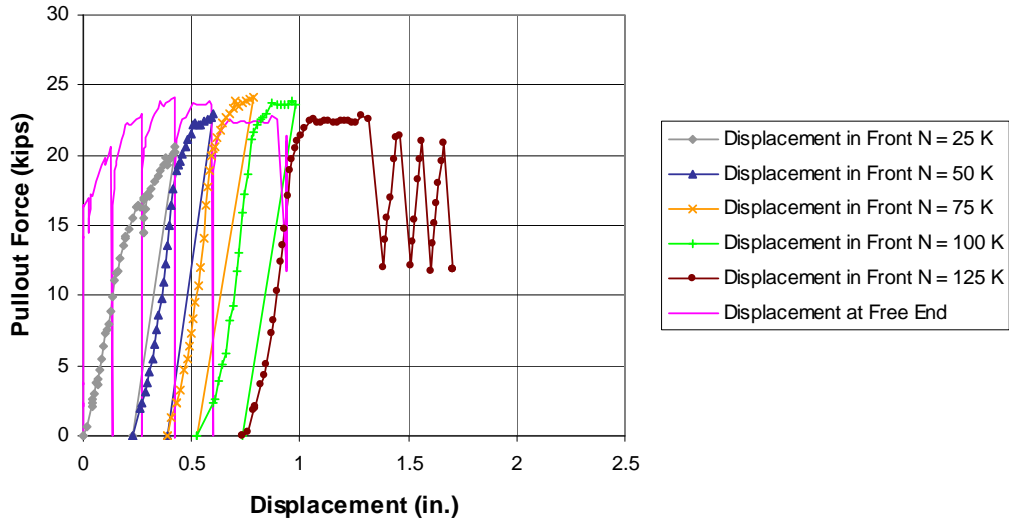


Figure C.10: Load-displacement Relationship for Strand BG1S_13R

Date Tested: August 9, 2001

Length embedded in concrete prior to test: 12.6 in. (0.32 m)

Average bond strength: 856 psi (5,900 kPa)

Table C.10: Summary of Test Results for Strand BG1S_13R

Clamping Load N	Slip Occurred or Resumed At
25 kips (111 kN)	16.97 kips (75.5 kN)
50 kips (222 kN)	18.94 kips (84.3 kN)
75 kips (334 kN)	19.96 kips (88.8 kN)
100 kips (445 kN)	21.16 kips (94.1 kN)
125 kips (556 kN)	20.46 kips (91.0 kN)

BG1S_17R: Pullout Force vs. Key Displacements

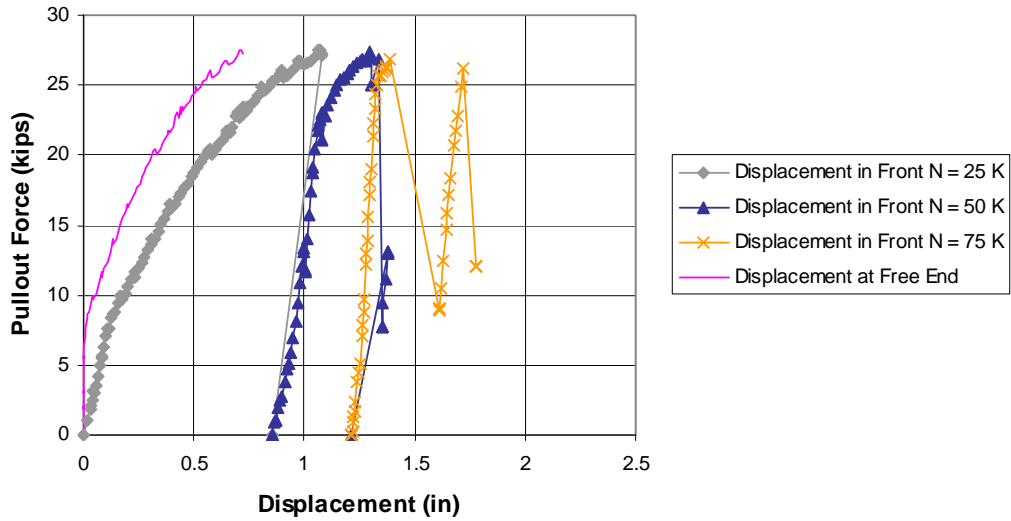


Figure C.11 Load-displacement Relationship for Strand BG1S_17R

Date Tested: July 31, 2001

Length embedded in concrete prior to test: 13.8 in. (0.35 m)

Average bond strength: 327 psi (2,250 kPa)

Table C.11: Summary of Test Results for Strand BG1S_17R

Clamping Load N	Slip Occurred or Resumed At
25 kips (111 kN)	7.06 kips (31.4 kN)
50 kips (222 kN)	21.76 kips (96.8 kN)
75 kips (334 kN)	25.7 kips (111.3 kN)

SLICE BG2N

BG2N_1L: Pullout Force vs. Key Displacements

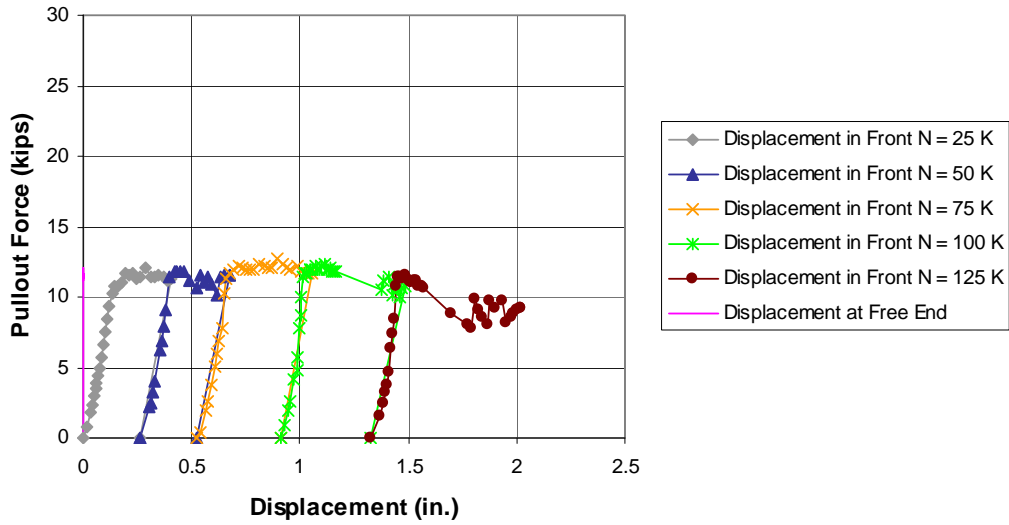


Figure C.12: Load-displacement Relationship for Strand BG2N_1L

Date Tested: October 19, 2001

Length embedded in concrete prior to test: 13 in. (0.33 m)

Average bond strength: 457 psi (3,150 kPa)

Table C.12: Summary of Test Results for Strand BG2N_1L

Clamping Load N	Slip Occurred or Resumed At
25 kips (111 kN)	9.34 kips (41.6 kN)
50 kips (222 kN)	11.39 kips (50.7 kN)
75 kips (334 kN)	11.36 kips (50.5 kN)
100 kips (445 kN)	11.49 kips (51.1 kN)
125 kips (556 kN)	10.79 kips (48.0 kN)

BG2N_4L: Pullout Force vs. Key Displacements

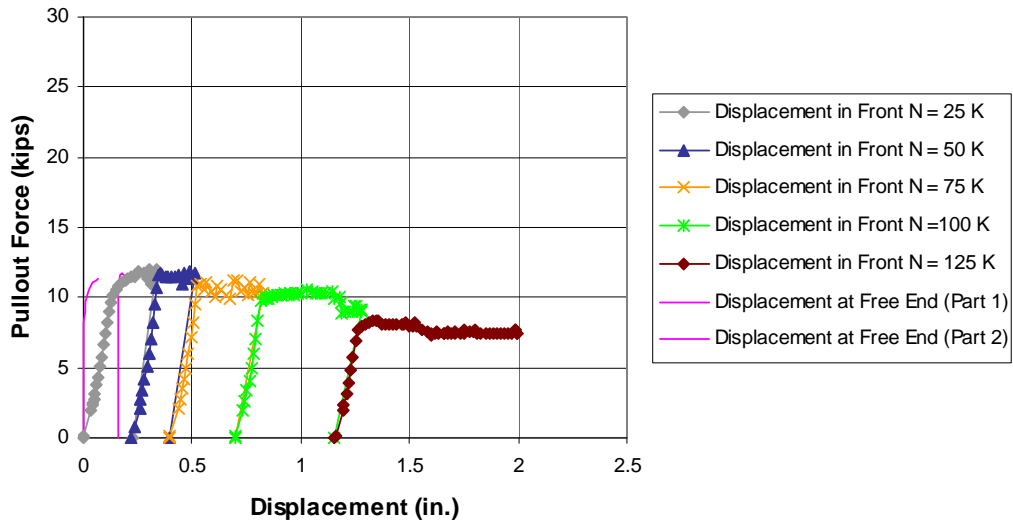


Figure C.13: Load-displacement Relationship for Strand BG2N_4L

Date Tested: October 26, 2001

Length embedded in concrete prior to test: 13.6 in. (0.35 m)

Average bond strength: 420 psi (2,900 kPa)

Table C.13: Summary of Test Results for Strand BG2N_4L

Clamping Load N	Slip Occurred or Resumed At
25 kips (111 kN)	8.99 kips (40.0 kN)
50 kips (222 kN)	11.56 kips (51.4 kN)
75 kips (334 kN)	10.89 kips (48.4 kN)
100 kips (445 kN)	10.09 kips (44.9 kN)
125 kips (556 kN)	7.96 kips (35.4 kN)

BG2N_6L: Pullout Force vs. Key Displacements

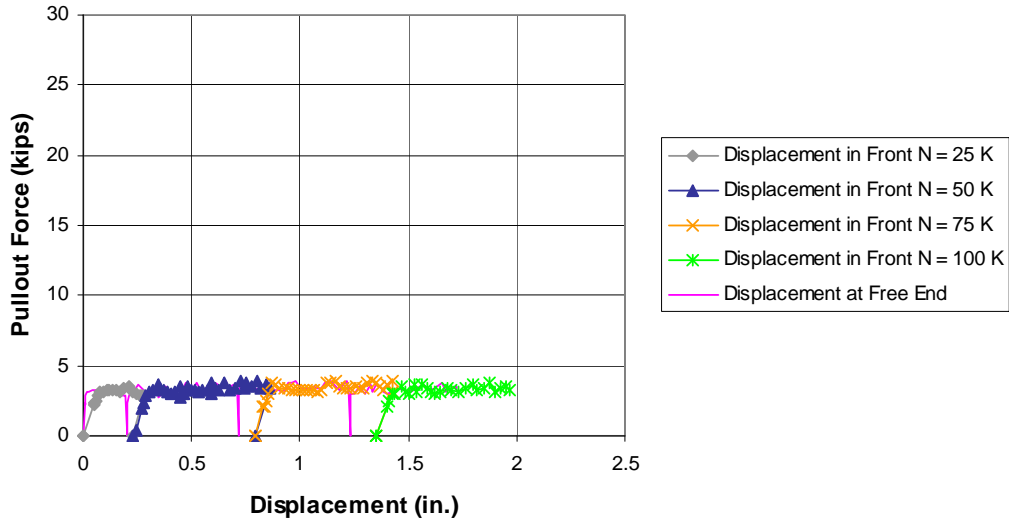


Figure C.14: Load-displacement Relationship for Strand BG2N_6L

Date Tested: October 26, 2001

Length embedded in concrete prior to test: 14.3 in. (0.36 m)

Average bond strength: 128 psi (880 kPa)

Table C.14: Summary of Test Results for Strand BG2N_6L

Clamping Load N	Slip Occurred or Resumed At
25 kips (111 kN)	2.86 kips (12.7 kN)
50 kips (222 kN)	2.89 kips (12.9 kN)
75 kips (334 kN)	3.03 kips (13.5 kN)
100 kips (445 kN)	3.01 kips (13.4 kN)

BG2N_8L: Pullout Force vs. Key Displacements

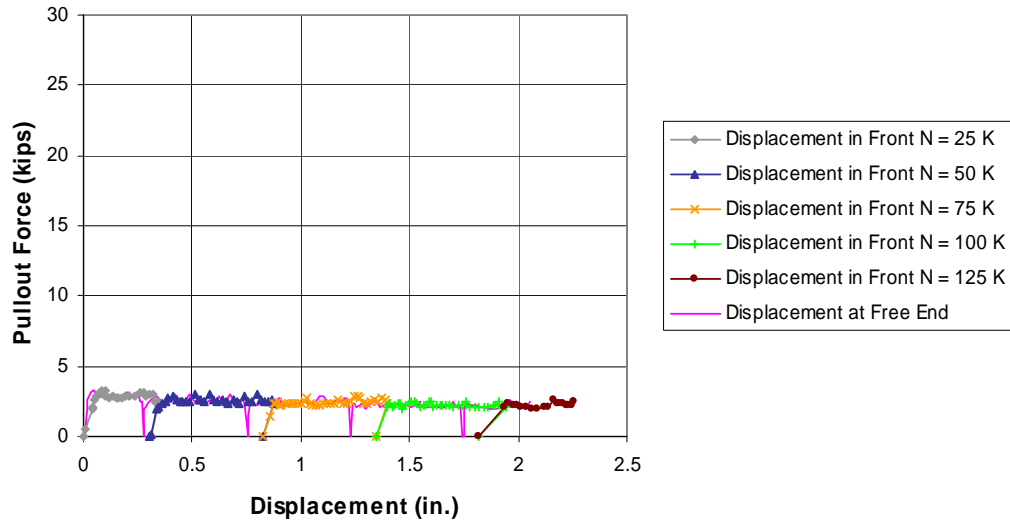


Figure C.15: Load-displacement Relationship for Strand BG2N_8L

Date Tested: October 25, 2001

Length embedded in concrete prior to test: 13 in. (0.33 m)

Average bond strength: 97 psi (670 kPa)

Table C.15: Summary of Test Results for Strand BG2N_8L

Clamping Load N	Slip Occurred or Resumed At
25 kips (111 kN)	1.98 kips (8.81 kN)
50 kips (222 kN)	2.15 kips (9.56 kN)
75 kips (334 kN)	2.32 kips (10.3 kN)
100 kips (445 kN)	2.35 kips (10.4 kN)
125 kips (556 kN)	2.37 kips (10.5 kN)

BG2N_15L: Pullout Force vs. Key Displacements

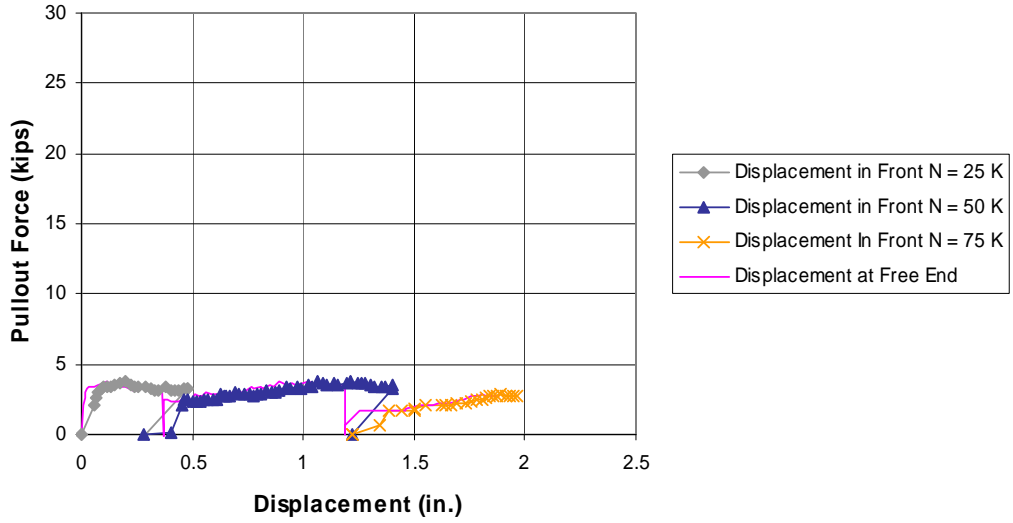


Figure C.16: Load-displacement Relationship for Strand BG2N_15L

Date Tested: October 18, 2001

Length embedded in concrete prior to test: 14.3 in. (0.36 m)

Average bond strength: 93 psi (640 kPa)

Table C.16: Summary of Test Results for Strand BG2N_15L

Clamping Load N	Slip Occurred or Resumed At
25 kips (111 kN)	2.09 kips (9.3 kN)
50 kips (222 kN)	2.46 kips (10.9 kN)
75 kips (334 kN)	1.7 kips (7.6 kN)

BG2N_17L_retest: Pullout Force vs. Key Displacements

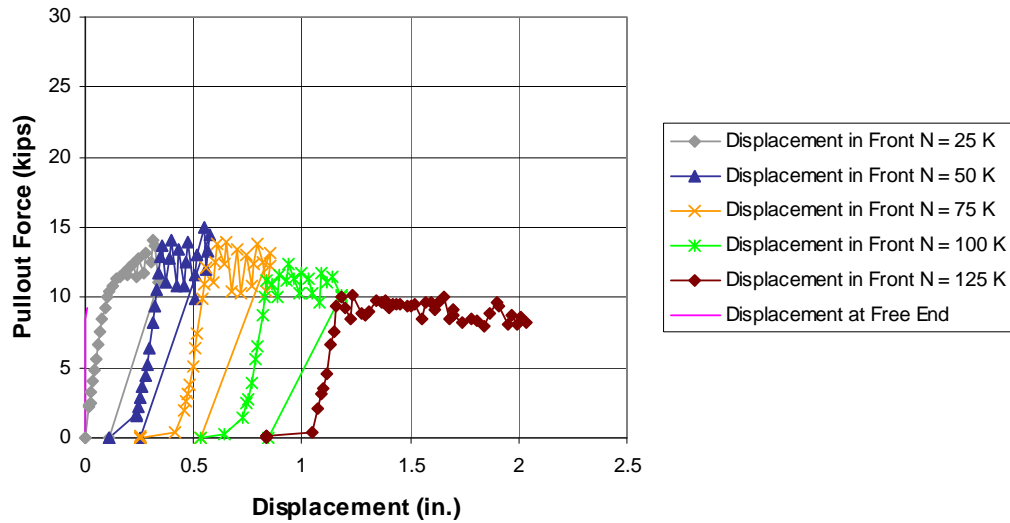


Figure C.17: Load-displacement Relationship for Strand BG2N_17L_retest

Date Tested: October 18, 2001

Length embedded in concrete prior to test: 13.8 in. (0.35 m)

Average bond strength: 392 psi (2,700 kPa)

Table C.17: Summary of Test Results for Strand BG2N_17L_retest

Clamping Load N	Slip Occurred or Resumed At
25 kips (111 kN)	8.47 kips (37.7 kN)
50 kips (222 kN)	13.74 kips (61.1 kN)
75 kips (334 kN)	12.15 kips (54.1 kN)
100 kips (445 kN)	11.25 kips (50.0 kN)
125 kips (556 kN)	10.01 kips (44.5 kN)

BG2N_18L: Pullout Force vs. Key Displacements

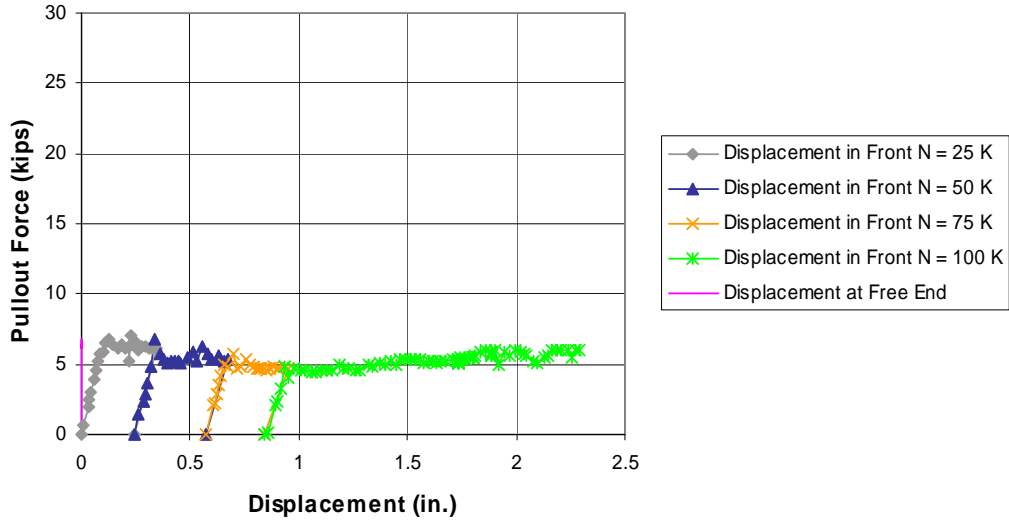


Figure C.18: Load-displacement Relationship for Strand BG2N_18L

Date Tested: October 19, 2001

Length embedded in concrete prior to test: 12.9 in. (0.33 m)

Average bond strength: 227 psi (1,560 kPa)

Table C.18: Summary of Test Results for Strand BG2N_18L

Clamping Load N	Slip Occurred or Resumed At
25 kips (111 kN)	4.59 kips (20.4 kN)
50 kips (222 kN)	6.82 kips (30.3 kN)
75 kips (334 kN)	4.99 kips (22.2 kN)
100 kips (445 kN)	4.78 kips (21.3 kN)

BG2N_2R: Pullout Force vs. Key Displacements

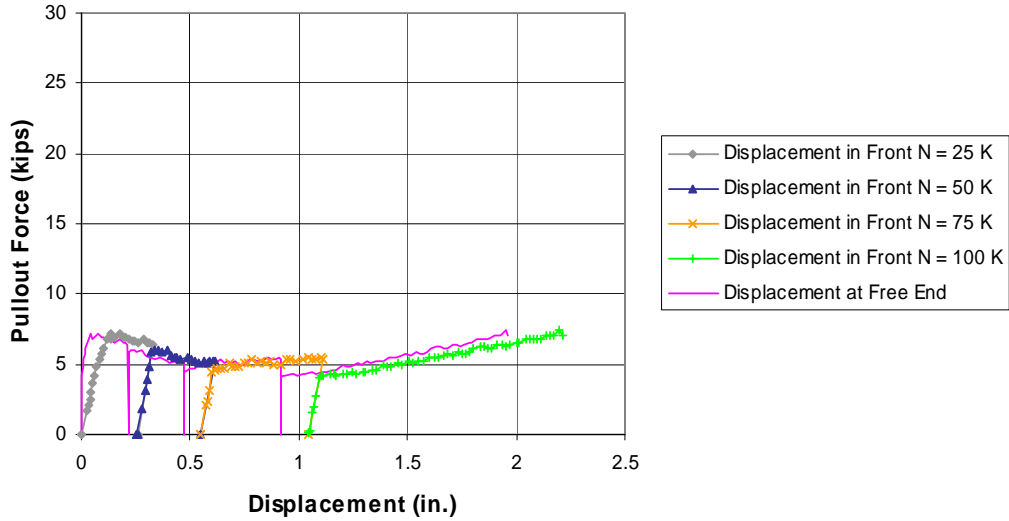


Figure C.19: Load-displacement Relationship for Strand BG2N_2R

Date Tested: November 9, 2001

Length embedded in concrete prior to test: 14 in. (0.36 m)

Average bond strength: 219 psi (1,510 kPa)

Table C.19: Summary of Test Results for Strand BG2N_2R

Clamping Load N	Slip Occurred or Resumed At
25 kips (111 kN)	4.81 kips (21.4 kN)
50 kips (222 kN)	6.06 kips (27.0 kN)
75 kips (334 kN)	4.61 kips (20.5 kN)
100 kips (445 kN)	4.2 kips (18.7 kN)

BG2N_4R: Pullout Force vs. Key Displacements

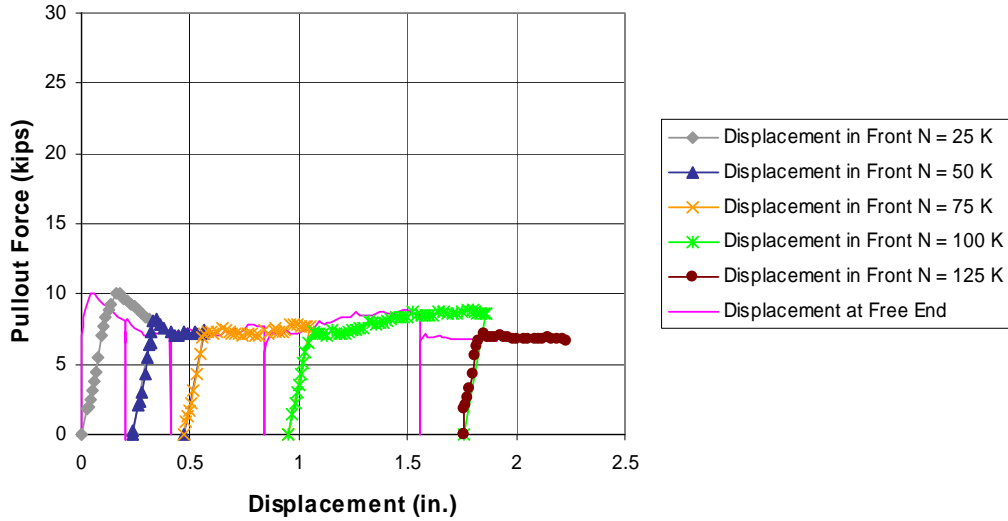


Figure C.20: Load-displacement Relationship for Strand BG2N_4R

Date Tested: November 5, 2001

Length embedded in concrete prior to test: 13.63 in. (0.35 m)

Average bond strength: 360 psi (2,480 kPa)

Table C.20: Summary of Test Results for Strand BG2N_4R

Clamping Load N	Slip Occurred or Resumed At
25 kips (111 kN)	7.71 kips (34.3 kN)
50 kips (222 kN)	8.21 kips (36.5 kN)
75 kips (334 kN)	7.22 kips (32.1 kN)
100 kips (445 kN)	6.53 kips (29.1 kN)
125 kips (556 kN)	6.68 kips (29.7 kN)

BG2N_7R: Pullout Force vs. Key Displacements

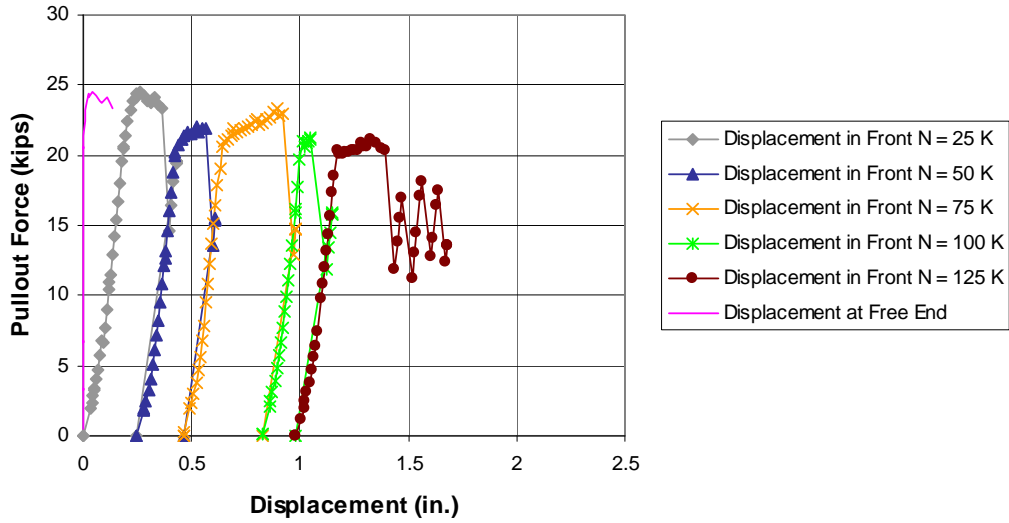


Figure C.21: Load-displacement Relationship for Strand BG2N_7R

Date Tested: November 5, 2001

Length embedded in concrete prior to test: 14.38 in. (0.37 m)

Average bond strength: 991 psi (6,840 kPa)

Table C.21: Summary of Test Results for Strand BG2N_7R

Clamping Load N	Slip Occurred or Resumed At
25 kips (111 kN)	22.39 kips (99.6 kN)
50 kips (222 kN)	20.16 kips (89.7 kN)
75 kips (334 kN)	20.56 kips (91.5 kN)
100 kips (445 kN)	19.69 kips (87.6 kN)
125 kips (556 kN)	20.37 kips (90.6 kN)

BG2N_9R: Pullout Force vs. Key Displacements

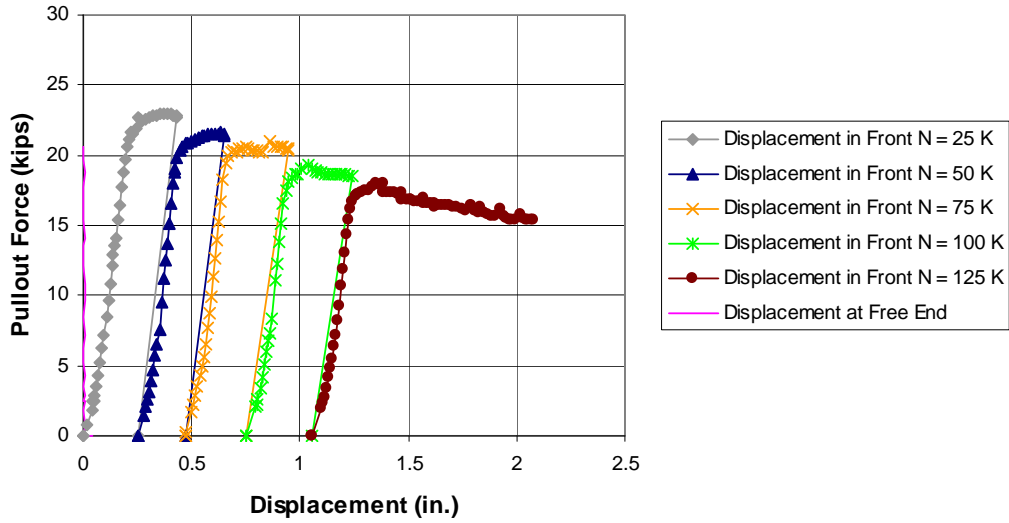


Figure C.22: Load-displacement Relationship for Strand BG2N_9R

Date Tested: November 5, 2001

Length embedded in concrete prior to test: 14.3 in. (0.36 m)

Average bond strength: 842 psi (5,800 kPa)

Table C.22: Summary of Test Results for Strand BG2N_9R

Clamping Load N	Slip Occurred or Resumed At
25 kips (111 kN)	18.84 kips (83.8 kN)
50 kips (222 kN)	19.82 kips (88.2 kN)
75 kips (334 kN)	19.46 kips (86.6 kN)
100 kips (445 kN)	17.51 kips (77.9 kN)
125 kips (556 kN)	16.17 kips (71.9 kN)

BG2N_13R: Pullout Force vs. Key Displacements

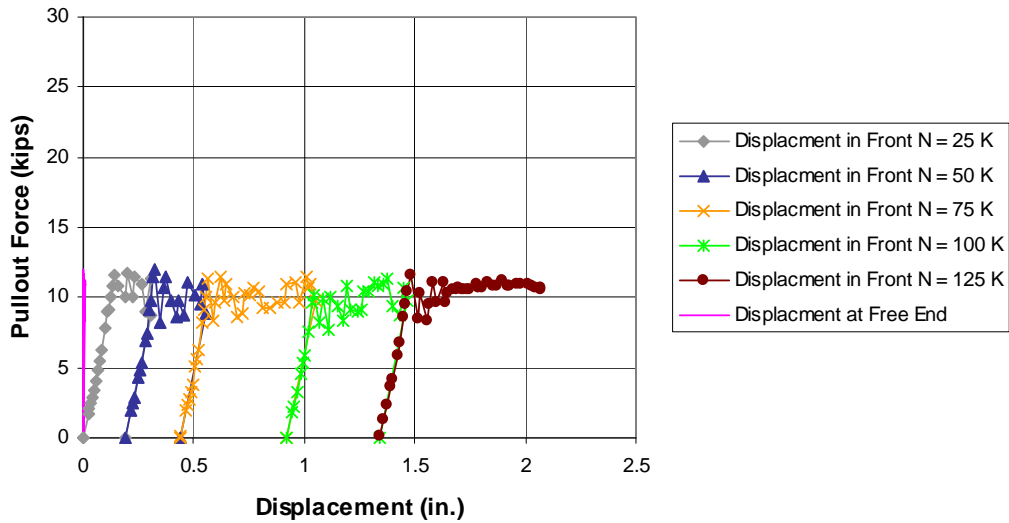


Figure C.23: Load-displacement Relationship for Strand BG2N_13R

Date Tested: November 9, 2001

Length embedded in concrete prior to test: 13.9 in. (0.35 m)

Average bond strength: 413 psi (2,850 kPa)

Table C.23: Summary of Test Results for Strand BG2N_13R

Clamping Load N	Slip Occurred or Resumed At
25 kips (111 kN)	9.00 kips (40.0 kN)
50 kips (222 kN)	11.96 kips (53.2 kN)
75 kips (334 kN)	11.32 kips (50.4 kN)
100 kips (445 kN)	10.22 kips (45.5 kN)
125 kips (556 kN)	10.45 kips (46.5 kN)

BG2N_15R: Pullout Force vs. Key Displacements

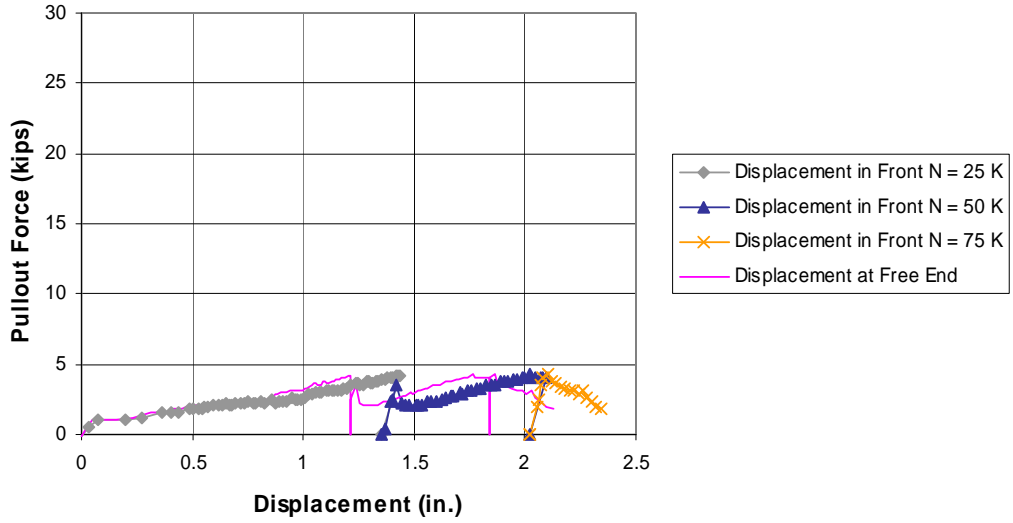


Figure C.24: Load-displacement Relationship for Strand BG2N_15R

Date Tested: November 9, 2001

Length embedded in concrete prior to test: 14 in. (0.36 m)

Average bond strength: 22 psi (150 kPa)

Table C.24: Summary of Test Results for Strand BG2N_15R

Clamping Load N	Slip Occurred or Resumed At
25 kips (111 kN)	0.48 kips (2.1 kN)
50 kips (222 kN)	3.58 kips (15.9 kN)
75 kips (334 kN)	4.25 kips (18.9 kN)

BG2N_17R: Pullout Force vs. Key Displacements

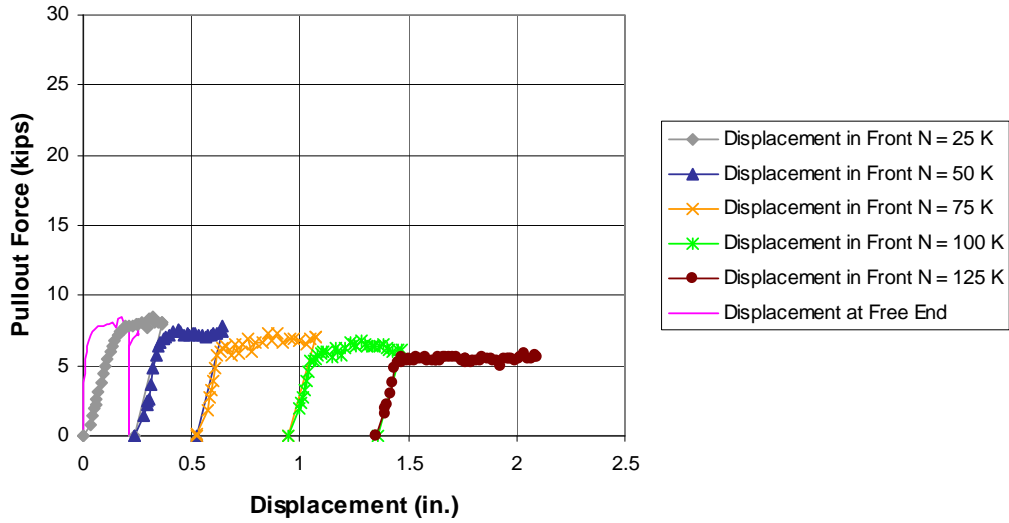


Figure C.25: Load-displacement Relationship for Strand BG2N_17R

Date Tested: November 9, 2001

Length embedded in concrete prior to test: 14.4 in. (0.37 m)

Average bond strength: 195 psi (1,340 kPa)

Table C.25: Summary of Test Results for Strand BG2N_17R

Clamping Load N	Slip Occurred or Resumed At
25 kips (111 kN)	4.4 kips (19.6 kN)
50 kips (222 kN)	6.7 kips (29.8 kN)
75 kips (334 kN)	5.99 kips (26.6 kN)
100 kips (445 kN)	5.35 kips (23.8 kN)
125 kips (556 kN)	5.22 kips (23.2 kN)

BG2N_18R: Pullout Force vs. Key Displacements

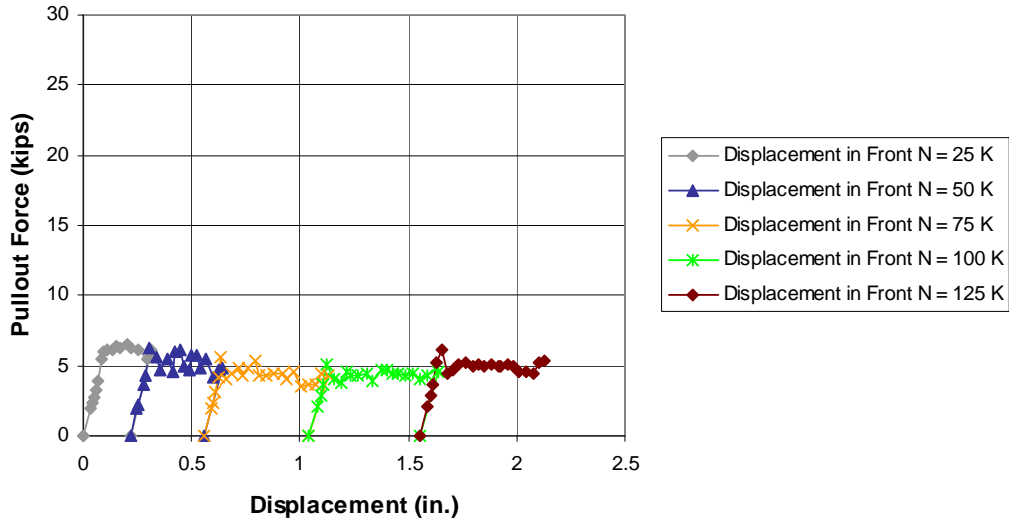


Figure C.26: Load-displacement Relationship for Strand BG2N_18R

Date Tested: November 9, 2001

Length embedded in concrete prior to test: 14.3 in. (0.36 m)

Average bond strength: 244 psi (1,680 kPa)

Table C.26: Summary of Test Results for Strand BG2N_18R

Clamping Load N	Slip Occurred or Resumed At
25 kips (111 kN)	5.46 kips (24.9 kN)
50 kips (222 kN)	6.21 kips (27.6 kN)
75 kips (334 kN)	5.58 kips (24.8 kN)
100 kips (445 kN)	5.07 kips (22.6 kN)
125 kips (556 kN)	6.16 kips (27.4 kN)

SLICE BG4S1

BG4S1_2L: Pullout Force vs. Key Displacements

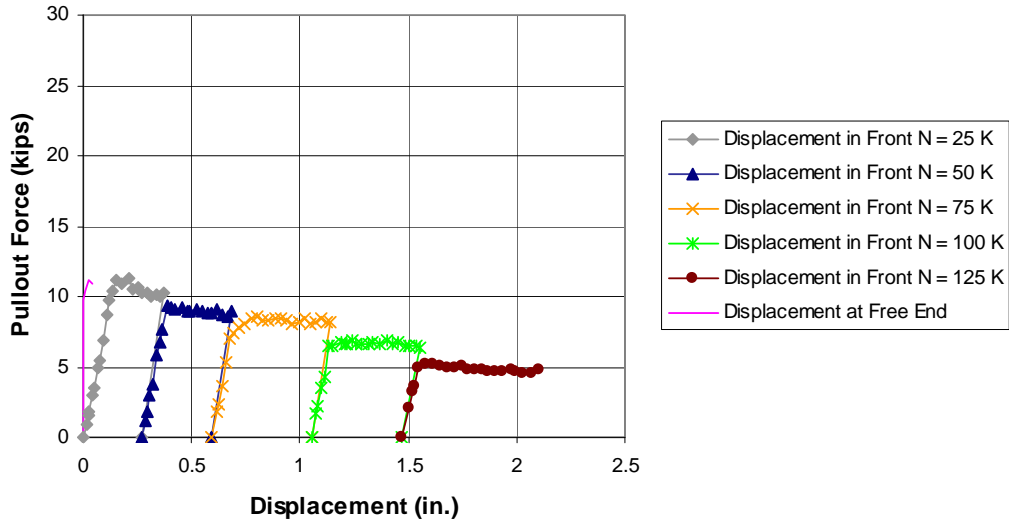


Figure C.27: Load-displacement Relationship for Strand BG4S1_2L

Date Tested: February 8, 2002

Length embedded in concrete prior to test: 13.5 in. (0.34 m)

Average bond strength: 491 psi (3,380 kPa)

Table C.27: Summary of Test Results for Strand BG4S1_2L

Clamping Load N	Slip Occurred or Resumed At
25 kips (111 kN)	10.41 kips (46.3 kN)
50 kips (222 kN)	9.41 kips (41.9 kN)
75 kips (334 kN)	7.38 kips (32.8 kN)
100 kips (445 kN)	6.5 kips (28.9 kN)
125 kips (556 kN)	4.88 kips (21.7 kN)

BG4S1_5L: Pullout Force vs. Key Displacements

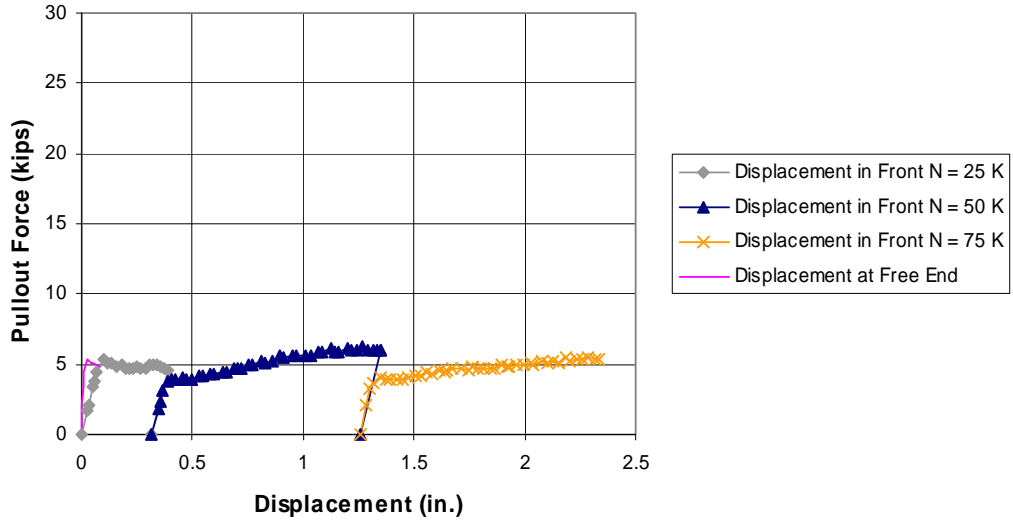


Figure C.28: Load-displacement Relationship for Strand BG4S1_5L

Date Tested: February 13, 2002

Length embedded in concrete prior to test: 12.8 in. (0.32 m)

Average bond strength: 265 psi (1,820 kPa)

Table C.28: Summary of Test Results for Strand BG4S1_5L

Clamping Load N	Slip Occurred or Resumed At
25 kips (111 kN)	5.30 kips (23.6 kN)
50 kips (222 kN)	3.83 kips (17.0 kN)
75 kips (334 kN)	3.65 kips (16.2 kN)

BG4S1_7L: Pullout Force vs. Key Displacements

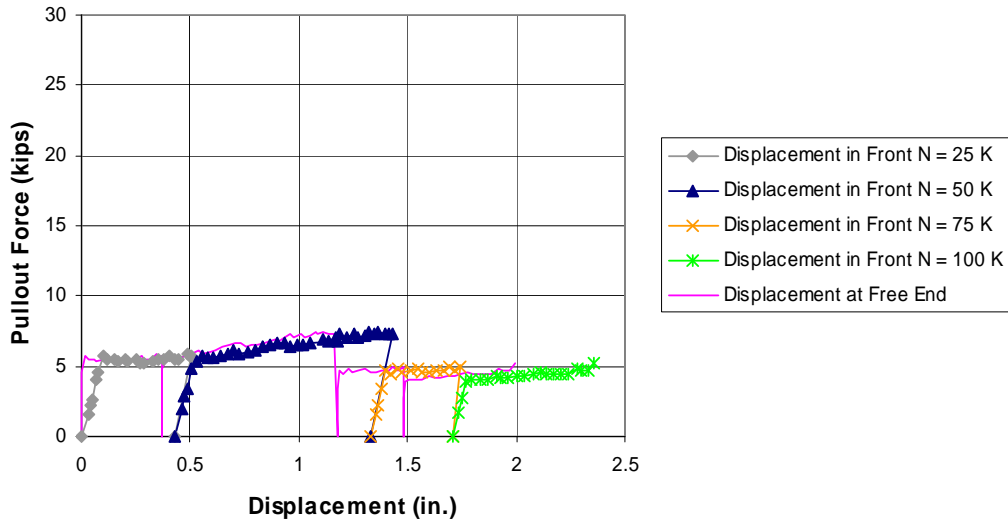


Figure C.29: Load-displacement Relationship for Strand BG4S1_7L

Date Tested: February 13, 2002

Length embedded in concrete prior to test: 14 in. (0.36 m)

Average bond strength: 259 psi (1,784 kPa)

Table C.29: Summary of Test Results for Strand BG4S1_7L

Clamping Load N	Slip Occurred or Resumed At
25 kips (111 kN)	5.69 kips (25.3 kN)
50 kips (222 kN)	5.35 kips (23.8 kN)
75 kips (334 kN)	4.66 kips (20.7 kN)
100 kips (445 kN)	3.96 kips (17.6 kN)

BG4S1_9L: Pullout Force vs. Key Displacements

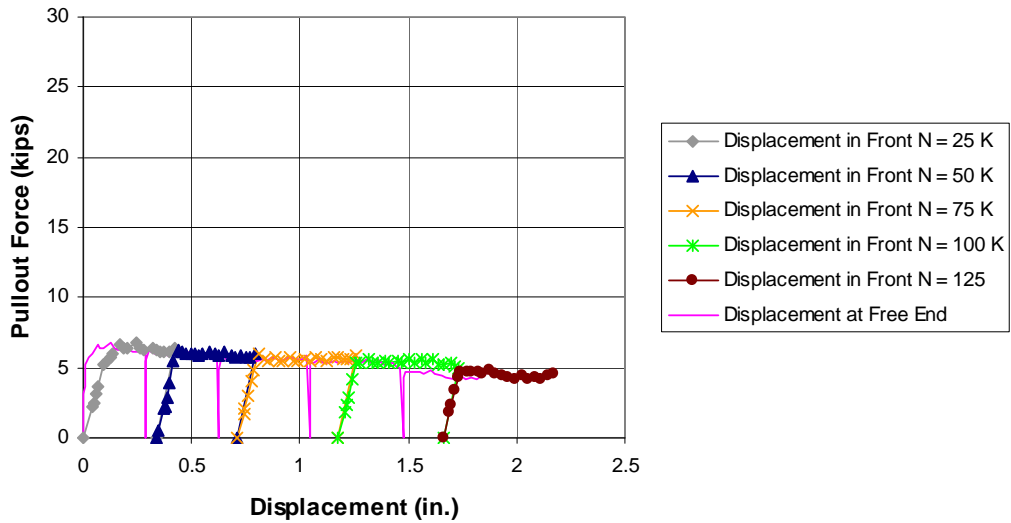


Figure C.30: Load-displacement Relationship for Strand BG4S1_9L

Date Tested: February 12, 2002

Length embedded in concrete prior to test: 12.3 in. (0.31 m)

Average bond strength: 269 psi (1,850 kPa)

Table C.30: Summary of Test Results for Strand BG4S1_9L

Clamping Load N	Slip Occurred or Resumed At
25 kips (111 kN)	5.17 kips (23 kN)
50 kips (222 kN)	6.26 kips (27.9 kN)
75 kips (334 kN)	5.94 kips (26.4 kN)
100 kips (445 kN)	5.36 kips (23.8 kN)
125 kips (556 kN)	4.63 kips (20.6 kN)

BG4S1_13L: Pullout Force vs. Key Displacements

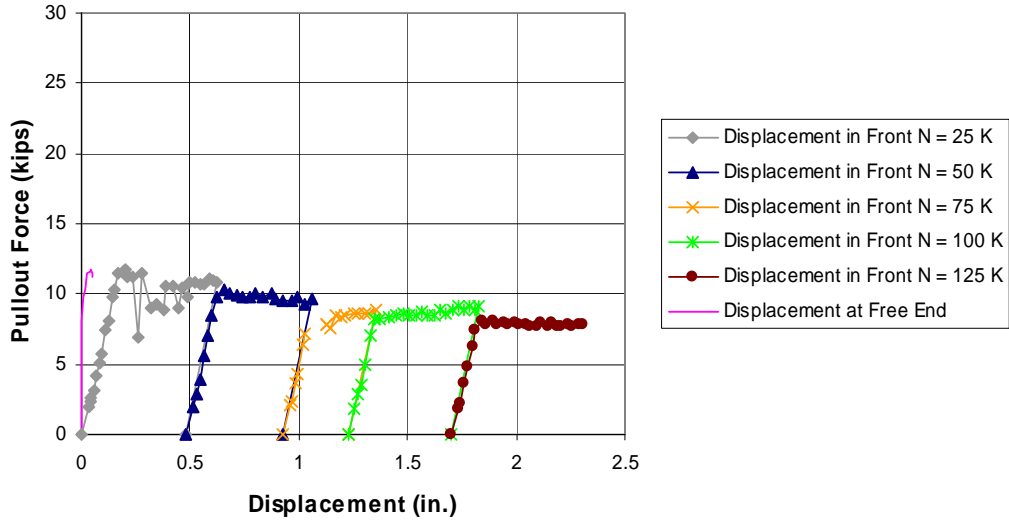


Figure C.31: Load-displacement Relationship for Strand BG4S1_13L

Date Tested: February 9, 2002

Length embedded in concrete prior to test: 14.3 in. (0.36 m)

Average bond strength: 439 psi (3,030 kPa)

Table C.31: Summary of Test Results for Strand BG4S1_13L

Clamping Load N	Slip Occurred or Resumed At
25 kips (111 kN)	9.83 kips (43.7 kN)
50 kips (222 kN)	9.83 kips (43.7 kN)
75 kips (334 kN)	7.2 kips (32.0 kN)
100 kips (445 kN)	8.18 kips (36.4 kN)
125 kips (556 kN)	8.09 kips (36 kN)

BG4S1_15L: Pullout Force vs. Key Displacements

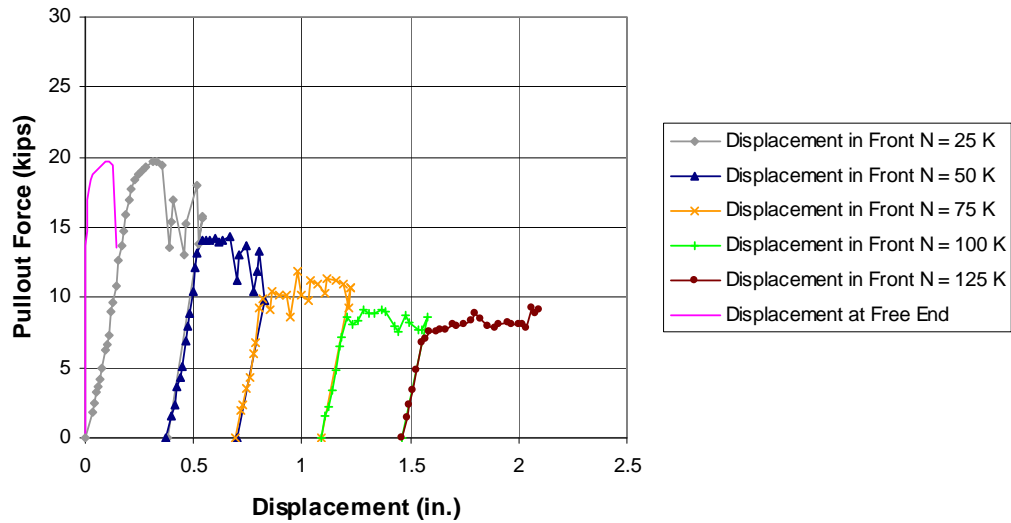


Figure C.32: Load-displacement Relationship for Strand BG4S1_15L

Date Tested: February 8, 2002

Length embedded in concrete prior to test: 14 in. (0.36 m)

Average bond strength: 672 psi (4,630 kPa)

Table C.32: Summary of Test Results for Strand BG4S1_15L

Clamping Load N	Slip Occurred or Resumed At
25 kips (111 kN)	14.77 kips (65.7 kN)
50 kips (222 kN)	14.02 kips (62.4 kN)
75 kips (334 kN)	9.97 kips (44.4 kN)
100 kips (445 kN)	8.63 kips (38.4 kN)
125 kips (556 kN)	7.06 kips (31.4 kN)

BG4S1_17L: Pullout Force vs. Key Displacements

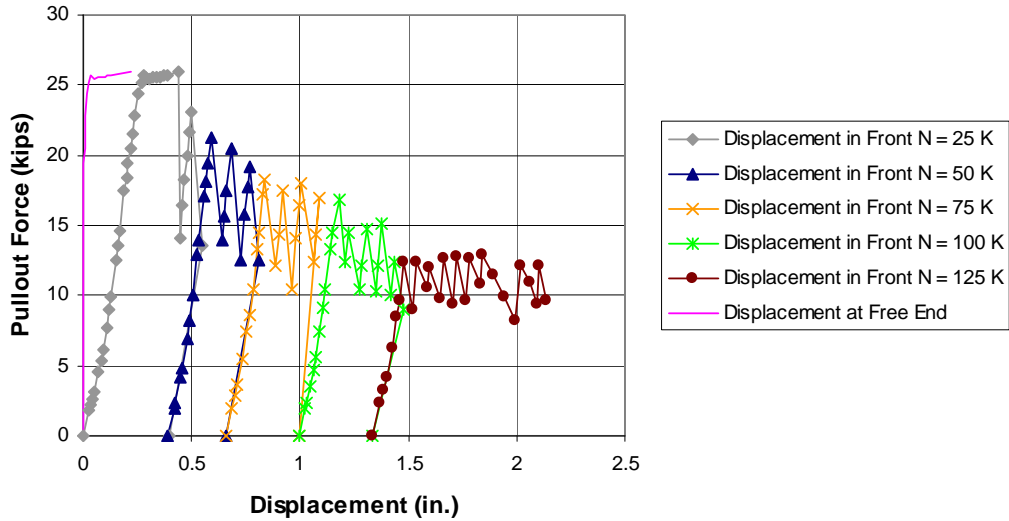


Figure C.33: Load-displacement Relationship for Strand BG4S1_17L

Date Tested: February 8, 2002

Length embedded in concrete prior to test: 14.5 in. (0.37 m)

Average bond strength: 901 psi (6,210 kPa)

Table C.33: Summary of Test Results for Strand BG4S1_17L

Clamping Load N	Slip Occurred or Resumed At
25 kips (111 kN)	20.52 kips (91.3 kN)
50 kips (222 kN)	17.04 kips (75.8 kN)
75 kips (334 kN)	18.24 kips (81.1 kN)
100 kips (445 kN)	14.45 kips (64.3 kN)
125 kips (556 kN)	12.39 kips (55.1 kN)

BG4S1_18L: Pullout Force vs. Key Displacements

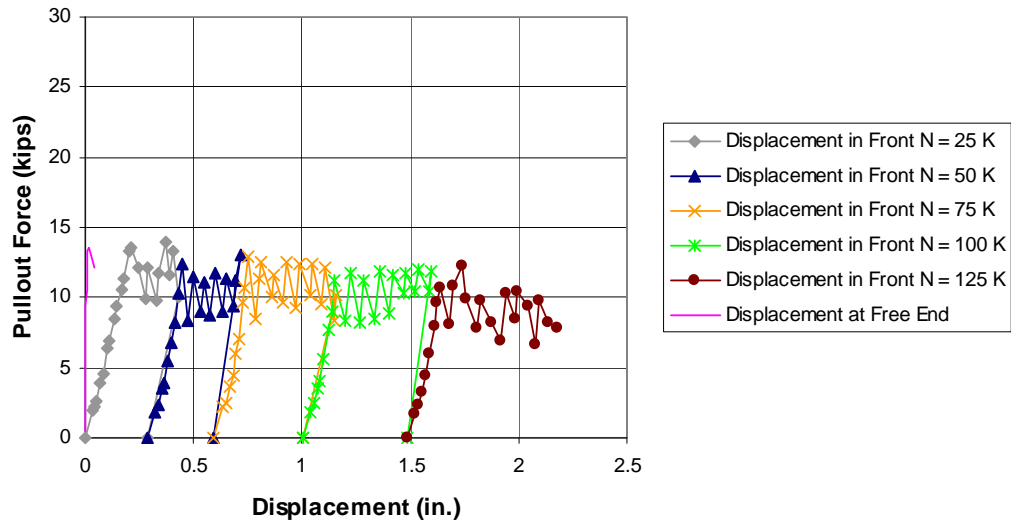


Figure C.34: Load-displacement Relationship for Strand BG4S1_18L

Date Tested: February 9, 2002

Length embedded in concrete prior to test: 12.8 in. (0.32 m)

Average bond strength: 664 psi (4,570 kPa)

Table C.34: Summary of Test Results for Strand BG4S1_18L

Clamping Load N	Slip Occurred or Resumed At
25 kips (111 kN)	13.29 kips (59.1 kN)
50 kips (222 kN)	12.43 kips (55.3 kN)
75 kips (334 kN)	12.96 kips (57.7 kN)
100 kips (445 kN)	11.28 kips (50.2 kN)
125 kips (556 kN)	10.74 kips (47.8 kN)

BG4S1_1R: Pullout Force vs. Key Displacements

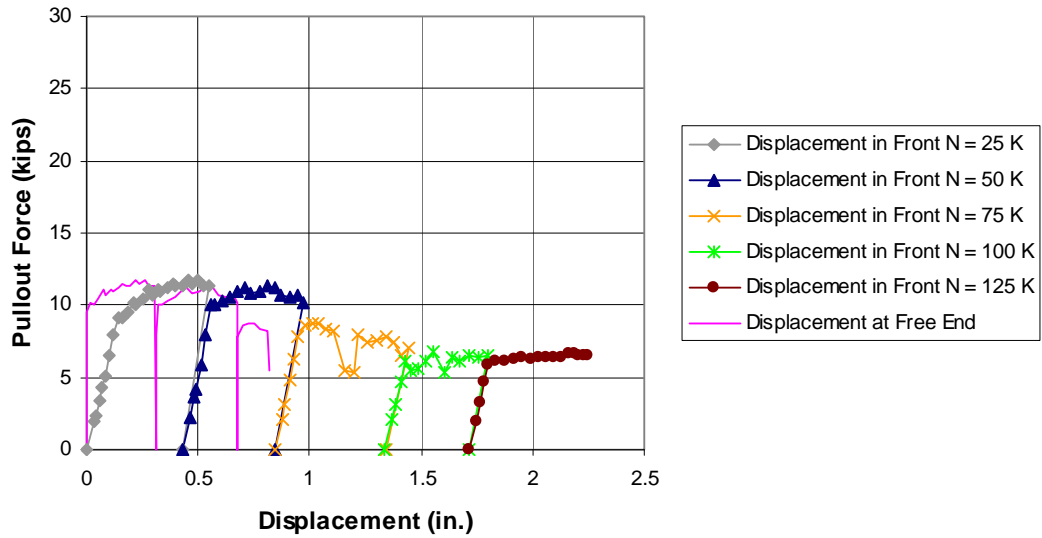


Figure C.35: Load-displacement Relationship for Strand BG4S1_1R

Date Tested: February 19, 2002

Length embedded in concrete prior to test: 13.5 in. (0.34 m)

Average bond strength: 481 psi (3,310 kPa)

Table C.35: Summary of Test Results for Strand BG4S1_1R

Clamping Load N	Slip Occurred or Resumed At
25 kips (111 kN)	10.19 kips (45.3 kN)
50 kips (222 kN)	10.03 kips (44.6 kN)
75 kips (334 kN)	8.66 kips (38.5 kN)
100 kips (445 kN)	6.19 kips (27.5 kN)
125 kips (556 kN)	5.86 kips (26.1 kN)

BG4S1_4R: Pullout Force vs. Key Displacements

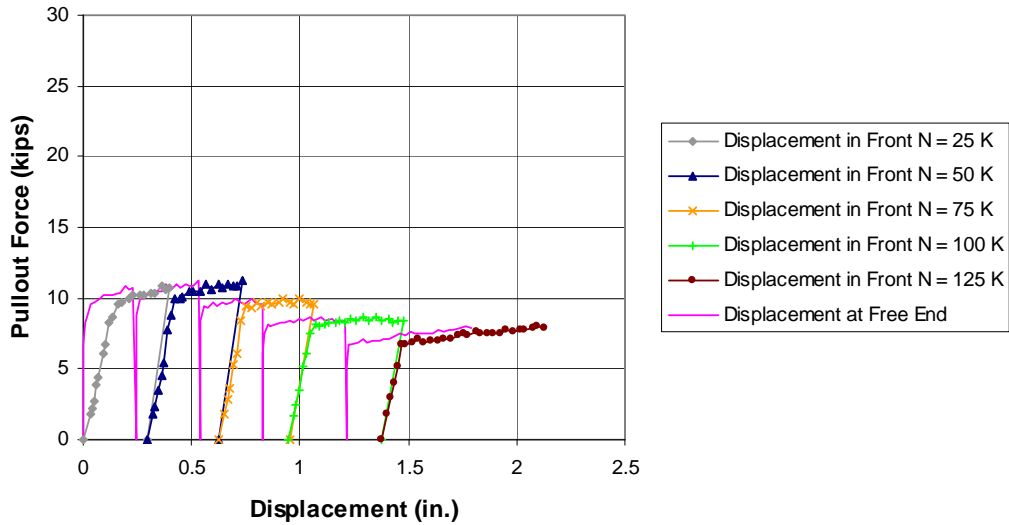


Figure C.36: Load-displacement Relationship for Strand BG4S1_4R

Date Tested: February 15, 2002

Length embedded in concrete prior to test: 13.8 in. (0.35 m)

Average bond strength: 384 psi (2,650 kPa)

Table C.36: Summary of Test Results for Strand BG4S1_4R

Clamping Load N	Slip Occurred or Resumed At
25 kips (111 kN)	8.3 kips (36.9 kN)
50 kips (222 kN)	9.99 kips (44.4 kN)
75 kips (334 kN)	9.49 kips (42.2 kN)
100 kips (445 kN)	8.12 kips (36.1 kN)
125 kips (556 kN)	6.75 kips (30.0 kN)

BG4S1_6R: Pullout Force vs. Key Displacements

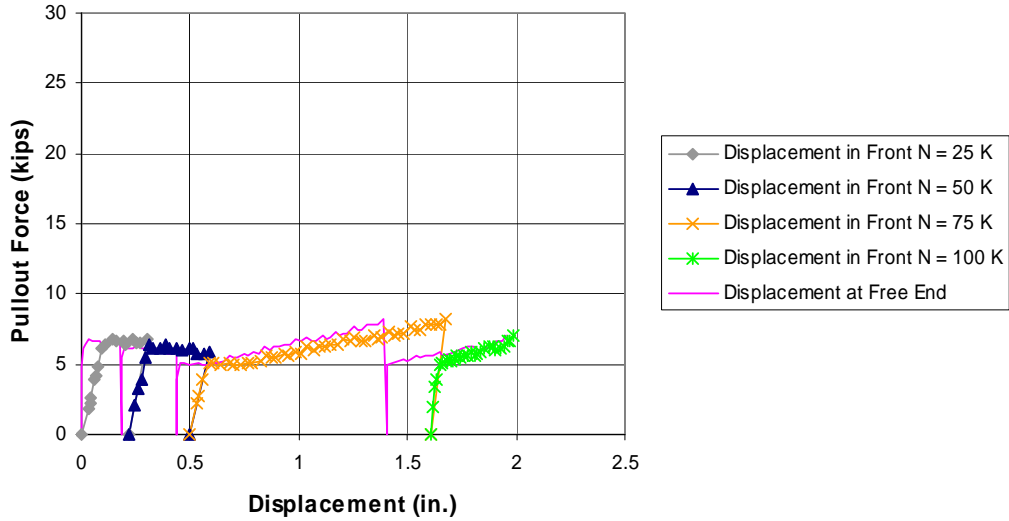


Figure C.37: Load-displacement Relationship for Strand BG4S1_6R

Date Tested: February 15, 2002

Length embedded in concrete prior to test: 12.25 in. (0.31 m)

Average bond strength: 322 psi (2,220 kPa)

Table C.37: Summary of Test Results for Strand BG4S1_6R

Clamping Load N	Slip Occurred or Resumed At
25 kips (111 kN)	6.19 kips (27.5 kN)
50 kips (222 kN)	6.44 kips (28.7 kN)
75 kips (334 kN)	5.14 kips (22.9 kN)
100 kips (445 kN)	4.93 kips (21.9 kN)

BG4S1_9R: Pullout Force vs. Key Displacements

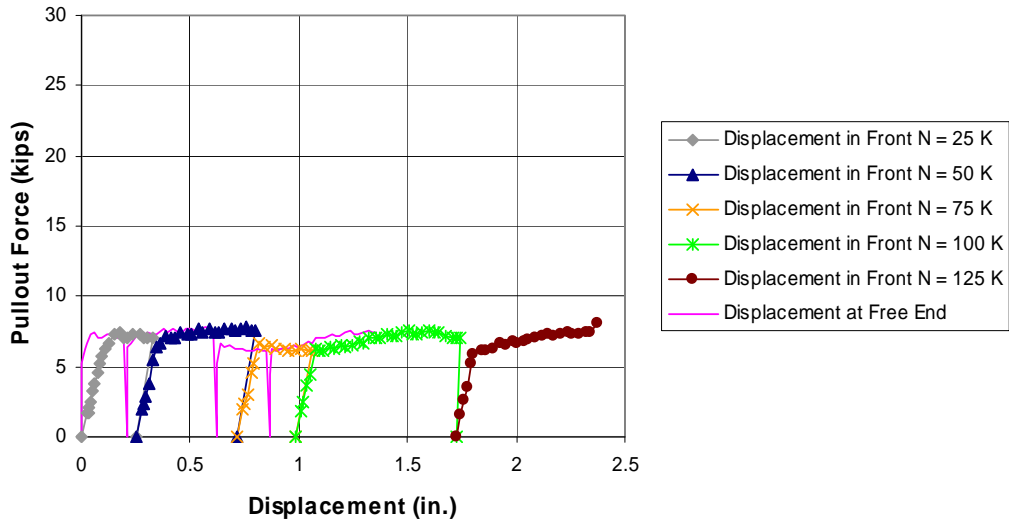


Figure C.38: Load-displacement Relationship for Strand BG4S1_9R

Date Tested: February 15, 2002

Length embedded in concrete prior to test: 13.8 in. (0.35 m)

Average bond strength: 266 psi (1,840 kPa)

Table C.38: Summary of Test Results for Strand BG4S1_9R

Clamping Load N	Slip Occurred or Resumed At
25 kips (111 kN)	5.75 kips (25.6 kN)
50 kips (222 kN)	6.61 kips (29.4 kN)
75 kips (334 kN)	6.64 kips (29.5 kN)
100 kips (445 kN)	6.26 kips (27.9 kN)
125 kips (556 kN)	5.84 kips (26.0 kN)

BG4S1_15R: Pullout Force vs. Key Displacements

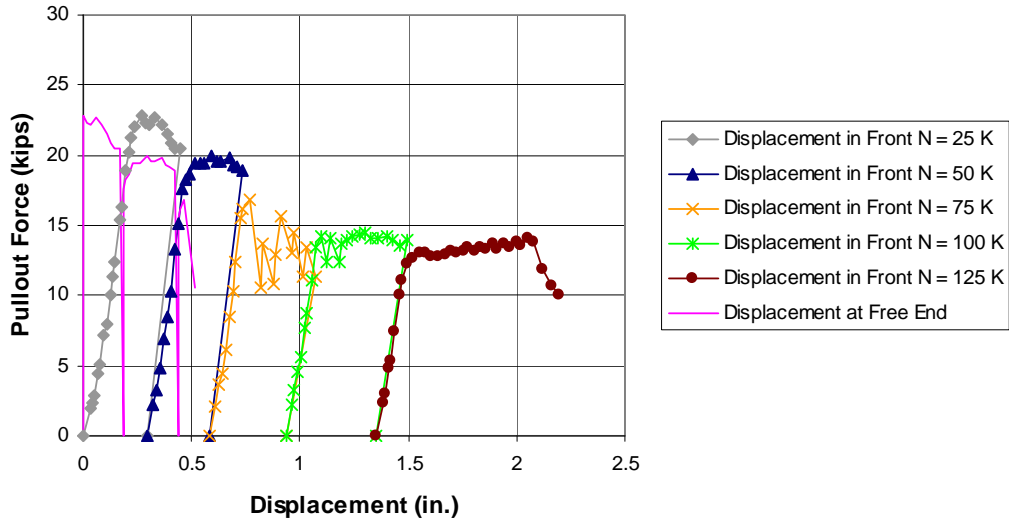


Figure C.39: Load-displacement Relationship for Strand BG4S1_15R

Date Tested: February 19, 2002

Length embedded in concrete prior to test: 14.5 in. (0.37 m)

Average bond strength: 1,003 psi (6,910 kPa)

Table C.39: Summary of Test Results for Strand BG4S1_15R

Clamping Load N	Slip Occurred or Resumed At
25 kips (111 kN)	22.84 kips (101.6 kN)
50 kips (222 kN)	17.65 kips (78.5 kN)
75 kips (334 kN)	16.19 kips (72.0 kN)
100 kips (445 kN)	14.17 kips (63.0 kN)
125 kips (556 kN)	12.25 kips (54.5 kN)

BG4S1_17R: Pullout Force vs. Key Displacements

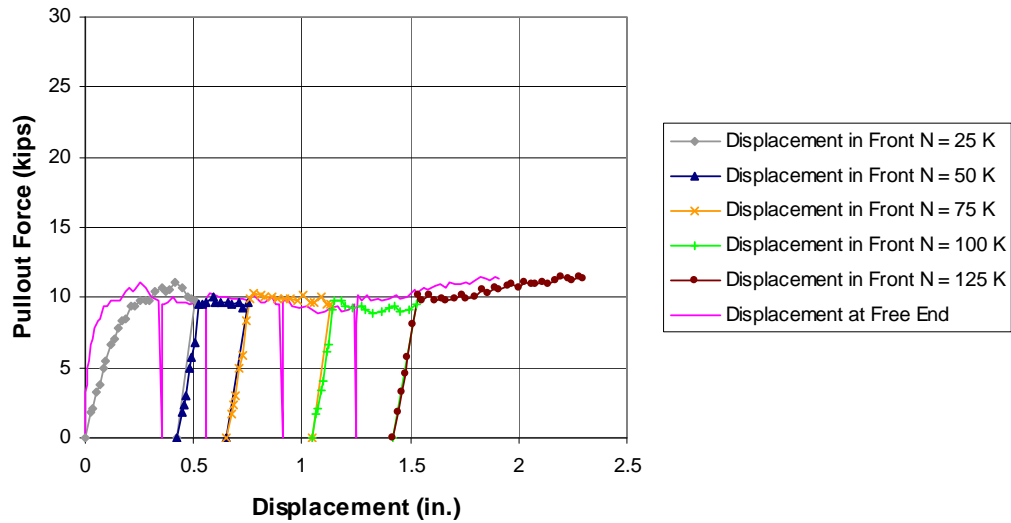


Figure C.40: Load-displacement Relationship for Strand BG4S1_17R

Date Tested: February 19, 2002

Length embedded in concrete prior to test: 15 in. (0.38 m)

Average bond strength: 158 psi (1,090 kPa)

Table C.40: Summary of Test Results for Strand BG4S1_17R

Clamping Load N	Slip Occurred or Resumed At
25 kips (111 kN)	3.72 kips (16.6 kN)
50 kips (222 kN)	9.56 kips (42.5 kN)
75 kips (334 kN)	10.32 kips (45.9 kN)
100 kips (445 kN)	9.76 kips (43.4 kN)
125 kips (556 kN)	10.24 kips (45.6 kN)

BG4S1_18R: Pullout Force vs. Key Displacements

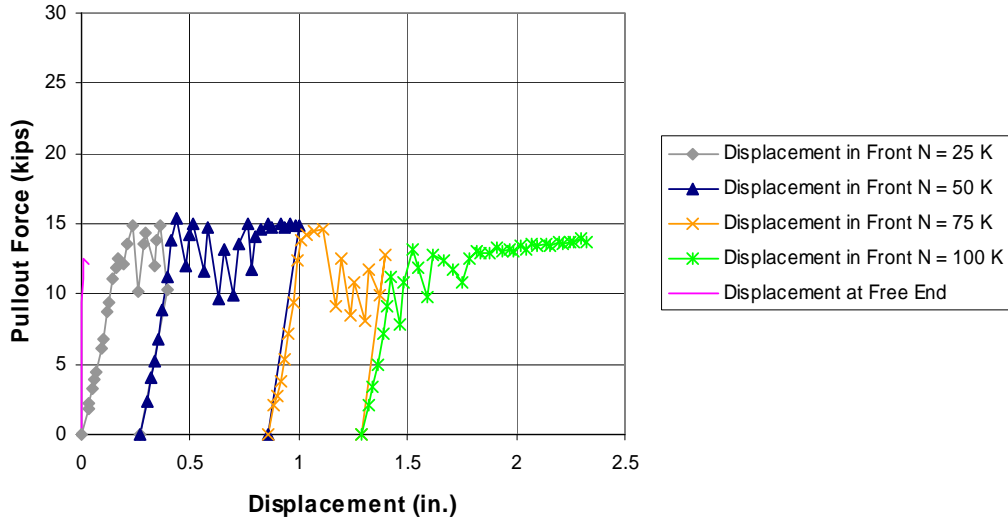


Figure C.41: Load-displacement Relationship for Strand BG4S1_18R

Date Tested: February 19, 2002

Length embedded in concrete prior to test: 13.6 in. (0.35 m)

Average bond strength: 554 psi (3,820 kPa)

Table C.41: Summary of Test Results for Strand BG4S1_18R

Clamping Load N	Slip Occurred or Resumed At
25 kips (111 kN)	11.85 kips (52.7 kN)
50 kips (222 kN)	13.76 kips (61.2 kN)
75 kips (334 kN)	13.84 kips (61.6 kN)
100 kips (445 kN)	11.2 kips (49.8 kN)

SLICE BG4S2

BG4S2_1L: Pullout Force vs. Key Displacements

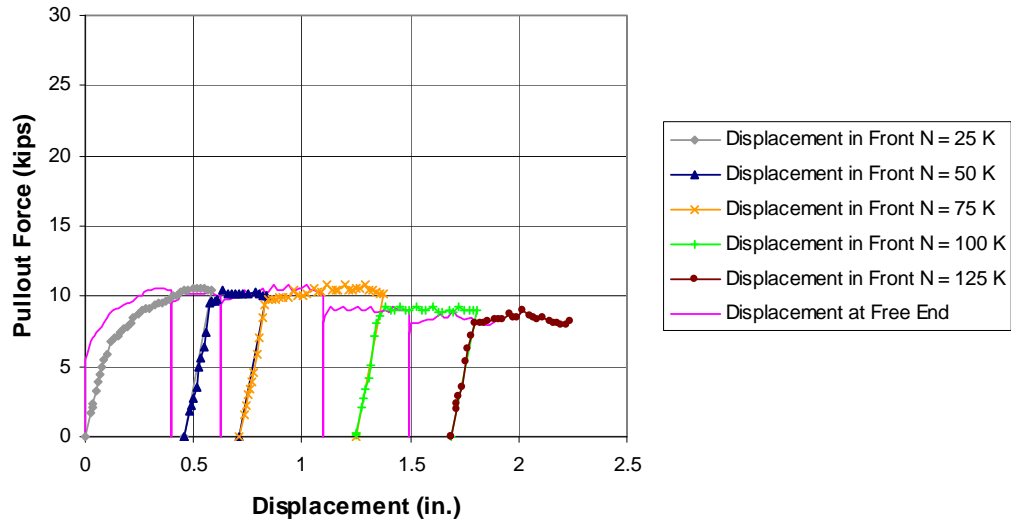


Figure C.42: Load-displacement Relationship for Strand BG4S2_1L

Date Tested: January 13, 2002

Length embedded in concrete prior to test: 13.2 in. (0.34 m)

Average bond strength: 280 psi (1,930 kPa)

Table C.42: Summary of Test Results for Strand BG4S2_1L

Clamping Load N	Slip Occurred or Resumed At
25 kips (111 kN)	5.81 kips (25.8 kN)
50 kips (222 kN)	9.61 kips (42.8 kN)
75 kips (334 kN)	9.72 kips (43.2 kN)
100 kips (445 kN)	8.63 kips (38.4 kN)
125 kips (556 kN)	8.1 kips (36.0 kN)

BG4S2_4L: Pullout Force vs. Key Displacements

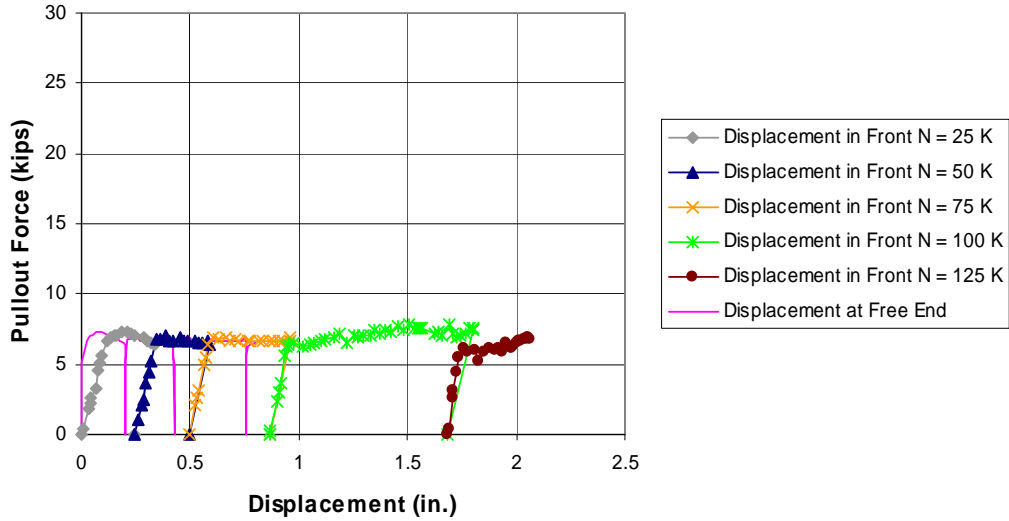


Figure C.43: Load-displacement Relationship for Strand BG4S2_4L

Date Tested: January 15, 2002

Length embedded in concrete prior to test: 13.5 in. (0.34 m)

Average bond strength: 265 psi (1,827 kPa)

Table C.43: Summary of Test Results for Strand BG4S2_4L

Clamping Load N	Slip Occurred or Resumed At
25 kips (111 kN)	5.62 kips (25 kN)
50 kips (222 kN)	6.8 kips (30.3 kN)
75 kips (334 kN)	6.89 kips (30.6 kN)
100 kips (445 kN)	6.35 kips (28.3 kN)
125 kips (556 kN)	6.11 kips (27.2 kN)

BG4S2_6L: Pullout Force vs. Key Displacements

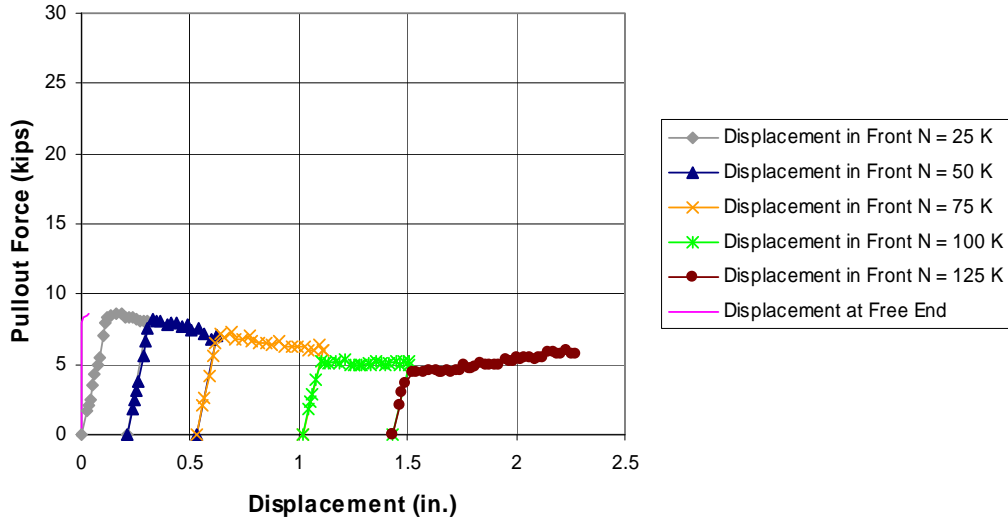


Figure C.44: Load-displacement Relationship for Strand BG4S2_6L

Date Tested: January 16, 2002

Length embedded in concrete prior to test: 13 in. (0.33 m)

Average bond strength: 407 psi (2,810 kPa)

Table C.44: Summary of Test Results for Strand BG4S2_6L

Clamping Load N	Slip Occurred or Resumed At
25 kips (111 kN)	8.32 kips (37.0 kN)
50 kips (222 kN)	8.2 kips (36.5 kN)
75 kips (334 kN)	7.13 kips (31.7 kN)
100 kips (445 kN)	5.24 kips (23.3 kN)
125 kips (556 kN)	4.37 kips (19.4 kN)

BG4S2_9L: Pullout Force vs. Key Displacements

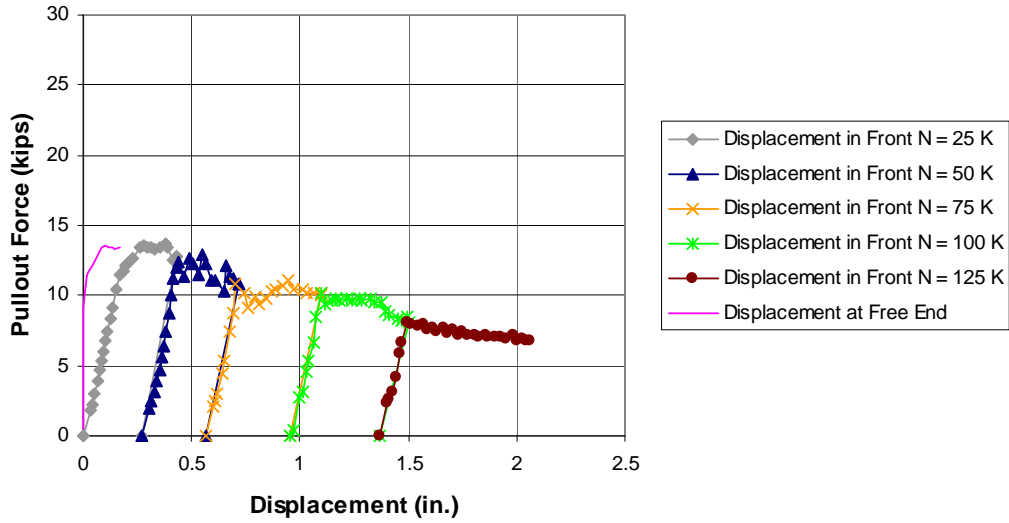


Figure C.45: Load-displacement Relationship for Strand BG4S2_9L

Date Tested: January 15, 2002

Length embedded in concrete prior to test: 13.3 in. (0.34 m)

Average bond strength: 499 psi (3,440 kPa)

Table C.45: Summary of Test Results for Strand BG4S2_9L

Clamping Load N	Slip Occurred or Resumed At
25 kips (111 kN)	10.39 kips (46.2 kN)
50 kips (222 kN)	12.02 kips (53.5 kN)
75 kips (334 kN)	10.82 kips (48.1 kN)
100 kips (445 kN)	10.21 kips (45.4 kN)
125 kips (556 kN)	8.09 kips (36.0 kN)

BG4S2_15L: Pullout Force vs. Key Displacements

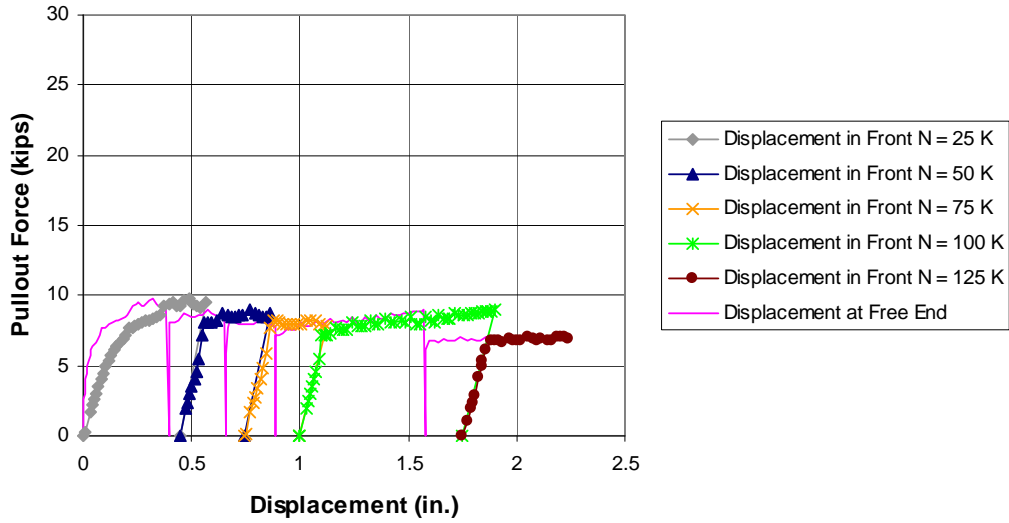


Figure C.46: Load-displacement Relationship for Strand BG4S2_15L

Date Tested: January 13, 2002

Length embedded in concrete prior to test: 13.6 in. (0.35 m)

Average bond strength: 139 psi (960 kPa)

Table C.46: Summary of Test Results for Strand BG4S2_15L

Clamping Load N	Slip Occurred or Resumed At
25 kips (111 kN)	2.98 kips (13.3 kN)
50 kips (222 kN)	8.09 kips (36.0 kN)
75 kips (334 kN)	7.66 kips (34.1 kN)
100 kips (445 kN)	7.13 kips (31.7 kN)
125 kips (556 kN)	6.13 kips (27.3 kN)

BG4S2_17L: Pullout Force vs. Key Displacements

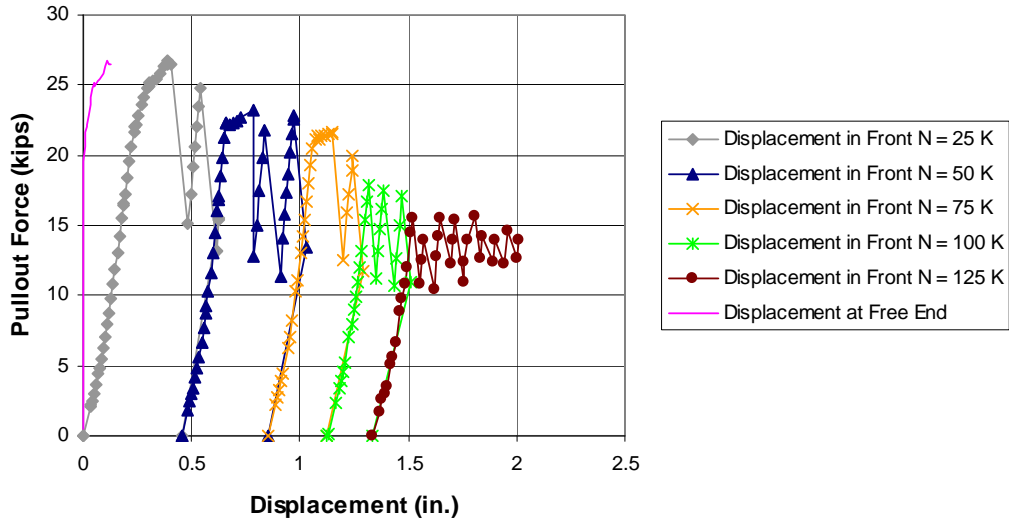


Figure C.47: Load-displacement Relationship for Strand BG4S2_17L

Date Tested: January 13, 2002

Length embedded in concrete prior to test: 13.6 in. (0.35 m)

Average bond strength: 963 psi (6,640 kPa)

Table C.47: Summary of Test Results for Strand BG4S2_17L

Clamping Load N	Slip Occurred or Resumed At
25 kips (111 kN)	20.61 kips (91.7 kN)
50 kips (222 kN)	22.3 kips (99.2 kN)
75 kips (334 kN)	20.52 kips (91.3 kN)
100 kips (445 kN)	17.83 kips (79.3 kN)
125 kips (556 kN)	15.52 kips (69.0 kN)

BG4S2_18L: Pullout Force vs. Key Displacements

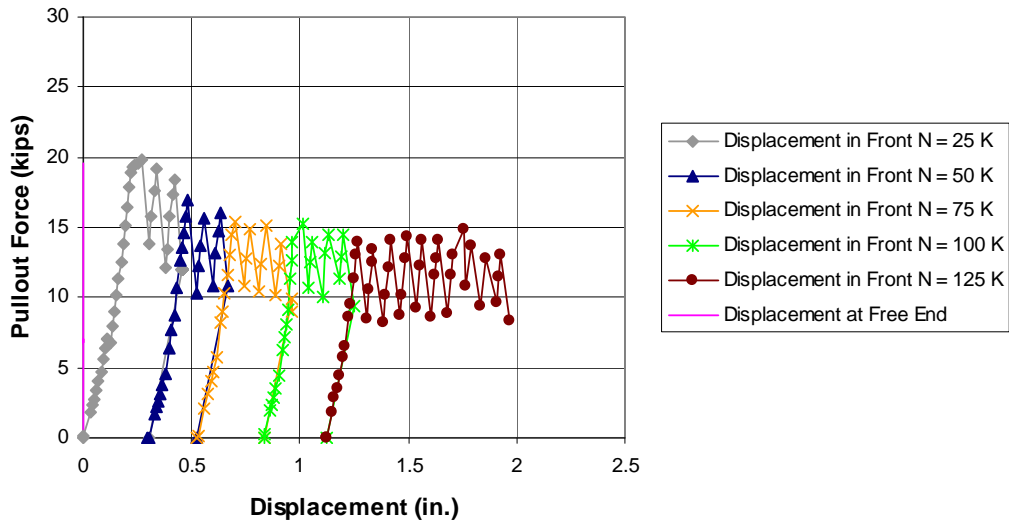


Figure C.48: Load-displacement Relationship for Strand BG4S2_18L

Date Tested: January 14, 2002

Length embedded in concrete prior to test: 13.1 in. (0.33 m)

Average bond strength: 667 psi (4,610 kPa)

Table C.48: Summary of Test Results for Strand BG4S2_18L

Clamping Load N	Slip Occurred or Resumed At
25 kips (111 kN)	13.79 kips (61.3 kN)
50 kips (222 kN)	14.63 kips (65.1 kN)
75 kips (334 kN)	13.09 kips (58.2 kN)
100 kips (445 kN)	13.98 kips (62.2 kN)
125 kips (556 kN)	12.99 kips (57.8 kN)

BG4S2_2R: Pullout Force vs. Key Displacements

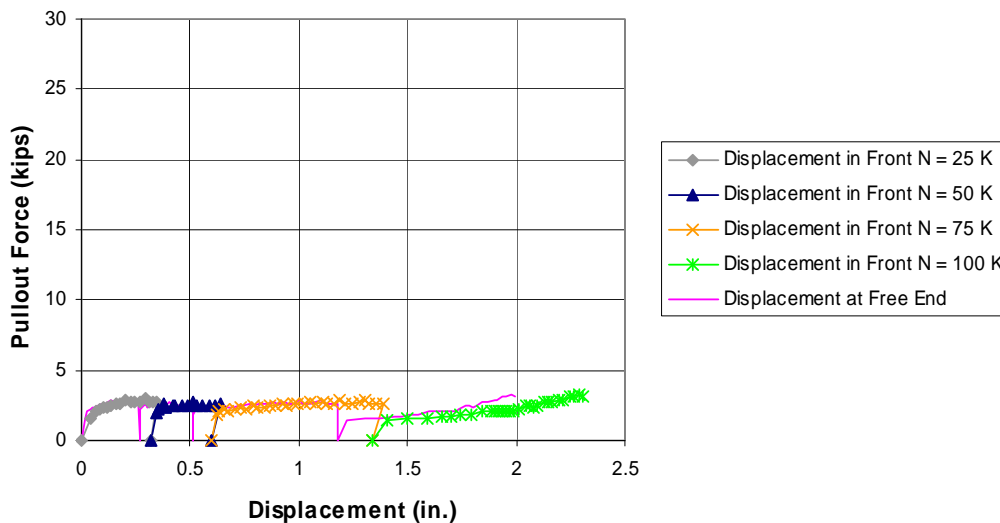


Figure C.49: Load-displacement Relationship for Strand BG4S2_2R

Date Tested: January 22, 2002

Length embedded in concrete prior to test: 12.6 in. (0.32 m)

Average bond strength: 76 psi (525 kPa)

Table C.49: Summary of Test Results for Strand BG4S2_2R

Clamping Load N	Slip Occurred or Resumed At
25 kips (111 kN)	1.51 kips (6.7 kN)
50 kips (222 kN)	2.59 kips (11.5 kN)
75 kips (334 kN)	2.1 kips (9.3 kN)
100 kips (445 kN)	1.39 kips (6.2 kN)

BG4S2_5R: Pullout Force vs. Key Displacements

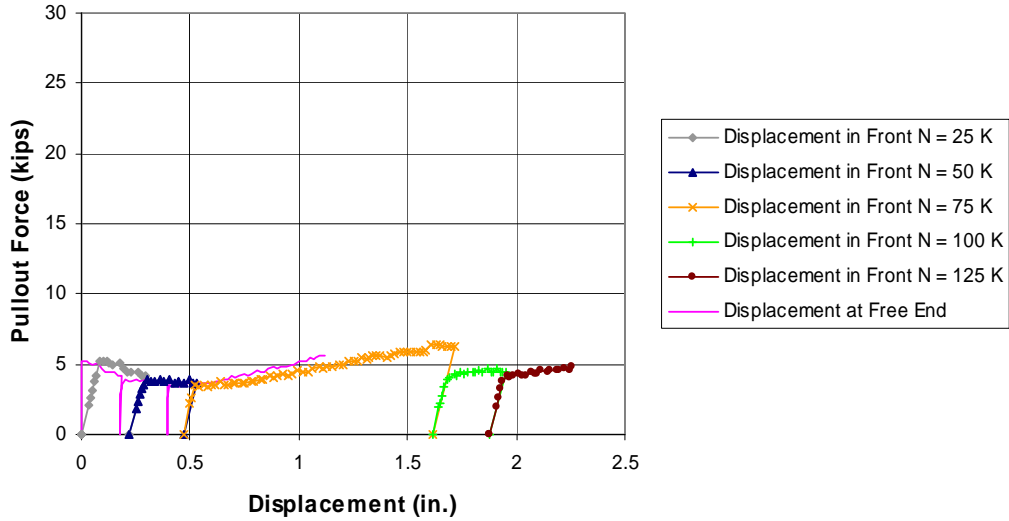


Figure C.50: Load-displacement Relationship for Strand BG4S2_5R

Date Tested: January 18, 2002

Length embedded in concrete prior to test: 12.4 in. (0.31 m)

Average bond strength: 272 psi (1,870 kPa)

Table C.50: Summary of Test Results for Strand BG4S2_5R

Clamping Load N	Slip Occurred or Resumed At
25 kips (111 kN)	5.28 kips (23.5 kN)
50 kips (222 kN)	3.56 kips (15.8 kN)
75 kips (334 kN)	3.49 kips (15.5 kN)
100 kips (445 kN)	4.01 kips (17.8 kN)
125 kips (556 kN)	4.14 kips (18.4 kN)

BG4S2_7R: Pullout Force vs. Key Displacements

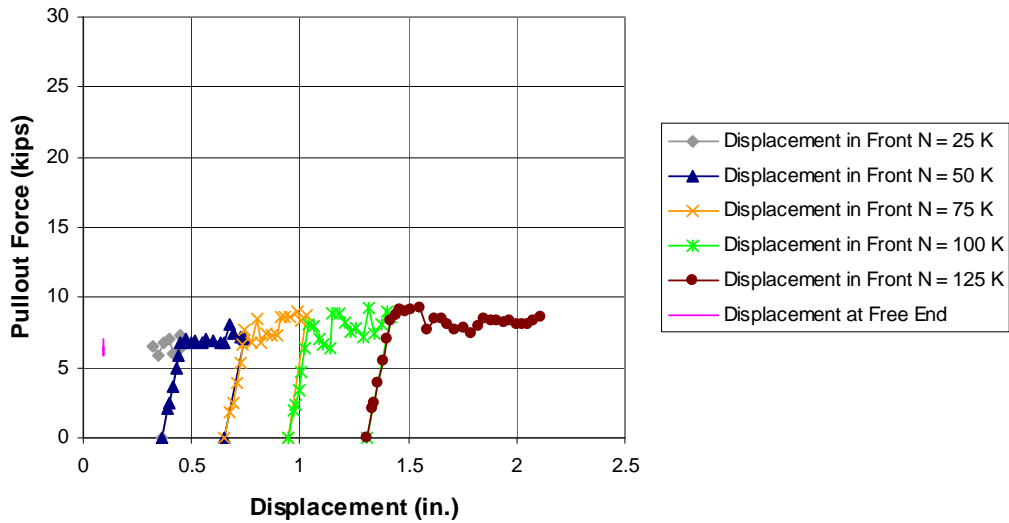


Figure C.51: Load-displacement Relationship for Strand BG4S2_7R

Date Tested: January 18, 2002

Length embedded in concrete prior to test: 12.6 in. (0.32 m)

Average bond strength: Unknown

Table C.51: Summary of Test Results for Strand BG4S2_7R

Clamping Load N	Slip Occurred or Resumed At
25 kips (111 kN)	Unknown
50 kips (222 kN)	7.11 kips (31.6 kN)
75 kips (334 kN)	7.67 kips (34.1 kN)
100 kips (445 kN)	8.12 kips (36.1 kN)
125 kips (556 kN)	8.74 kips (38.9 kN)

BG4S2_9R: Pullout Force vs. Key Displacements

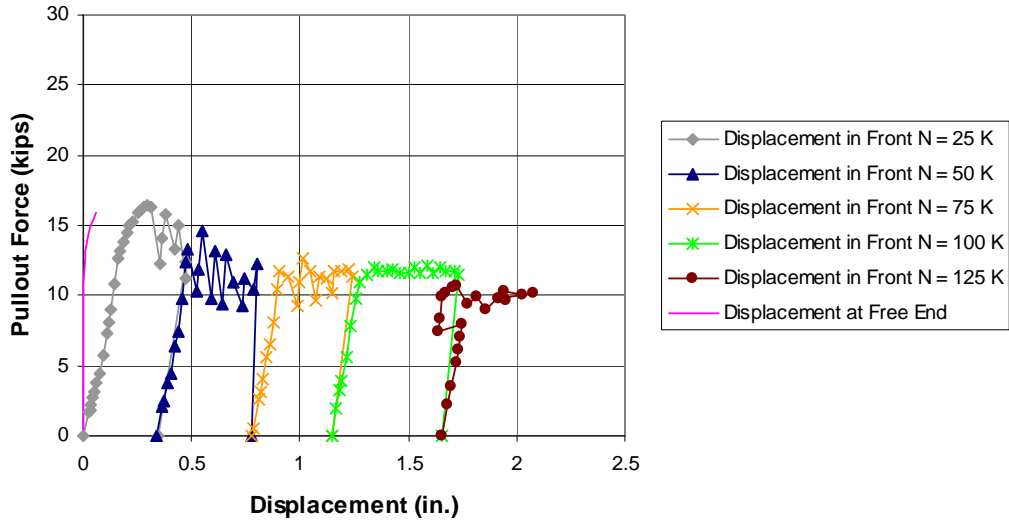


Figure C.52: Load-displacement Relationship for Strand BG4S2_9R

Date Tested: January 17, 2002

Length embedded in concrete prior to test: 12.8 in. (0.33 m)

Average bond strength: 628 psi (4,330 kPa)

Table C.52: Summary of Test Results for Strand BG4S2_9R

Clamping Load N	Slip Occurred or Resumed At
25 kips (111 kN)	12.63 kips (56.2 kN)
50 kips (222 kN)	13.34 kips (59.3 kN)
75 kips (334 kN)	11.69 kips (52 kN)
100 kips (445 kN)	10.99 kips (48.9 kN)
125 kips (556 kN)	10.23 kips (45.5 kN)

BG4S2_13R: Pullout Force vs. Key Displacements

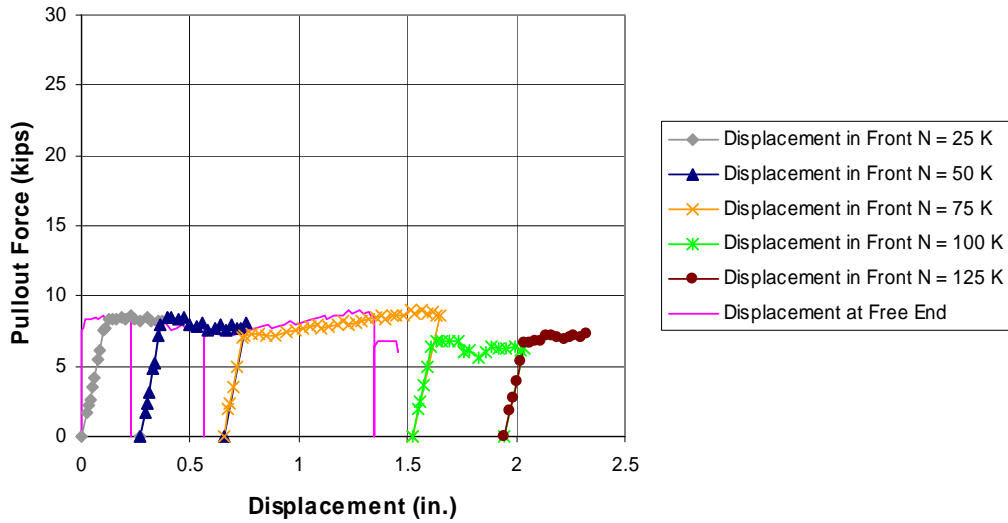


Figure C.53: Load-displacement Relationship for Strand BG4S2_13R

Date Tested: January 22, 2002

Length embedded in concrete prior to test: 12.5 in. (0.32 m)

Average bond strength: 391 psi (2,700 kPa)

Table C.53: Summary of Test Results for Strand BG4S2_13R

Clamping Load N	Slip Occurred or Resumed At
25 kips (111 kN)	7.68 kips (34.2 kN)
50 kips (222 kN)	8.46 kips (37.6 kN)
75 kips (334 kN)	7.24 kips (32.2 kN)
100 kips (445 kN)	6.78 kips (30.2 kN)
125 kips (556 kN)	6.63 kips (29.5 kN)

BG4S2_15R: Pullout Force vs. Key Displacements

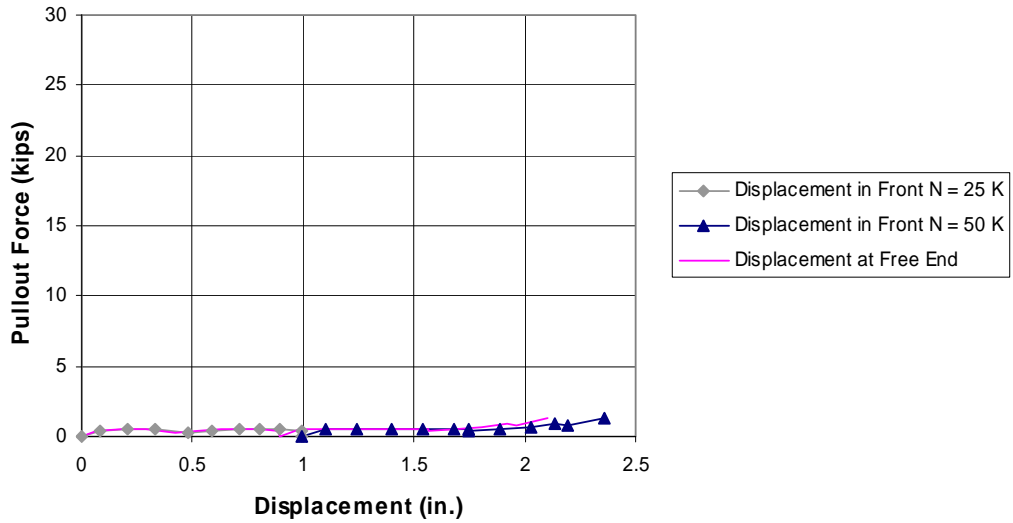


Figure C.54: Load-displacement Relationship for Strand BG4S2_15R

Date Tested: January 22, 2002

Length embedded in concrete prior to test: 13.3 in. (0.34 m)

Average bond strength: 0 psi (0 kPa)

Table C.54: Summary of Test Results for Strand BG4S2_15R

Clamping Load N	Slip Occurred or Resumed At
25 kips (111 kN)	0 kips (0 kN)
50 kips (222 kN)	0 kips (0 kN)

BG4S2_17R: Pullout Force vs. Key Displacements

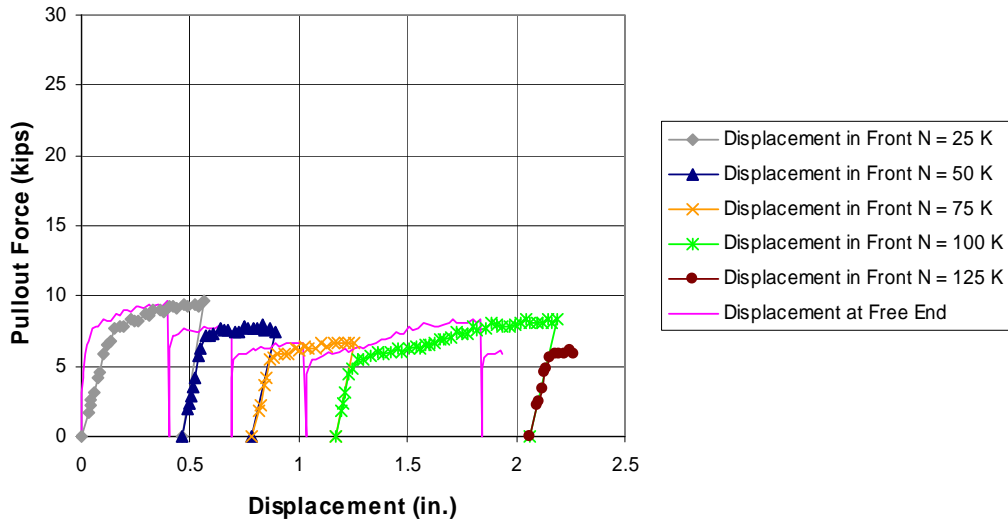


Figure C.55: Load-displacement Relationship for Strand BG4S2_17R

Date Tested: January 21, 2002

Length embedded in concrete prior to test: 12.8 in. (0.32 m)

Average bond strength: 206 psi (1,420 kPa)

Table C.55: Summary of Test Results for Strand BG4S2_17R

Clamping Load N	Slip Occurred or Resumed At
25 kips (111 kN)	4.13 kips (18.4 kN)
50 kips (222 kN)	7.16 kips (31.9 kN)
75 kips (334 kN)	5.61 kips (25.0 kN)
100 kips (445 kN)	4.88 kips (21.7 kN)
125 kips (556 kN)	5.59 kips (24.9 kN)

BG4S2_18R: Pullout Force vs. Key Displacements

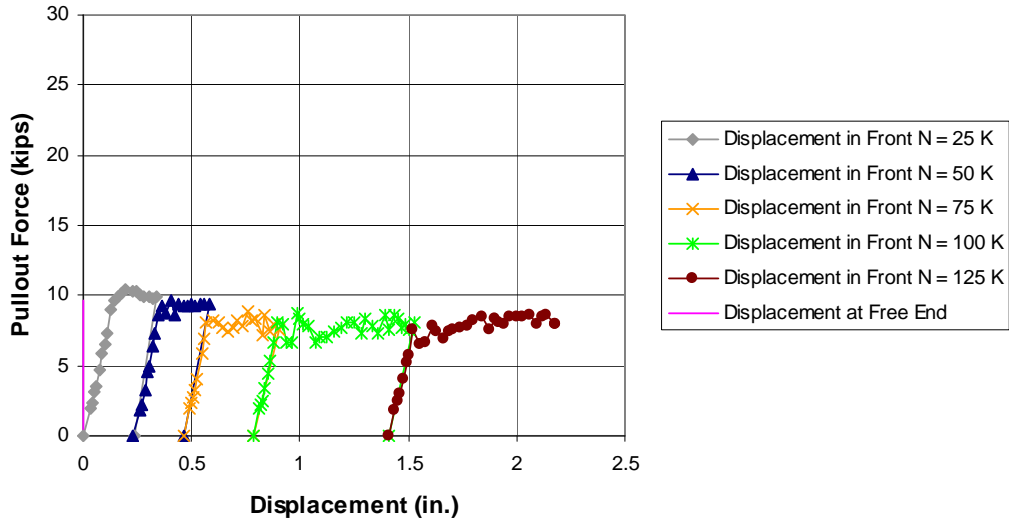


Figure C.56: Load-displacement Relationship for Strand BG4S2_18R

Date Tested: January 22, 2002

Length embedded in concrete prior to test: 12.3 in. (0.31 m)

Average bond strength: 471 psi (3,250 kPa)

Table C.56: Summary of Test Results for Strand BG4S2_18R

Clamping Load N	Slip Occurred or Resumed At
25 kips (111 kN)	9.06 kips (40.3 kN)
50 kips (222 kN)	9.26 kips (41.2 kN)
75 kips (334 kN)	8.06 kips (35.9 kN)
100 kips (445 kN)	8.06 kips (35.9 kN)
125 kips (556 kN)	7.59 kips (33.8 kN)

References

- Abrishami, H. H. and Mitchell, D., "Bond Characteristics of Pretensioned Strand." *ACI Materials Journal*, V. 90, No. 3, May-June 1993, pp. 228-235.
- ACI Committee 318 "Building Code Requirements for Structural Concrete (318-02) and Commentary (318R-02)," Farmington Hills, Michigan, 2002.
- Boenig, A., "Bridges with Premature Concrete Deterioration: Field Observations and Large-Scale Testing." Master's Thesis prepared for The Graduate School of The University of Texas at Austin, May 2000.
- Chotickai, P., "Acoustic Emission Monitoring of Prestressed Bridge Girders with Premature Concrete Deterioration." Master's Thesis prepared for The Graduate School of The University of Texas at Austin, May 2001.
- Eskridge, A. E., "Mitigation Techniques for In-Service Structures with Premature Concrete Deterioration." Master's Thesis prepared for The Graduate School of The University of Texas at Austin, May 2002.
- Fang, I.-K., Worley, J., Klingner, R. E. and Burns, N. H., "Behavior of Isotropic Concrete Bridge Decks on Steel Girders." *Structures Journal, ASCE*, V. 116, No. 3, March 1990, pp. 659-679.
- Fúnez, Luz Marina, "Field Observation of Bridges with Premature Concrete Deterioration: Structural Implications." MS Report, The University of Texas at Austin, December 1999.
- Janney, J. R., "Nature of Bond in Pre-Tensioned Prestressed Concrete." *Journal of the American Concrete Institute, Proceedings*, V. 50, No. 9, May 1954, pp. 717-736.
- Klingner, R. E. and Fowler, T. J., "Structural Assessment of In-service Bridges with Premature Concrete Deterioration." Proposal prepared for Texas Department of Transportation, 1998.
- Klingner, R. E., Fowler, T. J., and Kreger, M. E., "Mitigation Techniques for In-service Structures with Premature Concrete Deterioration." Proposal prepared for Texas Department of Transportation, 2000.

- Mains, R. M., "Measurement of the Distribution of Tensile and Bond Stresses Along Reinforcing Bars." *Journal of the American Concrete Institute, Proceedings*, V. 48, No. 3, November 1951, pp.225-252.
- Mylrea, T. D., "Bond and Anchorage." *Journal of the American Concrete Institute, Proceedings*, V. 44, No. 7, March 1948, pp. 521-552.
- National Climatic Data Center, National Oceanic & Atmospheric Administration, <http://lwf.ncdc.noaa.gov>, May 2002.
- Roche, J. M., "Bridges with Premature Concrete Deterioration: Fatigue Testing of Full-Scale, Prestressed Concrete Box Girders Failing in Shear." Master's Thesis prepared for The Graduate School of The University of Texas at Austin, May 2001.
- Rose, D.R. and Russell, B.W., "Investigation of Standardized Tests to Measure the Bond Performance of Prestressing Strand." *PCI Journal*, V. 42, No. 4, July-August 1997, pp.56-80.
- Salmons, J. R. and McCrate, T. E., "Bond Characteristics of Untensioned Prestressing Strand." *PCI Journal*, V. 22, No. 1, January-February, 1977, pp. 52-65.
- Stocker, M. F. and Sozen, M. A., "Investigation of Prestressed Reinforced Highway Bridges, Part V: Bond Characteristics of Prestressing Strand." *Engineering Experiment Station, Bulletin 503*, The University of Illinois, College of Engineering, 1970.
- Tinkey, B. V., "Nondestructive Testing of Prestressed Bridge Girders with Distributed Damage." Master's Thesis prepared for The Graduate School of The University of Texas at Austin, May 2000.
- Texas Department of Transportation "Standard Specifications for Construction of Highways, Streets and Bridges," Austin, Texas, 1993.

Vita

Larry Memberg was born in Atlanta, Georgia, on December 12, 1976, the son of Donald and Francine Memberg. After graduating from Chamblee High School in 1995, he attended the Georgia Institute of Technology (Georgia Tech) in Atlanta, Georgia. He received the degree of Bachelor of Science in Civil Engineering from Georgia Tech in August 2000. In August 2000, he entered The Graduate School of The University of Texas at Austin.

Permanent address: 3931 Granger Dr.
Chamblee, GA 30341

This thesis was typed by the author.